frontiers | Research Topics

Insights on the rise of animal life from Cambrian and Ordovician Lagerstätten

Edited by
Bertrand Lefebvre, Allison Daley, Farid Saleh and Khadija El Hariri

Published in
Frontiers in Ecology and Evolution
Frontiers in Earth Science

ISSN 1664-8714
ISBN 978-2-8325-4234-7
DOI 10.3389/978-2-8325-4234-7

About Frontiers

Frontiers is more than just an open access publisher of scholarly articles: it is a pioneering approach to the world of academia, radically improving the way scholarly research is managed. The grand vision of Frontiers is a world where all people have an equal opportunity to seek, share and generate knowledge. Frontiers provides immediate and permanent online open access to all its publications, but this alone is not enough to realize our grand goals.

Frontiers journal series

The Frontiers journal series is a multi-tier and interdisciplinary set of open-access, online journals, promising a paradigm shift from the current review, selection and dissemination processes in academic publishing. All Frontiers journals are driven by researchers for researchers; therefore, they constitute a service to the scholarly community. At the same time, the *Frontiers journal series* operates on a revolutionary invention, the tiered publishing system, initially addressing specific communities of scholars, and gradually climbing up to broader public understanding, thus serving the interests of the lay society, too.

Dedication to quality

Each Frontiers article is a landmark of the highest quality, thanks to genuinely collaborative interactions between authors and review editors, who include some of the world's best academicians. Research must be certified by peers before entering a stream of knowledge that may eventually reach the public - and shape society; therefore, Frontiers only applies the most rigorous and unbiased reviews. Frontiers revolutionizes research publishing by freely delivering the most outstanding research, evaluated with no bias from both the academic and social point of view. By applying the most advanced information technologies, Frontiers is catapulting scholarly publishing into a new generation.

What are Frontiers Research Topics?

Frontiers Research Topics are very popular trademarks of the *Frontiers journals series*: they are collections of at least ten articles, all centered on a particular subject. With their unique mix of varied contributions from Original Research to Review Articles, Frontiers Research Topics unify the most influential researchers, the latest key findings and historical advances in a hot research area.

Find out more on how to host your own Frontiers Research Topic or contribute to one as an author by contacting the Frontiers editorial office: frontiersin.org/about/contact

Insights on the rise of animal life from Cambrian and Ordovician Lagerstätten

Topic editors

Bertrand Lefebvre — Université Claude Bernard Lyon 1, France
Allison Daley — Université de Lausanne, Switzerland
Farid Saleh — Université de Lausanne, Switzerland
Khadija El Hariri — Cadi Ayyad University, Morocco

Citation

Lefebvre, B., Daley, A., Saleh, F., El Hariri, K., eds. (2023). *Insights on the rise of animal life from Cambrian and Ordovician Lagerstätten*. Lausanne: Frontiers Media SA. doi: 10.3389/978-2-8325-4234-7

Table of contents

frontiers | Frontiers in Earth Science

TYPE Editorial
PUBLISHED 18 December 2023
DOI 10.3389/feart.2023.1343862

OPEN ACCESS

EDITED AND REVIEWED BY
Bruce S. Lieberman,
University of Kansas, United States

*CORRESPONDENCE
Farid Saleh,
farid.nassim.saleh@gmail.com

RECEIVED 24 November 2023
ACCEPTED 04 December 2023
PUBLISHED 18 December 2023

CITATION
Saleh F, Daley AC, Lefebvre B and El Hariri K (2023), Editorial: Insights on the rise of animal life from Cambrian and Ordovician Lagerstätten.
Front. Earth Sci. 11:1343862.
doi: 10.3389/feart.2023.1343862

Editorial: Insights on the rise of animal life from Cambrian and Ordovician Lagerstätten

Farid Saleh[1]*, Allison C. Daley[1], Bertrand Lefebvre[2] and Khadija El Hariri[3]

[1]Institute of Earth Sciences, University of Lausanne, Lausanne, Switzerland, [2]Université de Lyon, Université Claude Bernard Lyon 1, École Normale Supérieure de Lyon, CNRS, UMR5276, LGL-TPE, Villeurbanne, France, [3]Laboratoire Laboratoire de Géoressources, Géoenvironnement et Génie Civil (L3G), Faculté des Sciences et Techniques, Université Cadi-Ayyad, Marrakesh, Morocco

KEYWORDS

Ordovician, Cambrian, animal radiation, ecology, evolution

Editorial on the Research Topic
Insights on the rise of animal life from Cambrian and Ordovician Lagerstätten

The Early Palaeozoic witnessed the swift emergence and diversification of most animal phyla alongside the establishment of modern-style ecosystems. Exceptionally well-preserved fossils from various Cambrian and Ordovician Lagerstätten provide valuable insights into this pivotal evolutionary phase. Palaeontological investigations describe taxonomic occurrences, anatomical innovations, and developmental patterns, and link these biological observations with characterisations of the abiotic environmental conditions, to achieve a holistic understanding of this time period.

This special volume gathers together publications on Cambrian and Early Ordovician Lagerstätten and provides detailed fossil descriptions for a variety of animals including annelids, arthropods, bryozoans, cnidarians, echinoderms, and scalidophorans. These works showcase the breadth of different approaches that can be applied beyond the descriptive, for example, with evolutionary analyses and studies on ontogeny, development, functional morphology and palaeoecology.

Important new results are revealed from a series of publications studying material from several Cambrian Lagerstätten in China. A new primitive polychaete is described from the Guanshan Biota by Zhao et al., who argue that this annelid likely possessed strong sensory abilities owing to its bicellular eyes and possible nuchal organs. Zhao et al. also describe new bryozoan and cnidarian taxa from the Guanshan Biota, demonstrating that the epibenthic diversity of this Lagerstätte is higher than previously thought. Our understanding of Cambrian ecosystems is also enhanced by the discovery of well-preserved microscopic medusozoans from the Zhangjiagou section. Zhang et al. describe the detailed three-dimensional morphology of multiple ontogenetic stages that allow for a complete reconstruction of anatomical shape change during the development of this early cnidarian. The ontogenetic sequence of scalidophorans from the same section is also established in more detail than possible previously based on the discovery of new material described by Qin et al. This study reveals that the sclerites of this undetermined worm became more numerous and increased in size during growth. Our knowledge of Cambrian diversity and development is further enriched by a study conducted by Ma et al., investigating the growth and development of the arthropod *Isoxys* from the

Qingjiang Biota. Tens of specimens of this arthropod reveal that its valves gradually elongated, and the ratio of cardinal spines and spherical eyes relative to the valve length significantly decreased during postembryonic development. The presence of evidence of brood care in some small specimens suggests that *Isoxys* may have exhibited reproductive abilities in its early life stage.

The special volume also features several publications focused on fossils from the Ordovician Fezouata Shale Lagerstätte in Morocco, focusing on two animal phyla—echinoderms and arthropods—that are relatively abundant at this site. Dupichaud et al. provide a detailed taxonomic treatment of solutan echinoderms, showing that they were more diverse than previously envisaged and establishing a new genus and species. Novel information on exceptionally preserved arthropods from the Fezouata Biota is also revealed in a series of papers. Potin et al. investigated over a hundred specimens of radiodonts and showed that filter-feeding taxa are more abundant than sediment-sifting or raptorial predators, which is likely a result of the Ordovician plankton revolution. Marrellid arthropods from the Fezouata Biota are also investigated. An article by Drage et al. describes marrellid exuviae, identifies the moulting suture location and suggests that the Fezouata marrellid likely exited the exoskeleton using posterior and upward movements, in a similar fashion to modern lobsters. Laibl et al. explore the morphology of early and late developmental stages of this marrellid and show similar appendage morphology and differentiation along the body between these stages, suggesting a simple model of niche differentiation between juveniles and adults living in nearby environments. Finally, in a broader paper examining fossils from several Palaeozoic Lagerstätten, Lustri et al. show that the developmental changes in Xiphosura are correlated with the exploitation of different environments throughout their evolutionary history. Taken together, all the studies from this special volume highlight the importance of establishing a clear taxonomic framework and considering both developmental and environmental parameters during ecological and evolutionary investigations.

In conclusion, it is rather clear that new palaeontological discoveries from fossil Lagerstätten and the application of a variety of conceptual approaches are driving recent advances in our understanding of the Early Palaeozoic. This special volume has delved into the ecology and evolution of numerous animal groups from that time interval. From newly discovered micro- and macro-organisms, annelid eyes, and the intricacies of early arthropod development to the role of plankton in shaping radiodont diversity and the fascinating realm of marrellid arthropods, these findings significantly contribute to our understanding of the diversity and dynamics of life in the Early Palaeozoic. As we peer through the lens provided by exceptionally well-preserved fossil Lagerstätten, the intricate evolutionary processes that have shaped life on our planet come increasingly into focus.

Author contributions

FS: Writing–original draft, Writing–review and editing. AD: Writing–review and editing. BL: Writing–review and editing. KE: Writing–review and editing.

Funding

The author(s) declare financial support was received for the research, authorship, and/or publication of this article. FS is funded by a Swiss National Science Foundation (SNF) Ambizione Grant (PZ00P2_209102). AD acknowledges funding from a SNF project grant (205321_179084) and a SNF Sinergia grant (198691).

Acknowledgments

We would like to thank all the authors who contributed to this volume, and all the reviewers who examined the manuscripts. We are grateful to Emily G. Mitchell, Sylvain Charbonnier, Tae-Yoon Park, Haijun Song, and Zhifei Zhang for serving as guest Associate Editors of some papers in this volume. This special volume is associated with the second annual meeting of the IGCP project 735 in Marrakech, Morocco in 2022 entitled "Filling knowledge gaps in the Early Palaeozoic Biodiversification and Promoting Geological Heritage" in 2022, and with the IGCP project 735 Symposium of the International Palaeontological Congress 2022 in Khon Kaen, Thailand, entitled "Recent advances on metazoan diversifications from Early Palaeozoic Lagerstätten".

Conflict of interest

The authors declare that the research was conducted in the absence of any commercial or financial relationships that could be construed as a potential conflict of interest.

The author(s) declared that they were an editorial board member of Frontiers, at the time of submission. This had no impact on the peer review process and the final decision.

Publisher's note

frontiers | Frontiers in Earth Science

TYPE Original Research
PUBLISHED 17 March 2023
DOI 10.3389/feart.2023.1038686

OPEN ACCESS

EDITED BY
Farid Saleh,
Yunnan University, China

REVIEWED BY
Jean Vannier,
Université Claude Bernard Lyon 1, France
Peiyun Cong,
Yunnan University, China
Jonathan Antcliffe,
Université de Lausanne, Switzerland

*CORRESPONDENCE
Yunhuan Liu,
yunhuanl@chd.edu.cn

SPECIALTY SECTION
This article was submitted to Paleontology, a section of the journal Frontiers in Earth Science

RECEIVED 07 September 2022
ACCEPTED 28 February 2023
PUBLISHED 17 March 2023

CITATION
Zhang Y, Liu Y, Shao T and Qin J (2023), New *Qinscyphus* material from the Fortunian of South China. *Front. Earth Sci.* 11:1038686. doi: 10.3389/feart.2023.1038686

New *Qinscyphus* material from the Fortunian of South China

Yanan Zhang, Yunhuan Liu*, Tiequan Shao and Jiachen Qin

School of Earth Science and Resources, Chang'an University, Xi'an, China

Microscopic medusozoans from the Cambrian Fortunian stage of South China are well known for their exceptionally preserved embryos and elongated tubes. However, additional details of their morphology remain unclear. This paper describes new medusozoan fossils showing the whole apical complement and covering the morphological integrity of *Qinscyphus*. The apical part of *Qinscyphus* is considered to be soft during early ontogeny, and the inverted pentagonal pyramid may gradually form with growth and development. This discovery of the apical complement of *Qinscyphus* is novel and essential to complement the external morphology of early medusozoan fossils. More importantly, the new specimens have different annuli with triangular thickenings, providing a more comprehensive view on the developmental sequence of *Qinscyphus*. Therefore, this work allows a better understanding of early medusozoans ecology and evolution.

KEYWORDS

medusozoan, olivooids, apical complement, Zhangjiagou section, developmental sequence

1 Introduction

The origin and evolution of medusa are the focus of both paleontologists and modern biologists (Park et al., 2012; Wang D et al., 2020). The most distinctive characteristics of medusozoans are their radial symmetry and their ability to swim (Han et al., 2020). Paleontologists have found numerous medusozoans in the early Cambrian (531.8–536.4 Ma) (Dong et al., 2013; Han et al., 2013; Liu et al., 2014a; Steiner et al., 2014; Dong et al., 2016; Liu et al., 2017; Wang et al., 2017; Shao et al., 2018b; Han et al., 2018; Shao et al., 2019a; Wang X et al., 2020). In the Zhangjiagou Section, South China, various Fortunian radial animals were found such as *Olivooides, Quadrapyrgites,* and *Hexaconularia* (Conway Morris and Chen, 1992; Van Iten et al., 2006; Van Iten et al., 2010; Liu et al., 2014b; Van Iten et al., 2014; Liu et al., 2017). These taxa were compared to cnidarians as they show a radial body plan with an apical–abapical differentiation (Conway Morris and Chen, 1992; Van Iten et al., 2006; Van Iten et al., 2010; Liu et al., 2014b; Van Iten et al., 2014; Liu et al., 2017). However, most olivooids structures are lacking from living cnidarians. Olivooid tubes had prominent annulations and fine longitudinal striations with the oral aperture being the only opening of these tubes (Liu et al., 2014a; Steiner et al., 2014). Therefore, olivooids were considered as coronate scyphozoans, and their elongate tubes were considered as polyp stages that develop after hatching (Conway Morris and Chen, 1992; Bengtson and Yue, 1997; Van Iten et al., 2006; Van Iten et al., 2010; Dong et al., 2013; Han et al., 2013; Liu et al., 2014a; Liu et al., 2017; Wang et al., 2017).

The microscopic animal, *Qinscyphus,* was first reported from the early Cambrian Kuanchuanpu Formation at the Zhangjiagou section in South China (Liu et al., 2017). *Qinscyphus necopinus* is a cup-shaped animal with an embryonic tissue (apical part) and a post-embryonic tissue (abapical part). The embryonic tissue formed an inverted pentagonal

pyramid with a smooth surface (Liu et al., 2017; Shao et al., 2018a). Post-embryonic tissue was tube-shaped with densely spaced and slightly raised annuli (Liu et al., 2017). Several circlets of triangular thickenings formed five longitudinal rows, pentaradially arranged on post-embryonic tissues, each straddling several annuli (Shao et al., 2018a). Moreover, *Qinscyphus* might be a direct developer due to the comparable morphology of the oral part in both embryos and adults (Shao et al., 2018a; Qin et al., 2020). *Qinscyphus* was interpreted as a possible coronate scyphozoan for its pentagonal symmetry, its tube (comparable to a periderm), and its oral part (its only opening) (Liu et al., 2017). This paper reports five new three-dimensionally phosphatized specimens of *Q. necopinus* from South China; from which four are complete, unlike the fragmentary nature of previously described material, including partially the holotype.

2 Materials and methods

The studied specimens are deposited at the University Museum of Chang'an University (UMCU), Xi'an, China. They were extracted from the phosphatic limestone of the lower part of the second member of the Kuanchuanpu Formation, Zhangjiagou section, Xixiang County, southern Shaanxi Province, South China (Figure 1). The lithostratigraphy and biostratigraphy of the Zhangjiagou section were studied by Li (1984) and Steiner et al. (2004a), Steiner et al. (2007). The same locality and horizon have previously yielded abundant and beautifully preserved microfossils, such as specimens of *Olivooides* (Liu et al., 2014a; Steiner et al., 2014; Liu et al., 2017; Shao et al., 2018b; Shao et al., 2019a), *Pseudooides*, the oldest known priapulid–like cycloneuralians as well as other scalidophorans (Liu et al., 2014b; Shao et al., 2016; Shao et al., 2018b; Shao et al., 2019b; Wang et al., 2019; Wang D et al., 2020) and possibe *Saccorhytus* (Han et al., 2017; Liu et al., 2022). The fossil-bearing horizon correlates with the *Anabarites trisulcatus–Protohertzina anabarica* assemblage zone (Steiner et al., 2007; Steiner et al., 2014), which has an estimated age of 531.8–536.4 Ma and falls within the Fortunian Stage (Peng et al., 2020).

Nearly 300 kg of rock samples from the key horizon at the Zhangjiagou section (Figure 1) were cracked into football-sized pieces. Each sample was put in a plastic pail or basin with a capacity of 20 L macerated using diluted acetic acid (~8%). The sieving and changing acid cycle requires three to 7 days, depending on the temperature (ambient temperature around 40°C in summer and 20°C in winter). Undissolvable residues dried naturally and were then handpicked under a binocular microscope. The microfossils were picked out and mounted on aluminium stubs for observation under a Hitachi S4800 environmental scanning electron microscope at Chang'an University, Xi'an. The figures were processed using Adobe Photoshop CS5.

3 Results

Qinscyphus is rarely found in the Kuanchuanpu Formation, and most specimens in the collection are fragmented. The newly discovered specimens are three-dimensionally preserved and only four intact tubes with a preserved apical complement have been found (Figures 2A,H and Figures 3A,F).

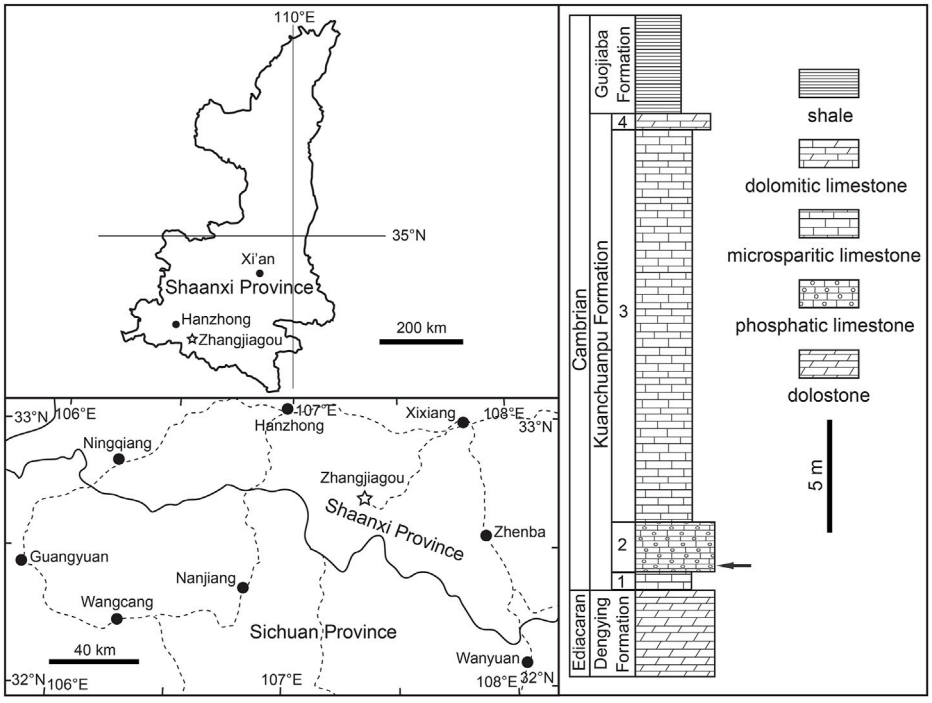

FIGURE 1
Location map and stratigraphic column of the Zhangjiagou Section in southern Shaanxi Province, South China. The key horizon yielding the current specimens is denoted by an arrow.

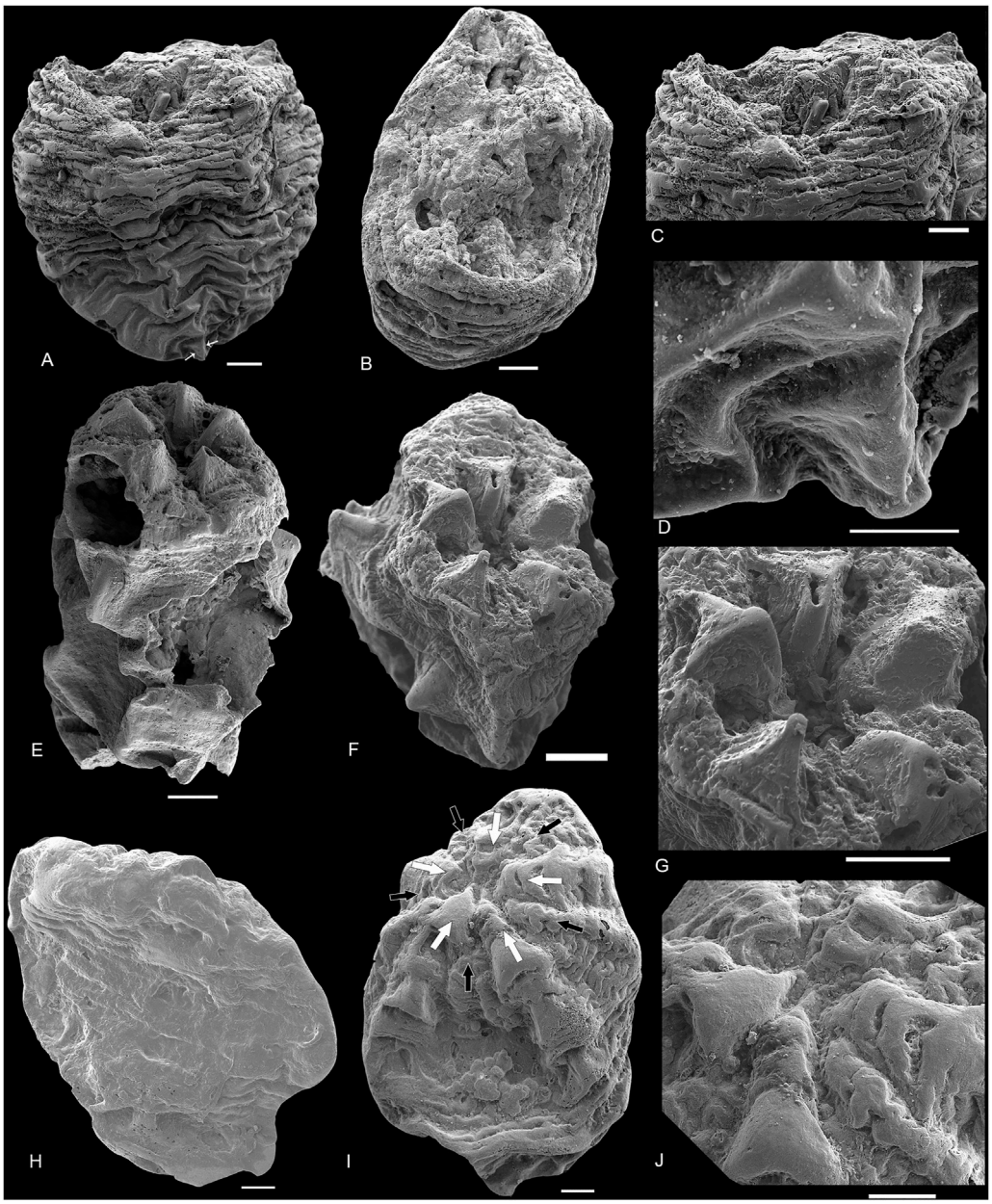

FIGURE 2
SEM images of *Qinscyphus necopinus* respectively with one to three circlets of triangular thickenings. **(A,E,H)** lateral views of 2021XQB102, 2021XQB211, 2021XQB107; **(B,F,I)** oral views; **(C,G,J)** close-up oral views of **(B,H,I)**; **(D)** the enlargement of the apical part of **(A)**; In **(I)**, white arrows denote the perradial belts with triangular thickenings, and black arrows denote the interradial belts. The scale bar represents 50 μm in **(F)**, and 100 μm in other images.

Only one specimen (Figure 2A) reveals five longitudinal edges by slight folds corresponding to five groups of triangular thickenings (Figure 2D). These edges merge at the apical end (Figure 2A), with both length and width of 950 μm. The apical end is similar to the shape of the hatchlings of *Olivooides* (Figure 4), but has a smooth surface (Figure 3B). The apical end represents a small percentage of the entire organism (Figure 2D). However, for the remaining specimens, the apical part shows multiple distinct transverse folds, with no apparent longitudinal edges (Figures 3A,B,G,H).

The post-embryonic tissue (abapical part) is tube-shaped with densely spaced and slightly raised annuli (Figures 3A,F). Five groups of triangular thickenings are developed radially on the abapical part (Figure 2I). In each group, the triangular thickening occurs repetitively every seven annuli, and straddles the next four to five annuli (Figures 3C,D). These annuli are only slightly raised, rather than strongly extended outwards to form ridges (Fig. 2C, 3D). The largest complete specimen with six circlets of triangular thickenings is 1.4 mm long and 1.1 mm wide (Figure 3F). Two oral views

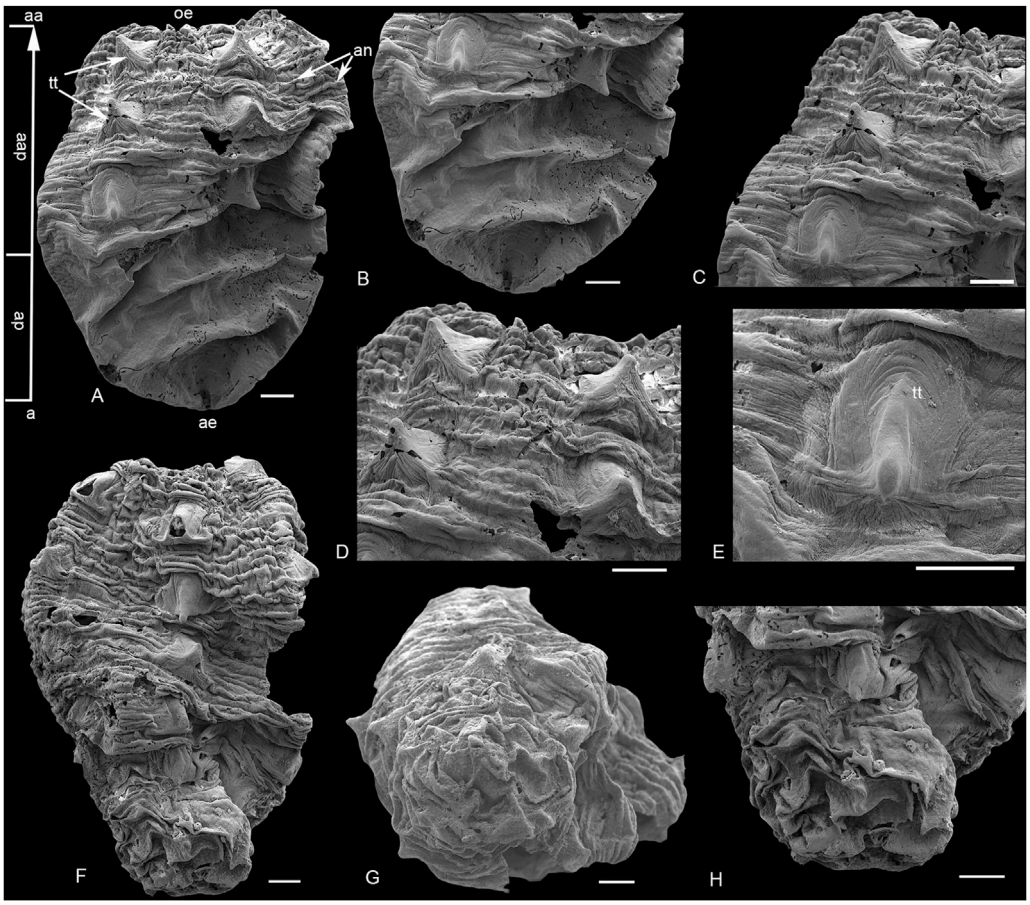

FIGURE 3
SEM images of *Qinscyphus necopinus* respectively with three and six circlets of triangular thickenings. **(A–E)** 2021XQB105; **(B)** apical part; **(C,D)** enlargement of postembryonic crests with triangular thickenings; **(E)** enlargement of triangular thickening; **(F–H)** 2021XQB106; **(G)** apical view; **(H)** enlargement of the apical part. Scale bars: 100 μm. a = apical; aa = abapical; ap = apical part; aap = abapical part; ae = apical end; an = annuli; e = edge; oe = oral end; tt = triangular thickening.

indicate that the new crest with five distinct triangular thickenings formed at the oral part (Figures 2F,I). Around the oral aperture, perradial belts and interradial belting are demarcated by marginal furrows, with a median furrow bisecting each interradial belt (Figures 2F,G,I,J). The morphology and number of triangular thickenings at the oral part are comparable to *Olivooides multisulcatus* (Figure 4F), while the new crest with triangular thickenings did not occur continuously but spaced several annuli to the next crest (Figure 3C). The new specimens are well preserved and have different circlets of triangular thickenings: one (Figure 2A), two (Figure 2E), three (Figure 2H, Figure 3A), and six circlets (Figure 3F). The surface of these triangular thickenings shows peristaltic deformation and distortion (Figure 3E), suggesting that the triangular tickenings were soft.

4 Discussion

The Cambrian fossil embryos are represented by taxa of *Markuelia, Pseudooides*, *Olivooides*, *Quadrapyrgites* and *Qinscyphus* (Dong et al., 2013; Steiner et al., 2014; Dong et al., 2016; Duan et al., 2017; Liu et al., 2017; Shao et al., 2018a). However, the affinity of many Fortunian radial animals remains debatable. For example, *Pseudooides* was previously regarded as the embryonic stage of some co-occurring arthropod-like fossil (Steiner et al., 2004b). But it was challenged because the features were unusual for any arthropod or even bilaterian (Donoghue et al., 2006). *Olivooides* was proposed as a coronate scyphozoan (Bengtson and Yue, 1997; Yue and Bengtson, 1999; Dong et al., 2013; Dong et al., 2016) or an echinoderm (Chen, 2004), a cubozoan (Han et al., 2016a; Han et al., 2016b), a stem-group cycloneuralian (Steiner et al., 2014) or a diploblastic stem-group eumetazoan (Yasui et al., 2013). *Quadrapyrgites* might be the sister group of *Olivooides* (Steiner et al., 2014), and has been proposed as a stem-group cycloneuralian (Steiner et al., 2014), a coronate scyphozoan (Liu et al., 2014b), or a cubozoan (Han et al., 2016a). *Qinscyphus* might also be a coronate scyphozoan (Liu et al., 2017; Shao et al., 2018a). The coronate scyphozoan hypothesis for *Olivooides*, *Quadrapyrgites* and *Qinscyphus* is favoured here.

The possible polypoid cnidarians from the Fortunian stage correspond to Anabaritidae (Conway Morris and Chen, 1989; Kouchinsky et al., 2009), Hexangulaconulariidae (Qian and Bengtson, 1989; Van Iten et al., 2010; Steiner et al., 2014),

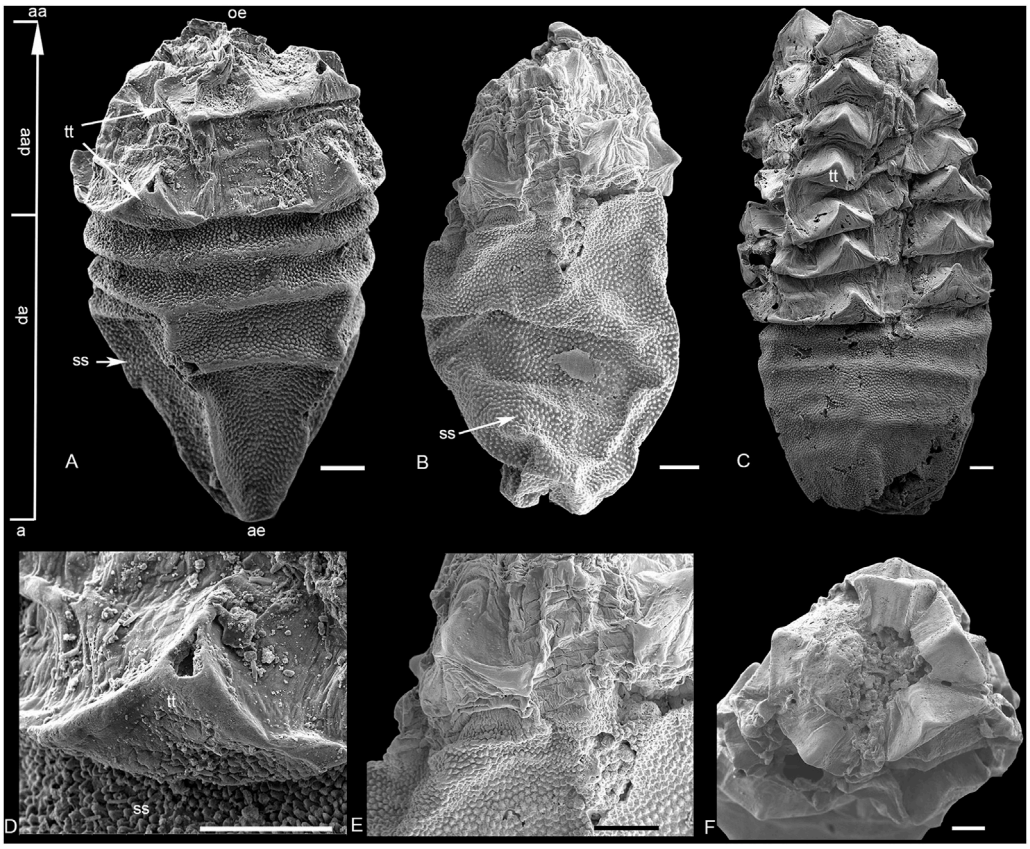

FIGURE 4
SEM images of *Olivooides multisulcatus*. **(A,D)** XX21CHD01-1; **(B,E)** XX19-b05; **(C,F)** XX21CHD01-1; **(D,E)** enlargement of triangular thickening; **(F)** close-up oral views. Scale bars: 100 μm. a = apical; aa = abapical; ap = apical part; aap = abapical part; ae = apical end; oe = oral end; ss = stellate structure; tt = triangular thickening.

Carinachitidae (Qian, 1977; Conway Morris and Chen, 1992; Yue and Bengtson, 1999; Liu et al., 2005; Liu et al., 2011; Han et al., 2018), Olivooidae (Steiner et al., 2010; Steiner et al., 2014; Han et al., 2016a; Han et al., 2016b) and Family uncertain (Steiner et al., 2004a; Dong et al., 2013; Shao et al., 2015). They had comparable radial symmetry, tube morphology, and developmental cycles. Furthermore, Olivooidae might include several genera with similar morphologies and developmental modes: *Olivooides* (Qian, 1977; Yasui et al., 2013; Steiner et al., 2014), *Quadrapyrgites* (Li, 1984; Li et al., 2007; Liu et al., 2009; Liu et al., 2014a; Steiner et al., 2014; Shao et al., 2019a), *Qinscyphus* (Liu et al., 2017; Shao et al., 2018a), *Octapyrgites* (Guo et al., 2020).

Olivooides multisulcatus (Figure 4) represents the closest analogue to *Q. necopinus*. Both are cup-shaped with an apical part and an abapical part (Figure 5). They had a similar body of pentaradial symmetry, five longitudinal rows of triangular thickenings and were found in coeval strata from South China. However, *Q. necopinus* and *O. multisulcatus* still had significant differences (Table 1). The apical part of *Q. necopinus* lacked tiny stellate protuberances on the external surface (Figures 4D,E). The newly described material shows multiple distinct transverse folds (Figure 2A) rather than an apparent longitudinal edge. Moreover, the triangular thickennings of *O. multisulcatus* occurred continuously and independently on each annulus (Figures 4A–C), whereas for *Q. necopinus* they appeared every four to seven annuli and straddled the next four to five annuli (Figures 3A,F and Figures 5C,D). *Qinscyphus necopinus* annuli were slightly raised rather than enormously extended ridged ones (Figures 3C,D). Those annuli might have contributed to a better stretching, contraction, and buffering in the living environment. *Qinscyphus necopinus* and *O. multisulcatus* also differed from each other by the absence/presence of stellate structures, and the shape of the perradial lobes and interradial belts in their embryonic stages. The perradial lobes of *Q. necopinus* had an elliptical end. The interradial belts had median and marginal furrows (Figure 5B). However, the interradial lobes of *O. multisulcatus* were strongly squeezed by the perradial lobes (Figure 5A) (see Shao et al., 2018a).

Previous work suggested that the apical part of *Q. necopinus* is an inverted pentagonal pyramid with five prominent longitudinal edges (Liu et al., 2017; Shao et al., 2018a; Qin et al., 2020). However, the new specimens did not show this feature (Figure 2; Figure 3). The apical part of the new specimens had multiple distinct transverse folds (Figures 3A,F), but no apparent longitudinal edges. Thus, there are two possible forms of the apical part of *Qinscyphus*: an inverted pentagonal cone or a circular one. This contrast might be resulting from intraspecific variations. However, considering that the new fossils show a circular cone in early ontogenetic stages (Liu et al., 2017), we suggest that the shape of the apical part might gradually become an inverted pentagonal pyramid with growth and development.

TABLE 1 Morphological comparisons of *Olivooides multisulcatus* and *Qinscyphus necopinus*.

Characteristics\taxa		*Olivooides multisulcatus*	*Qinscyphus necopinus*
Embryo	oral part	5 sharply V-shaped perradial lobes and 5 interradial lobes	5 perradial belts with elliptical end and 5 interradial belts
	lower part	stellate structures	smooth
Hatched stages	tube shape	cup-shaped	cup-shaped
	oral lobes	5	5
	apical/abapical differentiation	yes	yes
	apical part	stellate structures	smooth
	triangular thickenings	5 longitudinal rows (continuously and independently on each annulus)	5 longitudinal rows (every four to seven annuli and straddled the next four to five annuli)
	Annuli	enormously extended outwards to be ridges	slightly raised
radial symmetry		5	5
growth pattern		direct development	direct development

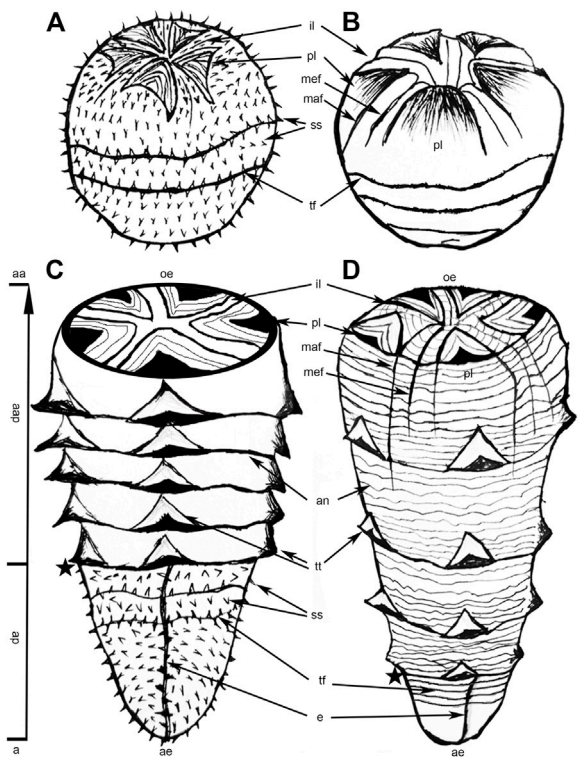

FIGURE 5
A comparative sketch of *Olivooides multisulcatus* and *Qinscyphus necopinus*. **(A)** Embryo of *Olivooides multisulcatus*; **(B)** embryo of *Qinscyphus necopinus*; **(C)** hatchling of *Olivooides multisulcatus*; **(D)** hatchling of *Qinscyphus necopinus*; Asterisks denote the boundary between the apical and abapical parts. **(B)** and **(D)** modified from Shao et al., 2018a. a = apical; aa = abapical; ap = apical part; aap = abapical part; ae = apical end; an = annuli; e = edge; il = interradial lobe; maf = marginal furrow; mef = median furrow; oe = oral end; pl = perradial lobe; ss = stellate structure; tf = transverse fold; tt = triangular thickening.

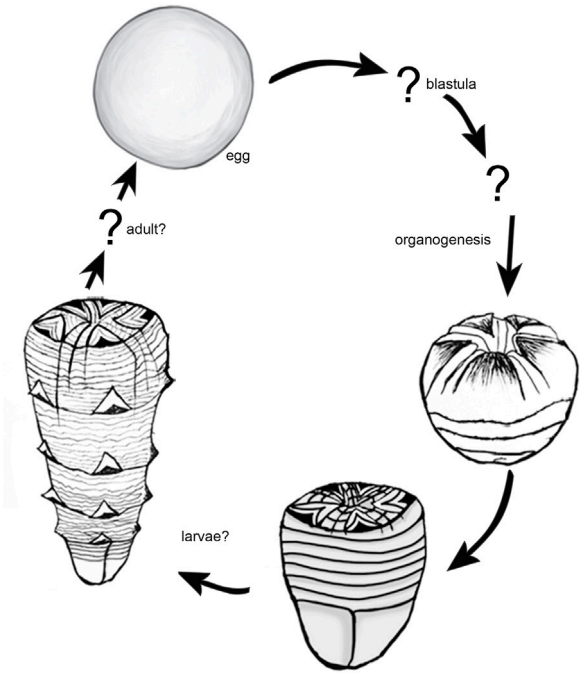

FIGURE 6
Reconstruction of the developmental cycle of *Qinscyphus necopinus*.

We consider that the embryonic tissue (apical part) of *Qinscyphus necopinus* was soft during early ontogeny (fossils with fewer circlets of triangular thickenings) (Figure 2A). As such, the transverse folds on the embryonic tissue might be taphonomic artifacts due to the soft nature of the apical part. And it is probable that this part was smooth during life. Even in adult individuals, the embryonic tissues could still show transverse folds in taxa such as *Qinscyphus*, *Olivooides*, and

Quadrapygites (Steiner et al., 2014; Dong et al., 2016). These soft transverse folds were absent in previous reconstructions of *Olivooides* and *Quadrapygites* (Steiner et al., 2014), with transverse folds only occurring on the upper part of the embryonic tissue. Therefore, we modified the reconstruction of *Q. necopinus* based on the newly described material, by adding transverse folds on the entire embryonic tissue (Figures 5A,D).

Previously reported *Qinscyphus* were mostly fragmented. The new specimens preserved intact tubes with apical and abapical parts. They also show one (Figure 2A), two (Figure 2E), three (Figure 2H and Figure 3A), and six (Figure 3F) circlets with triangular thickenings respectively. Combined with previous studies, the developmental sequence of *Qinscyphus* is reconstructed (Figure 6). The oral part of the embryo had a morphology that is comparable to that of the hatched stages (Shao et al., 2018a), demonstrating that *Qinscyphus* underwent direct development. After hatching, the tube with transverse annuli and pentaradially arranged triangular thickenings began to develop. New annuli and triangular thickenings might have regenerated from within the abapical end. The circlet of triangular thickenings at the abapical end would have evaginated to form a new circlet of triangular thickenings. *Qinscyphus* would have elongated its length through the addition of annuli and triangular thickenings at the abapical end (Liu et al., 2017; Shao et al., 2018a).

5 Conclusion

The newly discovered fossils with the whole apical part complete the morphology of *Qinscyphus*. The apical portion of *Q. necopinus* is assumed soft during early ontogenetic stages. And, it does not always manifest as an inverted pentagonal pyramid. More importantly, the new specimens have different annuli with triangular thickenings, completing the developmental sequence and expanding the morphological disparity of *Q. necopinus*.

Data availability statement

The original contributions presented in the study are included in the article/Supplementary Material, further inquiries can be directed to the corresponding author.

Author contributions

YZ coordinated the field work, preparation and curation of fossils, wrote the manuscript, and processed the images. YL edited the manuscript. TS and JQ assisted in collecting the rock samples in the field. All authors contributed to the article and approved the submitted version.

Funding

The National Natural Science Foundation of China (grant numbers 41872014, 41572007 and 41572009), the Strategic Priority Research Program of Chinese Academy of Sciences (grant number XDB26000000), the State Key Laboratory of Paleobiology and Stratigraphy, Nanjing Institute of Geology and Paleontology, Chinese Academy of Sciences (grant number 193123), the Basic Research Plan of Natural Science of Shaanxi Province (grant number 2018JM4002).

Acknowledgments

We thank Xiaoke Sun and Mingjin Liu, as they helped revise some of the manuscript's images and language issues.

Conflict of interest

The authors declare that the research was conducted in the absence of any commercial or financial relationships that could be construed as a potential conflict of interest.

Publisher's note

References

Bengtson, S., and Yue, Z. (1997). Fossilized metazoan embryos from the earliest Cambrian. *Science* 277, 1645–1648. doi:10.1126/science.277.5332.1645

Chen, J. (2004). *The dawn of animal world*. Nanjing: Jiangsu Science and Technology Press, 366.

Conway Morris, S., and Chen, M. G. (1989). Lower cambrian anabaritids from SouthSouth China. *Geol. Mag.* 126, 615–632. doi:10.1017/s0016756800006920

Conway Morris, S., and Chen, M. E. (1992). Carinachitids, hexaconulariids, and *punctatus*, problematic metazoans from the early cambrian of SouthSouth China. *J. Paleontol.* 66, 384–406. doi:10.1017/s0022336000033953

Dong, X., Cunningham, J. A., Bengtson, S., Thomas, C. W., Liu, J., Stampanoni, M., et al. (2013). Embryos, polyps and medusae of the early Cambrian scyphozoan *Olivooides*. *P. Roy. Soc. B–Biol. Sci.* 280, 20130071. doi:10.1098/rspb.2013.0071

Dong, X., Vargas, K., Cunningham, J. A., Zhang, H., Liu, T., Chen, F., et al. (2016). Developmental biology of the early Cambrian cnidarian*Olivooides*. *Olivooides, Palaeontol.* 59, 387–407. doi:10.1111/pala.12231

Donoghue, P. C. J., Bengtson, S., Dong, X., Gostling, N. J., Huldtgren, H., Cunningham, J. A., et al. (2006). Synchrotron x-ray tomographic microscopy of fossil embryos. *Nature* 442, 680–683. doi:10.1038/nature04890

Duan, B., Dong, X., Porras, L., Vargas, K., Cunnigham, J. A., and Donoghue, P. C. J. (2017). The early Cambrian fossil embryo Pseudooides is a direct - developing cnidarian, not an early ecdysozoan. *Proc. R. Soc. B* 284, 20172188. doi:10.1098/rspb.2017.2188

Guo, J., Han, J., Van Iten, H., Song, Z., Sun, J., Wang, W., et al. (2020). A new tetraradial olivooid (medusozoa) from the lower cambrian (stage 2) yanjiahe formation, south China. *J. Paleontol.* 94, 457–466. doi:10.1017/jpa.2019.101

Han, J., Kubota, S., Li, G., Yao, X., Yang, X., Shu, D., et al. (2013). Early Cambrian pentamerous cubozoan embryos from South China. *PloS One* 8, e70741. doi:10.1371/journal.pone.0070741

Han, J., Kubota, S., Li, G., Ou, Q., Wang, X., Yao, X., et al. (2016a). Divergent evolution of medusozoan symmetric patterns: Evidence from the microanatomy of

Cambrian tetramerous cubozoans from South China. *Gondwana Res.* 31, 150–163. doi:10.1016/j.gr.2015.01.003

Han, J., Li, G. X., Kubota, S., Ou, Q., Toshino, S., Eang, X., et al. (2016b). Internal microanatomy and zoological affinity of the early Cambrian*Olivooides*. *Olivooides, Acta Geol. Sin–Engl.* 90, 38–65. doi:10.1111/1755-6724.12641

Han, J., Morris, S. C., Ou, Q., Shu, D., and Huang, H. (2017). Meiofaunal deuterostomes from the basal cambrian of Shaanxi (China). *Nature* 542, 228–231. doi:10.1038/nature21072

Han, J., Li, G., Wang, X., Yang, X., Guo, J., Sasaki, O., et al. (2018). *Olivooides*–like tube aperture in early Cambrian carinachitids (Medusozoa, Cnidaria). *J. Paleontol.* 92, 3–13. doi:10.1017/jpa.2017.10

Han, J., Guo, J., Ou, Q., Song, Z., Liu, P., Hao, W., et al. (2020). Evolutionary framework of early Cambrian cnidarians from South China. *Earth Sci. Front.* 27, 067–078. doi:10.13745/j.esf.sf.2020.6.3

Kouchinsky, A., Bengtson, S., Feng, W., Kutygin, R., and Val'kov, A. (2009). The lower cambrian fossil anabaritids: Affinities, occurrences and systematics. *J. Syst. Palaeontol.* 7, 241–298. doi:10.1017/S1477201909002715

Li, P., Hua, H., Zhang, L., Zhang, D., Jin, X., and Liu, Z. (2007). Lower Cambrian phosphatized Punctatus from southern Shaanxi and their ontogeny sequence. *Chin. Sci. Bull.* 52, 2820–2828. doi:10.1007/s11434-007-0447-y

Li, Z. (1984). The discovery and its significance of small shelly fossils in Hexi area, Xixiang. *Geol. Shaanxi* 2, 73–77.

Liu, Y., Li, Y., Shao, T., Wang, Y., Yu, B., Han, H., et al. (2005). Two new species of protoconulariids from the early Cambrian in South Shaanxi, China. *Acta micropalaeontol. Sin.* 22, 311–321. doi:10.1360/gs050302

Liu, Y., Li, Y., Gong, H., Zhang, Z., and Yan, T. (2009). New date on *Quadrapyrgites* from the early cambrian of South Shaanxi. *Acta Palaeontol. Sin.* 48, 688–694. doi:10.1360/972009-495

Liu, Y., Li, Y., Shao, T., Zheng, X., and Wang, K. (2011). A new genus and specie of protoconulariids from the early Cambrian in the south Shaanxi, China. *Acta micropalaeontol. Sin.* 28, 245–249. doi:10.1631/jzus.B1000197

Liu, Y., Li, Y., Shao, T., Zhang, H., Wang, Q., and Qiao, J. (2014a). *Quadrapyrgites* from the lower Cambrian of South China: Growth pattern, post–embryonic development, and affinity. *Chin. Sci. Bull.* 59, 4086–4095. doi:10.1007/s11434-014-0481-5

Liu, Y., Xiao, S., Shao, T., Broce, J., and Zhang, H. (2014b). The oldest known priapulid–like scalidophoran animal and its implications for the early evolution of cycloneuralians and ecdysozoans. *Evol. Dev.* 16, 155–165. doi:10.1111/ede.12076

Liu, Y., Shao, T., Zhang, H., Wang, Q., Zhang, Y., Chen, C., et al. (2017). A new scyphozoan from the cambrian fortunian stage of SouthSouth China. *Palaeontology* 60, 511–518. doi:10.1111/pala.12306

Liu, Y., Carlisle, E., Zhang, H., Yang, B., Steiner, M., Shao, T., et al. (2022). *Saccorhytus* is an early ecdysozoan and not the earliest deuterostome. *Nature* 609, 541–546. doi:10.1038/s41586-022-05107-z

Park, E., Hwang, D., Lee, J., Song, J., Seo, T., and Won, Y. (2012). Estimation of divergence times in cnidarian evolution based on mitochondrial protein-coding genes and the fossil record. *Mol. Phylogenetics Evol.* 62, 329–345. doi:10.1016/j.ympev.2011.10.008

Peng, S. C., Babcock, L. E., and Ahlberg, P. (2020). "The Cambrian Period," in *Geological Time Scale 2020*. Editors F. M. Gradstein, J. G. Ogg, M. Schmitz, and G. M. Ogg (Oxford: Elsevier), 565–629.

Qian, Y., and Bengtson, S. (1989). Palaeontology and biostratigraphy of the early cambrian meishucunian stage in yunnan Province, south China. *Fossils Strata* 24, 293–294. doi:10.1016/0012-8252(91)90034-D

Qian, Y. (1977). Hyolitha and some problematica from the lower Cambrian Meishucun Stage in central and SW China. *Acta Palaeontol. Sin.* 16, 255–275. doi:10.19800/j.cnki.aps.1977.02.007

Qin, J., Liu, Y., Wang, Q., Zhang, H., Zhang, Y., Liu, M., et al. (2020). A new fortunian scyphozoa and its development. *Acta Geol. sin–engl.* 94, 1303–1304. doi:10.1111/1755-6724.13838

Shao, T., Liu, Y., Wang, Q., Zheng, Y., Tang, H., Cao, X., et al. (2015). Early Cambrian gastrozooid of polyp and problematic tubular microfossils from the southern Shaanxi, China. *Acta micropalaeontol. Sin.* 32, 194–199. doi:10.16087/j.cnki.1000-0674.2015.02.008

Shao, T., Liu, Y., Wang, Q., Zhang, H., Tang, H., and Li, Y. (2016). New material of the oldest known scalidophoran animal Eopriapulites sphinx. *Palaeoworld* 25, 1–11. doi:10.1016/j.palwor.2015.07.003

Shao, T., Liu, Y., Duan, B., Zhang, H., Zhang, H., Wang, Q., et al. (2018a). The Fortunian (lowermost Cambrian) *Qinscyphus necopinus* (Cnidaria, Scyphozoa, Coronatae) underwent direct development. *Neues Jahrb. Geol. P.–A.* 289, 149–159. doi:10.1127/njgpa/2018/0755

Shao, T., Tang, H., Liu, Y., Waloszek, D., Maas, A., and Zhang, H. (2018b). Diversity of cnidarians and cycloneuralians in the fortunian (early cambrian) Kuanchuanpu Formation at Zhangjiagou, south China. *Paleontology* 92, 115–129. doi:10.1017/jpa.2017.94

Shao, T., Hu, B., Shao, Y., Zhang, Y., Zhang, H., Qin, J., et al. (2019a). Intraspecific variation of radial symmetry number of a 535 million–year–old jellyfish. *Precambrian Res.* 349, 105412. doi:10.1016/j.precamres.2019.105412

Shao, T., Qin, J., Shao, Y., Liu, Y., and Zhang, H. (2019b). New macrobenthic cycloneuralians from the fortunian (lowermost cambrian) of SouthSouth China. *Precambrian Res.* 2019, 105413. doi:10.1016/j.precamres.2019.105413

Steiner, M., Li, G. X., Qian, Y., and Zhu, M. (2004a). Lower Cambrian small shelly fossils of northern Sichuan and southern Shaanxi (China), and their biostratigraphic importance. *Geobios* 37, 259–275. doi:10.1016/j.geobios2003.08.001

Steiner, M., Zhu, M., Li, G., Qian, Y., and Erdtmann, B. D. (2004b). New Early Cambrian bilaterian embryos and larvae from China. *Geology* 32, 833–836. doi:10.1130/g20567.1

Steiner, M., Li, G. X., Qian, Y., Zhu, M., and Erdtmann, B. D. (2007). Neoproterozoic to early Cambrian small shelly fossil assemblages and a revised biostratigraphic correlation of the Yangtze Platform (China). *Palaeogeogr. Palaeoclimatol. Palaeoecol.* 254, 67–99. doi:10.1016/j.palaeo.2007.03.046

Steiner, M., Li, G., Hu, S., and Keupp, H. (2010). Soft–tissue preservation in small shelly faunas. *Geol. Soc. Am. Annu. Meet.* 42, 539.

Steiner, M., Qian, Y., Li, G., Hagadorn, J. W., and Zhu, M. (2014). The developmental cycles of early cambrian Olivooidae fam. Novol. (? Cycloneuralia) from the yangtze platform (China). *Palaeogeogr. Palaeoclimatol. Palaeoecol.* 398, 97–124. doi:10.1016/j.palaeo.2013.08.016

Van Iten, H., de Moraes Leme, J., Simões, M. G., Marques, A. C., and Collins, A. G. (2006). Reassessment of the phylogenetic position of conulariids (? Ediacaran–Triassic) within the subphylum medusozoa (phylum Cnidaria). *J. Syst. Palaeontol.* 4, 109–118. doi:10.1017/S1477201905001793

Van Iten, H., Zhu, M., and Li, G. (2010). Redescription of Hexaconularia He and Yang, 1986 (lower Cambrian, South China): Implications for the affinities of conulariid–like small shelly fossils. *Palaeontology* 53, 191–199. doi:10.1111/j.1475-4983.2009.00925.x

Van Iten, H., Marques, A. C., Leme, J. d. M., Forancelli Pacheco, M. L. A., and Simões, M. G. (2014). Origin and early diversification of the phylum Cnidaria Verrill: Major developments in the analysis of the taxon's Proterozoic–Cambrian history. *Palaeontology* 57, 677–690. doi:10.1111/pala.12116

Wang, X., Han, J., Vannier, J., Ou, Q., Yang, X., Uesugi, K., et al. (2017). Anatomy and affinities of a new 535–million–year–old medusozoan from the Kuanchuanpu Formation, South China. *Palaeontology* 60, 853–867. doi:10.1111/pala.12320

Wang, D., Vannier, J., Schumann, I., Wang, X., Han, S. J., Komiya, T., et al. (2019). Origin of ecdysis: Fossil evidence from 535–million–year–old scalidophoran worms. *Proc. R. Soc. B* 286, 20190791. doi:10.1098/rspb.2019.0791

Wang, D., Vannier, J., Yang, X., Sun, J., Han, J., Hao, W. j., et al. (2020). Cuticular reticulation replicates the pattern of epidermal cells in lowermost Cambrian scalidophoran worms. *Proc. R. Soc. B* 287, 20200470. doi:10.1098/rspb.2020.0470

Wang X, X., Kubota, S., Ou, Q., Vannier, J., Han, J., Yao, X., et al. (2020). An intermediate type of medusa from the early Cambrian Kuanchuanpu Formation, South China. *Palaeontology* 4, 775–789. doi:10.1111/pala.12483

Yasui, K., Reimer, J., D., Liu, Y. H., Yang, X. G., Daisuke, K., Degan, S., et al. (2013). A diploblastic radiate animal at the dawn of cambrian diversification with a simple body plan: Distinct from Cnidaria? *PLoS ONE* 8, e65890. doi:10.1371/journal.pone.0065890

Yue, Z., and Bengtson, S. (1999). Embryonic and post–embryonic development of the early Cambrian cnidarian *Olivooides*. *Lethaia* 32, 181–195. doi:10.1111/j.1502-3931.1999.tb00538.x

frontiers | Frontiers in Ecology and Evolution

TYPE Original Research
PUBLISHED 31 March 2023
DOI 10.3389/fevo.2023.1160530

OPEN ACCESS

EDITED BY
Bertrand Lefebvre,
Université Claude Bernard Lyon 1, France

REVIEWED BY
Andrej Ernst,
University of Hamburg, Germany
Olev Vinn,
University of Tartu, Estonia

*CORRESPONDENCE
Yujing Li
✉ yujingli@ynnu.edu.cn

SPECIALTY SECTION
This article was submitted to Paleontology, a section of the journal Frontiers in Ecology and Evolution

RECEIVED 07 February 2023
ACCEPTED 14 March 2023
PUBLISHED 31 March 2023

CITATION
Zhao J, Li Y and Selden PA (2023) Two new metazoans from the Cambrian Guanshan biota of China.
Front. Ecol. Evol. 11:1160530.
doi: 10.3389/fevo.2023.1160530

Two new metazoans from the Cambrian Guanshan biota of China

Jun Zhao[1], Yujing Li[2]* and Paul A. Selden[3,4]

[1]Research Center of Paleobiology, Yuxi Normal University, Yuxi, Yunnan, China, [2]Yunnan Key Laboratory of Plateau Geographical Processes and Environmental Changes, Faculty of Geography, Yunnan Normal University, Kunming, Yunnan, China, [3]Department of Geology, University of Kansas, Lawrence, KS, United States, [4]Natural History Museum, London, United Kingdom

Sessile epibenthos were diverse and played important part in the process of energy flow in the Cambrian marine ecosystem. Based on new specimens from the Gaoloufang Section of the Wulongqing Formation, we describe two new representatives of the group that show character traits with cnidarians and bryozoans. If confirmed, the new material can help us understand the origin and early evolution of these two phyla. The discovery of more sessile epibenthos suggests that the benthic ecosystem of the Guanshan biota (Cambrian Series 2, Stage 4) is more diverse than previously thought.

KEYWORDS

Cnidaria, Bryozoa, Burgess Shale-type *Lagerstätten*, South China, Cambrian Series 2, Cambrian explosion

Introduction

As one of the most significant Burgess Shale-type *Lagerstätten*, the Guanshan biota (Cambrian Series 2, Stage 4) has yielded nearly 100 species classified into more than 10 metazoan groups from over 10 fossil sites (Hu et al., 2013, 2023; Chen et al., 2019; Zhao et al., 2020). Chronologically, the Guanshan biota lies among some famous Cambrian biotas (e.g., the Chengjiang and Xiaoshiba from Stage 3 and, Kaili and the Burgess Shale from Wuliuan), thus forming an important link in the history of the early evolution of marine animals (Hu et al., 2013; Liu et al., 2016; Chen et al., 2019). In addition to the detailed systematic assessments of metazoan groups, recent studies have also been focused on the ecological complexities and sedimentology of the Guanshan biota (Ding et al., 2020; Chen et al., 2022), which further reveal a comprehensive appearance of the exceptionally preserved fossil deposit.

Characterized by a body of radial symmetry, cnidarians (anthozoans + medusozoans) are among the most basal metazoans (Hou et al., 2017; Han et al., 2020; Ou et al., 2022); polypoid cnidarian adults live anchored to the sea floor and by collecting food with circumoral tentacles (Hou et al., 2017). Han et al. (2020) discussed the evolution of early Cambrian cnidarians from the Yangtze Block, and concluded that during the "Cambrian explosion" the abundance and diversity of cnidarians peaked at the very beginning and then declined in Stages 2 and 3 of the Cambrian, with this change possibly contributing to the rise of bilateral animals. A few taxa from the Chengjiang biota (Cambrian Series 2, Stage 3) have been previously interpreted as potential cnidarians, including *Xianguangia sinica* Chen and Erdtmann, 1991. Recently, *Xianguangia*, alongside with *Dinomischus venustus* Chen et al., 1989, and *Daihua sanqiong* Zhao et al., 2019 (two epibenthic metazoans also from the

Chengjiang biota), was included in the stem lineage of ctenophores (Zhao et al., 2019). However, the most recent phylogenetic analysis has proposed that *Xianguangia*, *Dinomischus*, *Daihua,* and *Nailiana elegans* Ou et al., 2022 (a polypoid form from the Chengjiang biota) were among the basal stem within Cnidaria (Ou et al., 2022). Only a tubular metazoan from the Guanshan biota was reported as a possible cnidarian (Hu et al., 2013), but its anatomy has not been documented in detail yet.

Bryozoa (also known as Ectoprocta) are a group of dominantly sessile, filter-feeding lophophorates that are abundant, diverse and widely distributed in marine, and freshwater environments (Taylor and Waeschenbach, 2015; Schwaha et al., 2020). They are colonial and characterized by iterated units (zooids) showing hierarchical levels of modularity (Lidgard et al., 2012; Zhang et al., 2021). Morphological data and molecular clock estimation strongly indicated a Cambrian origin for bryozoans (Taylor et al., 2015; Taylor and Waeschenbach, 2015; Hageman and Ernst, 2019; Ernst, 2020), and character traits expected in ancestral Cambrian representatives were also proposed (Taylor and Waeschenbach, 2015). No unequivocal fossil records of Cambrian bryozoans were accepted widely until Zhang et al. (2021) first recognized a bryozoan (*Protomelission gatehousei* Brock and Cooper, 1993) from Cambrian Stage 3 sections of Australia and South China, thus dating back the appearance of this phylum by approximately 35 million years. Recently, a potential bryozoan was described from the Cambrian Stage 4 Harkless Formation, USA, which could greatly push back the occurrence of mineralized skeletons in Bryozoa (Pruss et al., 2022).

Here, we describe two new epibenthos from the Guanshan biota (Cambrian Series 2, Stage 4). The first is soft-bodied and cnidarian-like; the second is preserved attached to trilobite fragments and lives in a skeletonized colony-like structure, with individuals (each with a suboval apical opening) being densely packed: some basic character traits of Bryozoa. If confirmed as representatives of Cnidaria and Bryozoa, the two new forms would provide new information about the early evolutionary history of these two phyla. Our findings will markedly increase the known taxonomic diversity and morphological disparity of the Guanshan biota. In addition, the new material also demonstrates that the epibenthic ecosystem of the Guanshan biota is rather sophisticated.

Materials and methods

One specimen of the cnidarian-like metazoan (RCP-ZJ-0002), with part and counterpart; two slabs of the bryozoan-like organism, with six colony-like assemblages (RCP-ZJ-0003-0008). All the fossils were collected from the Gaoloufang section (24.95916°N and 102.80539°E) in Kunming, Yunnan Province, southwest China. Digital photographs were taken using a Canon EOS 5D SR camera with a Canon MP-E 65 (1–5X) macro lens under cross-polarized light, with the brightness and contrast of the resulting images processed in Adobe Photoshop CS 5. The specimens are housed at the Research Center of Paleobiology, Yuxi Normal University (RCP).

The cnidarian-like metazoan (RCP-ZJ-0002)

Description

The body is 27 mm in length and has two distinct regions (upper portion and lower portion), which are delineated by a weak constriction in between (**Figure 1**).

The upper portion measures 12 mm long on the part of the specimen (**Figure 1A**) and is a cluster of tentacle-like structures that are thin, semi-transparent (**Figures 2A, B**), and preserved to be straight from base to top. "The supposed tentacles" are lamellar and overlapping (**Figure 2B**); although the exact number is hard to count due to the poor preservation, it is no fewer than eight.

The lower portion (trunk) is column-like, measuring 15 mm in length, and 9 mm in maximum width (at the midheight). Bumps and depressions are evident on the surface (**Figure 2C**), and prominent sub-parallel longitudinal ridges are located at the lower right of the trunk (**Figure 2C**). The bottom is flat and measures 6 mm in width. Remains of some comparatively rigid structures are visible at the lower left side and the bottom (**Figure 2C**), suggesting the trunk might be enclosed by a sheath-like structure in life. Dark remains (**Figure 1**) are concentrated on the lower part of the trunk, indicating the presence of an internal cavity.

No openings can be seen on this laterally compressed specimen.

Remarks

The overall profile and the presence of bumps and depressions demonstrate the new taxon is a sessile and soft-bodied epibenthos, with the bottom of the trunk attached to the seafloor in life. The lamellar structures of the upper portion are non-prehensile, reminiscent of the tentacle rods in *Xianguangia*. The relatively regular longitudinal ridges (**Figure 2C**) imply some internal supporting structures of the trunk, i.e., the presence of the mesenterial divisions. There are some similarities to the *Xianguangia* from the Chengjiang biota, which bears proximal tentacle rods, a preserving outline of gut in the trunk and the mesenteries inside. The bipartite body and the possession of possible tentacles portray a polypoid outline for the new taxon, suggesting some relationships with cnidarians.

Until now, the Chengjiang biota has produced the most diverse purported cnidarians from Cambrian Series 2, e.g., *Dinomischus*, *Xianguangia*, *Daihua,* and *Nailiana*. The new taxon resembles *Xianguangia* in having tentacular structures and a main body (figure 1 in Zhao et al., 2019), but tentacles of the latter are feather-like (figure 1 in Ou et al., 2017), a character not found in the former. It is similar to *Xianguangia* and *Daihua* in the overall profile of a bipartite body (figure 2 in Zhao et al., 2019), however, the presence/absence of circumoral domes and the lowermost part of the body being flat (figure 1) or tapering to a blunt tip (figure 2I in Zhao et al., 2019) clearly discriminate the two. The new taxon approximates *Nailiana* in the general shape of the body (composed of unbranched tentacles and a trunk), but the tentacles of *Nailiana* are prehensile (Ou et al., 2022), whereas those of the new taxon more likely function as sclerotized proximal tentacle rods. The absence of a stalk sets the new taxon apart from *Dinomischus*.

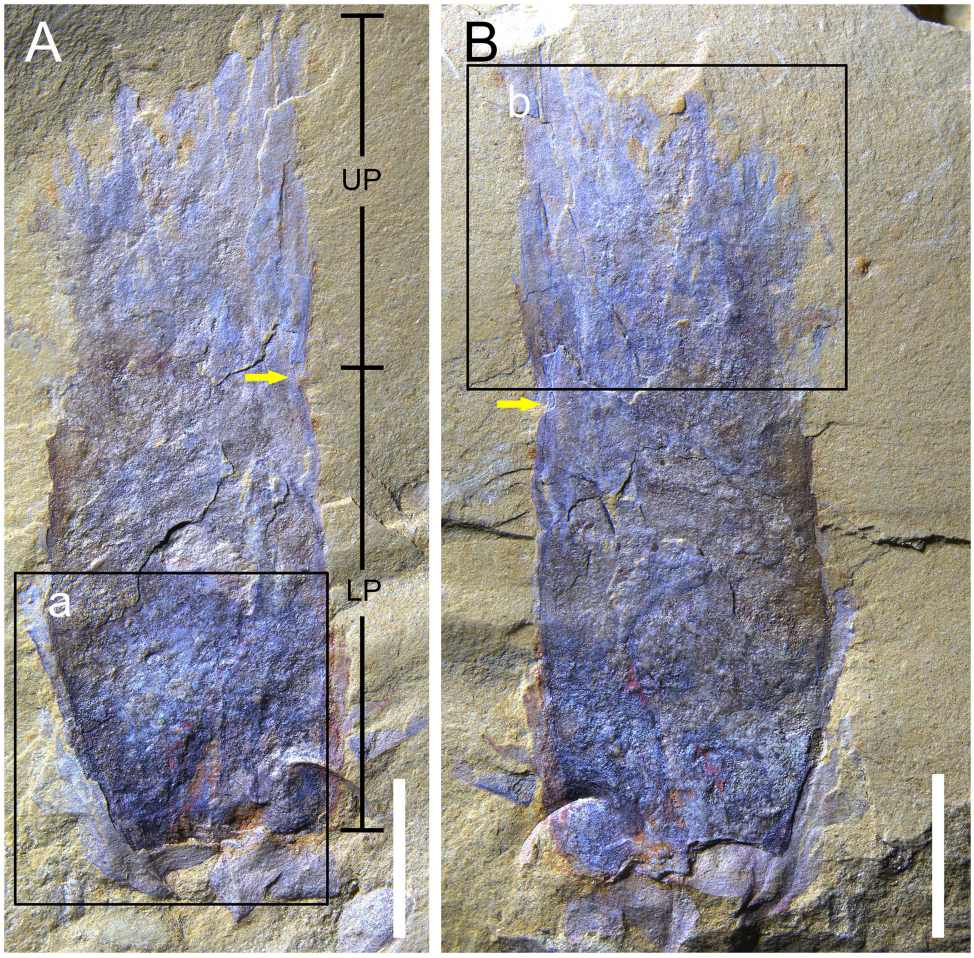

FIGURE 1
The unnamed cnidarian-like metazoan (RCP-ZJ-0002). **(A)** Part; yellow arrow indicates the weak constriction between the upper portion and the lower portion of the body; **(B)** counterpart; yellow arrow indicates the weak constriction between the upper portion and the lower portion of the body. The scale bars are 5 mm. UP, upper portion; LP, lower portion.

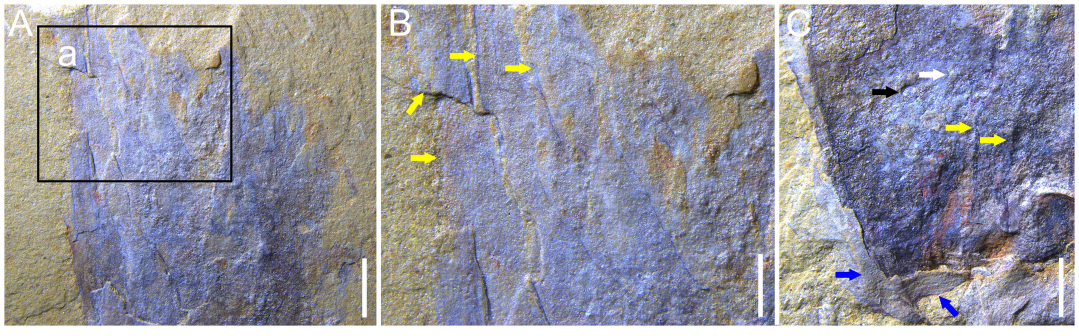

FIGURE 2
The unnamed cnidarian-like metazoan (RCP-ZJ-0002). **(A)** Detail of the tentacle-like structures on the counterpart (position marked by frame b in Figure 1B); **(B)** detail of the tentacle-like structures [position marked by frame a in panel **(A)**]; yellow arrows indicate the thin and overlapped tentacle-like structures; **(C)** detail of the lower portion of the body on the part (position marked by frame a in Figure 1A); white and black arrows indicate a bump and a depression, respectively, yellow arrows indicate longitudinal ridges; blue arrows indicate the sheath-like structure. The scale bars are 2 mm for panels **(A,C)** and 1 mm for panel **(B)**.

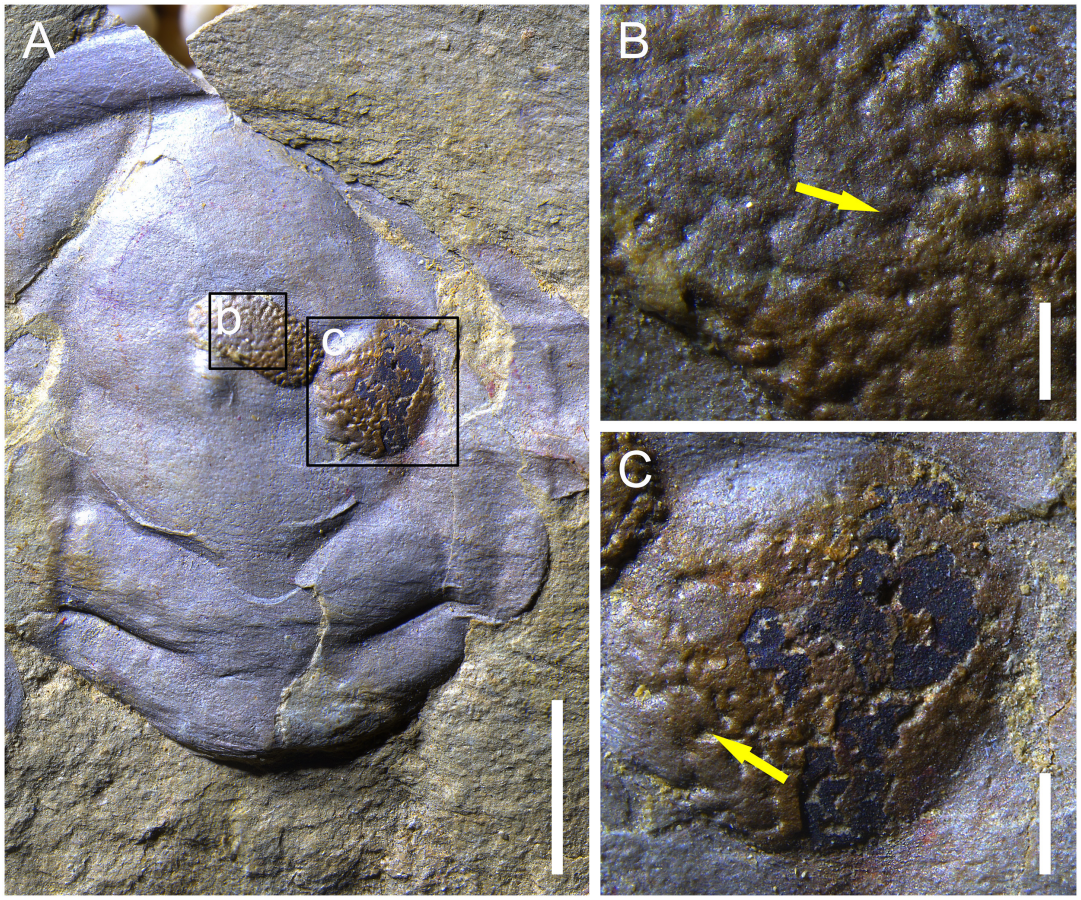

FIGURE 3
The unnamed bryozoan-like metazoan (RCP-ZJ-0003-0004). **(A)** RCP-ZJ-0003-0004 are preserved on a trilobite glabella; **(B)** detail of RCP-ZJ-0003 [position marked by frame b in panel **(A)**], yellow arrow indicates an opening of the specimen; **(C)** detail of RCP-ZJ-0004 [position marked by frame c in panel **(A)**], yellow arrow indicates an opening of the specimen. The scale bars are 5 mm for panel **(A)**, 0.5 mm for panel **(B)**, and 1 mm for panel **(C)**.

Based on the morphological similarities and discrepancies documented above with the purported cnidarians from the Chengjiang biota, we tentatively leave the new metazoan from the Guanshan biota in open nomenclature and describe it as a cnidarian-like metazoan. So far, no exact cnidarians have been documented from the Guanshan biota. If the new material can be confirmed as a representative of Cnidaria, it will provide us with very important evidence for the evolution of cnidarians from the Chengjiang to Guanshan biotas.

The bryozoan-like metazoan (RCP-ZJ-0003-0008)

Description

RCP-ZJ-0003-0004 are preserved on a molted trilobite glabella (Figure 3) and RCP-ZJ-0005-0008 on a librigena (Figure 4). The specimens are dark-brown and in high relief (e.g., Figures 3B, C), with each bearing numerous, densely packed openings (e.g., Figure 3B).

RCP-ZJ-0003 is oval in overall profile and, measures 4.5 × 3 mm (Figures 3A, B). The diameters of the openings range from 180 to 250 μm, with most being ca. 200 μm. RCP-ZJ-0004 is circular in outline and 4 mm in diameter (Figures 3A–C). The diameters of the openings measure 117 to 235 μm. RCP-ZJ-0005-0008 are counterparts (Figure 4); parts were collapsed into pieces during excavation and impossible to repair for photography. RCP-ZJ-0005 (Figure 4B) is sub-rectangular in general shape and measures 4.5 × 3.5 mm. The diameters of the openings vary from 114 to 286 μm. RCP-ZJ-0006-0008 are irregular in outline and, each comprises fewer openings (Figure 4C), with the diameters ranging from 91 to 152 μm.

Remarks

Morphological details cannot be observed clearly on these heavily mineralized specimens. In terms of the overall profile, each specimen resembles an assemblage of zooid tubes, i.e., a colony of bryozoans. Although it cannot be fully confirmed, the densely packed openings may represent the apical orifices of bryozoan zooids, which are used as the passage of the lophophore during life

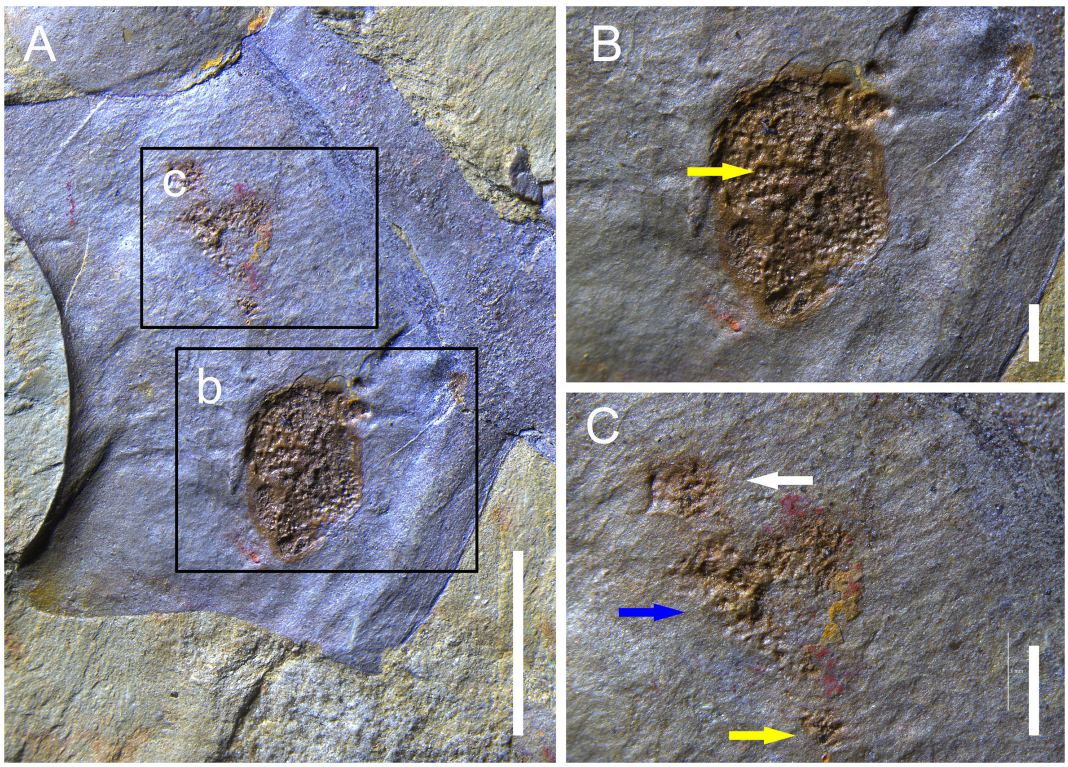

FIGURE 4
The unnamed bryozoan-like metazoan (RCP-ZJ-0005-0008). **(A)** RCP-ZJ-0005-0008 are preserved on a trilobite librigenal; **(B)** detail of RCP-ZJ-0005 [position marked by frame b in panel **(A)**], yellow arrow indicates an opening of the specimen; **(C)** detail of RCP-ZJ-0006-0008 [position marked by frame c in panel **(A)**], white arrow indicates RCP-ZJ-0006; blue arrow indicates RCP-ZJ-0007 and yellow arrow indicates RCP-ZJ-0008. The scale bars are 5 mm for panel **(A)** and 1 mm for panels **(B,C)**.

(e.g., figure 2 in Zhang et al., 2021; figure 3A in Pruss et al., 2022). Furthermore, the diameters of the openings also lie within the size range (ca. 50 μm–ca. 1 mm) of the orifices of zooids expected in ancestral Cambrian bryozoans (Taylor and Waeschenbach, 2015; Zhang et al., 2021). Attached to trilobite fragments, these fossils are definitively epibenthic metazoans, which add new epibenthos to the Guanshan biota. If confirmed as bryozoans, these specimens will further fill in the gap between the first fossil record of Cambrian Stage 3 to the diversity dynamics of Ordovician radiation of Bryozoa. The new material will represent the earliest known bryozoans from the Burgess Shale-type *Lagerstätten* and indicate that some representatives of Bryozoa were adapted for attaching to hard substrates in siliciclastic environments during Cambrian Stage 4.

Discussion

The "Cambrian explosion" (Brasier, 1979), beginning ca. 540 million years ago, was one of the most significant radiations of animal life in Earth's history, and all major animal phyla started appearing in the fossil record during this period (Maloof et al., 2010; Hu et al., 2013; Tihelka et al., 2022). Studies have shown that this important evolutionary event resulted in the formation of metazoan-dominated ecosystems in the Phanerozoic (Erwin and Tweedt, 2012; Zhang and Shu, 2014; Zhang et al., 2021). The Burgess Shale-type *Lagerstätten* from Cambrian Series 2 and Miaolingian worldwide (e.g., the Chengjiang and Guanshan biotas from China and, the Burgess Shale from Canada) witnessed the construction of diversified marine ecosystems in this time interval. In terms of ecological niches, animals from these *Lagerstätten* can be classified into five categories: pelagic, nekton, vagile epibenthos, sessile epibenthos, and infauna (e.g., Hou et al., 2017). In any ecosystem, the routes of energy flow and matter cycling are determined by trophic relationships (Zhang et al., 2021). In this respect, biotic constituents from these deposits can be listed as producers (e.g., algae), consumers (e.g., euarthropods, priapulids, and radiodonts), and decomposers (which remain to be recognized).

Sessile epibenthos are indispensable in any marine ecosystem and play important part in the process of energy flow. Representatives of this group are abundant in the Guanshan biota, including sponges, chancelloriids, echinoderms, and some enigmatic taxa, e.g., *Phlogites guangxiensis* Hu et al., 2010 and a kleptoparasitic tube-dwelling organism (Zhang et al., 2020). The two new metazoans documented above show character traits with cnidarians and bryozoans; confirmed or not, both can be included in sessile epibenthos. The discovery of more epibenthic organisms suggests that the benthic ecosystem of the Guanshan biota is much more diversified than previously thought, and hence implies a complex trophic structure and rather sophisticated epibenthic ecological interactions for the *Lagerstätte*.

Conclusion

We describe two new sessile epibenthos and, their general morphology indicates them to be possible cnidarians and bryozoans. Our new material demonstrates that the Guanshan biota has developed an epibenthic ecosystem much more complex than previously expected.

Data availability statement

The original contributions presented in this study are included in the article/supplementary material, further inquiries can be directed to the corresponding author.

Author contributions

JZ and YL designed the study and collected and prepared the fossil specimens. JZ photographed the specimens and prepared the figures. JZ and YL wrote the first draft of the manuscript with substantial input from PS. All authors described and interpreted the specimens, contributed to the article, and approved the submitted version.

Acknowledgments

We are grateful to Fei Li and Zhongwei Li for the assistance during field work.

Conflict of interest

The authors declare that the research was conducted in the absence of any commercial or financial relationships that could be construed as a potential conflict of interest.

Publisher's note

References

Brasier, M. D. (1979). "The Cambrian radiation event," in *The origin of major invertebrate groups*, ed. M. R. House (New York, NY: Academic Press), 103–159.

Brock, G. A., and Cooper, B. J. (1993). Shelly fossils from the early Cambrian (Toyonian) Wirrealpa, Aroona Creek, and Ramsay Limestones of South Australia. *J. Paleontol.* 67, 758–787. doi: 10.1017/S0022336000037045

Chen, F. Y., Topper, T. P., Skovsted, C. B., Strotz, L. C., Shen, J., and Zhang, Z. F. (2022). Cambrian ecological complexities: Perspectives from the earlies brachiopod-supported benthic communities in the early Cambrian Guanshan Lagerstätte. *Gondwana Res.* 107, 30–41. doi: 10.1016/j.gr.2022.02.008

Chen, F. Y., Zhang, Z. F., Betts, M. J., Zhang, Z. L., and Liu, F. (2019). First report on Guanshan biota (Cambrian Stage 4) at the stratotype area of Wulongqing formation in Malong County, Eastern Yunnan. *Geosci. Front.* 10, 1459–1476. doi: 10.1016/j.gsf.2018.09.010

Chen, J. Y., and Erdtmann, B. D. (1991). "Lower Cambrian lagerstätte from Chengjiang, Yunnan, China: Insights for reconstructing early metazoan life," in *The early evolution of metazoa and the significance of problematic taxa*, eds A. M. Simonetta and S. Conway Morris (Cambridge: Cambridge University Press), 57–76.

Chen, J. Y., Hou, X. G., and Lu, H. Z. (1989). Early Cambrian hock glass-like rare sea animal *Dinomischus* (Entoprocta) and its ecological features. *Acta Pal. Sin.* 28, 58–71.

Ding, Y., Liu, J. N., and Chen, F. F. (2020). Ichnology, palaeoenvironment, and ecosystem dynamics of the early Cambrian (stage 4, series 2) Guanshan biota, South China. *Geol. J.* 55, 77–94. doi: 10.1002/gj.3360

Ernst, A. (2020). "Fossil record and evolution of Bryozoa," in *Bryozoa*, eds J. G. Helmcke, D. Starck, and H. Wermuth (Berlin: De Gruyter), 11–55. doi: 10.1515/9783110586312-002

Erwin, D. H., and Tweedt, S. (2012). Ecological drivers of the Ediacaran-Cambrian diversification of metazoa. *Evol. Ecol.* 26, 417–433. doi: 10.1098/rspb.2014.0038

Hageman, S. J., and Ernst, A. (2019). The last phylum: Occupation of bryozoa morpho-ecospace (colony growth habits) during the early phase of the Great Ordovician Biodiversification Event. *Palaeogeogr. Palaeoclimatol. Palaeoecol.* 534:109270. doi: 10.1016/j.palaeo.2019.109270

Han, J., Guo, J. F., Ou, Q., Song, Z. C., Liu, P., Hao, W. J., et al. (2020). Evolutionary framework of early Cambrian cnidarians from South China. *Earth Sci. Front.* 27, 067–078. doi: 10.13745/j.esf.sf.2020.6.3

Hou, X. G., Siveter, D. J., Siveter, D. J., Aldridge, R. J., Cong, P. Y., Gabbott, S. E., et al. (2017). *The Cambrian fossils of Chengjiang, China: The flowering of early animal life*. Hoboken, NJ: John Wiley & Sons, 307. doi: 10.1002/9781118896372

Hu, S. X., Li, X. K., Tan, X. H., Zhao, D. Q., and Luo, H. L. (2010). Phlogites from the early Cambrian Guanshan fauna. *Acta Pal. Sin.* 49, 360–364.

Hu, S. X., Zhao, F. C., Liu, A. G., and Zhu, M. Y. (2023). A new Cambrian frondose organism: "Ediacaran survivor" or convergent evolution? *J. Geol. Soc.* 180. doi: 10.1144/jgs2022-088

Hu, S. X., Zhu, M. Y., Luo, H. L., Steiner, M., Zhao, F. C., Li, G. X., et al. (2013). *The Guanshan biota*. Kunming: Yunnan Science and Technology Press, 204.

Lidgard, S., Carter, M. C., Dick, M. H., Gordon, D. P., and Ostrovsky, A. N. (2012). Division of labor and recurrent evolution of polymorphisms in a group of colonial animals. *Evol. Ecol.* 26, 233–257. doi: 10.1007/s10682-011-9513-7

Liu, J. N., Han, J., Li, J. S., Wu, Y. C., Peng, J., Qi, N., et al. (2016). New localities and Palaeoscolecid worms from the Cambrian (Stage 4, Series 2) Guanshan biota in Kunming, Yunnan, South China. *Acta Geol. Sin.* 90, 1939–1945. doi: 10.1111/1755-6724.13013

Maloof, A. C., Porter, S. M., Moore, J. L., Dudas, F. Q., Bowring, S. A., Higgins, J. A., et al. (2010). The earliest Cambrian record of animals and ocean geochemical change. *Geol. Soc. Am. Bull.* 122, 1731–1774. doi: 10.1130/B30346.1

Ou, Q., Han, J., Zhang, Z. F., Shu, D. G., Su, G., and Mayer, G. (2017). Three Cambrian fossils assembled into an extinct body plan of cnidarian affinity. *Proc. Natl. Acad. Sci. U.S.A.* 114, 8835–8840. doi: 10.1073/pnas.1701650114

Ou, Q., Shu, D. G., Zhang, Z. F., Han, J., Iten, H. V., Cheng, M. R., et al. (2022). Dawn of complex animal food webs: A new predatory anthozoan (*Cnidaria*) from Cambrian. *Innovation* 3:100195. doi: 10.1016/j.xinn.2021.100195

Pruss, S. B., Leeser, L., Smith, E. F., Zhuravlev, A. Y., and Taylor, P. D. (2022). The oldest mineralized bryozoan? A possible palaeostomate in the lower Cambrian of Nevada, USA. *Sci. Adv.* 8:eabm8465. doi: 10.1126/sciadv.abm8465

Schwaha, T. F., Ostrovsky, A. N., and Wanninger, A. (2020). Key novelties in the evolution of the aquatic colonial phylum bryozoa: Evidence from soft body morphology. *Biol. Rev.* 95, 696–729. doi: 10.1111/brv.12583

Taylor, P. D., and Waeschenbach, A. (2015). Phylogeny and diversification of bryozoans. *Palaeontology* 58, 585–599. doi: 10.1111/pala.12170

Taylor, P. D., Lombardi, C., and Cocito, S. (2015). Biomineralization in bryozoans: Present, past and future: Bryozoan biomineralization. *Biol. Rev.* 90, 1118–1150. doi: 10.1111/brv.12148

Tihelka, E., Howard, R. J., Cai, C. Y., and Lozano-Fernandez, J. (2022). Was there a Cambrian explosion on land? The case of arthropod terrestrialization. *Biology* 11:1516. doi: 10.3390/biology11101516

Zhang, X. L., and Shu, D. G. (2014). Causes and consequences of the Cambrian explosion. *Sci. China Earth Sci.* 57, 930–942. doi: 10.1007/s11430-013-4751-x

Zhang, Z. F., Strotz, L. C., Topper, T. P., Chen, F. Y., Chen, Y. L., Liang, Y., et al. (2020). An encrusting kleptoparasite-host interaction from the early Cambrian. *Nat. Commun.* 11, 1–7. doi: 10.1038/s41467-020-16332-3

Zhang, Z. L., Zhang, Z. F., Ma, J. Y., Taylor, P. D., Strotz, L. C., Jacquet, S. M., et al. (2021). Fossil evidence unveils an early Cambrian origin for bryozoa. *Nature* 599, 251–255. doi: 10.1038/s41586-021-04033-w

Zhao, J., Li, Y. J., Selden, P. A., and Cong, P. Y. (2020). New occurrence of the Guanshan Lagerstätte (Cambrian Series 2, Stage 4) in the Kunming area, Yunnan, southwest China, with records of new taxa. *Alcheringa* 44, 343–355. doi: 10.1080/03115518.2020.1781257

Zhao, Y., Vinther, J., Parry, L. A., Wei, F., Green, E., Pisani, D., et al. (2019). Cambrian sessile, suspension feeding stem-group ctenophores and evolution of the comb jelly body plan. *Curr. Biol.* 29, 1112–1125. doi: 10.1016/j.cub.2019.02.036

frontiers | Frontiers in Ecology and Evolution

TYPE Original Research
PUBLISHED 26 April 2023
DOI 10.3389/fevo.2023.1128070

OPEN ACCESS

EDITED BY
Farid Saleh,
Yunnan University, China

REVIEWED BY
Danny Eibye-Jacobsen,
University of Copenhagen, Denmark
Jianni Liu,
Northwest University, China

*CORRESPONDENCE
Yujing Li
✉ yujingli@ynnu.edu.cn

RECEIVED 20 December 2022
ACCEPTED 28 March 2023
PUBLISHED 26 April 2023

CITATION
Zhao J, Li Y and Selden PA (2023) A new primitive polychaete with eyes from the lower Cambrian Guanshan biota of Yunnan Province, China. *Front. Ecol. Evol.* 11:1128070. doi: 10.3389/fevo.2023.1128070

A new primitive polychaete with eyes from the lower Cambrian Guanshan biota of Yunnan Province, China

Jun Zhao[1], Yujing Li[2]* and Paul A. Selden[3,4]

[1]Research Center of Paleobiology, Yuxi Normal University, Yuxi, China, [2]Yunnan Key Laboratory of Plateau Geographical Processes and Environmental Changes, Faculty of Geography, Yunnan Normal University, Kunming, China, [3]Department of Geology, University of Kansas, Lawrence, KS, United States, [4]Natural History Museum, London, United Kingdom

Annelids are abundant and speciose in the modern world but are comparatively few in the fossil record. Primitive annelids were expected to have developed eyes and nuchal organs, but until now definitive evidence is still lacking. Based on a new specimen from the Wulongqing Formation, we describe *Gaoloufangchaeta bifurcus* gen. et sp. nov. from the Guanshan biota (Cambrian Series 2, Stage 4) of Yunnan province, China. The overall profile of the body and the presence of tentacles and stout parapodia with simple chaetae establish it as a primitive polychaete. By bearing bicellular eyes and possible nuchal organs, the new form has developed relatively strong sensory abilities. Our material further confirms that polychaetes were already diverse by Cambrian Series 2, indicating a much earlier origin for the group.

KEYWORDS

Annelida, Burgess Shale-type *Lagerstätte*, South China, Cambrian explosion, soft-bodied organism

Introduction

Annelida is a highly diverse phylum that includes approximately 17,000 described species (Nanglu and Caron, 2018). The records of fossil representatives are sparse because annelids are entirely soft-bodied and decay rapidly (Briggs and Kear, 1993; Parry et al., 2014). Whole-body fossil annelids have been recovered from early Cambrian to Carboniferous strata (Conway Morris, 1979; Schram, 1979; Thompson, 1979; Briggs et al., 1996; Sutton et al., 2001; Huang et al., 2004; Farrel and Briggs, 2007; Vinther et al., 2008; Högström et al., 2009; Briggs and Bartels, 2010; Liu et al., 2015; Han et al., 2019). In particular, the Cambrian annelids are predominantly polychaetes, which are strikingly various and widely distributed, including *Burgessochaeta setigera* (Walcott, 1911), *Canadia spinosa* (Walcott, 1911), *Peronochaeta dubia* (Walcott, 1911), *Insolicorypha psygma* (Conway Morris, 1979), *Stephenscolex argutus* (Conway Morris, 1979), and *Kootenayscolex barbarensis* (Nanglu and Caron, 2018) from the Burgess Shale, *Phragmochaeta canicularis* (Conway Morris and Peel, 2008), and *Pygocirrus butyricampum* (Vinther et al., 2011) from Sirius Passet, *Ipoliknus avitus* (Han et al., 2019), and *Adelochaeta sinensis* (Han et al., 2019) from Chengjiang, *Dannychaeta tucolus* (Chen et al., 2020) from the Cambrian Canglangpu Formation of Yunnan, and *Guanshanchaeta felicia* (Liu et al., 2015) from Guanshan. Nanglu and Caron (2018) proposed that primitive annelids could have developed eyes and nuchal organs. However, of all the polychaetes documented above, none has been demonstrated to possess eyes thus far.

Here, we describe a new primitive polychaete, *Gaoloufangchaeta bifurcus* gen. et sp. nov., from the Guanshan biota, which is characterized by the presence of a possibly tripartite body profile, a pair of tentacles, bicellular eyes, possible nuchal organs, and a bifid pygidium. These are the first taxon-bearing visual organs among Cambrian annelids. Our material provides a new epibenthic soft-bodied metazoan for the Burgess Shale-type *Lagerstätte* and further confirms the diversity of polychaetes by Cambrian Series 2, demonstrating that the group originated in a deeper time.

Geological setting

The Guanshan biota occurs in the Wulongqing Formation (Cambrian Series 2, Stage 4), which is distributed widely in eastern Yunnan, southwest China, including the Kunming-Wuding and Malong-Yiliang areas. The best-studied sections include the Gaoloufang and Gangtoucun sections of Kunming, the Shijiangjun section of Wuding, the Lihuazhuang section of Yiliang, and the Wulongqing section of Malong (Hu et al., 2013; Figure 1).

The specimen described in this study was collected from the Gaoloufang section (24.95916°N, 102.80539°E), which is ~15 km southeast of the downtown area of Kunming (Figure 1). The Cambrian succession in this section mainly consists of the Hongjingshao and Wulongqing Formations. The former is composed of dark brown sandstones and gray argillaceous siltstones, while the latter comprises grayish-yellow silty mudstones interbedded with dark brown siltstones.

Materials and methods

The single specimen (RCP-ZJ-0001), preserved in a gray-yellow mudstone, was prepared using a fine needle under a Nikon SMZ 800 N microscope, revealing parts covered by matrix. Digital photographs were taken using a Canon EOS 5D SR camera with a Canon MP-E 65 (1-5X) macro lens under cross-polarized light, with the brightness and contrast of the resulting images processed in Adobe Photoshop CS 5. The specimen was imaged using an FEI Quanta 650 FEG scanning electron microscope. Elemental mapping was undertaken using an EDAX Pegasus energy dispersive X-ray spectroscopy (EDX) system, 112×magnification, 10.3 mm working distance, and an accelerating voltage of 20 kV. The specimen is housed in the Research Center of Paleobiology, Yuxi Normal University (RCP).

The specimen is of a bizarre appearance. Behind the second pair of uniramous parapodia, there is an apparent constriction, forming a neck-like structure, which is not known for any other Cambrian polychaetes (Figure 2). Based on the overall morphology of the body, we suspect that this is a taphonomic artifact. We tentatively divide the body into three regions as follows: anterior part, trunk, and pygidium, as shown in Figure 2.

The current publication and the new species are registered in ZooBank as urn:lsid:zoobank.org: act:54120A6E-2195-478E-A924-E686FD88D633 and urn:lsid:zoobank.org:act:D0F29632-9BDC-4CF6-9299-D84279B28A46, respectively.

Systematic paleontology

Phylum Annelida (Lamarck, 1809)
Class Polychaeta (Grube, 1850)
Gaoloufangchaeta gen. nov.

Derivation of name

Gaoloufang, referring to the location where the fossil was found; *chaeta*, a diagnostic characteristic of polychaetes.

Type species

Gaoloufangchaeta bifurcus sp. nov.

Diagnosis

Body tripartite (tentative) and elongated, bearing a pair of tentacles, bicellular eyes, and possible nuchal organs; the anterior part of the body being a reversed trapezoid in outline; at least seven pairs of uniramous parapodia with simple chaetae; pygidium large and bifid.

Gaoloufangchaeta bifurcus sp. nov.
Figures 2–4.

Derivation of name

From the Latin *bifurcus*, referring to the bifid structure on the pygidium.

Holotype

RCP-ZJ-0001, a complete specimen.

Type locality

Gaoloufang section, Kunming, Yunnan, China.

Type horizon

Wulongqing Formation (Cambrian Series 2, Stage 4).

Diagnosis

As for genus.

10.3389/fevo.2023.1128070

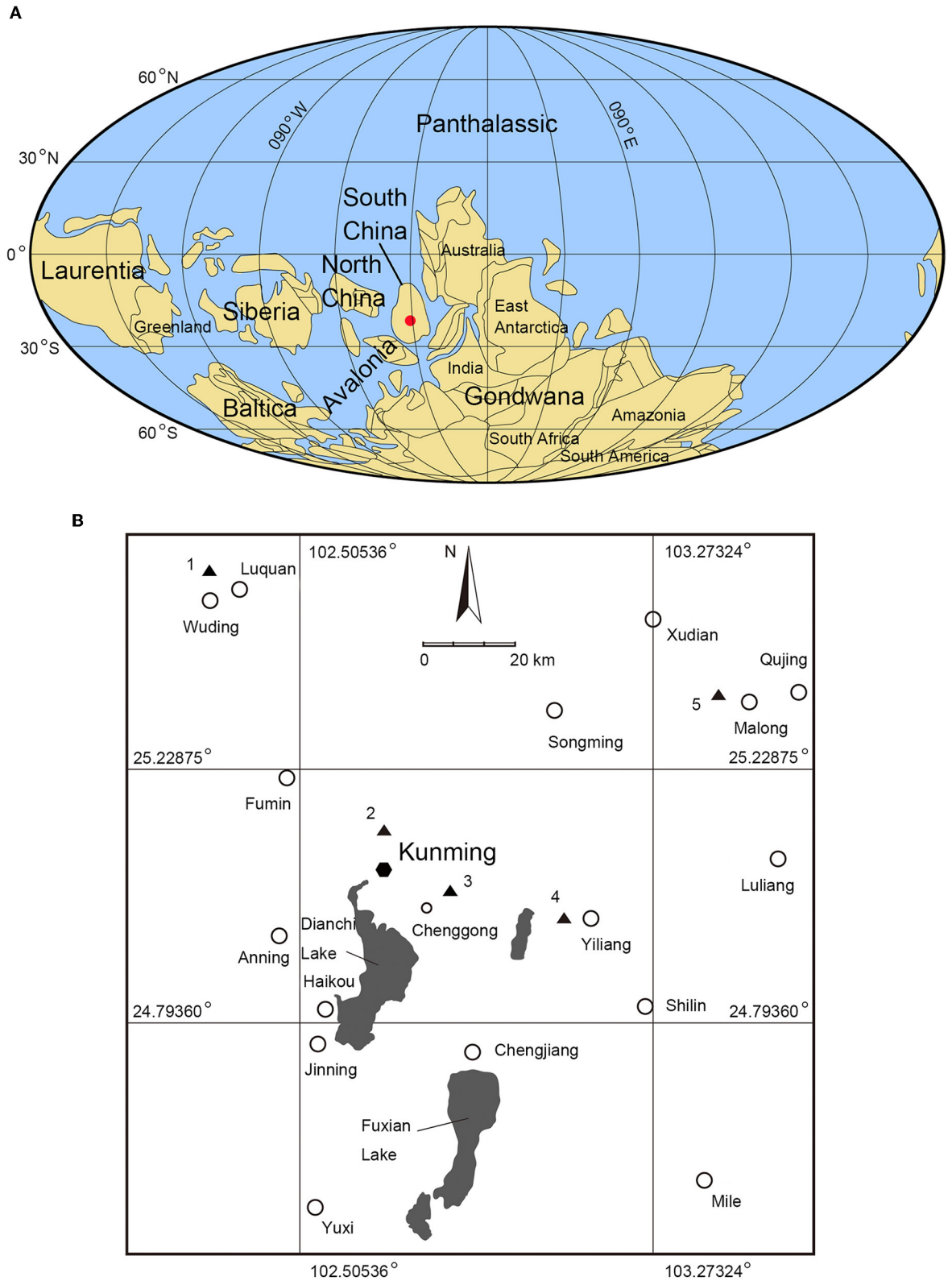

FIGURE 1
Paleogeographic and geographic maps, showing the occurrence of *Gaoloufangchaeta bifurcus* gen. et sp. nov. **(A)** paleogeographic reconstruction in early and middle Cambrian, modified from Torsvik and Cocks (2017); **(B)** the main fossil sites of the Guanshan biota in eastern Yunnan. 1, Shijiangjun; 2, Gangtoucun; 3, Gaoloufang; 4, Lihuazhang; 5, Wulongqing.

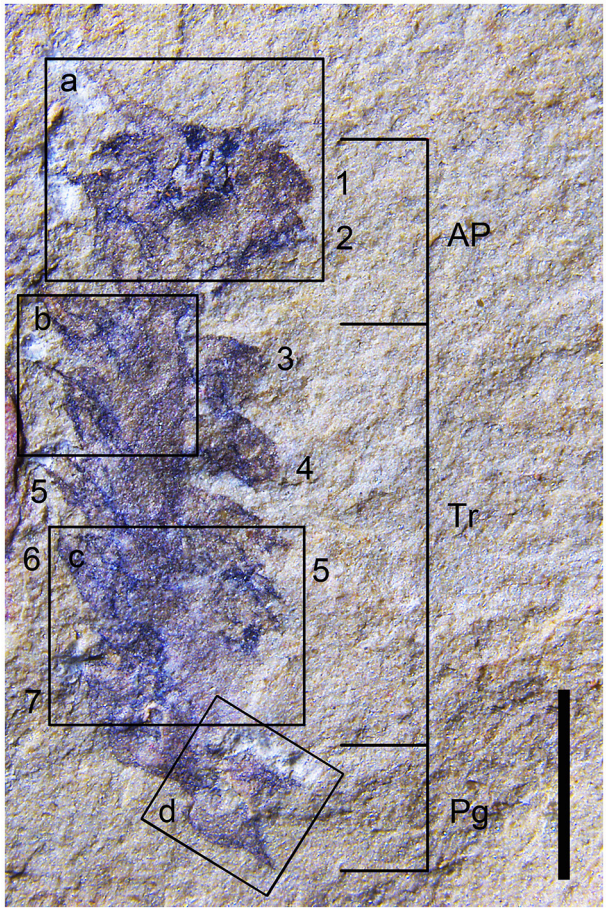

FIGURE 2
Gaoloufangchaeta bifurcus gen. et sp. nov. from the early Cambrian Guanshan biota (Yunnan Province, China). AP, anterior part; Pg, pygidium; Tr, trunk. The scale bar is 2 mm.

Description

The body is bilaterally symmetrical and possibly tripartite (composed of the anterior part, trunk, and pygidium) and preserved dorsoventrally flattened in parallel aspect, measuring 9 mm long (excluding tentacles).

The anterior part is a reversed trapezoid in the overall profile and measures 2 mm in length and 2.5 mm in maximum width (including parapodia, just above mid-length; Figures 2, 3A). A pair of tentacles stretches out anterolaterally from near the center of the anterior margin and tapers distally, with the best-preserved branch (left) measuring 1 mm long and 0.5 mm wide at the base (Figure 3). A pair of bicellular eyes is located behind the anterior margin and close to the bases of tentacles, with the diameter of each being 0.3 mm (Figure 3A). A total of two short longitudinal grooves, with each being 0.2 mm in length, are situated behind the eyes, which are interpreted here as possible nuchal organs (Figure 3A). A sub-ovoid dark patch lies behind the possible nuchal organs and may represent traces of the mouth or a partly preserved pharynx on the ventral side (Figure 3A). The posterior region of the anterior part is apparently constricted, forming a neck-like structure (Figure 2). Two pairs of uniramous parapodia are lined along both sides of the anterior part and are roughly triangular in outline (Figures 2, 3).

The trunk is elongated and tapers posteriorly, measuring 6 mm in length and approximately 3 mm in maximum width (at the first pair of parapodia). It comprises at least five homonomous segments, with each bearing a pair of uniramous parapodia that are broadly based and taper slightly distally, ending in blunt terminations (Figures 2, 4A, B). Chaetae are simple, thin, and situated at the distal ends of parapodia (Figures 4A, C). The posterior right side of the trunk is obscured, likely as a result of decay (Figure 4C). The boundaries of trunk segments are faint. The posterior part of the trunk is constricted slightly and associated with the pygidium and is devoid of any parapodia (Figure 4D). Column-like structures along the median trunk region are interpreted as traces of the gut (Figure 4A).

The pygidium is sub-rectangular in outline and measures 0.5 mm in length and 1.2 mm in width. From its posterior–lateral corners, two triangular structures arise (0.5 mm long for each), creating a more or less U-shaped morphology of the posterior margin (Figures 4D, E).

Remarks

The general shape of the body and the presence of tentacles, eyes, parapodia with chaetae, and pygidium clearly demonstrate that *Gaoloufangchaeta bifurcus* is a polychaete annelid. Chaetae are hard parts and most easily to be preserved, but they are absent in most parapodia of the new form. Decay could result in the detachment of chaetae in Cambrian polychaetes, e.g., *Canadia spinosa* (Walcott, 1911; Briggs et al., 1994; Parry et al., 2016). Traces of decay are present at the posterior right side of the trunk of *G. bifurcus* (Figure 4C), indicating that the body indeed experienced a period of decay prior to burial.

Gaoloufangchaeta bifurcus resembles *Guanshanchaeta felicia* (Liu et al., 2015) in having an elongated body, a pair of tentacles, and a bifid pygidium. However, *G. bifurcus* differs from *G. felicia* in that the body is much shorter and the trunk segments fewer; parapodia are uniramous and the first two pairs are followed by a constriction, forming a reversed trapezoid for the anterior part of the body (although this could be a taphonomic artifact; Figure 2). In addition, in *G. bifurcus,* the pygidium is strongly differentiated from the trunk and large relative to the body size (Figures 2, 4D, E), whereas it is poorly defined and rather smaller in *G. felicia* (figure 1 in Liu et al., 2015). *G. felicia* tapers both anteriorly and posteriorly, a morphological characteristic not found in *G. bifurcus*. Lastly, *G. bifurcus* differs from *G. felicia* in the presence of eyes and possible nuchal organs and the absence of a buccal tube. The differences above discriminate *G. bifurcus* from being a juvenile of *G. felicia*.

Han et al. (2019) described two polychaetes [*Ipoliknus avitus* (Han et al., 2019) and *Adelochaeta sinensis* (Han et al., 2019)] and three additional polychaete specimens from the earlier Chengjiang biota. *Gaoloufangchaeta bifurcus* differs from *Ipoliknus avitus,* in particular, in the absence of sclerites

FIGURE 3
Gaoloufangchaeta bifurcus gen. et sp. nov. **(A)** detail of Figure 2, position marked by frame a. **(B, C)** SEM-EDX maps of **(A)**, the specimen was rotated slightly to the left. Ey, eye; Mo?, possible mouth; NO?, possible nuchal organ; Pa, parapodium; Te, tentacle. The scale bars are 0.5 mm.

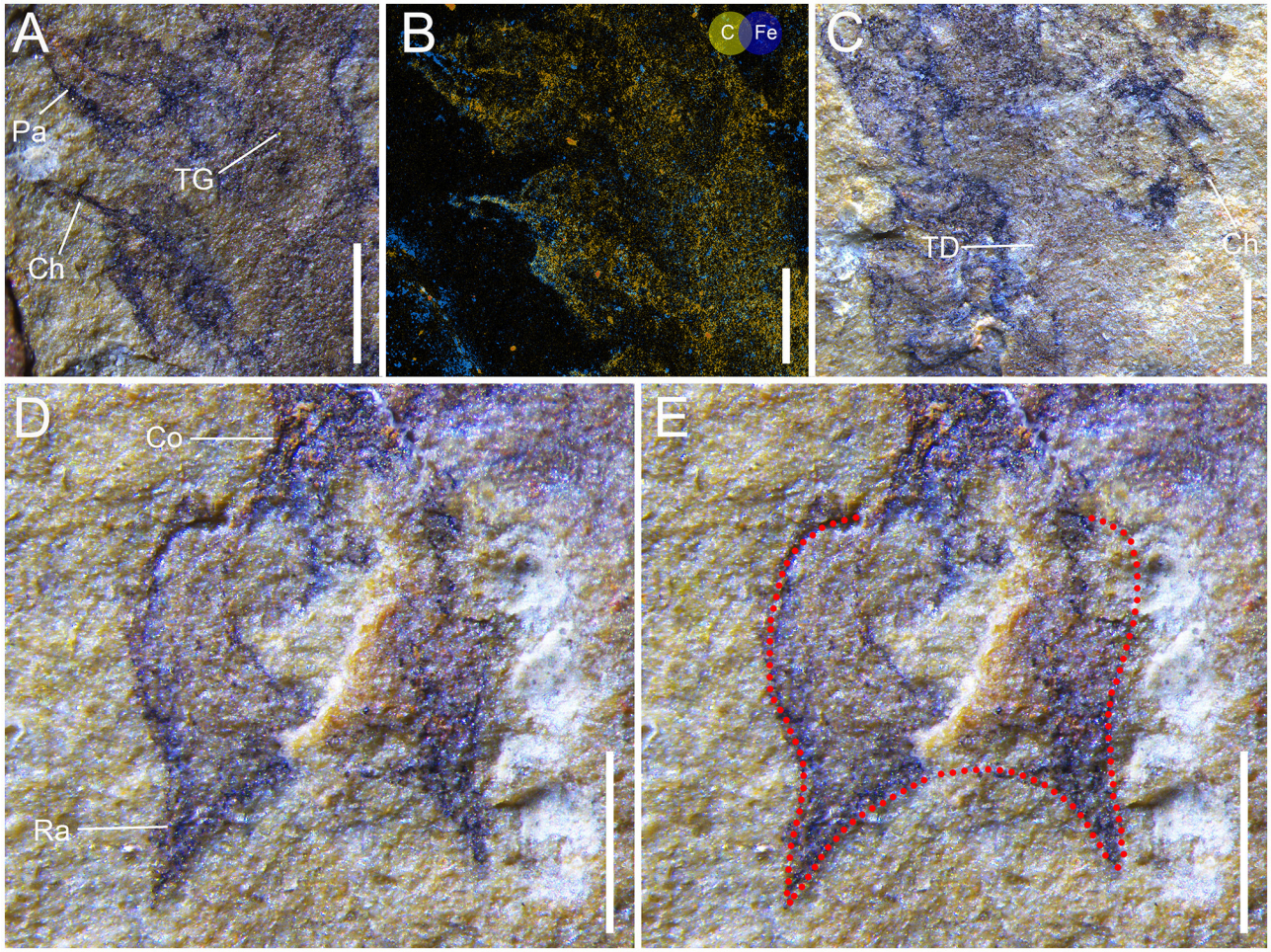

FIGURE 4
Gaoloufangchaeta bifurcus gen. et sp. nov. **(A)** detail of Figure 2, position marked by frame b. **(B)** EDX map of **(A)**, the specimen was rotated anticlockwise slightly. **(C)** Detail of Figure 2, position marked by frame c. **(D)** Detail of Figure 2, position marked by frame d; the specimen was rotated clockwise a little to show the pygidium in upright orientation. **(E)** Detail of Figure 2, position marked by frame d; the red dotted line shows the profile of the pygidium. Ch, chaeta; Co, constriction; Pa, parapodium; Ra, ramus; TD, traces of decay; TG, traces of gut. The scale bars are 0.5 mm.

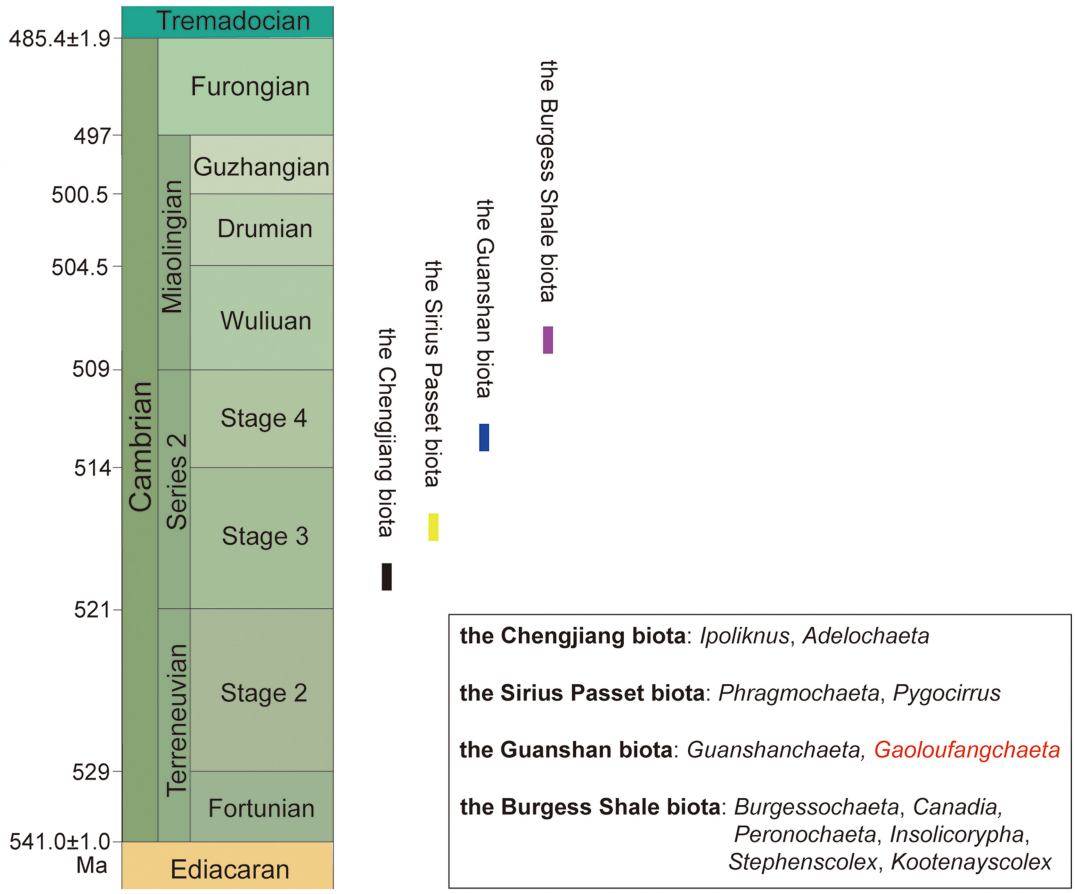

FIGURE 5
Main early and middle Cambrian fossil *Lagerstätten* yielding polychaetes.

and evident segment boundaries. *G. bifurcus* is different from *Adelochaeta sinensis* in that the latter has a clearly defined head region and aciculae, which are absent from the former. The most obvious similarity between *G. bifurcus* and the three unidentified polychaetes is the presence of chaetae; further comparisons are hard to make owing to the incomplete preservation of the three individuals. The absence of characteristics such as palps, prostomium, thorax, and parapodia with lateral lamellae discriminates *G. bifurcus* from *Dannychaeta tucolus* (Chen et al., 2020), a tube-dwelling polychaete from the Canglangpu formation (Cambrian Series 2, Stage 3) of Yunnan province.

Hitherto, the Burgess Shale has yielded the most abundant polychaetes of various morphologies in Cambrian *Lagerstätten*. *Gaoloufangchaeta bifurcus* approximates *Burgessochaeta setigera* and *Canadia spinosa* in the elongated profile of the body and by having uniramous parapodia. However, the number of body segments and the presence or absence of branchia discriminate the three taxa. *Peronochaeta dubia* and *Stephenscolex argutus* most differ from *G. bifurcus* in that they bear papillae at the anterior end of the body, instead of tentacles. *G. bifurcus* shares the same body length with *Insolicorypha psygma*, whereas the latter has a bipartite head region and more trunk segments. *Kootenayscolex barbarensis* bears a pair of large palps and a median antenna, which are absent from *G. bifurcus*.

Different from *Gaoloufangchaeta bifurcus*, *Phragmochaeta canicularis* (Conway Morris and Peel, 2008), a polychaete from the Sirius Passet *Lagerstätte*, has numerous long and thin chaetae and more trunk segments. The body terminating in a bifid structure is the most apparent similarity between *G. bifurcus* and *Pygocirrus butyricampum* (Vinther et al., 2011), another polychaete from the Sirius Passet. However, the profile of the bifid structure is different between the two taxa: V-shaped for *P. butyricampum* and more or less U-shaped for *G. bifurcus*. In addition, *P. butyricampum* has more trunk segments.

Discussion

Gaoloufangchaeta bifurcus gen. et sp. nov. is described based on a single specimen with decay traces, and thus, some of its characteristics cannot be confirmed as original. The neck-like structure (Figure 2) may be an artifact formed during burial given the soft nature of annelid bodies, and hence, the tripartite outline of the body of the new form is tentative in this study; the parapodia lined along both sides of the trunk appear to be too stout, and whether each is composed of two lobes (i.e., notopodium and neuropodium) cannot be confirmed on this comparatively poorly preserved specimen; they are

temporarily interpreted here as uniramous; the morphologies of the inferred nuchal organs and mouth are not clearly shown on the specimen, and their identities need to be confirmed by additional and better-preserved ones; decay traces obscure the morphology of the posterior part of the trunk (Figures 2, 4C).

Gaoloufangchaeta bifurcus from Cambrian Series 2 of southwest China is one of the oldest fossil annelids recovered so far. Structures such as eyes and nuchal organs have previously been expected but not found in ancestral annelids (Weigert et al., 2014; Nanglu and Caron, 2018). The specimen of *G. bifurcus* clearly shows evidence of eyes and possible nuchal organs (Figures 2, 3) for the first time in Cambrian polychaetes, demonstrating that the oldest annelids are not all devoid of these sensory organs. By having tentacles, eyes, possible nuchal organs, and stout parapodia, *G. bifurcus* clearly had comparatively strong sensory abilities and an active and epibenthic lifestyle. Although no evidence of a proboscis with jaws is found in the single specimen, the possibility of the new taxon being a predator or scavenger cannot be ruled out. Our material not only provides a new epibenthic representative for early Cambrian marine animals but also a new soft-bodied metazoan for the Guanshan biota.

Until now, fossil polychaetes are the most diversified and abundant in the Burgess Shale (Cambrian Miaolingian, Wuliuan); the earliest whole-body preserved ones date back to Cambrian Series 2, Stage 3, represented by *Phragmochaeta canicularis* and *Pygocirrus butyricampum* from Sirius Passet, and *Ipoliknus avitus* and *Adelochaeta sinensis* from Chengjiang. Together with *Gaoloufangchaeta bifurcus*, the slightly younger Guanshan biota (Figure 5) has yielded two types of polychaetes. These occurrences confirm that polychaetes were already diverse in morphology by Cambrian Series 2, indicating a much earlier origin for the group.

Gaoloufangchaeta shows the characteristics proposed for primitive annelids, i.e., errant polychaete body form, parapodia with simple chaetae, and prostomial sensory organs (Parry et al., 2014; Weigert et al., 2014), and thus, it is among the primitive representatives of Annelida. Of all the early and middle Cambrian polychaetes, only the bodies of *Pygocirrus*, *Guanshanchaeta,* and *Gaoloufangchaeta* terminate in a bifid structure, suggesting a similar phylogenetic grade in between. *Gaoloufangchaeta* bears eyes and possible nuchal organs that are absent from *Pygocirrus* and *Guanshanchaeta*, which implies that *Gaoloufangchaeta* might be comparatively more derived and/or even a representative of the last common ancestor of annelids.

Conclusion

We describe a new primitive polychaete, *Gaoloufangchaeta bifurcus* gen. et sp. nov., from the Cambrian Series 2, Stage 4 of southwest China. This is the second polychaete from the Guanshan biota and among the oldest records of fossil annelids globally. Our material not only demonstrates that relatively strong sensory organs had developed in Cambrian annelids but also further confirms that polychaetes were already diverse in morphology by Cambrian Series 2.

Data availability statement

The original contributions presented in the study are included in the article/supplementary material, further inquiries can be directed to the corresponding author.

Author contributions

JZ and YL designed the study, collected and prepared the fossil, and wrote the first draft of the manuscript with substantial input from PS. JZ photographed the specimen and prepared the figures. All authors described and interpreted the specimen. All authors contributed to the article and approved the submitted version.

Acknowledgments

We are grateful to Fei Li and Zhongwei Li for their assistance during fieldwork.

Conflict of interest

The authors declare that the research was conducted in the absence of any commercial or financial relationships that could be construed as a potential conflict of interest.

Publisher's note

References

Briggs, D. E. G., and Bartels, C. (2010). Annelids from the Lower Devonian Hunsrück Slate (Lower Emsian, Rhenish Massif, Germany). *Palaeontology* 53, 215–232. doi: 10.1111/j.1475-4983.2009.00927.x

Briggs, D. E. G., Erwin, D. H., and Collier, F. J. (1994). *The Fossils of the Burgess Shale*. Washington, DC; London: Smithsonian Institution Press.

Briggs, D. E. G., and Kear, A. J. (1993). Decay and preservation of polychaetes: taphonomic thresholds in soft-bodied organisms. *Paleobiology* 19, 107–135. doi: 10.1017/S0094837300012343

Briggs, D. E. G., Siveter, D. J., and Siveter, D. J. (1996). Soft-bodied fossils from a Silurian volcaniclastic deposit. *Nature* 382, 248–250. doi: 10.1038/382248a0

Chen, H., Parry, L. A., Vinther, J., Zhai, D. Y., Hou, X. G., and Ma, X. Y. (2020). A Cambrian crown annelid reconciles phylogenomics and the fossil record. *Nature* 583, 248–250. doi: 10.1038/s41586-020-2384-8

Conway Morris, S. (1979). Middle Cambrian polychaetes from the Burgess Shale of British Columbia. *Philos. Trans. R. Soc. of Lond. B*. 285, 227–274. doi: 10.1098/rstb.1979.0006

Conway Morris, S., and Peel, J. S. (2008). The earliest annelids: lower Cambrian polychaetes from the Sirius Passet *Lagerstätte*, Peary Land, north Greenland. *Acta Palaeontol. Pol.* 53, 137–148. doi: 10.4202/app.2008.0110

Farrel, Ú., and Briggs, D. E. G. (2007). A pyritized polychaete from the Devonian of Ontario. *Proc. R. Soc. B* 274, 499–504. doi: 10.1098/rspb.2006.0063

Grube, A. (1850). Die Familien der Anneliden. Arch. *Naturgesch*. 16, 249–364.

Han, J., Conway Morris, S., Hoyal Cuthill, J. F., and Shu, D. (2019). Sclerite-bearing annelids from the lower Cambrian of South China. *Sci. Rep.* 9, 1–11. doi: 10.1038/s41598-019-40841-x

Högström, A. E. S., Briggs, D. E. G., and Bartels, C. (2009). A pyritized lepidocoleid machaeridian from the Lower Devonian Hunsrück Slate, Germany. *Proc. R. Soc. B* 276, 1981–1986. doi: 10.1098/rspb.2008.1875

Hu, S. X., Zhu, M. Y., Luo, H. L., Steiner, M., Zhao, F. C., Li, G. X., et al. (2013). *The Guanshan Biota*. Kunming: Yunnan Science and Technology Press [in Chinese with English summary].

Huang, D. Y., Chen, J. Y., Vannier, J., and Saiz Salinas, J. (2004). Early Cambrian sipunculan worms from southwest China. *Proc. R. Soc. Lond. B* 271, 1671–1676. doi: 10.1098/rspb.2004.2774

Lamarck, J. B. P. A. (1809). *Philosophie Zoologique*. Paris: Dentu.

Liu, J., Ou, Q., Han, J., Li, J., Wu, Y., Jiao, G., et al. (2015). Lower Cambrian polychaete from China sheds light on early annelid evolution. *Sci. Nat.* 102, 1–7. doi: 10.1007/s00114-015-1285-4

Nanglu, K., and Caron, J. B. (2018). A new Burgess Shale polychaete and the origin of the annelid head revisted. *Curr. Biol.* 28, 319–326. doi: 10.1016/j.cub.2017.12.019

Parry, L., Tanner, A., and Vinther, J. (2014). The origin of annelids. *Palaeontology* 57, 1091–1103. doi: 10.1111/pala.12129

Parry, L. A., Edgecombe, G. D., Eibye-Jacobsen, D., and Vinther, J. (2016). The impact of fossil data on annelid phylogeny inferred from discrete morphological characters. *Proc. R. Soc. B* 283, 20161378. doi: 10.1098/rspb.2016.1378

Schram, F. R. (1979). *Worms of the Mississippian Bear Gulch Limestone of central Montana, USA*. San Diego, CA: Transactions of the San Diego Society of Natural History.

Sutton, M. D., Briggs, D. E. G., and Siveter, D. J. (2001). A three-dimensionally preserved fossil polychaete worm from the Silurian of Herefordshire England. *Proc. R. Soc. B* 268, 2355–2363. doi: 10.1098/rspb.2001.1788

Thompson, I. (1979). Errant polychaetes (Annelida) from the Pennsylvanian Essex fauna of northern Illinois. *Palaeontogr. A*. 163, 169–199.

Torsvik, T. H., and Cocks, L. R. M. (eds.). (2017). "Cambrian," in *Earth History and Palaeogeography* (Cambridge: Cambridge University Press), 85–100. doi: 10.1017/9781316225523.006

Vinther, J., Eibye-Jacobsen, D., and Harper, D. A. T. (2011). An early Cambrian stem polychaete with pygidial cirri. *Bio. Lett.* 7, 929–932. doi: 10.1098/rsbl.2011.0592

Vinther, J., Roy, P. V., and Briggs, D. E. G. (2008). Machaeridians are palaeozoic armoured annelids. *Nature* 451, 185–188. doi: 10.1038/nature06474

Walcott, C. D. (1911). "Middle Cambrian annelids," in *Cambrian Geology and Paleontology II* (Washington, DC: Smithsonian Institution), 109–144.

Weigert, A., Helm, C., Meyer, M., Nickel, B., Arendt, D., Hausdorf, B., et al. (2014). Illuminating the base of the annelid tree using transcriptomics. *Mol. Biol. Evol.* 31, 1394–1401. doi: 10.1093/molbev/msu080

frontiers | Frontiers in Ecology and Evolution

TYPE Original Research
PUBLISHED 25 May 2023
DOI 10.3389/fevo.2023.1174564

OPEN ACCESS

EDITED BY
Allison Daley,
Universitéde Lausanne, Switzerland

REVIEWED BY
Jean Vannier,
Université Claude Bernard Lyon 1, France
Yu Liu,
Yunnan University, China
Brigitte Schoenemann,
University of Cologne, Germany

*CORRESPONDENCE
Dongjing Fu
djfu@nwu.edu.cn

RECEIVED 26 February 2023
ACCEPTED 09 May 2023
PUBLISHED 25 May 2023

CITATION
Ma J, Pates S, Wu Y, Lin W, Liu C, Wu Y, Zhang M and Fu D (2023) Ontogeny and brooding strategy of the early Cambrian arthropod *Isoxys minor* from the Qingjiang biota.
Front. Ecol. Evol. 11:1174564.
doi: 10.3389/fevo.2023.1174564

Ontogeny and brooding strategy of the early Cambrian arthropod *Isoxys minor* from the Qingjiang biota

Jiaxin Ma[1], Stephen Pates[2], Yu Wu[1], Weiliang Lin[1], Cong Liu[1], Yuheng Wu[1], Mingjing Zhang[1] and Dongjing Fu[1]*

[1]State Key Laboratory of Continental Dynamics, Shaanxi Key Laboratory of Early Life and Environments and Department of Geology, Northwest University, Xi'an, China, [2]Department of Zoology, University of Cambridge, Cambridge, United Kingdom

†*Isoxys* is a worldwide distributed bivalved arthropod known almost exclusively from Cambrian Burgess Shale-type Lagerstätten. Outline analyses using 34 specimens of the iconic large bivalved arthropod †*Isoxys minor* from the Cambrian Stage 3 (~518Ma) Qingjiang biota and the Cambrian Stage 4 Guanshan biota, interpret that they are the same species and there is a very slight difference in the shape of the outlines of the carapaces between the two biotas. This suggests that environment might be driving intraspecific variation. Quantitative analysis of shape changes during growth using 51 specimens of †*I. minor* from the Qingjiang biota, reveals that its valves gradually elongate and the ratio of cardinal spines and spherical eyes relative to the valve length significantly decreases during postembryonic development. †*I. minor* has proportionally large cardinal spines and eyes in the earliest stages, and this allometric growth is beneficial for self-protection and foraging, which may have improved the survival rate of individuals with these characters. In addition, two of the specimens document the evidence of brood care in †*I. minor*, and the egg cluster occupies almost the entire dorsal region under the carapace. Compared to other early Paleozoic egg-carrying arthropods, †*I. minor* broods have the highest number (~300 per clutch) of small (Ø, ~0.5mm) eggs. Since the ovigerous individuals are almost half the size of the adults, †*I. minor* may have possessed reproductive ability during the early life stage. The results indicate that spines played an antipredatory role for †*I. minor*, and that it followed an r-strategy of reproducing with many individuals at an early stage. †*I. minor* also represents the earliest diverging arthropod from which brood care has been documented.

KEYWORDS

Cambrian, Qingjiang biota, Isoxys, allometry, brood care

1. Introduction

†*Isoxys* arthropod is a widely distributed taxon of the Cambrian marine ecosystem, with a large bivalved carapace bearing two prominent cardinal spines, which is occurred in Cambrian Series 2 and 3 and has a widespread paleogeographical distribution (Williams et al., 1996; Vannier and Chen, 2000; Stein et al., 2010; Fu et al., 2011; Legg and Vannier, 2013; Liu et al., 2018). Hitherto, up to 22 species of †*Isoxys* have been recorded from Australia (Glaessner, 1979; García-Bellido et al., 2009a), North America (Simonetta and Delle Cave, 1975; Butterfield and Nicholas, 1994; Williams et al.,

1996; Briggs et al., 2008; García-Bellido et al., 2009b), North Greenland (Stein et al., 2010; Nielsen et al., 2017), France (Vannier et al., 2005), Spain (Richter and Richter, 1927; Wang, 2014), Russia (Ivantsov, 1990, 2005), and China (Hou, 1987; Shu et al., 1995; Luo et al., 1999, 2006, 2008; Zhao et al., 2005, 2011; Wang et al., 2010; Fu et al., 2011, 2014; Wen et al., 2015; Liu et al., 2018; Du et al., 2020). It is widely distributed in the continental shelf, as well as in deep-water slope areas, recovered from deposits ranging between 30° N and 30° S paleolatitude (Vannier and Chen, 2000; Vannier et al., 2009; Huang and Wang, 2014; Liu et al., 2018).

Hundreds of †*Isoxys minor* specimens have been reported in the Guanshan biota making it the dominant †*Isoxys* species in this biota (Luo et al., 2008; Wang et al., 2012; Huang and Wang, 2014). This species was initially recognized as †*I. auritus* (Luo et al., 1999), but due to its carapace morphology being quite different from that of †*I. auritus*, in particular the morphology of the cardinal spines, size of carapaces and surface ornamentation, Luo et al. in 2006 considered it as an unidentified species (Luo et al., 2006). †*Isoxys minor* was established by Luo and Hu in 2008 (Luo et al., 2008) and subsequently revised by various authors (Wang et al., 2012; Hu et al., 2013; Huang and Wang, 2014; Wang, 2014). Although a high number of specimens have been obtained from the Guanshan biota, only a few have revealed the soft anatomy (Hu et al., 2013; Huang and Wang, 2014).

In this study, carapace outlines of †*I. minor* specimens from the Qingjiang and Guanshan biotas are compared. The quantitative analysis of new specimens of †*I. minor* is recovered from the Qingjiang biota (Fu et al., 2019). Meanwhile, the ontogeny of this species is described in detail. In addition, exceptionally preserved specimens of †*I. minor* which carried an extremely large number of small eggs, are also described for the first time. The growth strategy and brooding strategy of †*I. minor* may serve as a key factor in driving this taxon as the most abundant †*Isoxys* species in both Qingjiang and Guanshan paleoecosystems. Given the phylogenetic position of †*Isoxys* – as an early diverging deuteropod (e.g., Fu et al., 2022) – †*I. minor* may represent the earliest diverging deuteropod to utilize an egg-carrying brooding strategy.

2. Materials and methods

2.1. Materials

A total of 51 specimens of †*I. minor* from the Qingjiang biota were analyzed in this study. Among which, 20 specimens had the trunk appendages preserved, and 13 had eyes preserved. These materials were collected from the middle member of the Shuijingtuo formation (Cambrian Series 2, Stage 3) at the Jinyangkou (prefix JY) section, Changyang County, Hubei Province, South China (Fu et al., 2019; Ma et al., 2021; Li et al., 2022). These soft-bodied fossils are preserved as dark organic carbon on fresh grey shale (Fu et al., 2019). All the studied specimens are deposited in the Shaanxi Key Laboratory of Early Life and Environments (LELE) and Department of Geology, Northwest University (NWU), Xi'an, China.

2.2. Fossil preparation and imaging

All specimens here were gathered from the laminated calcareous claystones (Fu et al., 2019). Some were further prepared with fine needles at high magnification using a Nikon SMZ 100 stereomicroscope. The fossils were photographed with a Canon EOS 5D Mark II digital camera under an incandescent lamp, controlled for remote shooting with EOS Utility 3.2. The line drawings were prepared with the Corel Draw X9 software (Bouton, 2008). All images were processed in Adobe Photoshop CC to make minor adjustments to contrast, exposure, colour balance and sharpness (Press, 2010).

2.3. Terminology

The morphological terms used for the description of †*Isoxys minor* are in general accordance with those used by previous authors to describe the morphology of *Isoxys* (Williams et al., 1996; Vannier and Chen, 2000; García-Bellido et al., 2009a; Fu et al., 2011; Aria and Caron, 2015).

2.4. Comparison of carapace outlines from the Guanshan and Qingjiang biotas

A total of 34 intact, laterally compressed specimens without deformation were selected for outline analyses. We focused on 25 specimens from the Qingjiang biota and nine previously figured specimens from the Guanshan biota (Wang et al., 2012; Huang and Wang, 2014) in this analysis (Figure 1A; Supplementary Table S1). All selected specimens were imaged in lateral view with the anterior oriented to the left; those oriented to the right were mirrored. Photographs of specimens were converted to black silhouettes on a white background using Inkscape, and saved as .jpg files (Supplementary Figure S1). These were imported into the R environment using the import_jpg function (*Momocs* package; Bonhomme et al., 2014; R Core Team, 2021) and converted to outlines (Supplementary Data 1). Outlines were scaled, centered, and resampled at 64-point resolution, and subjected to elliptical Fourier analysis (efourier function, *Momocs* package), retaining harmonics that achieve 99.9% of the total harmonic power. Eliptical Fourier analysis results were then visualized using a principal components analysis. A hierarchical clustering analysis (CLUST function, *Momocs* package) was then used to group carapaces by shape similarity.

2.5. Quantification and statistical analysis

Size measurements were taken from the photographs using the software ImageJ 1.8.0 (Burger and Burge, 2006). Six parameters were documented, including the total length of the carapace, the length of the valve and cardinal spines, the height of the valve, and the diameter of the eyes (Supplementary Table S2). The valve length was measured with exclusion of' the two cardinal spines. Regression analysis of the length (independent variable) and the height (dependent variable) of the valve was performed in Microsoft Excel (Figure 2D; Supplementary Table S3). The violin plot (i.e., box plots made of Kernel density distributions) of the carapace and cardinal spines was performed with Power BI (Figure 2E).

3. Results

3.1. Outline analysis and hierarchical clustering

Nineteen harmonics were retained for the elliptical Fourier analysis. Principal components 1, 2, and 3 retained just under 90% of

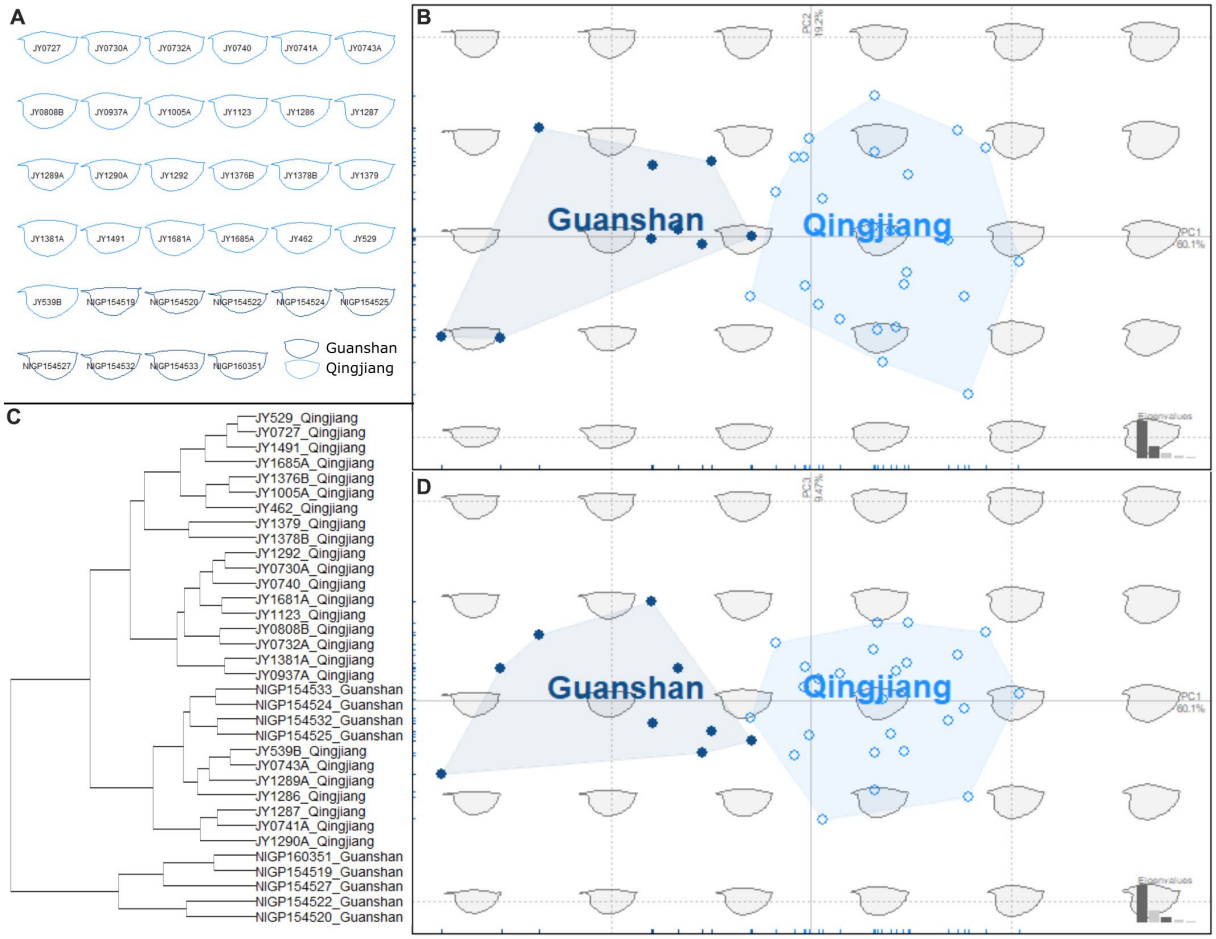

FIGURE 1
Analysis of †*Isoxys minor* carapace shape and comparison between the Guanshan and Qingjiang biotas. **(A)** Outlines of all specimens from the Qingjiang and Guanshan biotas analyzed in this study. Specimen number at centre of carapace, with outline color indicating biota. **(B)** Principal component analysis (PCA) visualizing PC1 and PC2 of results of elliptical Fourier analysis on †*I. minor* carapace outline shapes. **(C)** Hierarchical clustering results on elliptical Fourier analysis of †*Isoxys minor* carapace shapes. **(D)** Principal component analysis (PCA) visualizing PC1 and PC3 of results of elliptical Fourier analysis on †*I. minor* carapace outline shapes. Bars in bottom right of panels **(B,D)**, indicate contribution to overall variation of PCs, with plotted PCs in dark grey.

the total variation (60.1, 19.2, and 9.5% respectively). Carapaces have greater height relative to length and more robust spines with increasing values of Principal component 1 (PC1), and the anterior spine changes orientation from pointing dorsally to ventrally from negative values to positive values across this axis (Figure 1B). Spine length increases with PC2 (Figure 1B), and PC3 describes finer changes in the carapace outline (Figure 1D). Guanshan and Qingjiang specimens are separated in the PCA space, due to non-overlapping PC1 values. Guanshan carapaces have more negative PC1 values than those from Qingjiang. Guanshan and Qingjiang carapaces overlap across PC2 and PC3. The cluster analysis did not separate all Guanshan and Qingjiang specimens, instead a subset of Guanshan specimens cluster within the Qingjiang specimens (Figure 1C).

3.2. Ontogeny of †*Isoxys minor*

51 specimens from the Qingjiang biota were quantified and statistically analyzed to unravel the morphological changes in carapaces and soft bodies during ontogeny.

3.2.1. Carapace

The carapace length of specimens in the study ranges from 10.4 mm (JY1287) to 27.1 mm (JY1005), and the valve length ranges from 8.7 mm to 24 mm (Figures 2A,C,E). Dorsal margin clearly curved, ventral outline semicircular, the maximum height being in the mid-length of carapace. The valve L:H ratio is an average of 1.5 to 1.7 (Figures 2A–C). Regression analysis of the length of the valve against the height of the valve was performed using the 36 complete laterally compressed specimens. We analyzed the ontogenetic relationship of †*I. minor* by the allometric equation $Y = aX^b$ (a, the slope of the line; b, the allometric coefficient), and linearized the equation to $\ln Y = \ln a + b \ln X$. The result shows the valve of †*Isoxys* grew allometrically (Lv–Hv: $\ln Lv = -0.2204 + 0.9005 \ln Hv$; $b < 1$, $N = 36$, $R^2 = 0.9725$; *N*, number of specimens; R^2, the determination coefficient), gradually elongating during postembryonic development (Figure 2D).

The anterior spine is long and slightly curved, with lengths ranging from 1.6 mm to 2.1 mm (Figures 2C,E, 3). The ratio of anterior spine to valve length in the smallest individuals of †*I. minor* is 18.4%. This decreases significantly during ontogeny to a minimum ratio of

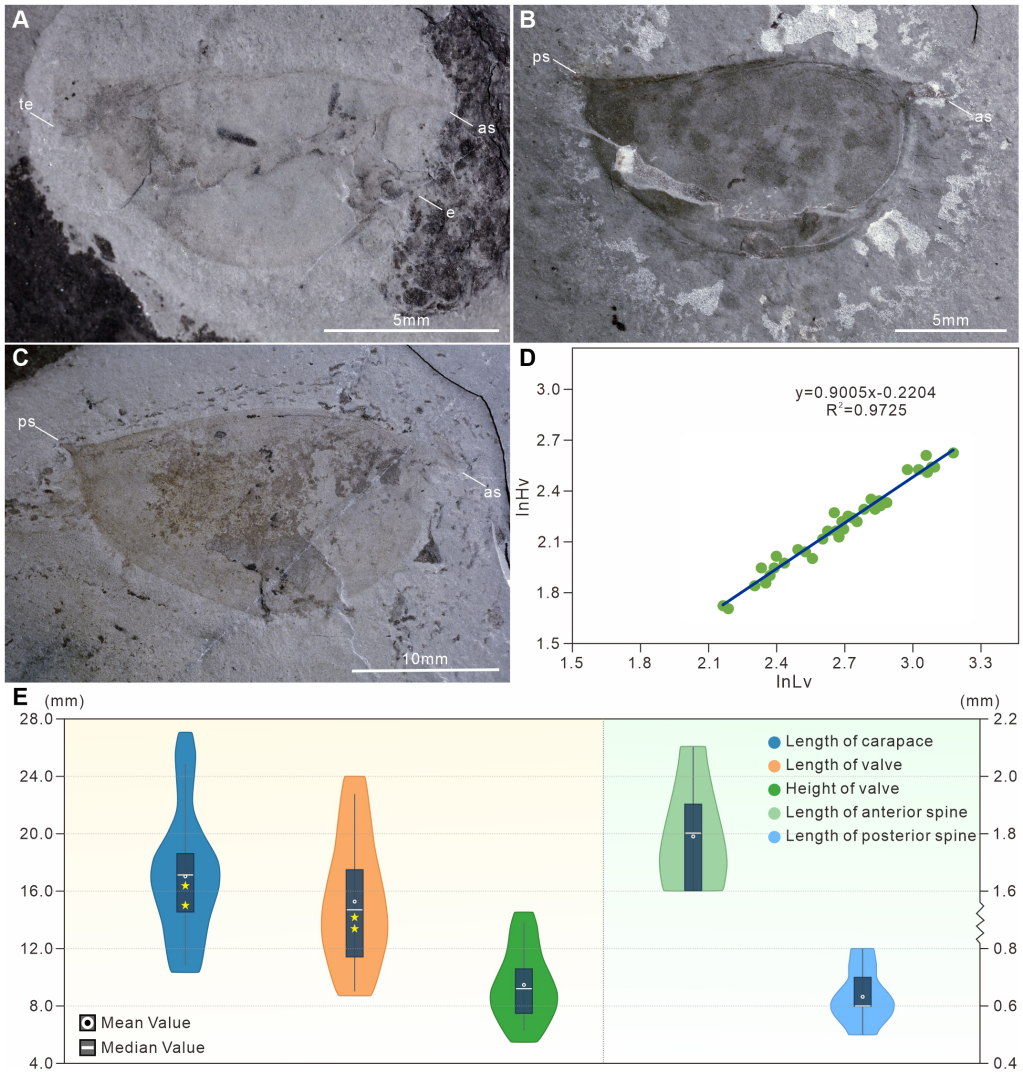

FIGURE 2
Statistical analysis of †*Isoxys minor* from the Qingjiang biota. **(A)** The smallest specimen with complete carapace, indistinct eyes and telson, JY1287. **(B)** The medium specimen with complete carapace, JY1123. **(C)** The largest specimen with complete carapace, JY1005. **(D)** Ontogenetic relationship between the length (Lv) and height (Hv) of †*I. minor* valve, showing the slow increase of the height with respect to the length. Regression analysis of Lv and Hv: lnLv=−0.2204+0.9005lnHv (N=36, R^2=0.9725). N, number of specimens; R^2, the determination coefficient. **(E)** The violin plot of the valve and cardinal spines of †*I. minor*. as, anterior spine; e, eye; ps, posterior spine; te, telson.

7.8% (Figures 2A,C, 3). The posterior spine is short and upturned, ranging from 0.5 mm to 0.8 mm in length (Figures 2A–C,E, 3). The ratio of posterior spine to valve length in the smallest individuals of †*I. minor* is 5.6%. This decreases significantly during ontogeny to a minimum ratio of 2.6% (Figures 2A–C,E, 3). Thus growth of cardinal spines was also allometric, with those of small individuals nearly the same length as those of the large individuals.

3.2.2. Eyes

A pair of large spheroidal eyes projects anteroventrally (Figures 3A–C). The spherical eye is connected to the head with a stalk, whose length is equal to, and its width is proximately half of the diameter of the eye (Figures 3A,B). Eye size remained almost constant during ontogeny (Figures 3A–C), and thus was largest in relation to the body size for the smallest individuals of the species (diameter *ca.* 16.1% of valve height and 11.1% of the body length) (Figures 2A, 3A).

3.3. Egg clusters in †*Isoxys minor*

Clusters of ovoid objects are present in two of the 51 specimens. In both specimens, these objects occur in the anterior and middle of the body beneath the bivalved carapace (Figures 4A,D,E). Their consistent location between the anterodorsal part of the body and the inner wall of the carapace, as well as the similar size of each ovoid object, all suggest that these clusters are eggs. The eggs are particularly prominent in JY0874 (Figures 4A–C). Clusters seem to consist of a single layer of eggs with no or limited overlap among eggs. Eggs of JY1381 are poorly preserved with more than 121 eggs in the cluster, while those of JY0874 are preserved more clearly, with 153 eggs in the cluster (Table 1). Extrapolation from previous reports on the egg-carrying behavior of Cambrian bivalved arthropods, considering the number of eggs beneath left and right valves to be approximately equal, the total number of †*I. minor* eggs may reach 306 per female

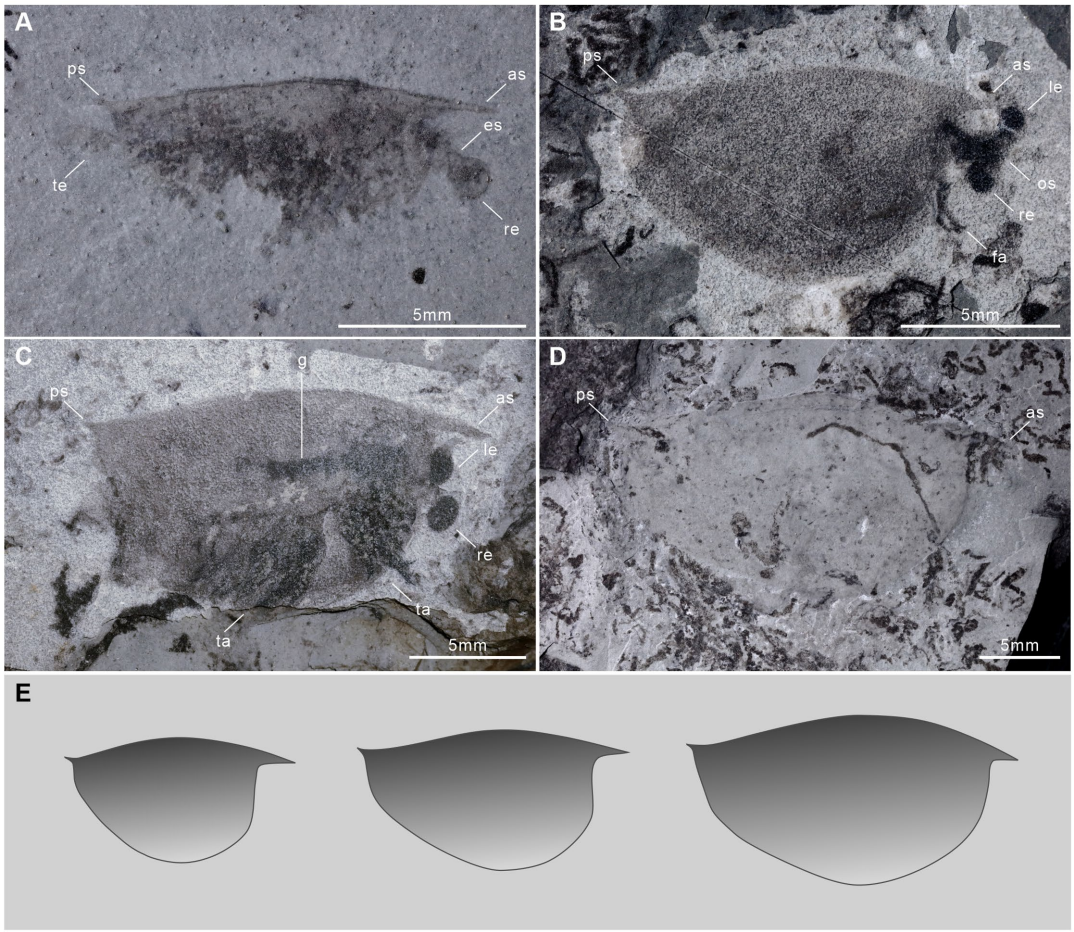

FIGURE 3
†*Isoxys minor* specimens of varying sizes from the Qingjiang biota. **(A)** The small specimen with complete cardinal spines and indistinct telson, showing eye stalk and eye sphere, JY1401. **(B)** The small specimen with complete carapace, a pair of frontal appendages, paired compound eyes and the ocular segment, JY1681A. **(C)** The medium specimen with distinct paired eyes, trunk appendages, and gut, JY1290A. **(D)** The large specimen with complete carapace, JY1491. es, eye stalk; fa, frontal appendages; g, gut; le, left eye; os, ocular segment; re, right eye; ta, trunk appendages. **(E)** The outline of the carapace of a small, medium and large †*I. minor* changes through ontogeny.

(Caron and Vannier, 2016; Ou et al., 2020). Clusters of eggs occupy about 43.87 and 40.52% of the lateral surface area of the valves of each specimen (Figures 4A,B,E). Egg diameter does not vary much within individual clusters, nor between the two specimens, with means of 0.41 mm and 0.47 mm, representing a ratio of *ca.* 2.9% (JY1381) and 3.5% (JY0874) of the valve length (Table 1). The valve length of egg-bearing females is 13.4 mm (JY0874) and 14.2 mm (JY1381). The egg-carrying individuals are small compared to other †*I. minor* from the Qingjiang biota – the carapace length is about half that of the largest specimen of this species (Figure 2E).

4. Discussion

4.1. Intraspecific variation in †*Isoxys minor*

The carapaces of specimens from the Qingjiang and the Guanshan biotas have many same morphological characteristics: (i) valves nearly semicircular (slightly pentagonal), dorsal margin curved, (ii) anterior spines long and strong, posterior spines short and slightly upturned, and (iii) carapace surface smooth (Wang et al., 2012). The outline analysis demonstrates that the specimens from the Guanshan biota are typically slenderer and display a different orientation of the anterior spine than those from the Qingjiang biota (Figures 1B,D). These differences are very slight, and, in fact, our hierarchical clustering analysis (Figure 1C) did not support them being two different species. Such differences are, therefore, considered as intraspecific variation. Other morphological differences visualized in the PCA space, such as the relative length of spines to body length, are shown to change during ontogeny (section below).

The Wulongqing Formation that hosts the Guanshan biota likely represents a shallower setting than most other Cambrian Konservat-Lagerstätten (Hu et al., 2013; Chen et al., 2019, 2020; Ding et al., 2020; Zhao et al., 2020). By contrast, the part of the Shuijingtuo Formation that hosts the Qingjiang biota represents a distal shelf setting, further from the coast and deeper than most other Cambrian Konservat-Lagerstätten (Fu et al., 2019). These two environments may have placed distinct selection pressures on †*I. minor*, both, environmentally, and ecologically, that could possibly have influenced these slight morphological differences. The energy of the environment would

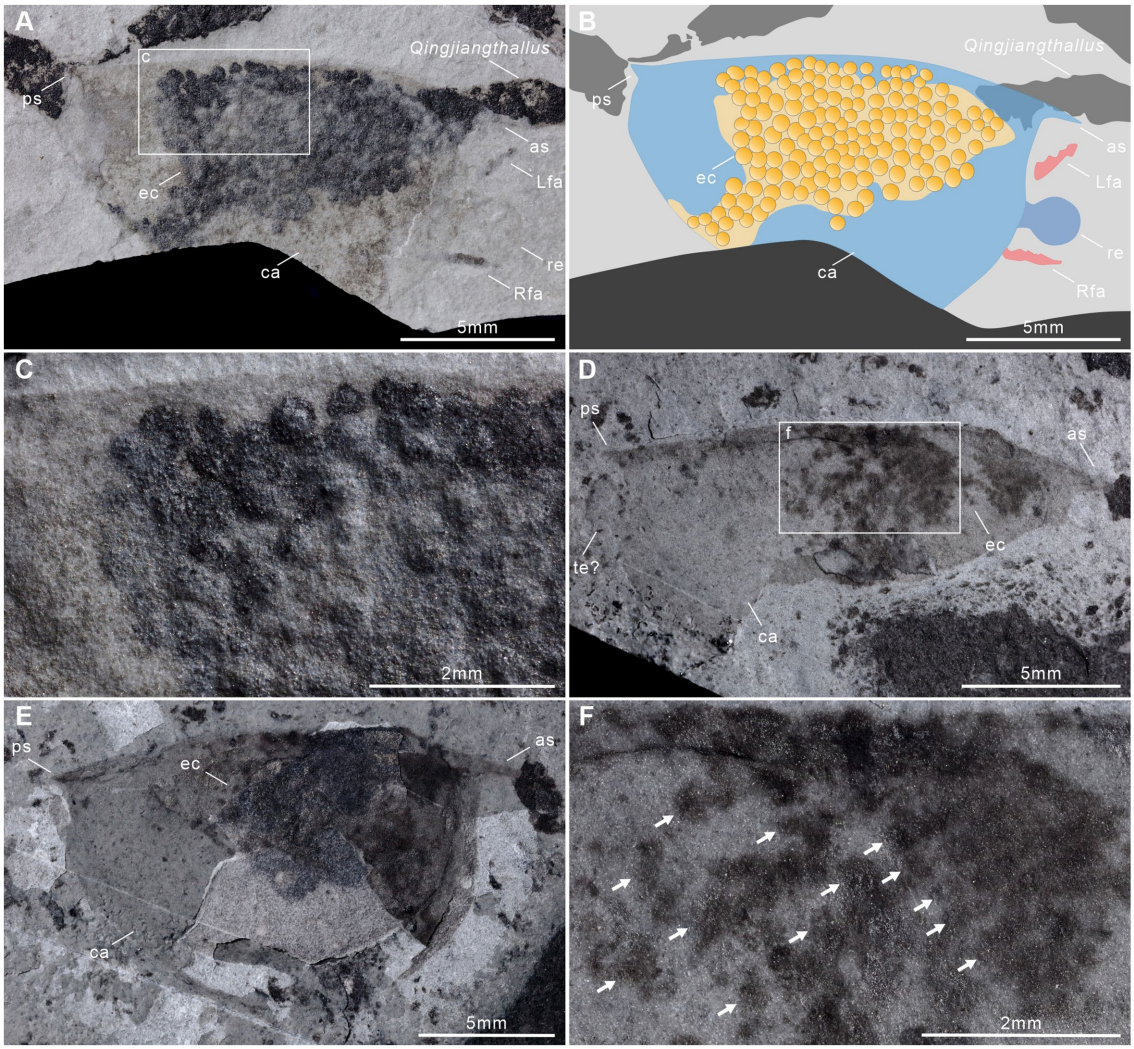

FIGURE 4
Egg clusters in †*Isoxys minor* from the Qingjiang biota. **(A)** Laterally compressed specimen (JY0874) with eggs, surrounded by the red alga (*Qingjiangthallus*). **(B)** Interpretative drawing of **(A)**. **(C)** Detail of egg cluster in **(A)**. **(D)** The incomplete specimen (JY1381B) with poorly-preserved eggs. **(E)** The counterpart of **(D)** with complete carapace, JY1381A. **(F)** Detail of egg cluster in **(D)**. ca, carapace; ec, egg cluster; Lfa, left frontal appendage; Rfa, right frontal appendage.

be expected to be higher in shallower waters (Jiao et al., 2021), thus the observed differences in carapace morphology perhaps may reflect slightly improved streamlining required in higher energy environments and/or to escape from predators, while the upturned and longer anterior spines may have also enhanced antipredation or defense. In addition, the changes of carapaces of †*I. minor* may also facilitate its extensive vertical migration in the water column and improve swimming efficiency, such as the external structure of pelagic halocypridid ostracods plays a role in retarding sinking in the water column (Vannier and Chen, 2000; Perrier et al., 2007).

4.2. Allometric growth of †*Isoxys minor*

Among Cambrian bivalved arthropods, allometric growth is relatively common, for instance the carapace development of †*Isoxys communis* (García-Bellido et al., 2009a) and *Tuzoia bispinosa* (Wen et al., 2015), the ontogeny and trunk segmentation of †*Isoxys auritus* (Fu et al., 2014), and the development of the posterior tagma of †*Chuandianella ovata* (Liu et al., 2022). By contrast, isometric growth is rare in Cambrian bivalved arthropod postembryonic development, having been only reported in the carapace of †*Branchiocaris*? *Yunnanensis* (Wu et al., 2016) and †*C. ovata* (Liu et al., 2021).

In †*Isoxys minor*, allometry is evident in the changing shape of the valve outline, and the relative sizes of eyes and spines to valve length. Both of these latter two features reach the size of those of large individuals early on in ontogeny (Figures 3A–C). †*Isoxys* is a visual predator whose eyes are very effective in order to recognize small prey and provide sufficient depth perception (Vannier et al., 2009; Schoenemann and Clarkson, 2011). Thus, the allometry of eyes of †*I. minor* may indicate that it acquired good vision early on to facilitate predation by small individuals. Generally, the cardinal spines of †*Isoxys* are thought to play an indirect role in locomotion and be helpful in defending against predators (Williams et al., 1996;

TABLE 1 Measurements of ovigerous specimens of Cambrian bivalved arthropods.

Specimen	Occurrence	*N*	Min *D* (mm)	Max *D* (mm)	Ave *D* (mm)	Tl (mm)	Vl (mm)	Vh (mm)	Es (mm^2)	*Vs* (mm^2)	Es/*Vs* (%)
†*Isoxys minor*											
JY0874	Qingjiang biota	153	0.38	0.56	0.47	NA	13.4	NA	38.89	88.65*	43.87
JY1381	Qingjiang biota	>121	0.37	0.48	0.43	NA	14.2	9.7	41.97	103.57	40.52
†*Chuandianella ovata* (Ou et al., 2020)											
ELEL-SJ081254	Chengjiang biota	50	0.41	0.59	0.52	22.50	9.88	6.56	10.62	50.95	20.84
ELEL-MF140101	Chengjiang biota	38	0.44	0.62	0.55	22.85	9.80	6.40	7.51	46.26	16.23
†*Waptia fieldensis* (Caron and Vannier, 2016; Ou et al., 2020)											
ROM 63357	Burgess Shale	13	2.25	2.62	2.4	63.7	20.7	NA	58.8	288*	20.4
ROM 63354	Burgess Shale	12	2.06	2.36	2.18	NA	19.6	17.0	44.8	280	16.0
†*Kunmingella douvillei* (Duan et al., 2014)											
ELI-YLS-1001A	Chengjiang biota	57	0.12	0.23	0.15	NA	4.91	3.69	4.55	17.86	25.48
ELI-EJ-0209A	Chengjiang biota	40	0.04	0.11	0.08	NA	NA	NA	NA	NA	NA

Ave *D*, average diameter of eggs; Es, egg cluster surface area; Es/Cs, ratio of Es to *Vs*; Max *D*, maximum diameter of eggs; Min *D*, minimal diameter of eggs; *N*, number of eggs (unilateral carapace); NA, not applicable; Tl, total length; Vh, valve height; Vl, valve length; *Vs*, valve surface area; *, extrapolated measurement.

Vannier and Chen, 2000; Luo et al., 2006; Liu et al., 2018; Pates et al., 2021). For †*Isoxys minor*, the allometric growth indicates that the spines more likely played a defensive rather than hydrodynamic role. The relatively larger size of the spines in smaller individuals indicates a defensive or deterrent role, which became reduced during ontogeny. This is comparable to the spiny carapaces of some extant malacostracan larvae (e.g., Vannier and Chen, 2000, Figure 11), which deter predation by fish but do not play a clear hydryodynamic role (Morgan, 1989; Vannier and Chen, 2000; García-Guerrero et al., 2006). By contrast, hydrodynamic streamlining would become more important at larger sizes, at higher Reynolds numbers. In †*Isoxys minor*, spines are shorter relative to body size in larger individuals, indicating that the changing morphology with growth in this species does not lead to improved hydrodynamic performance.

4.3. Brood care of †*Isoxys minor*

Since male egg-carrying is generally a rare phenomenon in extant arthropods (Trumbo, 2012; Caron and Vannier, 2016), it is most likely that the egg-carrying specimens represent mature females. The two ovigerous individuals from the Qingjiang biota are smaller and the carapace length is about half that of the largest specimen of this species (Figure 2E). This suggests that †*I. minor* may have possessed reproductive ability during comparatively early stages of development, and kept growing after becoming sexually mature. Detection of potential sexual dimorphism is precluded by the small sample size.

Egg clusters of †*I. minor* represent another record of brood care using carapaces in early arthropods. The dark stain around the egg clusters might be the remnants of mucus or other adhesive substances extruded from the eggs. There is no evidence of egg stalks or ovigerous setae in †*I. minor*, but the compact arrangement of eggs indicates that they may be attached to the inner wall of the carapace, similar to what has been observed in waptiids and extant branchiopod crustaceans (e.g., *Limnadia texana*) (Caron and Vannier, 2016; Ou et al., 2020). This location might have provided the eggs with optimal protection against physical damage, predators, and might have formed a suitable microenvironment to limited parasite or fungal infestation (Caron and Vannier, 2016). Movement of the trunk appendages might also have generated water currents between the body and the carapace to ensure ventilation over egg clusters (Ou et al., 2020). A coeval bivalved arthropod †*Kunmingella douvillei* carried eggs using three pairs of posterior appendages, although the type of its brood care was different from †*I. minor*, the carapaces also provided protection (Duan et al., 2014). Therefore, the bivalved carapace is pivotal to egg protection and incubation.

4.4. Reproductive trade-off in Cambrian arthropods

Trade-offs play a crucial role in the reproduction of organisms, which enhance their adaptations to the environment to obtain the maximum available resources by choosing between the offspring number and energy allocated to individual offspring (e.g., nutrition, parental care, etc.). Different organisms differ not only in exoskeleton and soft anatomy but also in their egg production. By comparing the brood care in Cambrian arthropods, we explored the evidence of trade-offs in reproduction of different taxa.

Egg clutches of †*I. minor* are attached between the inner surface of the carapace and the body, like †*Waptia fieldensis* and †*C. ovata* (Caron and Vannier, 2016; Ou et al., 2020; Liu, 2022). By contrast, the eggs of †*K. douvillei* are carried by the endopods and gathered ventrally (Duan et al., 2014). In spite of the similar valve length and egg size of ovigerous specimens between †*I. minor* and †*C. ovata*, †*I. minor* (≤306 per clutch; Ø, ~0.45 mm) has approximately three times as many eggs as †*C. ovata* (≤100 per clutch; Ø, ~0.5 mm) (Table 1). In addition, the brooded egg mass occupies a larger proportion (up to 40%) of †*I. minor* valve surface (Es/*Vs*), and a similar and small proportion (*ca.* 20–25%) of the valve surface of other Cambrian arthropods, which might correspond to their maximum brooding capacity. †*W. fieldensis* has a small clutch size of up to 26

eggs with a large mean diameter (Ø, ~2.0 mm) in well-preserved specimens, which is obviously different from the other three species (Figure 5; Table 1).

Our findings identify the distinct brooding strategy of the Cambrian arthropods: a mature female of †*I. minor* can brood an extremely high number of small eggs, those of †*C. ovata* and †*K. douvillei* brooded a relatively large number of small eggs, whereas those of †*W. fieldensis* carried a low number of large eggs (Figure 5). The largest number of small eggs might have allowed †*I. minor* to maximize the offspring number while investing minimum resources in each one. By comparison, the large and yolky eggs in †*W. fieldensis* might supply offspring with greater nutrient during embryonic development in response to adverse environmental factors (Fox and Czesak, 2000). Hence, †*W. fieldensis* greatly reduces the egg number, while increasing the brood care and the probability for individual offspring to survive to adulthood. Cambrian arthropods reproduced with trade-offs between the quantity and quality of their offspring: †*W. fieldensis* chooses to invest more resources for offspring; †*I. minor*, †*C. ovata*, and †*K. douvillei* choose to increase the offspring number to improve individual survival, and in particular †*I. minor* is an extreme case of this strategy in Cambrian arthropods where egg clutches have been observed.

4.5. Survival strategy of †*Isoxys minor* and evolutionary implications of brood care

A dominant species is one that has high abundance compared to other species in the same community, having proportionate effects on environmental conditions, community diversity, and ecosystem function (Avolio et al., 2019). †*I. minor* is the dominant species of †*Isoxys* in both Qingjiang and Guanshan biotas. At present, a total of 85 †*Isoxys* specimens have been identified from the Qingjiang biota, among which 51 are recognized as †*I. minor* (*ca.* 60% of †*Isoxys*). According to previous reports, there are more than 300 †*I. minor* specimens from the Guanshan biota (up to 96.7% of †*Isoxys*), while no more than 10 specimens of other species (Huang and Wang, 2014; Wang, 2014). Based on the study of †*I. minor* from the Qingjiang biota, we assumed that it may have become the dominant species in the two biotas by improving its interspecific competitiveness through allometric growth and r-strategy of reproducing: (i) cardinal spines and eyes have reached the size of those of large individuals in the early stage, which is beneficial for self-protection and foraging, thus increasing small individual survival, (ii) it may have possessed reproductive ability during the early stage of development, allowing it to move quickly into breeding, and (iii) it improves the survival rate of offspring by maximizing egg production. To sum up, these three aspects may have contributed to the dominance of †*I. minor* in the interspecific competition, and thus it gradually became the dominant species in the two biotas.

The position of †*Isoxys* as an early diverging deuteropod (e.g., Fu et al., 2022) also makes this taxon the earliest diverging arthropod from which brood care has been described. Brood care has appeared very early in arthropod evolution well before the first mandibulates (e.g., *Waptia*, *Chuandianella*) appeared. At the same time, primitive arthropods seem to favor r-strategy of reproducing, and with the evolution of arthropods, parents gradually reduce the number of offspring and invest more in quality. Thus, this life strategy appears to have had a deep root in the phylum, and evolved multiple times within the group.

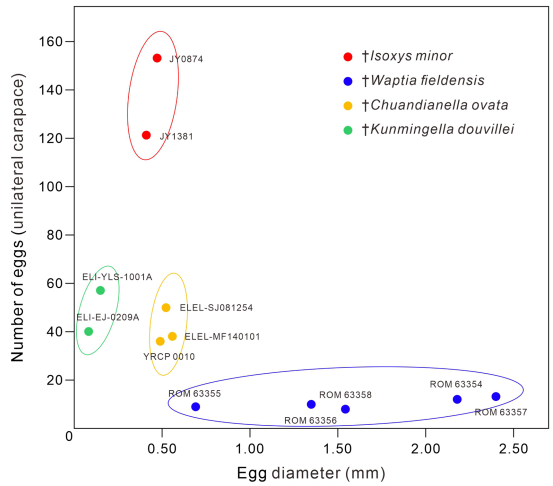

FIGURE 5
Diameter versus number of eggs brooded (unilateral carapace) by Cambrian arthropods.

Data availability statement

The original contributions presented in the study are included in the article/Supplementary material, further inquiries can be directed to the corresponding author.

Author contributions

DF conceived the project. JM interpreted the fossil material and wrote the draft manuscript. SP was involved in analyzing the fossil morphology and discussing the results. YW, WL, CL, YHW, and MZ were involved in discussing the method and the results. All authors contributed to the article and approved the submitted version.

Funding

This research was supported by funds from the Natural Science Foundation of China (41930319, 41890844, and 42242201), the Strategic Priority Research Program of the Chinese Academy of Sciences (XDB26000000), and 111 Project (D17013), Natural Science Basic Research Plan of Shaanxi Province (2022JC-DW5-01). SP was supported by a Herchel Smith Postdoctoral Fellowship (University of Cambridge).

Acknowledgments

The authors are grateful to Jean Vannier, Yu Liu, and Brigitte Schoenemann for constructive comments on the manuscript.

Conflict of interest

The authors declare that the research was conducted in the absence of any commercial or financial relationships that could be construed as a potential conflict of interest.

Publisher's note

All claims expressed in this article are solely those of the authors and do not necessarily represent those of their affiliated organizations, or those of the publisher, the editors and the reviewers. Any product that may be evaluated in this article, or claim that may be made by its manufacturer, is not guaranteed or endorsed by the publisher.

Supplementary material

The Supplementary material for this article can be found online at: https://www.frontiersin.org/articles/10.3389/fevo.2023.1174564/full#supplementary-material

References

Aria, C., and Caron, J. B. (2015). Cephalic and limb anatomy of a new Isoxyid from the burgess shale and the role of "stem bivalved arthropods" in the disparity of the frontalmost appendage. *PLoS One* 10:e0124979. doi: 10.1371/journal.pone.0124979

Avolio, M. L., Forrestel, E. J., Chang, C. C., La Pierre, K. J., Burghardt, K. T., and Smith, M. D. (2019). Demystifying dominant species. *New Phytol.* 223, 1106–1126. doi: 10.1111/nph.15789

Bonhomme, V., Picq, S., Gaucherel, C., and Claude, J. (2014). Momocs: outline analysis using R. *J. Stat. Softw.* 56, 1–24. doi: 10.18637/jss.v056.i13

Bouton, G. D. (2008). Corel DRAW: The official guide (Mcgraw-hill Osborne), ISBN: 9780071545709.

Briggs, D. E. G., Lieberman, B. S., Hendricks, J. R., Halgedahl, S. L., and Jarrard, R. D. (2008). Middle Cambrian arthropods from Utah. *J. Paleontol.* 82, 238–254. doi: 10.1666/06-086.1

Burger, W., and Burge, M. J. (2006). Image J. Springer Berlin Heidelberg Press.

Butterfield, N. J., and Nicholas, C. J. (1994). Exceptionally preserved fossils from the lower-middle Cambrian mount cap formation, Northwest Territories, Canada. *Palaeontology Newsletter* 24:16.

Caron, J. B., and Vannier, J. (2016). Waptia and the diversification of brood care in early arthropods. *Curr. Biol.* 26, 69–74. doi: 10.1016/j.cub.2015.11.006

Chen, F., Brock, G. A., Zhang, Z., Laing, B., Ren, X., and Zhang, Z. (2020). Brachiopod-dominated communities and depositional environment of the Guanshan Konservat-Lagerstätte, eastern Yunnan, China. *J. Geol. Soc.* 178, 1–19. doi: 10.1144/jgs2020-043

Chen, F., Zhang, Z., Betts, M. J., Zhang, Z., and Liu, F. (2019). First report on Guanshan biota (Cambrian stage 4) at the stratotype area of Wulongqing formation in Malong County, eastern Yunnan, China. *Geosci. Front.* 10, 1459–1476. doi: 10.1016/j.gsf.2018.09.010

Ding, Y., Liu, J., and Chen, F. (2020). Ichnology, palaeoenvironment, and ecosystem dynamics of the early Cambrian (stage 4, series 2) Guanshan biota, South China. *Geol. J.* 55, 77–94. doi: 10.1002/gj.3360

Du, K., Ortega-Hernández, J., Yang, J., Yang, X., Guo, Q., Li, W., et al. (2020). A new early Cambrian Konservat-Lagerstätte expands the occurrence of burgess shale-type deposits on the Yangtze platform. *Earth Sci. Rev.* 211:103409. doi: 10.1016/j.earscirev.2020.103409

Duan, Y., Han, J., Fu, D., Zhang, X., Yang, X., Komiya, T., et al. (2014). Reproductive strategy of the bradoriid arthropod Kunmingella douvillei from the lower Cambrian Chengjiang Lagerstätte, South China. *Gondwana Res.* 25, 983–990. doi: 10.1016/j.gr.2013.03.011

Fox, C. W., and Czesak, M. E. (2000). Evolutionary ecology of progeny size in arthropods. *Annu. Rev. Entomol.* 45, 341–369. doi: 10.1146/annurev.ento.45.1.341

Fu, D., Legg, D. A., Daley, A. C., Budd, G. E., Wu, Y., and Zhang, X. (2022). The evolution of biramous appendages revealed by a carapace-bearing Cambrian arthropod. *Phil. Trans. R. Soc. B* 377:20210034. doi: 10.1098/rstb.2021.00342022

Fu, D., Tong, G., Dai, T., Liu, W., Yang, Y., Zhang, Y., et al. (2019). The Qingjiang biota—a burgess shale-type fossil Lagerstätte from the early Cambrian of South China. *Science* 363, 1338–1342. doi: 10.1126/science.aau8800

Fu, D., Zhang, X., Budd, G. E., Liu, W., and Pan, X. (2014). Ontogeny and dimorphism of Isoxys auritus (Arthropoda) from the early Cambrian Chengjiang biota, South China. *Gondwana Res.* 25, 975–982. doi: 10.1016/j.gr.2013.06.007

Fu, D., Zhang, X., and Shu, D. (2011). Soft anatomy of the early Cambrian arthropod Isoxys curvirostratus from the Chengjiang biota of South China with a discussion on the origination of great appendages. *Acta Palaeontol. Pol.* 56, 843–852. doi: 10.4202/app.2010.0090

García-Bellido, D. C., Paterson, J. R., Edgecombe, G. D., Jago, J. B., Gehling, J. G., and Lee, M. S. Y. (2009a). The bivalved arthropods Isoxys and Tuzoia with soft-part preservation from the lower Cambrian Emu Bay shale Lagerstätte (Kangaroo Island, Australia). *Palaeontology* 52, 1221–1241. doi: 10.1111/j.1475-4983.2009.00914.x

García-Bellido, D. C., Vannier, J., and Collins, D. (2009b). Soft-part preservation in two species of the arthropod Isoxys from the middle Cambrian burgess shale of British Columbia, Canada. *Acta Palaeontol. Pol.* 54, 699–712. doi: 10.4202/app.2009.0024

García-Guerrero, M. U., Rodríguez, A., and Hendrickx, M. E. (2006). Larval development of the eastern Pacific anomuran crab Porcellana cancrisocialis (Crustacea: Decapoda: Anomura: Porcellanidae) described from laboratory reared material. *J. Mar. Biol. Assoc. UK* 86, 1123–1132. doi: 10.1017/S002531540601410X

Glaessner, M. F. (1979). Lower Cambrian Crustacea and annelid worms from Kangaroo Island, South Australia. *Alcheringa* 3, 21–31. doi: 10.1080/03115517908565437

Hou, X. (1987). Early Cambrian large bivalved Arthropoda from Chengjiang, Eastern Yunnan. *Acta Palaeontol. Sinica* 26, 286–298. [in Chinese with English abstract]

Hu, S., Zhu, M., Luo, H., Steiner, M., Zhao, F., Li, G., et al. (2013). *The Guanshan biota*. Yunnan Science and Technology Press, Yunnan.

Huang, D., and Wang, Y. (2014). The soft anatomy of Isoxys minor from the Guanshan fauna, lower Cambrian of Southwest China. *Palaeoworld* 23, 225–228. doi: 10.1016/j.palwor.2014.10.006

Ivantsov, A. I. (1990). Pervye hakhodki fillokarid v nizhnem kembrii Iakutii. *Palaeontologičeskij Žurnal* 34, 130–132. [in Russian]

Ivantsov, A. I. (2005). "Tardipolypodians, 112–113" in *Unique Sinsk localities of early Cambrian organisms (Siberian platform)*. ed. A. G. Ponomarenko (Moscow: Nauka) [in Russian]

Jiao, D., Pates, S., Lerosey-Aubril, R., Ortega-Hernández, J., Yang, J., Lan, T., et al. (2021). The endemic radiodionts of the Cambrian stage 4 Guanshan biota of South China. *Acta Palaeontol. Pol.* 66, 255–274. doi: 10.4202/app.00870.2020

Legg, D. A., and Vannier, J. (2013). The affinities of the cosmopolitan arthropod Isoxys and its implications for the origin of arthropods. *Lethaia* 46, 540–550. doi: 10.1111/let.12032

Li, R., Cui, L., Fu, D., and Zhang, X. (2022). A new red alga preserved with possible reproductive bodies from the 518-million-year-old Qingjiang biota. *J. Syst. Evol.* 1–11. doi: 10.1111/jse.12942

Liu, C. (2022). Cambrian arthropod Chuandianella ovata: morphology, taxonomy, ontogeny, ecology, mineralization and phylogeny. PhD thesis, Northwest University. [in Chinese with English abstract]

Liu, C., Fu, D., and Zhang, X. (2021). Phosphatic carapace of the waptiid arthropod Chuandianella ovata and biomineralization of ecdysozoans. *Palaeontology* 64, 755–763. doi: 10.1111/pala.12570

Liu, C., Fu, D., and Zhang, X. (2022). Developmental dynamics is revealed in the early Cambrian arthropod Chuandianella ovata. *iScience* 25:103591. doi: 10.1016/j.isci.2021.103591

Liu, S., Peng, J., Wen, R., and Liang, B. (2018). New data for Isoxys of the Balang Fauna (Cambrian stage 4), South China. *Bull. Geosci.* 93, 147–162. doi: 10.3140/bull.geosci.1673

Luo, H., Fu, X., Hu, S., Li, Y., Chen, L., You, T., et al. (2006). New bivalved arthropods from the early Cambrian Guanshan fauna in the Kunming and Wuding area. *Acta Palaeontol. Sin.* 45, 460–472. [in Chinese with English summary]

Luo, H., Li, Y., Hu, S., Fu, X., Hou, S., Liu, X., et al. (2008). *Early Cambrian Malong Fauna and Guanshan Fauna from Eastern Yunnan, China*. Yunnan: Yunnan Science and Technology Press.

Luo, H., Hu, S., Chen, L., Zhang, S., and Tao, Y. (1999). *Early Cambrian Chengjiang Fauna from Kunming region*. 129 pp. Yunnan Science of Technology Press, Kunming. [in Chinese with English summary]

Ma, J., Lin, W., Liu, C., Sun, A., Wu, Y., Wu, Y., et al. (2021). A new bivalved arthropod from the Cambrian (stage 3) Qingjiang biota expands the palaeogeographical distribution and increases the diversity of Tuzoiidae. *J. Geol. Soc.* 179:jgs2020-229. doi: 10.1144/jgs2020-229

Morgan, S. G. (1989). Adaptive significance of Spination in estuarine crab Zoeae. *Ecology* 70, 464–482. doi: 10.2307/1937551

Nielsen, M. L., Rasmussen, J. A., and Harper, D. A. T. (2017). Sexual dimorphism within the stem-group arthropod Isoxys volucris from the Sirius Passet Lagerstätte, North Greenland. *Bull. Geol. Soc. Den.* 65, 47–58. doi: 10.37570/bgsd-2017-65-04

Ou, Q., Vannier, J., Yang, X., Chen, A., Mai, H., Shu, D., et al. (2020). Evolutionary trade-off in reproduction of Cambrian arthropods. *Sci. Adv.* 6, eaaz3376–eaaz3405. doi: 10.1126/sciadv.aaz3376

Pates, S., Daley, A. C., Legg, D. A., and Rahman, I. A. (2021). Vertically migrating Isoxys and the early Cambrian biological pump. *Proc. R. Soc. B* 288:20210464. doi: 10.1098/rspb.2021.0464

Perrier, V., Vannier, J., and Siveter, D. J. (2007). The Silurian pelagic myodocope ostracod Richteria migrans. *Earth Environ. Sci. Trans. R. Soc. Edinb.* 98, 151–163. doi: 10.1017/S1755691007006147

Press, A. (2010). Adobe Photoshop CS5- classroom in a book. *J. Vis. Commun. Med.* 34, 125–152. doi: 10.3109/17453054.2011.604842

R Core Team. (2021). *R: a language and environment for statistical computing*. R Foundation for Statistical Computing, Vienna, Austria. Available at: https://www.R-project.org/

Richter, R., and Richter, E. (1927). Eine Cruseacee (Isoxys carbonelii n. sp.) in den Archaeocyathus-Bildungen der Sierra Morena und ihre stratigraphische Beurteilung. *Senckenbergiana* 9, 188–195.

Schoenemann, B., and Clarkson, E. N. (2011). Eyes and vision in the Chengjiang arthropod Isoxys indicating adaptation to habitat. *Lethaia* 44, 223–230. doi: 10.1111/j.1502-3931.2010.00239.x

Shu, D., Zhang, X., and Geyer, G. (1995). Anatomy and systematic affinities of the lower Cambrian bivalved arthropod Isoxys auritus. *Alcheringa* 19, 333–342. doi: 10.1080/03115519508619512

Simonetta, A. M., and Delle Cave, L. D. (1975). The Cambrian non-trilobite arthropods from the burgess shale of British Columbia. A study of their comparative morphology, taxonomy and evolutionary significance. *Palaeontogr. Ital.* 69, 1–37.

Stein, M., Peel, J. S., Siveter, D. J., and Williams, M. (2010). Isoxys (Arthropoda) with preserved soft anatomy from the Sirius Passet Lagerstätte, lower Cambrian of North Greenland. *Lethaia* 43, 258–265. doi: 10.1111/j.1502-3931.2009.00189.x

Trumbo, S. T. (2012). "Patterns of parental care in invertebrates" in *The evolution of parental care*. eds. N. J. Royle, P. T. Smiseth and M. Kölliker. *First* ed (Oxford University Press, New York), 81–100.

Vannier, J., and Chen, J. (2000). The early Cambrian colonization of pelagic niches exemplified by Isoxys (Arthropoda). *Lethaia* 33, 295–311. doi: 10.1080/00241600750053862

Vannier, J., García-Bellido, D. C., Hu, S., and Chen, A. (2009). Arthropod visual predators in the early pelagic ecosystem: evidence from the burgess shale and Chengjiang biotas. *Proc. R. Soc. Lond. B Biol. Sci.* 276, 2567–2574. doi: 10.1098/rspb.2009.0361

Vannier, J., Williams, M., Alvaro, J. J., Vizcaïno, D., Monceret, S., and Monceret, E. (2005). New early Cambrian bivalved arthropods from southern France. *Geol. Mag.* 142, 751–763. doi: 10.1017/S0016756805001093

Wang, Y. (2014). The diversity and systematics of Isoxys and Tuzoia from the Cambrian of China. PhD thesis, Nanjing Institute of Geology and Palaeontology, Chinese Academy of Science. [in Chinese with English abstract].

Wang, Y., Huang, D., and Lieberman, B. S. (2010). New Isoxys (Arthropoda) from the Cambrian, Mantou Fromation, Shandong Province. *Acta Palaeontol. Sinica* 49, 398–406. [in Chinese with English abstract]

Wang, Y., Huang, D., Liu, Q., and Hu, S. (2012). Isoxys from the Cambrian Guanshan Fauna, Yunnan Province. *Earth Sci. J China University Geosci.* 37, 156–164. doi: 10.3799/dpkx.2012.So.016

Wen, R., Zhao, Y., and Peng, J. (2015). Morphology and ontogeny of Tuzoia bispinosa from the Kaili biota (Cambrian stage 5) of eastern Guizhou, China. *Palaeoworld* 24, 61–70. doi: 10.1016/j.palwor.2014.12.005

Williams, M., Siveter, D. J., and Peel, J. S. (1996). Isoxys (Arthropoda) from the early Cambrian Sirius Passet Lagerstätte, North Greenland. *J. Paleontol.* 70, 947–954. doi: 10.1017/S0022336000038646

Wu, Y., Fu, D., Zhang, X., Daley, A. C., and Shu, D. (2016). Dimorphism of Bivalved arthropod Branchiocaris? Yunnanensis from the early Cambrian Chengjiang biota, South China. *Acta Geol. Sinica* 90, 818–826. doi: 10.1111/1755-6724.12725

Zhao, J., Li, Y., Selden, P. A., and Cong, P. (2020). New occurrence of the Guanshan Lagerstätte (Cambrian series 2, stage 4) in the Kunming area, Yunnan, Southwest China, with records of new taxa. *Alcheringa An Australasian J. Palaeontol.* 44, 343–355. doi: 10.1080/03115518.2020.1781257

Zhao, Y., Zhu, M., Babcock, L. E., and Peng, J. (2011). *The Kaili biota-marine organisms from 508 million years ago*. 251 Guizhou Science and Technology Press, Guiyang.

Zhao, Y., Zhu, M., Babcock, L. E., Yuan, J., Parsley, R. L., and Peng, J. (2005). Kaili biota: a taphonomic window on diversification of metazoans from the basal middle Cambrian: Guizhou, China. *Acta Geol. Sinica* 79, 751–765. doi: 10.1111/j.1755-6724.2005.tb00928.x

frontiers | Frontiers in Earth Science

TYPE Original Research
PUBLISHED 27 June 2023
DOI 10.3389/feart.2023.1210062

OPEN ACCESS

EDITED BY
Bertrand Lefebvre,
Université Claude Bernard Lyon 1, France

REVIEWED BY
Martin Vinther Sørensen,
University of Copenhagen, Denmark
Deng Wang,
Northwest University, China
Timothy Topper,
Swedish Museum of Natural History, Sweden

*CORRESPONDENCE
Yunhuan Liu,
yunhuanl@chd.edu.cn
Tiequan Shao,
stotto@163.com

RECEIVED 21 April 2023
ACCEPTED 14 June 2023
PUBLISHED 27 June 2023

CITATION
Qin J, Liu Y, Shao T, Liu M and Zhang Y (2023), Growth pattern of Fortunian scalidophoran sclerites.
Front. Earth Sci. 11:1210062.
doi: 10.3389/feart.2023.1210062

Growth pattern of Fortunian scalidophoran sclerites

Jiachen Qin, Yunhuan Liu*, Tiequan Shao*, Mingjin Liu and Yanan Zhang

School of Earth Science and Resources, Chang'an University, Xi'an, China

Fortunian scalidophoran worms have shown high diversity, with 7 genera and species and 10 indeterminate forms. Current studies have mainly focused on morphology as well as early evolution, and studies on ontogeny have not been carried out due to the limited number of specimens. Here, we report new material of an Orsten-type preserved Indeterminate Form 3 from the Zhangjiagou section. Collected specimens of Indeterminate Form 3 with different annulus widths indicate the presence of several ontogenetic stages. We found newly formed sclerites on the annulus of Indeterminate Form 3 at different ontogenetic stages, suggesting that the sclerites of Indeterminate Form 3 become more numerous in addition to increasing in size during growth. The size of the large sclerites may also increase as the worms grow, however, their number may not change.

KEYWORDS

scalidophora, ontogeny, Fortunian stage, Zhangjiagou section, South China

1 Introduction

As the earliest unambiguous fossil record of ecdysozoans, scalidophorans showed high diversity during the early Cambrian Fortunian stage (~535 Ma), with 7 genera and species and 10 indeterminate forms (Liu et al., 2014a; 2019; Zhang et al., 2015; 2018; Shao et al., 2018a; 2020a; 2020b; Zhang, 2021; Qin et al., 2023). This is consistent with the hypothesis of molecular clock studies, which posits cycloneuralians may have originated in the Ediacaran and radiated during the early Cambrian period (Rota-Stabelli et al., 2013; dos Reis et al., 2016; Erwin. 2020).

These fossils have gone through three-dimensional phosphatization, i.e., Orsten-type preservation (Maas et al., 2006). Orsten-type fossils preserve the most primitive three-dimensional structures of organisms. This facilitates the reconstruction of body structures and means Orsten-type fossils are more conducive to the discussion of morphological functions, affinities, and paleoecology. In addition, the preservation of Orsten-types can preserve successive developmental stages of a species, thus facilitating the reconstruction of ontogeny (Maas et al., 2006). Contemporaneous cnidarians (*Olivooides*, *Quadrapyrgites*, *Qinscyphus*, and *Hexaconularia*) have been found in a large number of fossils at different developmental stages, and more complete developmental sequences have been established on this basis (Dong et al., 2013; Han et al., 2013; Liu et al., 2014b; 2017; Steiner et al., 2014; Wang et al., 2017; Shao et al., 2018b; Zhang et al., 2023). In more recent strata, the developmental patterns of some paleoscolecids have also been discussed (Brock and Cooper, 1993; Müller and HinzSchallreuter, 1993; Zhang and Pratt, 1996; Duan and Dong, 2013; Xian et al., 2023).

In contrast to those, most Fortunian scalidophoran fossils are fragmented, and except for a little preserved introvert information, most of them only preserve the trunk part. The fossils of Fortunian scalidophorans are also relatively rare, and most of the species are only

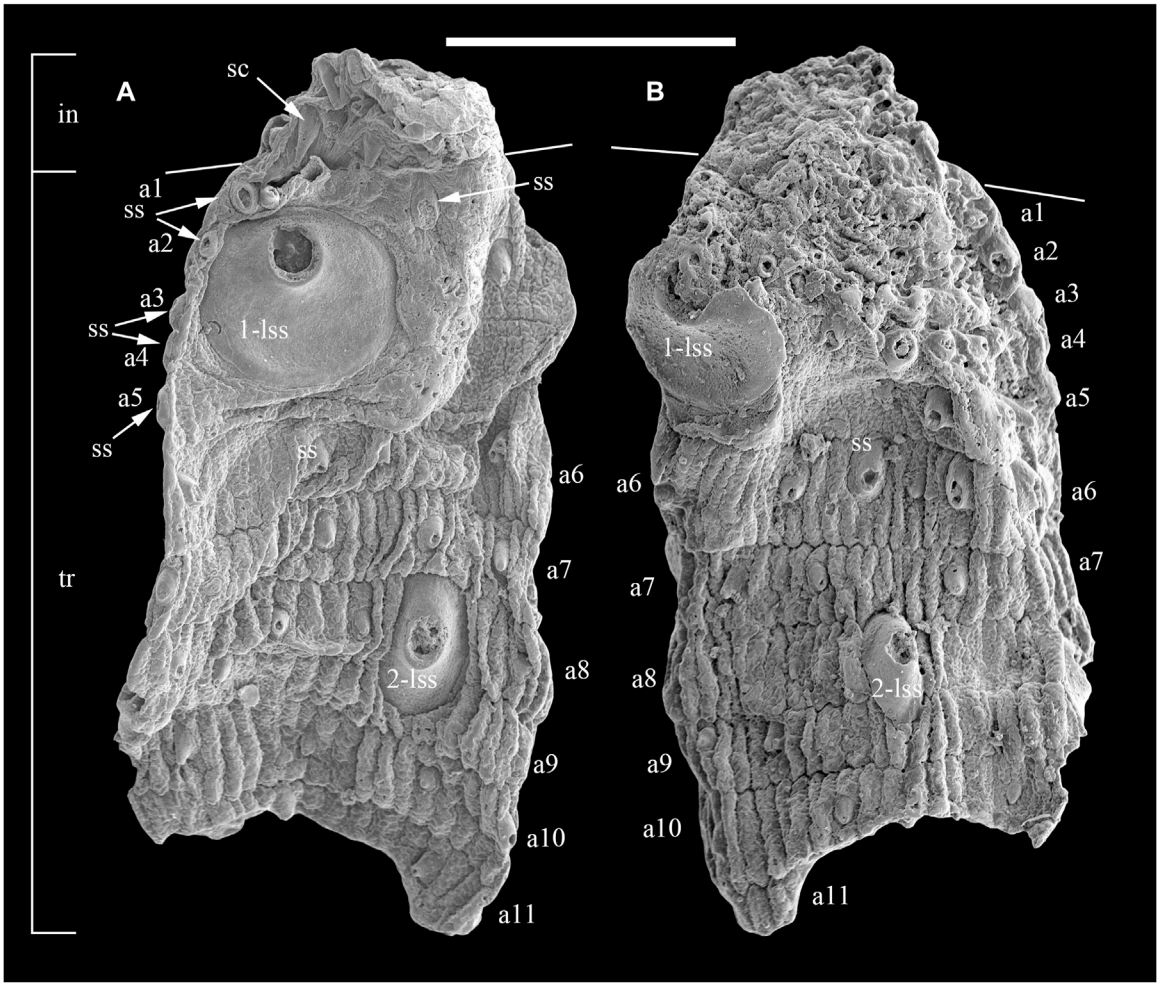

FIGURE 1
SEM images of Indeterminate Form 3 *sensu* Liu et al., 2019 from the Fortunian Zhangjiagou Section. **(A and B)** Two opposite sides of UMCU 23XX01. Abbreviations: in, introvert; tr, trunk; sc, scalid; ss, spinose sclerite; 1-lss, first large spinose sclerite; 2-lss, second large spinose sclerite; (a1–a11), the 1st to 11th annuli. The scale bar represents 500 μm.

represented by a single specimen. Thus, the previous studies mainly focus on morphology, while a study of ontogenetic development has not been carried out.

Here, we describe a new specimen of Indeterminate Form 3 *sensu* Liu et al., 2019 (hereafter referred to as Form 3), which has narrower annuli and is probably at a younger developmental stage than the specimens already reported. This specimen also has a smaller number of sclerites and preserves some sclerites that are not yet fully developed. It is suggested that Form 3's armor will change as it grows, mainly by appearing larger and having more sclerites as it grows.

2 Material and methods

The studied specimens are now deposited at the University Museum of Chang'an University (UMCU), Xi'an, China. They were collected from the bottom of the Kuanchuanpu Formation in the Zhangjiagou section, Xijiang Country, Southern Shaanxi. This fossil-rich horizon falls within the *Anabarites trisulcatus—Protohertzina anabarica* Assemblage Zone, with an estimated age of 531.8–536.4 Ma (Steiner et al., 2007; 2014), and belongs to the Fortunian Stage (Peng et al., 2020).

Rock samples were processed through standard acetic acid etching methods. Fossils were obtained from the undissolvable residues and picked out under a binocular microscope. Selected microfossils were mounted on stubs and coated with gold for observation under a Quanta 650 field-emission environmental scanning electron microscope at Chang'an University.

The specimens were measured using the ruler tool in Adobe Photoshop CS5, and the annuli with less deformation were mainly selected for the measurement.

3 Systematic paleontology

Ecdysozoa Aguinaldo et al., 1997.
Cycloneuralia Ahlrichs, 1995.

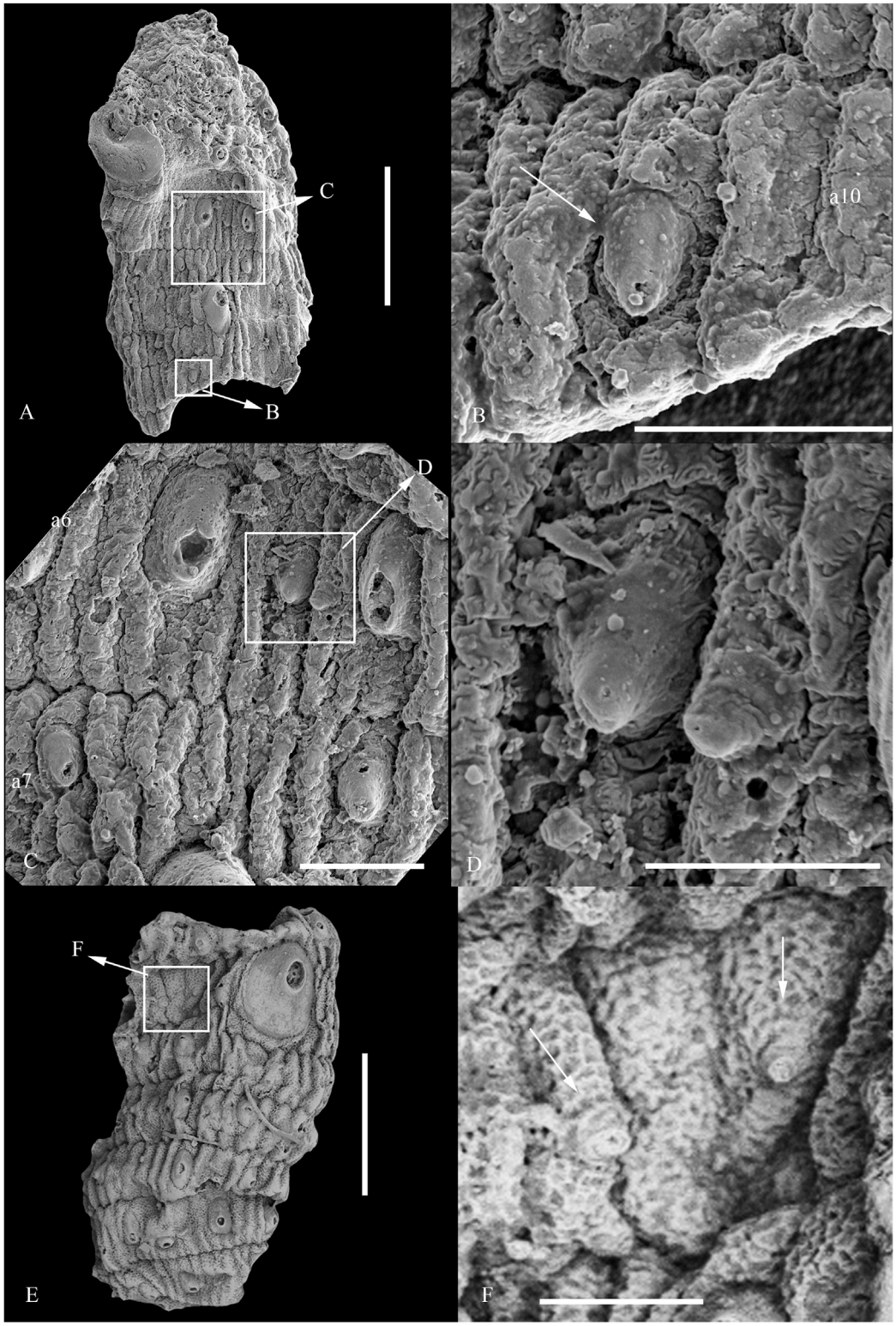

FIGURE 2
Newly formed sclerites of Indeterminate Form 3 *sensu* Liu et al., 2019. **(A–D)** UMCU 23XX01; **(E–F)** UMCU 22XX02; **(B–C)** close-up of A; **(D)** close-up of C; **(F)** close-up of **(E)**. The scale bars represent 500 μm **(A and E)**, 100 μm (B, C, and **(F)**, and 50 μm **(D)**.

Scalidophora Lemburg, 1995.
Indeterminate Form 3 *sensu* Liu et al., 2019.
(Figure 1Figure 2; Figure 3A–H)

2018 Form B Zhang et al., Fig. 5.4.
2019 Indeterminate Forms 3 Liu et al., Fig 9D.
2023 Indeterminate Form 3 Qin et al., Figures 1–3.

10.3389/feart.2023.1210062

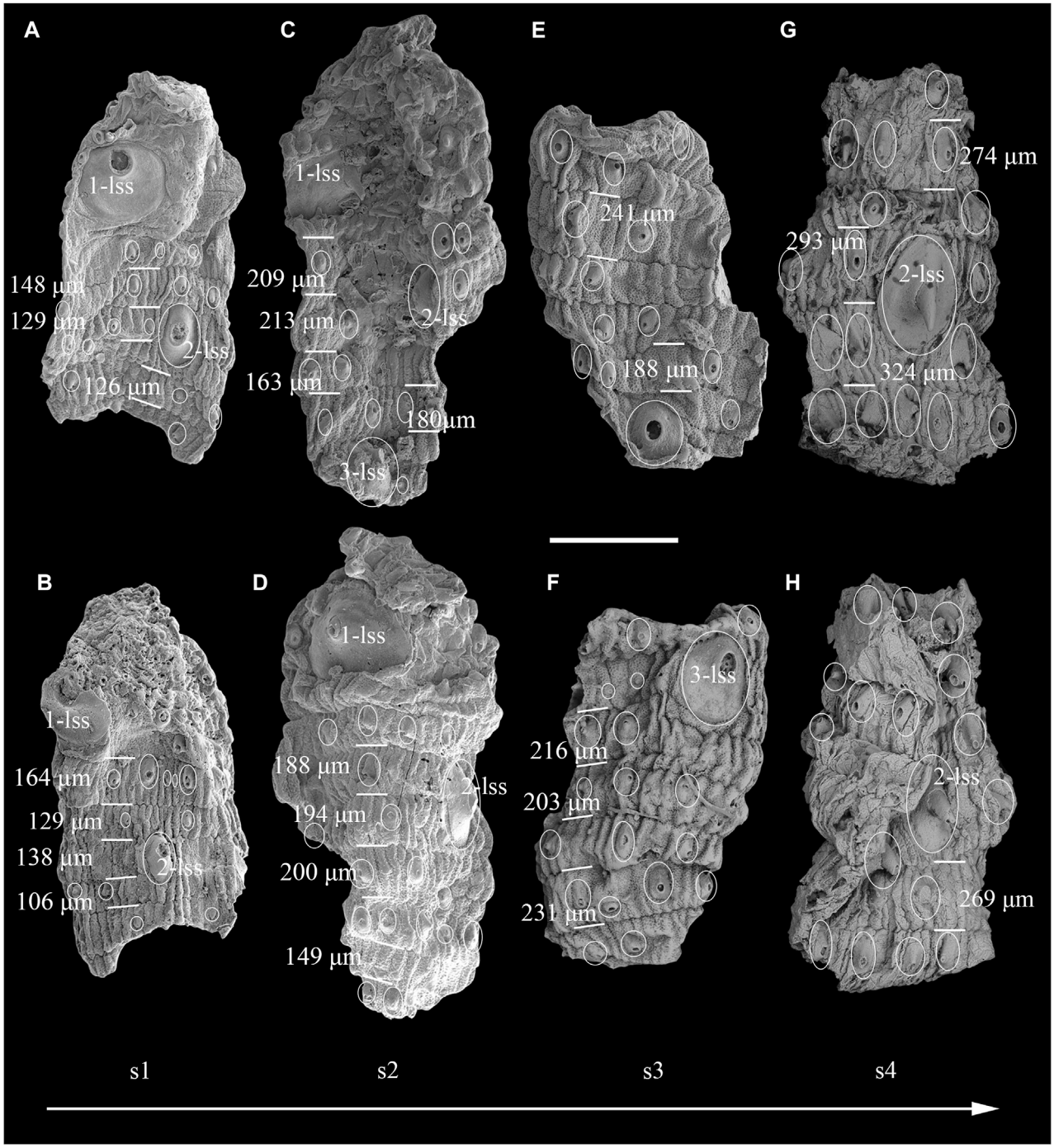

FIGURE 3
The possible developmental sequence of Indeterminate Form 3 *sensu* Liu et al., 2019. **(A,B)** UMCU 23XX01; **(C,D)** UMCU 22XX01; **(E,F)** UMCU 22XX02; **(G,H)** UMCU 16CHD0409-004. **(C, D, E, and F)** as cited in Qin et al., 2023; **(G and H)** as cited in Liu et al., 2019. The outlines of sclerites are marked by circles. Abbreviations: 1-lss, first large spinose sclerite; 2-lss, second large spinose sclerite; 3-lss, third large spinose sclerite; **(s1–s4)**, developmental stages 1-4. The scale bar represents 500 μm.

3.1 Material

UMCU 23XX01 (Figure 1; Figure 2A–D; Figure 3A,B), UMCU 22XX01 (Figures 3C,D), UMCU 22XX02 (Figures 2E,F; Figure 3E,F), UMCU 16CHD0409-004 (Figures 3G,H).

3.2 Description

UMCU 23XX01 has two parts; the anterior part is the introvert and the posterior part is the trunk. The introvert has long, spine-link, internally hollow scalds. The trunk has 11 annuli with spinose sclerites, each with an enlarged base and a spine. The spinose

sclerites on the same annulus vary in size and are randomly and sparsely distributed. A pair of rounded large spinose sclerites are located at the anterior part of the trunk, and a pair of large oval spinose sclerites are located on the eighth and ninth annuli.

UMCU 22XX01 is described in Qin et al., 2023; UMCU 16CHD0409-004 is described in Liu et al., 2019. The description of UMCU 22XX02 follows Qin et al., 2023, with only minor revisions to the sclerites. Two small sclerites appear on its second annulus (Figure 3B in Qin et al., 2023; Figures 2E,F); they seem to be newly formed.

3.3 Occurrence

Kuanchuanpu Formation (Fortunian Stage), Zhangjiagou section, Xixiang County, Shaanxi Province, South China; *Anabarites trisulcatus-Protohertzina anabarica* Assemblage zone.

3.4 Comparison

The main part of the trunk of these specimens is very similar, upon which similarly shaped sclerites are randomly and sparsely distributed. Both UMCU 23XX01 and UMCU 22XX01 have two pairs of large sclerites, and the first pair of large sclerites are both found in the anterior part of the trunk, and the second pair of large sclerites are both found in the middle of the trunk. This suggests that these specimens are from the same species, and the position of the large sclerites on the trunk may be fixed. There are at least five large sclerites (lss, Figure 1; Figure 3) on the trunk, in order from anterior to posterior: the first pair of large sclerites (1-lss), the second pair of large sclerites (2-lss), and the third large single sclerite (3-lss). Comparisons of Form 3 with other worms can be found in Liu et al., 2019 and Qin et al., 2023 and will not be repeated here.

Because the position of the large sclerites on the trunk may be fixed, when using UMCU 22XX01 as a reference, UMCU 23XX01 may represent the first two-thirds of it. UMCU 16CHD0409-004 has a pair of oval large spinose sclerites that may represent the middle part of UMCU 22XX01. The large rounded sclerites in UMCU 22XX02 may not correspond to the first large paired sclerites in UMCU 23XX01 and UMCU 22XX01: 1) the large sclerites in UMCU 22XX02 are not paired (also possibly due to incomplete preservation); 2) the first large paired sclerites in UMCU 22XX01 are next to triangular sclerites rather than oval sclerites as in UMCU 22XX02. Therefore, the large sclerite in UMCU 22XX02 may correspond to the single large sclerite located at the posterior part of the trunk in UMCU 22XX01.

3.5 Remarks

It is generally accepted that the annulus widens as the worm grows, both in extant scalidophorans (Neuhaus, 1995) and in paleoscolecids, which are considered to be early scalidophorans (cycloneuralians) (Brock and Cooper, 1993; Müller and HinzSchallreuter, 1993; Zhang and Pratt, 1996; Duan and Dong, 2013; Xian et al., 2023), so we divided these four specimens into four developmental stages according to the width of the annulus (Table 1; Figure 3s1-s4). According to these specimens, the size of the sclerites also gradually increases with growth (Table 1).

4 Discussion

Among the previously reported Fortunian armored scalidophorans, most of them have similar morphology and size to the sclerites within the same annulus, such as *Zhongpingscolex* (Shao et al., 2020a), *Shanscolex* (Liu et al., 2019), and *Dahescolex* (Shao et al., 2020b), Forms 1-3 and 5-6 (Liu et al., 2019; Qin et al., 2023).

UMCU 23XX01 was identified as Form 3, but its sclerites within the same annulus are clearly different in size, and some of the sclerites appear to be recently formed and are only one-fifth the size of other sclerites in the same annulus (Figure 2D). We re-examined the material previously attributed to Form 3 and also found two small sclerites in UMCU 22XX02 (Figures 2E,F). Compared to UMCU 23XX01, UMCU 22XX02 is at a more advanced developmental stage, and newly formed sclerites were found in worms at different developmental stages, possibly suggesting that the sclerites of worms not only become larger in size during development but also increase in number.

UMCU 23XX01 (Figure 3s1, Figure 1; Figure 2A–D; Figure 3A,B) has a low number of sclerites (about 4-5 sclerites on one annulus on average) and a high percentage of newly formed sclerites (if the sclerite in the middle of the a6 in UMCU 23XX01 (Figure 1B; Figure 2C) is considered as normal size, all other sclerites of the same type in UMCU 23XX01 are may be newly or recently formed, they are morphologically similar and differ only in size). At this stage, the number of newly formed sclerites is high, indicating a peak in sclerite development and that the sclerites are developing faster. In addition, there are smaller sclerites on almost every annulus of UMCU 23XX01, which means that the increase in sclerites may occur simultaneously throughout the trunk of the worm. The number and size of sclerites are greater in UMCU 22XX02 (Figure 3s3, Figures 2E,F and Figure 3E,F); there are only two newly formed sclerites at this stage, and the number of newly formed sclerites is reduced, indicating that the sclerite development is slowed down at this time. The high number of sclerites in UMCU 16CHD0409-004 (Figure 3s4, Figures 3G,H) (about six sclerites on one annulus on average: this specimen is partially folded and there should be a higher number of sclerites) did not reveal newly formed sclerites, indicating that the number of sclerites may not be increasing at this stage. However, because these fossils are fragmented, we cannot be sure whether newly formed sclerites are still present in the unpreserved parts of these fossils so it is also possible that the number of sclerites continues to increase. Whether or not the number of sclerites increases after Figure 3s4, the worms may continue to grow and the size of the sclerites may increase accordingly.

The common sclerites develop within a single annulus; the large sclerite is more unusual in that it can span 2-3 annuli. The size of large sclerites may also increase as the worms grow (Table 1), however, based on the specimens at hand, their numbers may not change (Figure 3).

The growth of the worm is accompanied by periodic molting, with the annulus widening as the worm grows. However, it is not

TABLE 1 Measurements.

Collected number	Annulus	Sclerites		First large paired sclerites (1-lss)		second large paired sclerites (2-lss)		Large single sclerite (3-lss)	
	L (μm)	L (μm)	W (μm)	L (μm)	W (μm)	L (μm)	W (μm)	L (μm)	W (μm)
UMCU 23XX01	106-164	23-105	11-58	326	279	233	140		
UMCU 22XX01	149-213	100	60	385	420	330	140	285	150
UMCU 22XX02	188-241	104	70					344	266
UMCU 16CHD0409-004	269-324	200	95			460	280		

clear whether sclerites increase and grow simultaneously with worm growth or whether an increase in sclerites requires more frequent molting. Therefore, the rate of increase in the number of sclerites does not represent the growth rate of the worms, and there may be no correlation between them.

5 Conclusion

We have reported new material of Indeterminate Form 3 *sensu* Liu et al., 2019 from the Fortunian Zhangjiagou section, southern Shannxi, South China. Based on the material at hand, we established a possible partial developmental sequence of Indeterminate Form 3 *sensu* Liu et al., 2019, which illustrates that during its growth, in addition to the size of the sclerites increasing, the number of sclerites also increases. Large sclerites only increase in size with growth but not in number.

Data availability statement

The original contributions presented in the study are included in the article/supplementary material, further inquiries can be directed to the corresponding authors.

Author contributions

JQ coordinated the field work, preparation and curation of fossils, wrote the manuscript, and processed the images. YL edited the manuscript. ML, TS, and YZ assisted in collecting the rock samples in the field. All authors contributed to the article and approved the submitted version.

Funding

This work was supported by the National Natural Science Foundation of China (grant numbers 41872014), the Strategic Priority Research Program of the Chinese Academy of Sciences (grant number XDB26000000), the State Key Laboratory of Paleobiology and Stratigraphy, the Nanjing Institute of Geology and Paleontology, the Chinese Academy of Sciences (grant number 193123), and the Basic Research Plan of Natural Science of Shaanxi Province (grant number 2018JM4002).

Acknowledgments

We thank three reviewers for providing reviews and suggestions.

Conflict of interest

The authors declare that the research was conducted in the absence of any commercial or financial relationships that could be construed as a potential conflict of interest.

Publisher's note

References

Aguinaldo, A., Turbeville, J., Linford, L., Rivera, M., Garey, J., Raff, R., and Lake, J. A., (1997). Evidence for a clade of nematodes, arthropods and other moulting animals. *Nature* 387, 489–493. doi:10.1038/387489a0

Ahlrichs, W. (1995). *Ultrastruktur und Phylogenie von Seison nebaliae (Gruber 1859) und Seison annulatus (Claus 1876). Hypothesen zu phylogenetischen Verwandtschaftsverhältnissen innerhalb der Bilateria*. Göttingen, Germany: Georg-August-University of Göttingen.

Brock, G., and Cooper, B. (1993). Shelly fossils from the early cambrian (toyonian) wirrealpa, aroona creek, and ramsay limestones of south Australia. *J. Paleontol.* 67, 758–787. doi:10.1017/s0022336000037045

Dong, X., Cunningham, J. A., Bengtson, S., Thomas, C. W., Liu, J., Stampanoni, M., and Donoghue, P. C. J., (2013). Embryos, polyps and medusae of the early Cambrian scyphozoan Olivooides. *P. Roy. Soc. B–Biol. Sci.* 280, 20130071. doi:10.1098/rspb.2013.0071

Dos Reis, M., Thawornwattana, Y., Angelis, K., Telford, M., Donoghue, P. J., and Yang, Z. (2015). Uncertainty in the timing of origin of animals and the limits of precision in molecular timescales. *Curr. Biol.* 25, 2939–2950. doi:10.1016/j.cub.2015.09.066

Duan, B., and Dong, X. (2013). Furongian (late cambrian) palaeoscolecid cuticles from hunan Province, South China: The growth impact on the worm cuticle. *Acta Sci. Nat. Univ. Pekin.* 49, 591–602. doi:10.13209/j.0479-8023.2013.083

Erwin, D. H. (2020). The origin of animal body plans: A view from fossil evidence and the regulatory genome. *Development* 147, dev182899. doi:10.1242/dev.182899

Han, J., Kubota, S., Li, G., Yao, X., Yang, X., Shu, D., Li, Y., Kinoshita, S., Sasaki, O., Komiya, T., and Yan, G. (2013). Early Cambrian pentamerous cubozoan embryos from South China. *PloS One* 8, e70741. doi:10.1371/journal.pone.0070741

Lemburg, C. (1995). Ultrastructure of sense organs and receptor cells of the neck and lorica of the Halicryptus spinulosus larva (Priapulida). *Microfauna Mar.* 10, 7–30. doi:10.1007/BF00397931

Liu, Y. H., Qin, J. C., Wang, Q., Maas, A., Duan, B. C., and Zhang, Y. N., (2019). New armoured scalidophorans (ecdysozoa, cycloneuralia) from the cambrian Fortunian Zhangjiagou lagerstätte, south China. *Pap. Palaeontol* 5, 241–260. doi:10.1002/spp2.1239

Liu, Y., Li, Y., Shao, T., Zhang, H., Wang, Q., and Qiao, J. (2014). *Quadrapyrgites* from the lower Cambrian of South China: Growth pattern, post–embryonic development, and affinity. *Chin. Sci. Bull.* 59, 4086–4095. doi:10.1007/s11434-014-0481-5

Liu, Y., Shao, T., Zhang, H., Wang, Q., Zhang, Y., and Chen, C., (2017). A new scyphozoan from the cambrian Fortunian stage of south China. *Palaeontology* 60, 511–518. doi:10.1111/pala.12306

Liu, Y., Xiao, S., Shao, T., Broce, J., and Zhang, H. (2014b). The oldest known priapulid–like scalidophoran animal and its implications for the early evolution of cycloneuralians and ecdysozoans. *Evol. Dev.* 16, 155–165. doi:10.1111/ede.12076

Maas, A., Braun, A., Dong, X. P., Donoghue, P. C. J., Müller, K. J., and Olempska, E., (2006). The 'orsten': More than a cambrian konservat-lagerstätte yielding exceptional preservation. *Palaeoworld* 15, 266–282. doi:10.1016/j.palwor.2006.10.005

Müller, K., and Hinz-Schallreuter, I. (1993). Palaeoscolecid worms from the middle cambrian of Australia. *Palaeontology* 36, 549–592. doi:10.1016/0031-0182(93)90137-8

Neuhaus, B. (1995). Postembryonic development of *Paracentrophyes praedictus* (homalorhagida): Neoteny questionable among the kinorhyncha. *Zool. Scr.* 24, 179–192. doi:10.1111/j.1463-6409.1995.tb00398.x

Peng, S., Babcock, L., and Ahlberg, P. (2020). "The Cambrian period," in *Geological time scale 2020*. Editors F. M. Gradstein, J. G. Ogg, M. Schmitz, and G. M. Ogg (oxford, United Kingdom: Elsevier), 565–629.

Qin, J., Liu, Y., Shao, T., Wang, Q., Zhang, Y., and Zhou, X., (2023). Three indeterminate forms of scalidophoran worms from the cambrian Fortunian of south China. *Acta Geol. Sin-Engl.* doi:10.1111/1755-6724.15052

Rota-Stabelli, O., Daley, A., and Pisani, D. (2013). Molecular timetrees reveal a Cambrian colonization of land and a new scenario for ecdysozoan evolution. *Curr. Biol.* 23, 392–398. doi:10.1016/j.cub.2013.01.026

Shao, T., Liu, Y., Duan, B., Zhang, H., Zhang, H., and Wang, Q., (2018b). The Fortunian (lowermost Cambrian) *Qinscyphus necopinus* (Cnidaria, Scyphozoa, Coronatae) underwent direct development. *Neues Jahrb. Geol. P.–A.* 289, 149–159. doi:10.1127/njgpa/2018/0755

Shao, T., Qin, J., Shao, Y., Liu, Y., Waloszek, D., and Mass, A., (2020b). New macrobenthic cycloneuralians from the Fortunian (lowermost cambrian) of south China. *Precambrian Res.* 349 (6632), 105413. doi:10.1016/j.precamres.2019.105413

Shao, T., Tang, H., Liu, Y., Waloszek, D., Maas, A., and Zhang, H. (2018a). Diversity of cnidarians and cycloneuralians in the Fortunian (early cambrian) Kuanchuanpu Formation at Zhangjiagou, south China. *Paleontology* 92, 115–129. doi:10.1017/jpa.2017.94

Shao, T., Wang, Q., Liu, Y., Qin, J., Zhang, Y., and Liu, M., (2020). A new scalidophoran animal from the Cambrian Fortunian Stage of South China and its implications for the origin and early evolution of Kinorhyncha. *Precambrian Res.* 349 (6632), 105616. doi:10.1016/j.precamres.2020.105616

Steiner, M., Li, G. X., Qian, Y., Zhu, M., and Erdtmann, B. D. (2007). Neoproterozoic to early Cambrian small shelly fossil assemblages and a revised biostratigraphic correlation of the Yangtze Platform (China). *Palaeogeogr. Palaeoclimatol. Palaeoecol.* 254, 67–99. doi:10.1016/j.palaeo.2007.03.046

Steiner, M., Qian, Y., Li, G., Hagadorn, J. W., and Zhu, M. (2014). The developmental cycles of early cambrian olivooidae fam. Novol. (? Cycloneuralia) from the yangtze platform (China). *Palaeogeogr. Palaeoclimatol. Palaeoecol.* 398, 97–124. doi:10.1016/j.palaeo.2013.08.016

Wang, X., Han, J., Vannier, J., Ou, Q., Yang, X., and Uesugi, K., (2017). Anatomy and affinities of a new 535–million–year–old medusozoan from the Kuanchuanpu Formation, South China. *Palaeontology* 60, 853–867. doi:10.1111/pala.12320

Xian, X., Eriksson, M., and Zhang, H. (2023). Growth patterns of palaeoscolecid sclerites from the furongian (upper cambrian) wangcun section, Western hunan, south China. *Palaeoworld*. doi:10.1016/j.palwor.2023.03.005

Zhang, H., Maas, A., and Waloszek, D. (2018). New material of scalidophoran worms in orsten-type preservation from the cambrian Fortunian stage of south China. *J. Paleontol.* 92, 14–25. doi:10.1017/jpa.2017.39

Zhang, H. (2021). The evolutionary relationships of the earliest known cycloneuralians and a new record from the Cambrian Fortunian of South China. *Palaeoworld*, 31, 389–401. doi:10.1016/j.palwor.2021.09.003

Zhang, H., Xiao, S., Liu, Y., Yuan, X., Wan, B., and Muscente, A., (2015). Armored kinorhynch-like scalidophoran animals from the early Cambrian. *Sci. Rep.* 5, 16521. doi:10.1038/SREP16521

Zhang, X., and Pratt, B. (1996). Early cambrian palaeoscolecid cuticles from Shaanxi, China. *J. Paleontol.* 70, 275–279. doi:10.1017/s0022336000023350

Zhang, Y., Liu, Y., Shao, T., and Qin, J. (2023). New Qinscyphus material from the Fortunian of south China. *Front. Earth Sci.* 11, 1038686. doi:10.3389/feart.2023.1038686

frontiers | Frontiers in Ecology and Evolution

TYPE Original Research
PUBLISHED 09 August 2023
DOI 10.3389/fevo.2023.1214109

OPEN ACCESS

EDITED BY
Emily G. Mitchell,
University of Cambridge, United Kingdom

REVIEWED BY
Dongjing Fu,
Northwest University, China
Peiyun Cong,
Yunnan University, China
Han Zeng,
Chinese Academy of Sciences (CAS), China

*CORRESPONDENCE
Gaëtan J.-M. Potin
gaetan.jm.potin@outlook.fr

RECEIVED 28 April 2023
ACCEPTED 30 June 2023
PUBLISHED 09 August 2023

CITATION
Potin GJ-M, Gueriau P and Daley AC (2023) Radiodont frontal appendages from the Fezouata Biota (Morocco) reveal high diversity and ecological adaptations to suspension-feeding during the Early Ordovician.
Front. Ecol. Evol. 11:1214109.
doi: 10.3389/fevo.2023.1214109

Radiodont frontal appendages from the Fezouata Biota (Morocco) reveal high diversity and ecological adaptations to suspension-feeding during the Early Ordovician

Gaëtan J.-M. Potin[1,2]*, Pierre Gueriau[1] and Allison C. Daley[1]

[1]Institute of Earth Sciences, University of Lausanne, Lausanne, Switzerland, [2]Géosciences Rennes, CNRS, UMR 6118, Univ Rennes, Rennes, France

Introduction: The Early Ordovician Fezouata Shale Formation (485–475Ma, Morocco) is a critical source of evidence for the unfolding Great Ordovician Biodiversification Event (GOBE), the largest radiation in animal diversity during the Paleozoic. The Fezouata Shale preserves abundant remains of ancient marine organisms, including hundreds of specimens of radiodonts, a diverse and globally distributed group of stem lineage arthropods that first appeared as raptorial predators during the Cambrian Explosion.

Methods: In this work, we study 121 radiodont frontal appendages from the Fezouata Shale. Frontal appendages are the most commonly preserved body parts of radiodonts, and their well-preserved anatomical characters are crucial for describing taxonomic diversity at the species level, while also providing essential data on mode of life, paleoecology, and feeding behaviour.

Results: Our data allow for a systematic review of suspension-feeding Hurdiidae radiodonts from Fezouata. The genus *Pseudoangustidontus* is recognised as a radiodont and ascribed to Hurdiidae, and a new second species of this genus is identified, *Pseudoangustidontus izdigua* sp. nov. *Aegirocassis benmoulai* is also reviewed and its diagnosis amended with new details of differentiated endites in this appendage. The morphological similarity between both genera allows us to erect Aegirocassisinae subfam. nov., which groups together the suspension-feeding hurdiids of the Fezouata Shale.

Discussion: Suspension-feeding radiodont appendages are more abundant than those of sediment sifting or raptorial radiodonts, with the Fezouata Shale showing the highest diversity of suspension-feeding radiodonts in the history of the group. This dominance and diversity of frontal filter-feeding appendages follows the "Ordovician Plankton Revolution", which started in the upper Cambrian and saw a huge radiation in plankton diversity.

KEYWORDS

Arthropoda, Radiodonta, evolution, frontal appendages, Fezouata Shale Formation, Early Ordovician, GOBE, suspension-feeder

1 Introduction

The Fezouata Shale, located near the city of Zagora, in the central Anti-Atlas in Morocco (figure 1D in Saleh et al., 2018); (Martin et al., 2016a; Saleh et al., 2018; Vannier et al., 2019; Saleh et al., 2021c), is the only Burgess Shale-type *Lagerstätte* known in the Early Ordovician (Tremadocian-Floian) that yields a rich and diverse assemblage of marine organisms (Gutiérrez-Marco et al., 2017; Lefebvre et al., 2018; Saleh et al., 2020a). The Fezouata Shale is a vital data point in understanding the transition between the Cambrian Explosion and Great Ordovician Biodiversification Event (GOBE) (Martin et al., 2016c; Servais et al., 2016; Vaucher et al., 2016; Saleh et al., 2021c; Saleh et al., 2022a). In the Fezouata shale non-mineralized taxa are abundant and preserve soft tissues with microscopic fidelity. The assemblage consists of a mix of the classic Cambrian Explosion fauna, including aglaspid, nektaspid or Radiodonta well known from Cambrian *Lagerstätten* such as the Burgess Shale (Canada), and Paleozoic animals characteristic of the Ordovician and later Paleozoic such as trilobites, orthoceratids, and chelicerates (Van Roy et al., 2015a; Ortega-Hernández et al., 2016; Pérez-Peris et al., 2021a; Pérez-Peris et al., 2021b).

Radiodonta Collins, 1996 is an order of early Paleozoic (Cambrian, Series 2, Stage 3 to Early Ordovician, and possibly to the basal Devonian) marine nektonic stem lineage members of Arthropoda von Siebold, 1848, which were important apex predators in early animal communities (Daley and Budd, 2010; Zeng et al., 2017; Liu et al., 2018; Guo et al., 2019; Pates and Daley, 2019; Potin and Daley, 2023). Subject to many interpretations since their first discovery, they have a particular and disparate morphology (Walcott, 1911; Conway Morris and Whittington, 1979; Collins, 1996). With adults measuring between 10 and 200cm in length (substantially larger than most other nektonic predators at the time) and a host of unique and highly diagnostic morphological characters, for example circular mouthparts and elaborate frontal feeding appendages (Collins, 1996; Van Roy and Briggs, 2011; Daley et al., 2013a; Van Roy et al., 2015a; Cong et al., 2018; Pates et al., 2019; Moysiuk and Caron, 2022; Potin and Daley, 2023), they are distinctive members of early Paleozoic ecosystems. The frontal appendages are the most common body part found in fossil *Lagerstätten*, owing to their high preservation potential, and they provide crucial information about the feeding strategy, which includes raptorial predation, sediment-sifting generalised predation, and suspension feeding (Briggs, 1979; Nedin, 1999; Daley and Budd, 2010; Daley et al., 2013a; Van Roy et al., 2015b; Servais et al., 2016; Pates et al., 2019; Pates et al., 2021a; Potin and Daley, 2023).

Phylogenetic analyses identify four radiodont families globally (Vinther et al., 2014; Lerosey-Aubril and Pates, 2018; Potin and Daley, 2023), only one of which, the Hurdiidae, has so far been identified from the Fezouata Shale (Van Roy and Briggs, 2011; Van Roy et al., 2015b). Hurdiidae are typically characterized by frontal appendages with podomeres that bear long, blade-like spines call endites (Lerosey-Aubril and Pates, 2018; Moysiuk and Caron, 2022; Wu et al., 2022). They first appeared during Cambrian Epoch 2 Age 3, and are abundant, diverse and globally distributed throughout the Cambrian (Zhu et al., 2021). In the Early Ordovician Fezouata Shale, the two meter long suspension-feeding *Aegirocassis benmoulai* is the only hurdiid/radiodont taxon formally described from the site (Van Roy et al., 2015b), interpreted as occupying the same ecological niche as some present-day whales or whale sharks (Van Roy et al., 2015b). Other specimens of hurdiids from Fezouata have been identified but no formal taxonomic description provided (Van Roy and Briggs, 2011).

This study focuses on hurdiid frontal appendages from the Fezouata Shale, expanding upon the known diversity and increasing the disparity of known functions at this site. Owing to newly discovered specimens, this paper provides new insight into radiodont evolution, particularly for the family Hurdiidae. The internal taxonomy of the Hurdiidae is re-evaluated with the creation of the suspension-feeding clade Aegirocassisinae, which unites *Aegirocassis benmoulai* and the genus *Pseudoangustidontus*, here identified as a Hurdiidae. The re-evaluation of *Pseudoangustidontus* results in the separation of *P. duplospineus* and *P. izdigua* sp. nov. The new specimens also provide data on the mineral composition of the frontal appendages fossils, and allows for a new perspective into radiodont ecology and evolution.

2 Geological context

The Fezouata Shale is an Early Ordovician *Konservat-Lagerstätte* of the Anti-Atlas of Morocco (Martin et al., 2016c; Drage et al., 2019; Saleh et al., 2019; Saleh et al., 2020a). This *Lagerstätte* formed on the northern Gondwanan margin at approximately 65° South of latitude, near the Ordovician south polar circle, consequently in a cold-water depositional context (figure 1D in Saleh et al., 2018) (Martin et al., 2016c; Saleh et al., 2018; Drage et al., 2019; Saleh et al., 2019; Saleh et al., 2020a; Saleh et al., 2021c). The sediments were deposited during the tectonic rifting that led to the formation of the Rheic ocean between the Avalonian and Gondwanan paleocontinents (figure 1D in Saleh et al., 2018) (Martin et al., 2016c; Vaucher et al., 2016; Lebrun, 2017; Saleh et al., 2018).

The Fezouata Shale Formation (between 900 and 1000 meters) is mainly composed of argillites and siltstones (Vidal, 1998; Lebrun, 2017; Vaucher et al., 2017). It is a subdivision of "External Feijas Group" which is one of the four big lithostratigraphic units of the Ordovician in modern day Morocco (Martin et al., 2016c). The Fezouata Formation is composed of the lower and upper Fezouata Shale units, which are separated by a surface that corresponds to a glauconitic and ferruginous horizon reflecting a maximum flooding interval (Martin et al., 2016c). Sediments were deposited almost exclusively in environments between the fair-weather wave base and just below the storm weather wave base (Vidal, 1998; Martin et al., 2016c; Vaucher et al., 2016; Saleh et al., 2018; Saleh et al., 2021b).

Several modes of fossilisation have been described for the *Konservat-Lagerstätte* aspects of the Fezouata Shale. Giant radiodont carcasses (e.g. of *Aegirocassis*) are preserved three-dimensionally within large (>1 m) silica-chlorite concretions, resulting from the microbial decomposition of their organic tissues (Gaines et al., 2012; Van Roy et al., 2015b). A similar mechanism led to the preservation of large trilobites from the

temporally and spatially (<50 km) coeval locality of Ouled Slimane (Saleh et al., 2021c). In the second mode, which concerns the great majority of the Fezouata taxa (i.e. smaller mineralised and soft-bodied organisms or tissues, as well as shed exoskeletal remains), fossils are preserved as two-dimensional iron oxide compressions within mudstone (Van Roy et al., 2010; Martin et al., 2016b). These compressed soft-body fossils resulted from burial *in situ* under storm-induced deposits (Vaucher et al., 2016; Lefebvre et al., 2018; Saleh et al., 2018). Pre-burial degradation was slowed by the deposition of a favourable clay mineralogy (Saleh et al., 2019) that allowed for the preservation of decay-prone structures such as internal and cuticularized tissues (Saleh et al., 2020c). It has been shown (Vaucher et al., 2016; Saleh et al., 2020c; Saleh et al., 2021b) that originally these fossils first turned into carbonaceous films and/or were replicated in rapidly forming authigenic minerals particularly pyrite (Saleh et al., 2020c; Saleh et al., 2021b). There are two main intervals of this mode of preservation (figure 1A in Saleh et al., 2018), dated to the Tremadocian and Floian (Vaucher et al., 2016; Lefebvre et al., 2018; Saleh et al., 2018). The lower interval is dated to the terminal Tremadocian based on the graptolite biozone *Sagenograptus murrayi* (previously called *Araneograptus murrayi*) and the beginning of *Hunnegraptus copiosus*, at the top of the lower member of the Fezouata Shale Formation (Martin et al., 2016b; Vaucher et al., 2016; Lefebvre et al., 2018; Saleh et al., 2018; Saleh et al., 2022c). The upper interval dates from the Floian based on the *Baltograptus jacksoni* biozone (figure 1A in Saleh et al., 2018) (Lefebvre et al., 2018; Saleh et al., 2018). The *Konzentrat-Lagerstätte* in the upper member dates to the Middle Floian, probably in the *Azygograptus suecicus* biozone, which formed in a more proximal area of the basin (Martin et al., 2016b; Vaucher et al., 2016). A third mode of preservation yielding non-biomineralised fossils has also been reported from the upper Floian of the Fezouata Shale, dominated by three-dimensionally preserved sclerotized fragments of large bivalve and/or radiodont arthropods together with brachiopods, echinoderms and graptolites (Saleh et al., 2022c). Fossils in this study derive from the Tremadocian interval of exceptional preservation in the form of two-dimensional iron oxide compressions.

3 Material and methods

3.1 Fossil specimens

This study is based on 112 specimens of frontal appendages belonging to suspension feeding hurdiids found in the Tremadocian (about 478 million years ago), from the exceptionally well-preserved lower member of the Fezouata Shale (Supplementary Table 1) (Martin et al., 2016b; Vaucher et al., 2016). All appendages examined for this study are housed in the collections of the Muséum cantonal des sciences naturelles, département de géologie, Lausanne (MGL), the Peabody Museum of Natural History of the Yale University (YPM), and the Marrakech Collections of the Cadi Ayyad University. The MGL and YPM material has been collected by authorized and academically recognized Moroccan collector Mohamed Ben Moula and his family over the period of 2015 to 2016 (MGL collection), and between 2009 to 2015 (YPM collection). The MGL fossil collection was purchased with funds from the University of Lausanne and the Swiss National Science Foundation, following all regulations for purchases. The fossil collection was transported to Casablanca and subjected to export approval by the Ministry of Energy, Mines and the Environment of the federal government of the Kingdom of Morocco and approved for shipment to Switzerland on 11.05.2017 (export permits curated with the collection). Fossils were shipped by sea and land to the University of Lausanne, where they are curated as part of the MGL collection. The collections of the Yale Peabody Museum of Natural history were obtained both through collection of specimens by Peter Van Roy during field work, and through purchase using dedicated museum funds for the acquisition of scientific collections. Export permits were obtained through the Moroccan Ministry of Energy, Mines and the Environment, with specimens being transported from Casablanca by sea. In addition, some data come from previous publications and are cited accordingly.

An additional 9 hurdiid radiodont appendages that do not show characteristics of suspension feeding morphology were examined and included in the analyses of proportions of feeding modes found in the Fezouata Shale (see list of specimens in Supplementary Table 1). These taxa, some of which have been previously published with brief descriptions (Van Roy and Briggs, 2011), have morphologies similar to *Hurdia* and *Peytoia*, and their detailed systematics will be the subject of a future study.

3.2 Terminology

In this work we follow the terminology of Potin and Daley (2023) for the anatomical features of the frontal appendages. As exemplified by the nearly complete *Aegirocassis benmoulai* appendages, the overall morphology consist of series of articulated podomeres divided into three regions: the 'proximal region' that usually includes a single podomere with an endite at the distal margin (referred to as the 'base', 'shaft' or 'peduncle' in previous publications, see Supplementary Table S1 in Potin and Daley, 2023); an 'intermediate region' of five or six podomeres that bear elongate blade-like endites; and a 'distal region' of one or several podomeres bearing short endites or no endites at all (Wu et al., 2022; Potin and Daley, 2023) (Figure 1). Endites in all three regions can bear 'auxiliary spines', distributed along the anterior or posterior (or both) margins. In suspension feeding taxa, the thin, densely-packed auxiliary spines of the elongated endites of the intermediate region are called 'setae', to which fine 'spinules' can be attached (Figure 1) (Van Roy et al., 2015b; Lerosey-Aubril and Pates, 2018; Potin and Daley, 2023).

3.3 Specimen examination, Photography, and Illustrations

Specimens were examined with a binocular microscope WILD typ 308700 (X6.4, 16, 40) to identify the microstructures, while camera lucida drawings were made in order to illustrate and record the morphological details. Photos were taken with a Canon 8000D

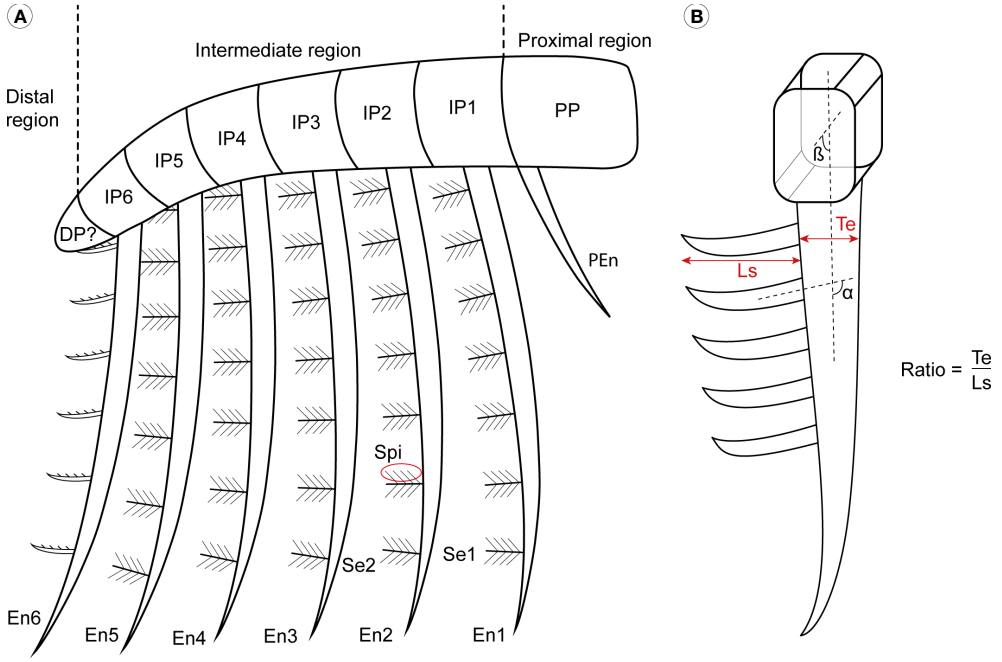

FIGURE 1
General morphology of Aegirocassisinae frontal appendages. **(A)** Simple drawing inspired by *Aegirocassis benmoulai* to show the general frontal appendage organisation. **(B)** Measurements and calculations applied to the specimens. α insertion angle between the setae and the endite; β, insertion angle between the podomere and the setae; DP, distal podomeres; En, intermediate region endite; IP, intermediate podomeres; Ls, length of the setae; PEn, proximal region endite; PP, proximal podomere; Se, setae from intermediate region endite; Spi, spinule; Te, thickness of the endite. Drawing credit: G. Potin.

camera couple with a Canon EFS 60mm 1:2.8, and EOS Utility photo software was used to adjust contrast and sharpness. Fossils were imaged using different lighting conditions, including high and low angle incident and polarised lighting. Drawings and figures were digitised using Wacom Intuos Pro graphic tab, and further prepared with the software Adobe Photoshop and Adobe Illustrator under license to the University of Lausanne. The expression of relief on the drawings corresponds to the method of (Whittington, 1975), with hachures starting on the point of high relief and moving downwards.

3.4 Measurements

Primary measurements (Supplementary Table 2) were made, using digital callipers, of the height, length, and thickness of the major morphological characters (podomeres, endites, setae and spinules), and the angle (α) between a seta and the margin of the endite to which it attaches was also measured. If the angle measure α is more than 90°, the seta is oriented to the ventral margin and, if less than 90° it is oriented to the dorsal margin (Figure 1). A number of morphometric parameters were then calculated using these baseline measurements, for use as quantitative variables that distinguish between genera and species. The first parameter is dimensionless and compares setae length and the thickness of the endite where it is attached, such that the ratio T_e/L_s consist of the endite thickness (T_e) divided by the setae length (L_s) (Figure 1). The ratio is calculated to see if there are differences between the dimensions of endites of the different species, and also if there are some intraspecific differences. To examine the suspension feeding mode of life, primary measurements was also used to calculate mesh sizes as either the space between the setae, or by the space between the spinules (if they are present), on the elongated endites of the intermediate region. The mesh size measurement allows for an estimate of the size of the plankton that can be captured during suspension feeding (Robison and Richards, 1981; Vinther et al., 2014).

3.5 Analyses

A study of the mode of insertion of the setae on the 6th endite of *Aegirocassis benmoulai* and *Pseudoangustidontus izdigua* sp. nov. was used to test for a significant difference of insertion angle between these taxa. The 6th endite was chosen because is the endite that clearly showed the insertion angle in the highest number of specimens, giving a total sample size of 29 appendages (Supplementary Table 3). Using PAST version 4 (Hammer et al., 2001), a Shapiro-Wilk test for normality was conducted, followed by a two-sample Kolmogorov-Smirnov test with Monte Carlo permutation to compare the overall two-sample distribution with their cumulative probability distribution (Hammer and Harper, 2008; Antcliffe et al., 2019). Violin and box plot were made to compare the results of the two insertion modes, which were then modified for the figures using Adobe Illustrator.

RStudio was used to generate a pie chart by using the function pie in order to visualize the proportion of the different radiodont taxa found in the Fezouata Shale.

The graph showing the size of particles captured by suspension-feeding radiodonts has been modified from (Vinther et al., 2014).

Data concerning *Pahvantia* mesh size were exported from (Lerosey-Aubril and Pates, 2018), and the data for *Tamisiocaris* derive from (Van Roy et al., 2015b). Our data come from a selection of well-preserved specimens, showing multiple well-preserved setae and/or spinules associated with the five first endites of the intermediate region (see Supplementary Table 2).

3.6 X-ray microtomography

X-ray computed microtomography (μCT) was conducted on the *Pseudoangustidontus izdigua* sp. nov. paratype MGL 103606 at the Institute of Earth Sciences, University of Lausanne, using a Skyscan 1273 CT scanner (Bruker-microCT, Kontich, Belgium) operating under a voltage of 130 kV and a current of 115 μA. Projections were collected with a pixel size of 40 μm using a rotation step of 0.15° over 360° (around the vertical axis), a 1005 ms exposure time with 3 averaged images per projection, and a 2.0 mm thick copper filter. Tomographic slices were reconstructed using NRecon v. 1.7.1.0 software (SkyScan 1273; Bruker-microCT, Kontich, Belgium), using a beam hardening correction of 20%, a ring artifact correction of 10, and a smoothing of 1. Segmentation and 3D rendering were performed using 3D Slicer (https://www.slicer.org/) on a slightly reduced version of the dataset (2×2×2 binning, resulting in a voxel size of 80 μm) to facilitate 3D data processing.

3.7 Raman microspectroscopy

Raman microspectroscopy was performed on MGL 103593b, 103606b, 103613a and 103596a at the Institute of Earth Sciences, University of Lausanne, using a Horiba Jobin Yvon LabRAM 800 HR spectrometer in a confocal configuration, equipped with an Ar+ laser (532 nm) excitation source and an electron multiplying charge-coupled device (EMCCD). Spectra were collected at constant room temperature, directly on the sample surface, by focusing the laser beam with a 400 μm confocal hole using a long working distance ×50 objective (NA = 0.70). This configuration provided a ≈4 μm spot size for a laser power delivered at the sample surface below 1 mW. Light was dispersed using a 1800 gr/mm diffraction grating. Mineral identification was carried out using references from the RRUFF database (https://rruff.info/).

3.8 Elemental mapping

Synchrotron micro X-ray fluorescence (μXRF) major-to-trace elemental mapping of MGL 103593b was performed at the DiffAbs beamline of the SOLEIL synchrotron source (France), using a monochromatic beam of 18 keV, selected for excitation of all chemical elements of the periodic table commonly present in geological materials, i.e. up to uranium (physically speaking, 18 keV X rays lead to the excitation of K-lines up to yttrium and L-lines from cadmium to uranium). In practice, however, the experiment is performed in air and as such detection of light elements up to phosphorous is not possible or very limited. In order to map the specimen with a high resolution, the beam was reduced down to a diameter of 50 μm using a molybdenum pinhole. The sample was mounted on a scanner stage allowing 90 mm movements (in both horizontal and vertical directions) with micrometre accuracy, and orientated at 45° to the incident beam. XRF was collected using a 4-element silicon drift detector (SDD, Vortex ME4, Hitachi High-Technologies Science America, Inc., total active area: 170 mm^2) oriented at 90° to the incident beam, in the horizontal plane. A two-dimensional spectral image, *i.e.* an image for which each pixel is characterized by a full XRF spectrum, was collected on the fly (Leclercq et al., 2015) over most the specimen at a 70 μm lateral resolution with a 25 ms dwell time (effective counting time 23 ms). The obtained dataset comprises 1'267'716 spectra (1068×1187 pixels; covering an area of 75×83 mm^2). μXRF elemental distributions presented in Figure 2C were produced through the collection of integrated intensities (sum of the four-elements XRF detector) within 100-eV-wide regions of the spectra corresponding to emission from elements of interest. Average μXRF spectra and main elemental contributions shown in Figure 2D were extracted and obtained using the PyMCA data-analysis freeware (Solé et al., 2007).

3.9 Abbreviations

Systematic abbreviations. a/b, indicates that there are part and counter-part; NC, indicates there is only one side.

Anatomical abbreviations. See Figure 1.

Institutional abbreviations. MGL, Musée Cantonal de Géologie Lausanne, Lausanne, Suisse; NMS, The National Museums of Scotland, Edinburgh, Scotland; NMW, National Museum Wales, Cardiff, Wales; YPM, Yale Peabody Museum of Natural History, Yale, USA.

4 Results

This report provides new anatomical data for two previously published taxa, *Aegirocassis benmoulai* and *Pseudoangustidontus duplospineus*, and describes one new species *Pseudoangustidontus izdigua*. Moreover, we erect the new subfamily Aegirocassisinae to include these two genera, uniting the suspension-feeding radiodonts from the Fezouata Shale by their shared morphological adaptations for that mode of life.

4.1 Preservation

Mineral characterization using Raman microspectroscopy of four of the specimens investigated herein confirm an iron oxide composition for these fossils, in line with previously published reports on the mode of preservation of these compressed non-mineralised fossils (Vaucher et al., 2016; Lefebvre et al., 2018; Saleh et al., 2018; Saleh et al., 2019; Saleh et al., 2020a; Saleh et al., 2020b; Saleh et al., 2020c; Saleh et al., 2021b). Quartz and clay minerals are the

10.3389/fevo.2023.1214109

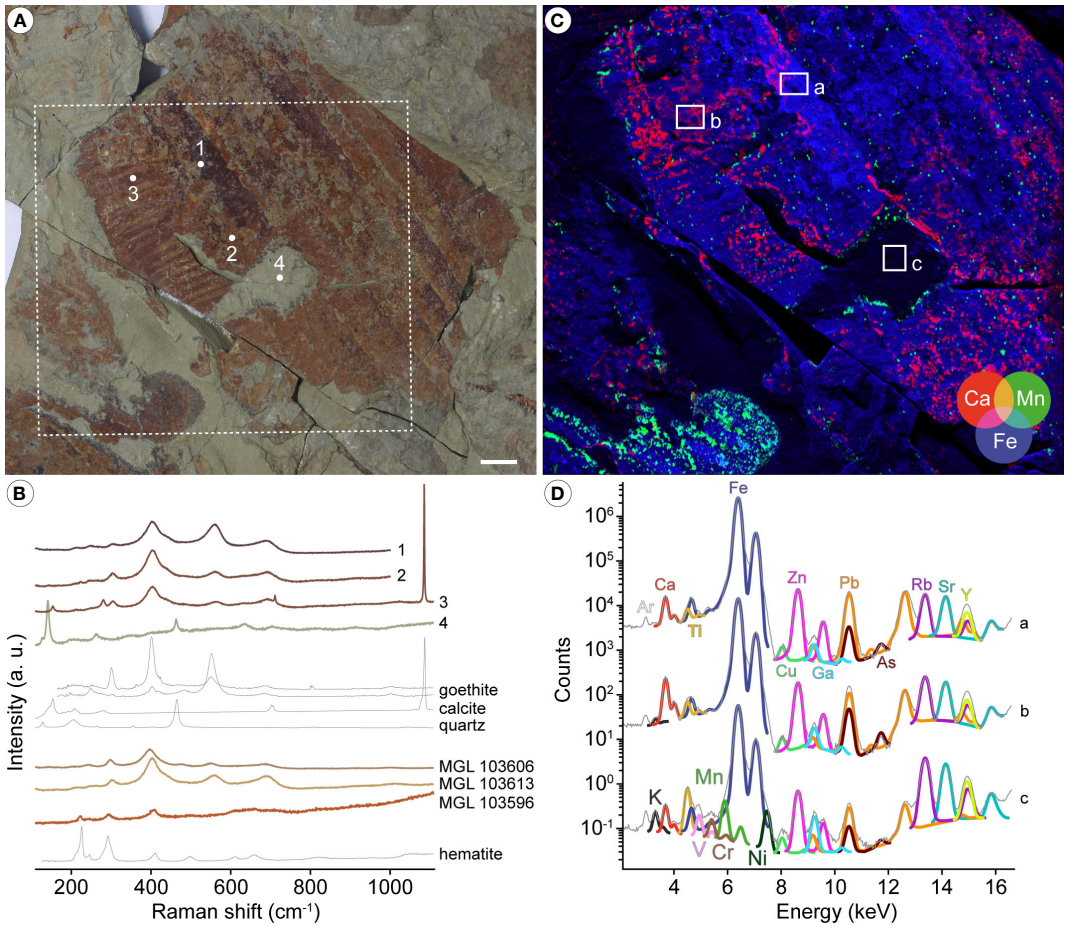

FIGURE 2
Mineralogical and elemental composition of radiodont frontal appendages from the Fezouata Shale. **(A)** Optical photograph of *Aegirocassis benmoulai* (Van Roy et al., 2015b) specimen MGL 103593b. **(B)** Raman microspectroscopy of MGL 103593b (spectra 1 to 4 from the corresponding points in A), as well as of *Pseudoangustidontus izdigua* sp. nov. paratype MGL 103606b, and of *Pseudoangustidontus duplospineus* (Van Roy and Tetlie, 2006) specimens MGL103613a and 103596a. Mineral reference spectra are taken from the RRUFF database; goethite is represented by two spectra collected using directions of polarization of the laser of 90° (top) and 0° (bottom). **(C)** False-color overlay of calcium (red), manganese (green), and iron (blue) distributions from the dotted white box in A. **(D)** Average µXRF spectra and main elemental contributions from the corresponding white boxes in C. Scale bars: 1cm. Image credit: P. Gueriau.

main constituents of the surrounding sedimentary mudstone matrix (Figures 2A, B). Characteristic spectral features identify the oxides as goethite (α-FeO(OH)) in MGL 103593 (*A. benmoulai*), MGL 103606 (*P. izdigua* sp. nov.) and MGL 103613 (*P. duplospineus*), and as hematite (α-Fe_2O_3) in MGL 103596 (*P. duplospineus*) (Figure 2B), highlighting variability in the formation and/or deposition of the iron oxides. The composition of MGL 103593 also locally includes calcite (Figures 2A, B), which is present over many regions of the specimen as evidenced by the distribution of Ca obtained using µXRF major-to-trace elemental mapping (Figure 2C). The random distribution pattern of calcite and the fact that carbonates from the matrix and from the skeletal elements of animals such as echinoderms are known to have dissolved under the action of modern water circulations (Saleh et al., 2020b; Saleh et al., 2021b) suggest that these phases deposited recently and therefore do not represent any biomineralization of the cuticularized tissue. µXRF spectra further indicate that the iron oxides have incorporated trace metals, particularly Zn, As and Pb (Figure 2D). Altogether, the geochemical data indicate that preservation of the material studied herein follows the taphonomic model proposed for other organisms preserved as two-dimensional iron oxide compressions within mudstone (Saleh et al., 2021b). Consequently, the lack of biomineralized structures within the studied appendages should be treated as a real absence, whereas the lack of soft cellular structures in direct contact with seawater is most likely taphonomic (Saleh et al., 2020a; Saleh et al., 2021a; Saleh et al., 2021b). By distinguishing between real biological and taphonomic absences, it becomes possible to identify and account for the biases that may have influenced the recorded faunal composition. In the context of the current study, this distinction provides a more reliable and comprehensive understanding of the original composition of the radiodont appendage (for similar consideration in the Chengjiang Biota, see Saleh et al., 2022b).

4.2 Dimorphism analysis

A new morphology of Hurdiidae endite is identified and well preserved on 29 specimens, some of which represent isolated

10.3389/fevo.2023.1214109

specimens of a single endite and some of which are associated with more endites and podomeres of the rest of the appendage. Consequently this either represents a new species of Hurdiidae or it represents a dimorphic endite from a known taxon. Detailed study of the most complete specimens of (MGL 103599, MGL 103604, MGL 103614, YPM IP 523428) allows us to confirm that dimorphism of endites is the most likely solution to this errant morphology. The dimorphic endite corresponds of the 6th endite of the intermediate region of *Pseudoangustidontus izdigua* sp. nov. and *Aegirocassis benmoulai*.

The dimorphic endites from *Aegirocassis* and *Pseudoangustidontus* are similar, however the insertion of the setae on the endite and the presence or absence of spinules allow for distinction of the dimorphic endites between the taxa. Three variables were revealed as crucial for this distinction: the insertion mode (simple or triangle) and the angle of insertion (between 75° and 135°) of setae on the endites, and the spinules (present or absent). Given that the distribution of measurements of the angle of insertion for both simple (Shapiro-Wilks test, n=20, W=0.8184, p=0.001649) and triangular (Shapiro-Wilks test, n=9, W=0.773, p=0.01001) insertions were significantly different from normal, a two-sample Kolmogorov Smirnov test with a Monte Carlo permutation was used to determine if there was a significantly different angle of insertion associated with the two insertion modes (Figure 3). It was found that there is a significantly higher insertion angle observed for setae with a simple insertion on the endite (between 100° and 135°) as compared to those with a triangular insertion (75° and 92°) (two sample Kolmogorov-Smirnov test, n=35, p=0.001). Moreover, all the specimens showing spinules attached to the setae correspond to those that have a simple insertion of 100° and 135° (Supplementary Table 3). These results allow us to say that there are

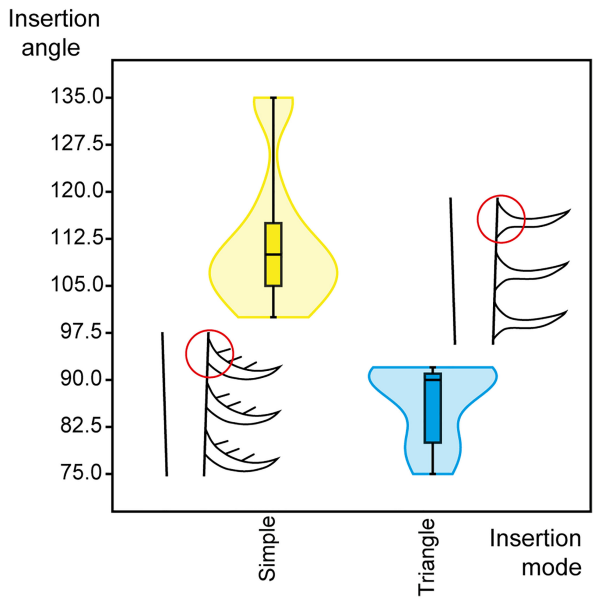

FIGURE 3
Violin plot representing the insertion angles of simple and triangular insertion types in *Aegirocassis benmoulai* (Van Roy et al., 2015b) and *Pseudoangustidontus izdigua* sp. nov. Insertion angles measured (n=29) as shown in Figure 1B. Line drawings with red circles show the simple versus triangular insertion modes. Image credit: G. Potin.

two morphotypes of the dimorphic endites. Owing to the most complete specimens YPM IP 523428, MGL 103599 and MGL 103614 for *Aegirocassis benmoulai* and MGL 103604 for *Pseudoangustidontus izdigua* sp. nov., we are able to associate the two morphotypes to these two taxa. The setae of the 6th endite of *Aegirocassis benmoulai* bear spinules and have simple insertions with angles ranging between 100° and 135°, except in specimens such as MGL 103593 that likely lost them taphonomically. The second morphotype is associated with *Pseudoangustidontus izdigua* sp. nov., where the 6th endite has setae attached with a triangle insertion of between 75° and 92°, none of which shows spinules. There is no specimen complete enough to show the dimorphic endite morphotype in *Pseudoangustidontus duplospineus*.

4.3 Mesh size

The mesh size calculation was made using measurements from the five first endites of the intermediate region of the frontal appendages. The mesh size of *Aegirocassis benmoulai* was measured for eleven specimens (MGL 103594, MGL 103600, MGL 103601, MGL 103627, MGL 103634, MGL 103665, MGL 104310, YPM IP 523428, YPM IP 525217, YPM IP 527123, YPM IP 527125) as these specimens show sufficient spinules preservation to allow measurements and calculation of mesh size, giving a mean of 0.56mm. For the species *Pseudoangustidontus duplospineus* measurements were possible on all specimens (n=7) (MGL 102360, MGL 103596, MGL 103609, MGL 103612, MGL 103613, MGL 104332, NMS G.2005.119.1) giving a mean of 0.49mm. Finally, *Pseudoangustidontus izdigua* sp. nov. has a mean of 0.51mm based on eighteen specimens (MGL 103027, MGL 103603, MGL 103604, MGL 103606, MGL 103607, MGL 103611, MGL 103616, MGL 103621, MGL 103622, MGL 104052_1, MGL 104101, MGL 107733, YPM IP 226560, YPM IP 226561, YPM IP 517614, YPM IP 517616, YPM IP 524840, YPM IP 525219). These data were plotted on the graph showing the size of particles captured by suspension-feeding radiodonts (Supplementary Table 2), modified from Vinther et al. (2014), giving a mesoplankton (0.2-20mm) size range of prey for both *Pseudoangustidontus* species and *Aegirocassis*.

4.4 Feeding strategy proportions

A total of hundred and twenty-one frontal appendages specimens were studied of which seventy-eight were possible to identify to species level, yielding forty three *Aegirocassis benmoulai*, seven *Pseudoangustidontus duplospineus* and twenty-eight *Pseudoangustidontus izdigua* sp. nov. A further nine specimens could be confidently assigned to the genus *Pseudoangustidontus* but not allocated to a species. There are a further eight specimens that can be allocated to the broader Aegirocassisinae subfam. nov. that are suspension-feeding radiodonts from Fezouata but without allocation to a genus. Finally, there are nine sediment-sifter radiodont appendages from the Hurdiidae family. The total number of suspension-feeding specimens is therefore 112 out of

121 specimens (≃92.6%), whereas only ≃7.4% of the radiodont appendage specimens are non-suspension-feeding appendages (Supplementary Table 1).

5 Systematic paleontology

Super-phylum Panarthropoda Nielsen, 1995

Phylum (stem-group) Arthropoda von Siebold, 1848

Order Radiodonta Collins, 1996

Family Hurdiidae Lerosey-Aubril and Pates, 2018

Type genus: *Hurdia* Walcott, 1912

Other genera included: *Aegirocassis* Van Roy et al., 2015b, *Buccaspinea* Pates et al., 2021b, *Cambroraster* Moysiuk and Caron, 2019, *Cordaticaris* Sun et al., 2020a, *Pahvantia* Robison and Richards, 1981, *Peytoia* Walcott, 1911, *Pseudoangustidontus* Van Roy and Tetlie, 2006, *Stanleycaris* Caron et al., 2010, *Titanokorys* Moysiuk and Caron, 2021, *Ursulinacaris* Pates et al., 2019.

Questionably: *Schinderhannes* Kühl et al., 2009

Emended diagnosis: Radiodonts with frontal appendages composed of proximal, intermediate, and distal regions: proximal region comprising one or more podomeres a single or no endites; intermediate region composed of at least five podomeres that are usually twice as high as they are long, and bearing paired or unpaired endites longer than podomere heights; distal region characterized by podomeres reduced in height, length, or both, bearing short or no endites. Endites in the form of thin or thick blades, not alternating in size between odd and even podomeres, typically curved towards the appendage distal tip, and bearing auxiliary structures (spines or setae) projecting from their anterior margins only. Oral cone comprises four large plates at right angles to each other. Large tripartite cephalic carapace extending about as long as half the length of the rest of the body, consisting of a large central element with tapering anterior and notched or flanged postero-lateral margins, flanked by a pair of slightly smaller ovoid or lenticular lateral elements with or without posterior notches. Body bearing two sets of flaps, dorsally and ventrally located, on each main body segment (Emended from Moysiuk and Caron, 2022).

Subfamilly Aegirocassisinae subfam. nov.

Figures 4–9.

Etymology: In recognition of *Aegirocassis benmoulai* species, the first recognised member of this group.

Included taxa: *Aegirocassis* Van Roy et al., 2015b, *Pseudoangustidontus* Van Roy and Tetlie, 2006.

Diagnosis: Hurdiids with multisegmented anterior frontal appendages comprising at least 6 podomeres in the intermediate region. The 6 podomeres of the intermediate region bear one endite each, 6 to 10 times longer than the podomere height. The first 5 most proximal endites bear thin setae (less than 1 mm in width, but at least as long as the endite thickness), either single or in pairs, with a triangle insertion to the endite. The 6th most distal endite is dimorphic in bearing curved setae thicker (more than 1 mm wide) but shorter as compared to the setae of the 5 first endites. The tip of all endites is curved toward the inner margin. The distal region of the appendage is short, consisting of only a few podomeres, possibly bearing a terminal spine.

Remark: All members of Aegirocassisinae had a suspension-feeding ecology, but it does not include all radiodonts interpreted as having a suspension-feeding paleoecology (i.e. *Tamisiocaris* and the possible *Pahvantia*, *Cambroraster*, *Echidnacaris briggsi*). So far, it only includes suspension-feeding radiodonts from the Fezouata Shale. It is named in recognition of *Aegirocassis benmoulai* and not *Pseudoangustidontus* because the latter was not definitively considered to be a radiodont before this study. So far, no proximal podomere has been observed in *Pseudoangustidontus*, and the distal appendage region in *Aegirocassis* and *Pseudoangustidontus* remain poorly known.

Genus *Aegirocassis* Van Roy et al., 2015b

Emended diagnosis for genus and species: Aegirocassisinae with tripartite frontal carapace having a central element at least as long as trunk, with an axial carina, pointed tip, rounded posterior margin and narrow down turned postero-ventral triangular extensions tapering towards rear and overlapping the lateral carapace elements dorsally. Lateral carapace elements oval, with rounded antero-dorsal expansion and longitudinal carina just below midline. Multisegmented anterior appendages consisting of seven podomeres. Proximal podomere longest, with one shorter, comb-like endite proximally. Succeeding six intermediate region podomeres bearing a single elongate, inward-angled endite that is 7 to 10 times longer than the podomere height. First five endites of the intermediate region bearing a single row of setae that are at least twice the length of the endite thickness (ratio T_e/L_s >0.5), each adorned with spinules in a 'V' orientation. The sixth intermediate endite dimorphic and bearing a single row of setae with a simple insertions oriented ventrally with an angle of 100° to 135° from the endite axis. Setae bearing single spinules. Terminal podomere stout, with pointed tip. Flat, broad trunk of 11 segments attaining maximum width at third segment and tapering to a blunt tip. Two pairs of non-overlapping flaps per segment: dorsal flaps pointed with recurving anterior and posterior margins, width about 13 the length of their attachment; ventral flaps narrow, triangular, width about 1.53 the length of their attachment. Continuous band of dorsal setal blades attached to base of each pair of dorsal flaps, traversing the trunk (Emended from Van Roy et al., 2015b).

Type species: *Aegirocassis benmoulai* Van Roy et al., 2015b.

Remark: The orientation of the setae in the first 5 endites from the intermediate region are not relevant because they are flexible.

Aegirocassis benmoulai Van Roy et al., 2015b

v. 2015b *Aegirocassis benmoulae* sp. nov. Van Roy et al.: figures 1–3; Extended data figures 1–7.

2015a *Aegirocassis benmoulai* Van Roy et al.,: figure 3.

Figures 2A, C, 4, 9A; Supplementary Figures 1, 2A, B.

Holotype (published): YPM IP 237172,

Paratypes (published): YPM IP 522227, YPM IP 527123, YPM IP 527125,

Plesiotypes: MGL 103593, MGL 108059, YPM IP 523428 (was published as additional material),

Published additional materials: YPM IP 523423, YPM IP 523425, YPM IP 523810, YPM IP 525217, YPM IP 527124, YPM IP 531183,

10.3389/fevo.2023.1214109

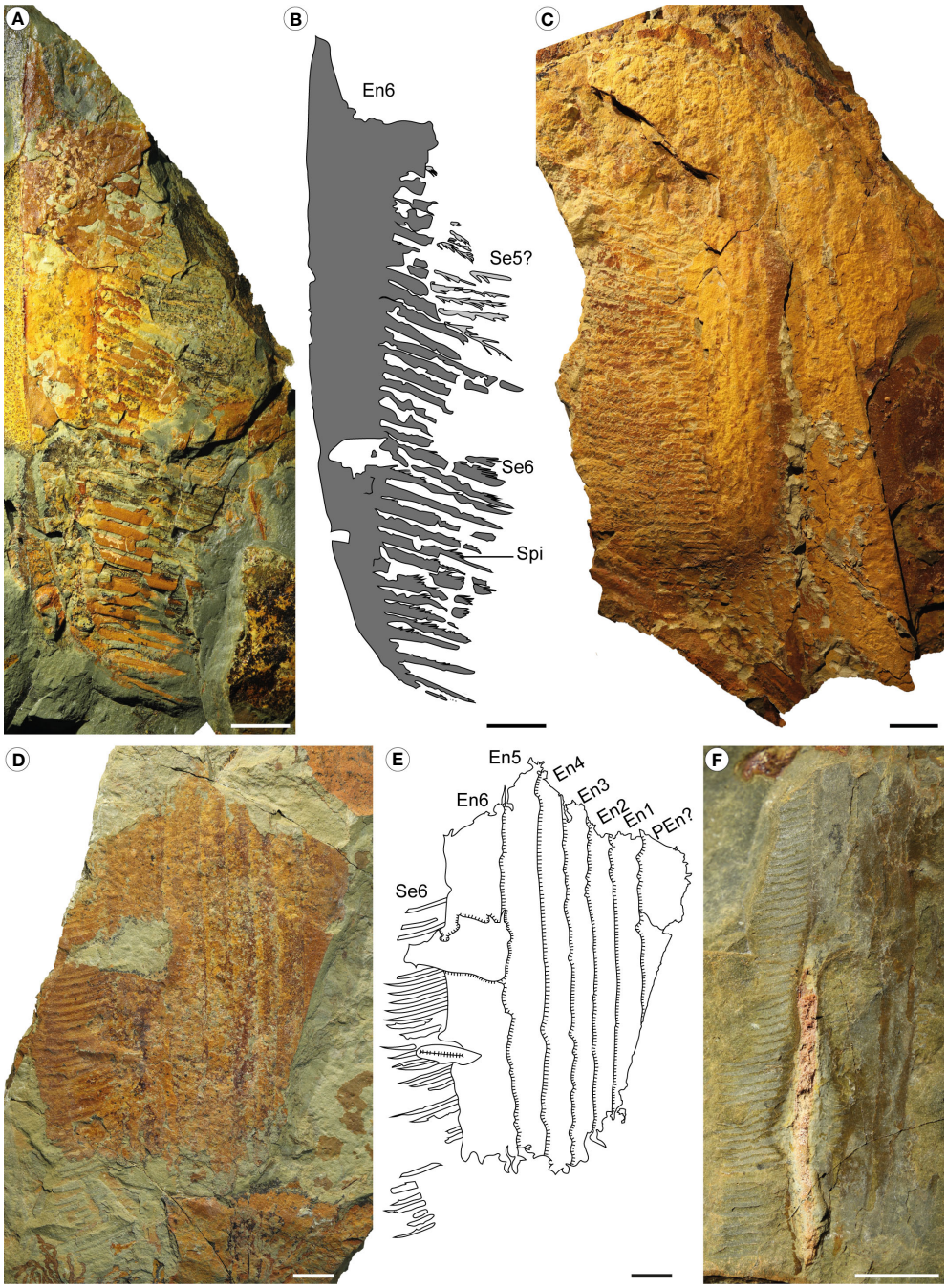

FIGURE 4
Aegirocassis benmoulai from the Fezouata Shale Formation, *Sagenograptus murrayi* biozone, Morocco. **(A, B)** YPM IP 523428 (plesiotype), showing the 6th endite showing setae and spinules, with the setae of one the 5 other intermediate region endites. **(A)** Picture under polarized filter. **(B)** Camera lucida drawing. **(C)** MGL 103594, picture under polarized filter of intermediate region podomeres and two of the 5 first intermediate region endite, with setae and pair of spinules. **(D, E)** MGL 103593 (plesiotype), showing the 6 intermediate region endites, the 6th one showing the setae. **(D)** Picture under polarized filter. **(E)** Camera lucida drawing. **(F)** MGL 103614, picture under polarized filter of the endites 4, 5 and 6 from the intermediate regions showing setae and spinules. Abbreviations: same as Figure 1. Scale bars: 1cm. Images and drawings credit: G. Potin

Additional material: MGL 103017, MGL 103594, MGL 103595, MGL 103598, MGL 103599, MGL 103600, MGL 103601, MGL103602, MGL 103608_1, MGL 103614, MGL 103615, MGL 103618, MGL 103620, MGL 103627, MGL 103628, MGL 103629, MGL 103630, MGL 103631, MGL 103633, MGL 103634, MGL 103635, MGL 103636, MGL 103665, MGL 104052_2, MGL 104310, MGL 104322, MGL 107387, MGL 107718, MGL 107912, MGL 107914, MGL 107915, MGL 108047_2, MGL 108053, MGL 108054, MGL 108056, MGL 108058, MGL 108061, MGL 108062, YPM IP 521575, AA.BIZ22.OI.4.

Locality: Specimens collected from outcrops in the Ternata plain, c. 18 km NW of the city of Zagora (Morocco) and c. 6 km NNE of the village of Beni Zouli. GPS coordinates are curated with specimens.

Horizon and age: Lower Fezouata Shale, Late Tremadocian, *Sagenograptus murrayi* biozone.

Diagnosis: As for the genus.

Description: Most of the specimens are incomplete, but together contribute to the overall description. Measurements and quantitative data can be seen in Supplementary Table 2.

MGL 103594 a/b (Figure 4C; Supplementary Figures 1A, B) shows many of the typical features of the appendages of this taxon as previously described by Van Roy et al. (2015b). It consists in one proximal podomere bearing a short endite and five intermediate podomeres, with the last one being fragmented. The podomeres are curved along the dorsal margin. Endites, setae and spinules are most complete on the first two podomeres (IP1 & IP2) in the intermediate region, which shows the typical anatomy of a single row of long setae on the anterior margin with spinules oriented towards the inner margin. Endites and setae are not completely preserved, but there are at least thirty-two setae and they are >2cm in length (Figure 4).

YPM IP 523428NC, (already mentioned in Van Roy et al., 2015b) is here reinterpreted as showing the dimorphic endite on the 6th podomere of the intermediate region endite, only the most distal part, bearing thick, short and curved setae (Figures 4A, B), some of which show multiple single spinules on their dorsal margin. Setae of another endite (that we cannot see because the more distal endites is overlapping it) are also visible, showing setae that bear rare spinules in the "V" orientation, thus confirming that the dimorphic endite is found in the same appendage as other endites with the previously described morphology. Other specimens also show the newly identified dimorphic endite.

MGL 103593a/b exhibits the 6 endites of the intermediate region, overlapping each other, and possible a short endite of the proximal region (Figures 4D, E). The 6th endite is the only one showing setae, which are reduced and measure less than 20mm in length, but which are relatively thick (more than 1mm).

MGL 108059NC (Supplementary Figure 1D) is also one of the rare specimen showing the two morphologies of the setae. It consist of three long (146.7 mm) fragmented intermediate region endites (the 4th, 5th and 6th). Endite 4 exhibits rare thin setae (length not complete), with a few spinules visible that are arranged in a "V". Endite 6 has several thick setae attached, with only a few spinules preserved.

MLG 103614a/b (Figure 4F; Supplementary Figures 1E, F) is a small specimen consisting of endites 4 to 6 of the intermediate region. The dimorphic 6th endite bears curved and thick setae that have single spinules on the dorsal margin. Endites 3, 4 and 5 show the triangular insertion points of the thin setae, but the setae are mostly covered by endite 6.

MGL 103599a/b (Supplementary Figure 1G) consists of endites 3 to 6 of the intermediate region, with visible long and thin setae bearing rare spinules on endites 4 and 5, and thicker setae on the 6th endite, with a simple insertion of 110°.

The largest specimen, MGL 103620NC, consists in endites 4 to 6, with endite 6 exhibiting fragmented setae. Despite the fact that it is fragmented, this endite measures 250mm in length.

Comments: First named *Aegirocassis benmoulae* in Van Roy et al. (2015b), a nomenclature correction in Van Roy et al. (2015a) renamed the species *Aegirocassis benmoulai*. The new material matches the previous published description, except for the new features described for the dimorphic endite. The holotype YPM 237172 is the only non-frontal appendage specimen listed above, so it is not used in the statistics. YPM IP 523428 was considered as Supplementary Materials in Van Roy et al. (2015b) (Extended Data figure 6) but in this paper, it is considered as a plesiotype owing to the new morphological characters (Supplementary Table 1). The isolated setae from YPM IP 523428 have been identified as belonging to the same specimen because they are oriented in the exact same direction, and covered by the visible endite.

Genus *Pseudoangustidontus* Van Roy and Tetlie, 2006

Diagnosis (emended): Aegirocassisinae with appendages characterised by the first 5 intermediate region endites bearing paired setae that are thin, at least as long as the endite thickness, and not bearing any spinules. Endites have a carina on the outer margin. The 6th intermediate, dimorphic, endite bearing single curved setae, shorter (around twice the endite thickness length) with a triangle insertion and oriented ventrally with an angle of 75° to 90° from the endite axis (Modified from Van Roy and Tetlie, 2006).

Type species: *Pseudoangustidontus duplospineus* Van Roy and Tetlie, 2006

Pseudoangustidontus duplospineus Van Roy and Tetlie, 2006

2006 *Pseudoangustidontus duplospineus* Van Roy and Tetlie: figures 3, 4.

Figure 5.

Holotype: NMS G.2005.119.1

Additional material: MGL 102360, MGL 103596, MGL 103609, MGL 103612, MGL 103613, MGL 104332.

Locality: Specimens collected from outcrops in the Ternata plain, c. 18 km NW of the city of Zagora (Morocco) and c. 6 km NNE of the village of Beni Zouli. GPS coordinates are curated with specimens.

Horizon: Lower Fezouata Shale, end of the Tremadocian, *Sagenograptus murrayi* biozone. According to Van Roy and Tetlie (2006), Upper Fezouata Shale, from Middle Arenig to end of the Floian.

Diagnosis (emended): *Pseudoangustidontus* with paired setae alternating in length short/long. Shorter setae around the same length as endite thickness/height and long ones at least twice the length of endite thickness/height (Modified from Van Roy and Tetlie, 2006).

Description: MGL 103596 a/b (Figures 5A, B) consists of a fragmented endite of a frontal appendage. The endite has a carina on the outer margin with a thickness of 0.5 mm. The setae are organized in pairs but is only visible on some setae owing to the incomplete preservation. Longest setae are almost 3 times longer than the small ones. MGL 103613 a/b (Figure 5C) is a long endite. The endite extremity is curved inwards. Paired setae are badly preserved, but are in pairs, with alternation in length visible for 3 of them.

Pseudoangustidontus izdigua sp. nov.

Life Science Identifier (LSID): urn:lsid:zoobank.org:act:53D86B6F-65DF-490C-B8EB-BEC30A2C49D1

v. 2010 spinose arthropod appendage Van Roy et al.: figure 1I.

Figures 6–8, 5B; Supplementary Figure 2A.

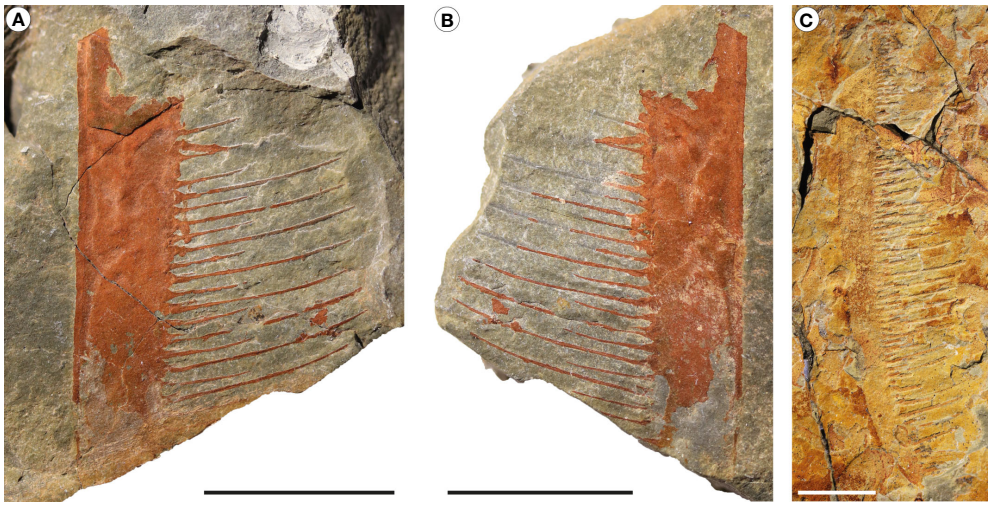

FIGURE 5
Pseudoangustidontus duplospineus from the Fezouata Shale Formation, *Sagenograptus murrayi* biozone, Morocco. **(A, B)** MGL 103596, picture under polarized filter of a single endite showing the alternative sizes of the paired setae. **(A)** Part. **(B)** Counterpart. **(C)** MGL 103613, picture under polarized filter of a single endite showing the alternative sizes of the paired setae. Scale bars: 1cm. Images credit: G. Potin.

Etymology: The species *izdigua* refers to the Tamazight language translation for filter, izdigue, as this species is considered to be a suspension-feeding radiodont.

Holotype: MGL 108047_1

Paratypes: MGL 103606, MGL 104052_1, YPM IP 226559,

Additional material: MGL 102153_2, MGL 102181_2, MGL 102237_2, MGL 103027, MGL 103597, MGL 103603, MGL 103604, MGL 103607, MGL 103608_2, MGL 103611, MGL 103616, MGL 103621, MGL 103622, MGL 104101, MGL 104227, MGL 104414, MGL 107733, YPM IP 226560, YPM IP 226561, YPM IP 517614, YPM IP 517616, YPM IP 518318, YPM IP 524840, YPM IP 525219, YPM IP 532033.

Locality: Specimens collected from outcrops in the Ternata plain, c. 18 km NW of the city of Zagora (Morocco) and c. 6 km NNE of the village of Beni Zouli. GPS coordinates are curated with specimens.

Horizon: Lower Fezouata Shale, Late Tremadocian, *Sagenograptus murrayi* biozone.

Diagnosis: *Pseudoangustidontus* with frontal appendage bearing endites with setae that are all the same length (no long/short alternation). The length of the setae is at least twice as long as the endite thickness.

Description: MGL 108047_1 NC (Figure 6; Supplementary Figure 2A) is divided in two parts, a lower (Figure 6C) and an upper part (Figures 6D, E), separated by the overlapping specimen MGL 108047_3. This specimen consists of four podomeres (visible in the upper part), probably from the intermediate region. It exhibits at least 5 intermediate region endites (the 2nd to the 6th) visible in the lower part. Those endites all have attachment sockets, in which setae would have attached. No setae are present in the lower part of endites 2 to 6. Endite 6 has several thick, short and curved setae attached (19.8mm in length and 2.7mm width). Their insertion mode is obscured by the visible sockets and the patchy preservation. In the upper part, there are three visible endites in the intermediate region, but the overlying setae make it impossible to determine which of the five non-dimorphic endites they are and to which podomeres they are associated. These endites in the upper part bear long and thin setae (29.9mm long and 0.2mm in width), and in several places the paired attachment of setae is clearly visible. The insertion mode of these setae is triangular, and insertion sockets are visible for some setae (Figures 6D, E).

Specimen MGL 103606a/b/c/d consists of 6 intermediate region endites (Figure 7). MGL 103606a/b/c shows that endites 1 to 5 have setae in pairs, which are long and thin with equal length and 103606c/d shows that the 6th endite bears single curved setae that are shorter and thicker, with a triangle insertion of 90°. On MGL 103606a/b the carina on the outer margin can be distinguished. There is an unidentified carapace fragment of 3mm diameter preserved amongst the setae of the endites 1 and 2 of this specimen.

Specimen MGL 104052_1 a/b (Figures 8A–E) consist of 6 podomeres, at least 4 of which are from the intermediate region because they are associated with long endites bearing long and thin setae in pairs that have a regular non-alternating length. The other endites cannot be identified because incompleteness of the appendage prevents determining an orientation. The podomeres are preserved oblique to the sediment surface and in section, showing a U-shaped outline that is 12 mm in width.

YPM IP 226559 (Figure 8F) consist of 6 endites from the intermediate region, on which the 6th endite clearly possesses thick and short setae that have the triangle insertion of 90°. Some of the other endites show the triangle base of the paired setae, which are occasionally fragmented.

MGL 103611NC (Figure 8G), the smallest specimen, consists of a fragmented curved endite bearing setae in pairs. The tip is curved.

10.3389/fevo.2023.1214109

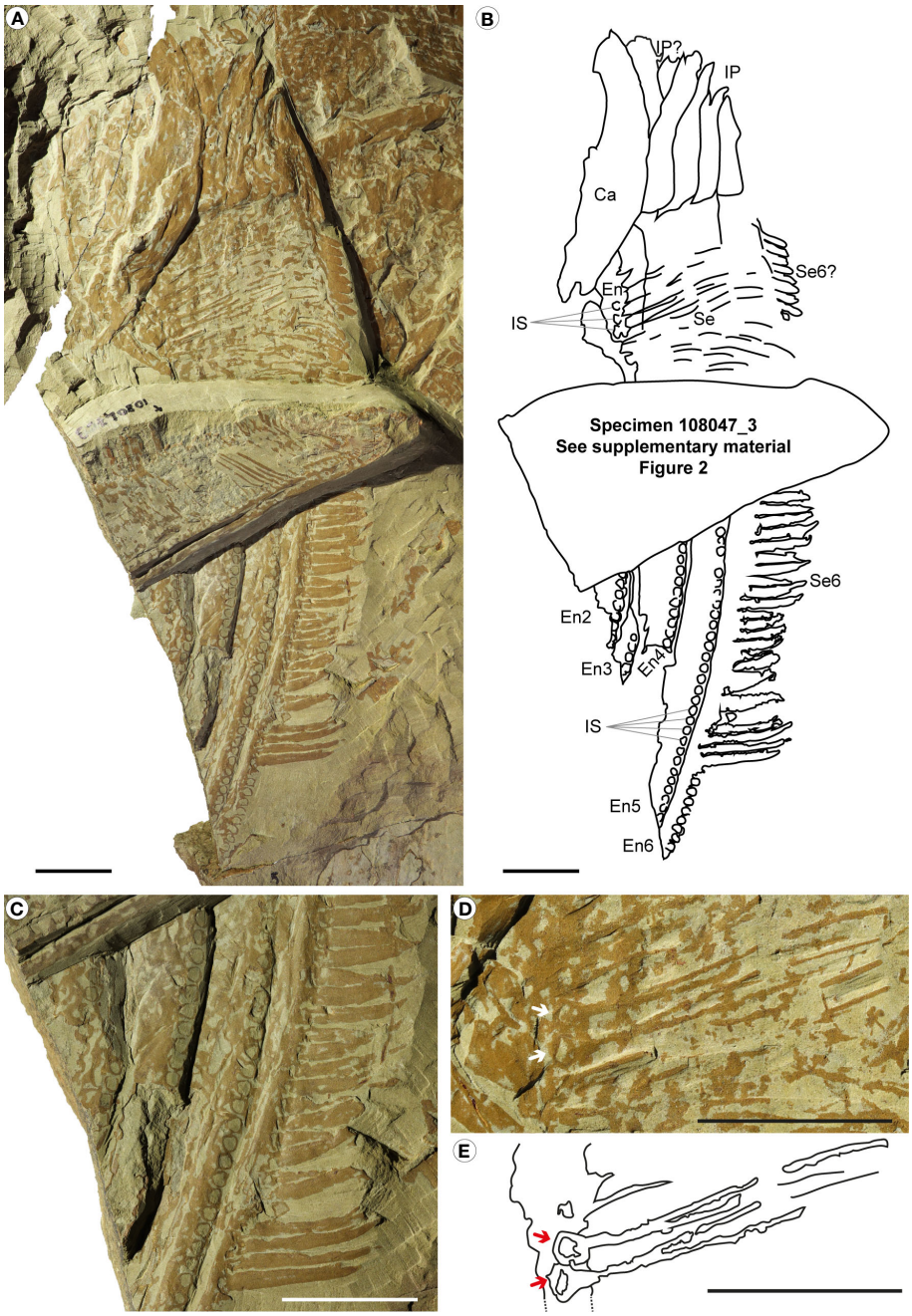

FIGURE 6
Pseudoangustidontus izdigua, MGL 108047_1 (holotype) from the Fezouata Shale Formation, *Sagenograptus murrayi* biozone, Morocco. **(A, B)** Entire specimen showing 4 intermediate region podomeres, with, at least 5 intermediate region endites (the 2nd to the 6th) with the two morphologies of setae and the insertion sockets. **(A)** Picture under polarized filter. **(B)** Camera lucida drawing. **(C)** Picture under polarized filter of the lower part of the specimen with endites 2 to 6 of the intermediate region, all showing the insertion sockets and the 6th endite showing the setae. **(D)** Picture under polarized filter of the upper part of the specimen with 4 (maybe 5) podomeres, with the 6th endite of the intermediate region with setae, and non-recognizable intermediate region endites, some showing the pairs of setae and some insertions sockets associated. **(E)** Camera lucida drawing of the setae in pairs with insertion sockets associated. Ca, carapace; other abbreviations as in Figure 1. Scale bars: 2cm. Images and drawing credit: G. Potin.

MGL 103027a/b is a fragment of curved endite with setae showing length irregularities due to the incomplete preservation. It is bearing setae in pairs with clear triangular insertions.

MGL 103603a/b (Figure 8H) consist of a small fragmented endite with the inner margin bear setae, in pairs, with a regular size.

Remark: The major difference compared to *Pseudoangustidontus duplospineus* is that the setae all have the same length. There is no size alternance between even and odd setae, as seen in *Pseudoangustidontus izdigua*. MGL 104052_1 is the first *Pseudoangustidontus* that shows podomeres and confirms that the genus belongs to Radiodonta and the

10.3389/fevo.2023.1214109

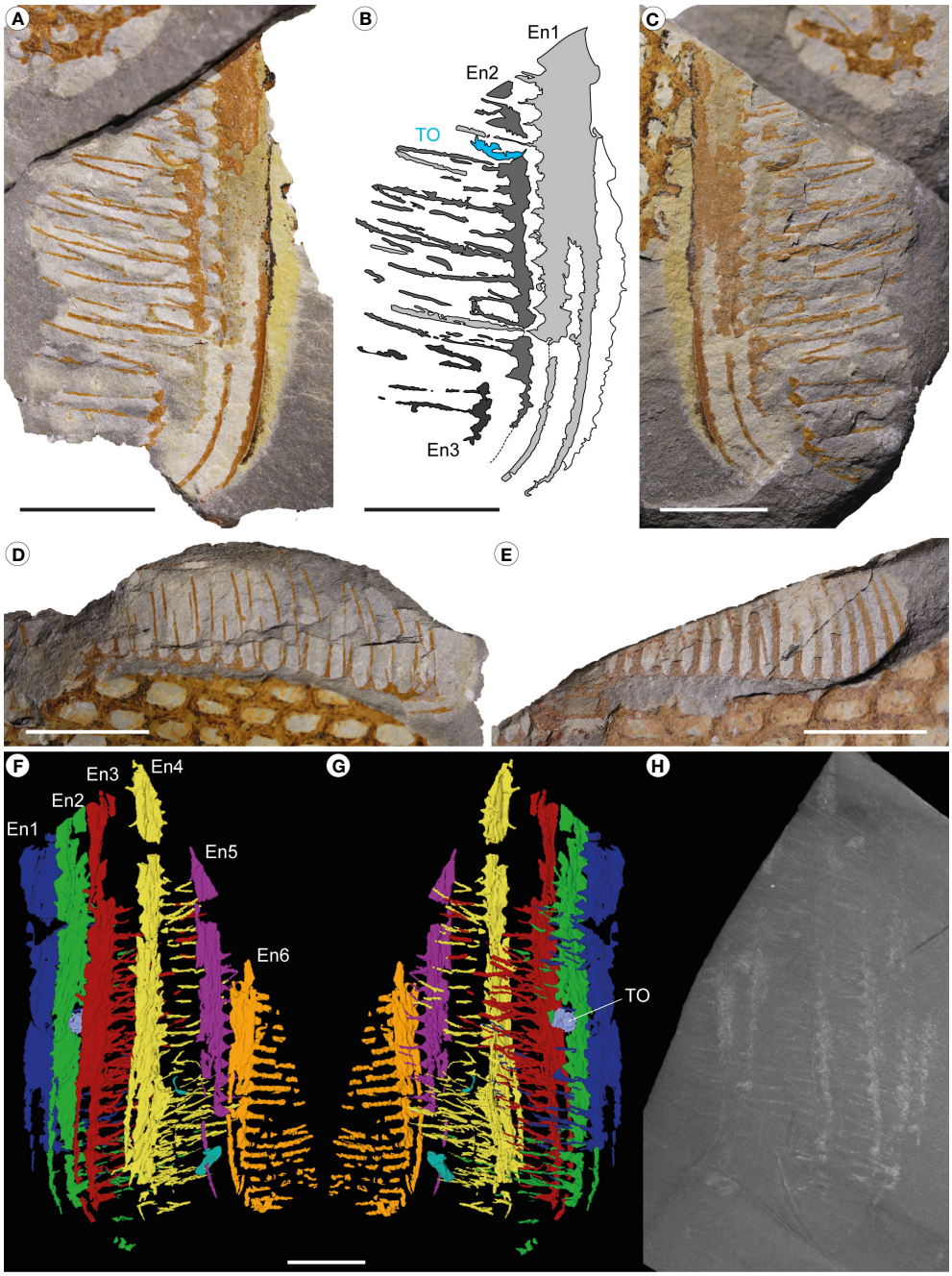

FIGURE 7
Pseudoangustidontus izdigua, MGL 103606 (paratype) from the Fezouata Shale Formation, *Sagenograptus murrayi* biozone, Morocco. **(A–C)** Intermediate region endites 1 to 3 showing setae in pairs and a trapped shelly prey. **(A, C)** Picture under polarized filter. **(B)** Camera lucida drawing. **(D)** Intermediate region endite 5 showing setae in pairs, and the setae of the 4th endite. **(E)** Intermediate region endite 6 showing setae. **(F–H)** X-ray computed microtomography. **(F)** 3D rendering of endites 1–6 in left lateral view. **(G)** 3D rendering in right lateral view. **(H)** Max intensity projection of 100 tomograms. TO, trapped organism; other abbreviations as in Figure 1. Scale bars: 1cm. Images and drawing credit: **(A–G)** G. Potin, **(H)** P. Gueriau.

Hurdiidae family. Sockets are visible in this species, but have not yet been observed in *P. duplospineus*.

Pseudoangustidontus sp.

Additional material MGL 102323, MGL 102326, MGL 103623_1, MGL 103624, MGL 103632, MGL 103637, MGL 107951, MGL 108052, YPM IP 517619.

Locality: Specimens collected from outcrops in the Ternata plain, c. 18 km NW of the city of Zagora (Morocco) and c. 6 km NNE of the village of Beni Zouli. GPS coordinates are curated with specimens.

Horizon: Lower Fezouata Shale, Late Tremadocian, *Sagenograptus murrayi* biozone.

10.3389/fevo.2023.1214109

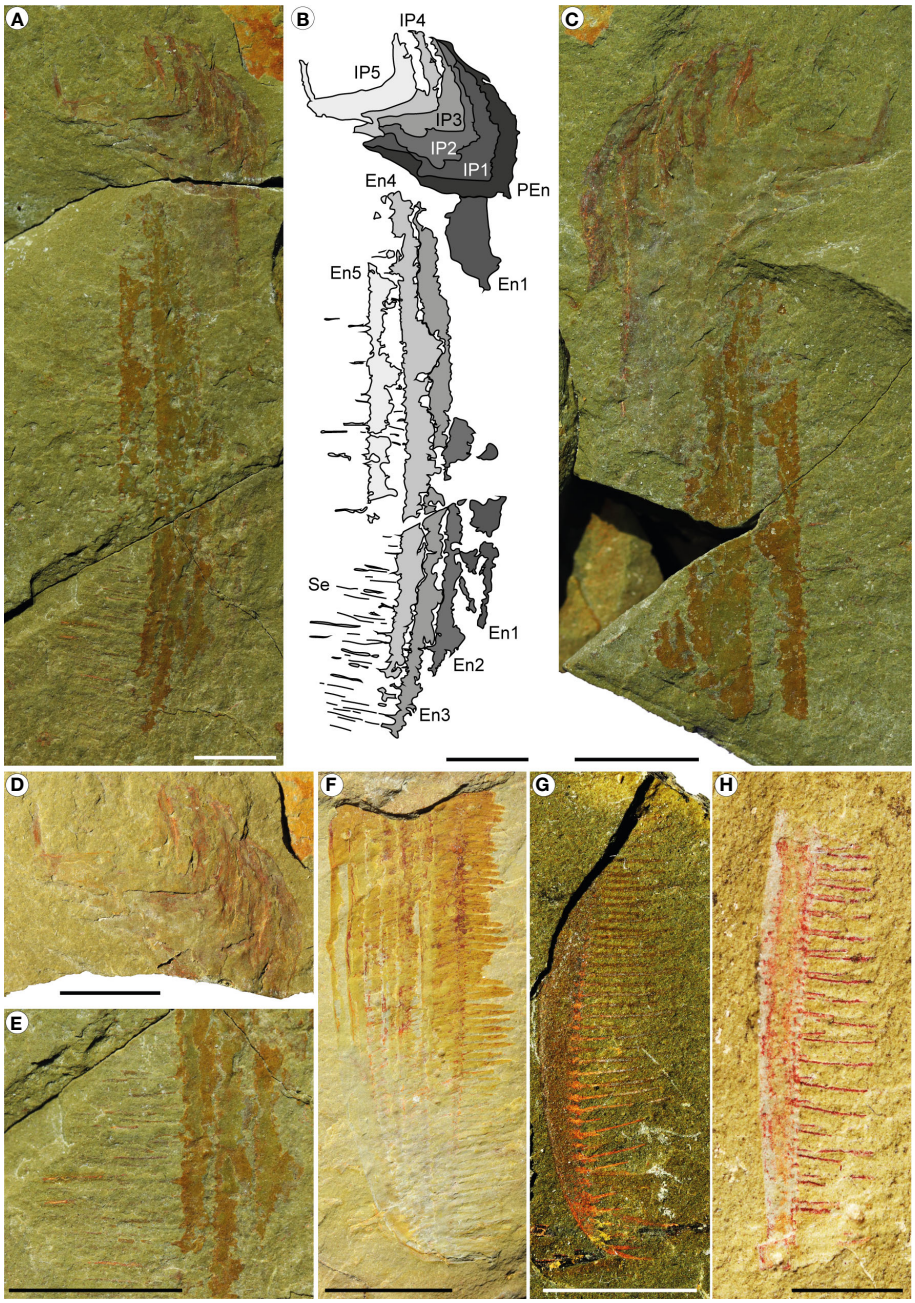

FIGURE 8
Pseudoangustidontus izdigua, from the Fezouata Shale Formation, *Sagenograptus murrayi* biozone, Morocco. **(A–E)** MGL 104052_1 (paratype). **(A, B)** Part with a series of 6 podomeres, probably the shaft podomere from the proximal region and the intermediate region podomeres 1 to 5, with the intermediate region endites 1 to 5, some with setae in pairs. **(A)** Picture under polarized filter. **(B)** Camera lucida drawing. **(C)** Counterpart. **(D)** Picture under polarized filter with a focus on the part podomeres. **(E)** Picture under polarized filter with a focus on the lower part of the endites and the setae in pairs. **(F)** YPM IP 226559 (paratype), picture under polarized filter with the 6 intermediate region endites showing setae. **(G)** MGL 103611, picture under polarized filter of the tip of a single intermediate region endite (one of the 5th firsts) showing setae in pairs. **(H)** MGL 103603 picture under polarized filter a single intermediate region endite (one of the 5th firsts) showing setae in pairs. Scale bars: **(A–F)**: 1cm; **(G, H)**: 0.5cm. Images and drawings credit: G. Potin.

Description: The specimens consist of endite(s) on which setae in pairs are attached, but the preservation does not allow us to distinguish if the setae size is alternating or regular.

Comments: The lack of well-preserved setae prevents identification to the species level, but they have morphological features that allow them to be identified as *Pseudoangustidontus*.

AEGIROCASSISINAE indet.

Additional material: MGL 102328, MGL 103617, MGL 103638, MGL 103651, MGL 103936_1, MGL 104062, MGL 104377, MGL 107468, MGL 108047_3, MGL 108050, MGL 108051, MGL 108055, MGL 108057, MGL 108060, YPM IP 530361.

Locality: Specimens collected from outcrops in the Ternata plain, c. 18 km NW of the city of Zagora (Morocco) and c. 6 km NNE of the village of Beni Zouli. GPS coordinates are curated with specimens.

Description: The specimens consist of endite(s) associated with setae. The preservation does not allow us to distinguish if the setae are in pairs, or if they have spinules.

Comments: The absence of well-preserved setae does not allow us to identify them to a genus level, but enough to identify the clade and therefore their feeding strategy.

6 Discussion

6.1 Implications for Systematic Paleontology

The family Hurdiidae, first mentioned by Vinther et al. (2014) and first formally described and defined by Lerosey-Aubril and Pates (2018), is characterized by possessing five podomeres each bearing at least one long endite. However, some specimens belonging to the Aegirocassisinae show six long endites, *Cordaticaris* has at least eight long endites (Sun et al., 2020a), and *Buccaspinea* has six endites with twelve podomeres (Pates et al., 2021b). Therefore, there are now several species in the Hurdiidae that have more than five long endites in the intermediate region.

Within Aegirocassisinae, a proximal region podomere with endite has only been observed in *Aegirocassis* so far (YPM IP 527125; MGL 103593; MGL 103594), so we did not include this character in the diagnosis of the broader group. Proximal region podomeres and endites are sometimes present in other Hurdiidae, e.g. *Hurdia* and questionably *Pahvantia* (Daley et al., 2013a; Lerosey-Aubril and Pates, 2018; Caron and Moysiuk, 2021), so this endite on the proximal podomere may be a character for all Hurdiidae.

Van Roy and Tetlie (2006) could not confidently place the genus *Pseudoangustidontus* in a stable phylogenetic position within Arthropoda owing to a lack of characters. *Pseudoangustidontus duplospineus* shares similarities and was named after the genus *Angustidontus* Cooper, 1936, an abundant and widespread Late Devonian fossil with enigmatic affinities at the time, but later recognized as a crustacean (Rolfe and Dzik, 2006) likely related to decapods (Gueriau et al., 2014). Van Roy and Tetlie (2006) also suggested that *Pseudoangustidontus duplospineus* could be a radiodont based upon morphological resemblance to *Echidnacaris briggsi* (Van Roy and Tetlie, 2006). With the discovery and description of *Pseudoangustidontus izdigua* sp. nov. herein, the genus can definitively be attributed to hurdiid radiodonts. Evidence comes mainly from two specimens that are sufficiently complete to demonstrate that *Pseudoangustidontus* is a radiodont. Specimen MGL 104052_1 preserves five aligned and overlapping *Pseudoangustidontus*-like "appendage fragments" in close association with six podomeres (Figures 8A–E), undoubtedly identifying them as the endites of a radiodont frontal appendage. Another specimen, MGL 103606 (Figure 7), shows a set of associated endites, aligned in parallel in the same plane but without podomeres, which are blade-like and indicate a Hurdiidae affinity. Most of the others fossils of *Pseudoangustidontus* consist of a single endite fragment with setae, suggesting a high degree of taphonomic disarticulation before preservation. This study allows for *Pseudoangustidontus duplospineus* and *Pseudoangustidontus izdigua* sp. nov. to be assigned to the order Radiodonta and the family Hurdiidae.

The new subfamily clade Aegirocassisinae within the family Hurdiidae has been erected due to the strong similarities between *Pseudoangustidontus* and *Aegirocassis*, with both genera having long endites bearing numerous, closely spaced, thin setae that are well adapted for suspension feeding (Figure 9). The erection of the new subfamily allows for the separation of the suspension-feeding versus the non-suspension-feeding Hurdiidae, at least within the Fezouata Shale. The only other possible suspension-feeding hurdiids, *Pahvantia* (as interpreted by Lerosey-Aubril and Pates, 2018), and *Cambroraster* (as interpreted in De Vivo et al., 2021) cannot be placed in Aegirocassisinae because of the lower number of endites, the absence of a distal dimorphic endite, and presence of at least two differentiated proximal endites. Note, however, that this purported suspension-feeding frontal appendage originally described for *Pahvantia* (Lerosey-Aubril and Pates, 2018) has since been re-interpretated as setal blades, with the appendage being re-described as having robust and distantly space auxiliary spines on the endites (Caron and Moysiuk, 2021), meaning it may actually be a sediment-sifter. *Pahvantia* can therefore be excluded from the subfamily Aegirocassisinae. As far as *Cambroraster* is concerned, De Vivo et al. (2021) consider as a suspension-feeder while Caron and Moysiuk (2021) interpret this taxon as a macrophagous sediment-sifter.

Owing to its consistent placement in the Tamisiocarididae familly, the other suspension-feeder *Tamisiocaris* cannot be placed in the Aegirocassisinae (Vinther et al., 2014; Paterson et al., 2023; Potin and Daley, 2023). This is also the case for the debated *Echidnacaris briggsi*, which is also placed in the Tamisiocarididae familly (Vinther et al., 2014; Paterson et al., 2023; Potin and Daley, 2023). *E. briggsi* is a debated specimen concerning the feeding strategy, with Paterson et al. (2020) having interpreted it as a suspension-feeder and Caron and Moysiuk (2021) considering the feeding ecology as unknown.

6.2 Ecology

Radiodonts are a group with a large diversity of feeding ecologies, as indicated by the morphology of their frontal appendages (Collins, 1996; Daley and Budd, 2010; Lerosey-Aubril and Pates, 2018; Guo et al., 2019; Caron and Moysiuk, 2021; Potin and Daley, 2023). Some, including *Amplectobelua* and *Anomalocaris*, are active raptorial predators, and have well-articulated appendages characterised by a large number of podomeres with short endites used to catch soft and lightly sclerotised prey (Daley and Budd, 2010; Guo et al., 2019; Caron and Moysiuk, 2021; Potin and Daley, 2023). The others are filter-feeders, as can be identified by their appendage having a smaller number of podomeres bearing long, usually straight and parallel endites with auxiliary spines (Daley and Budd, 2010; Caron and Moysiuk, 2021). The latter can be divided in two subgroups: the sediment-sifters and the suspension-feeders that can be differentiated by the robustness of the auxiliary structures on the endites, the interspace between them, and the length of the endites (Caron and

10.3389/fevo.2023.1214109

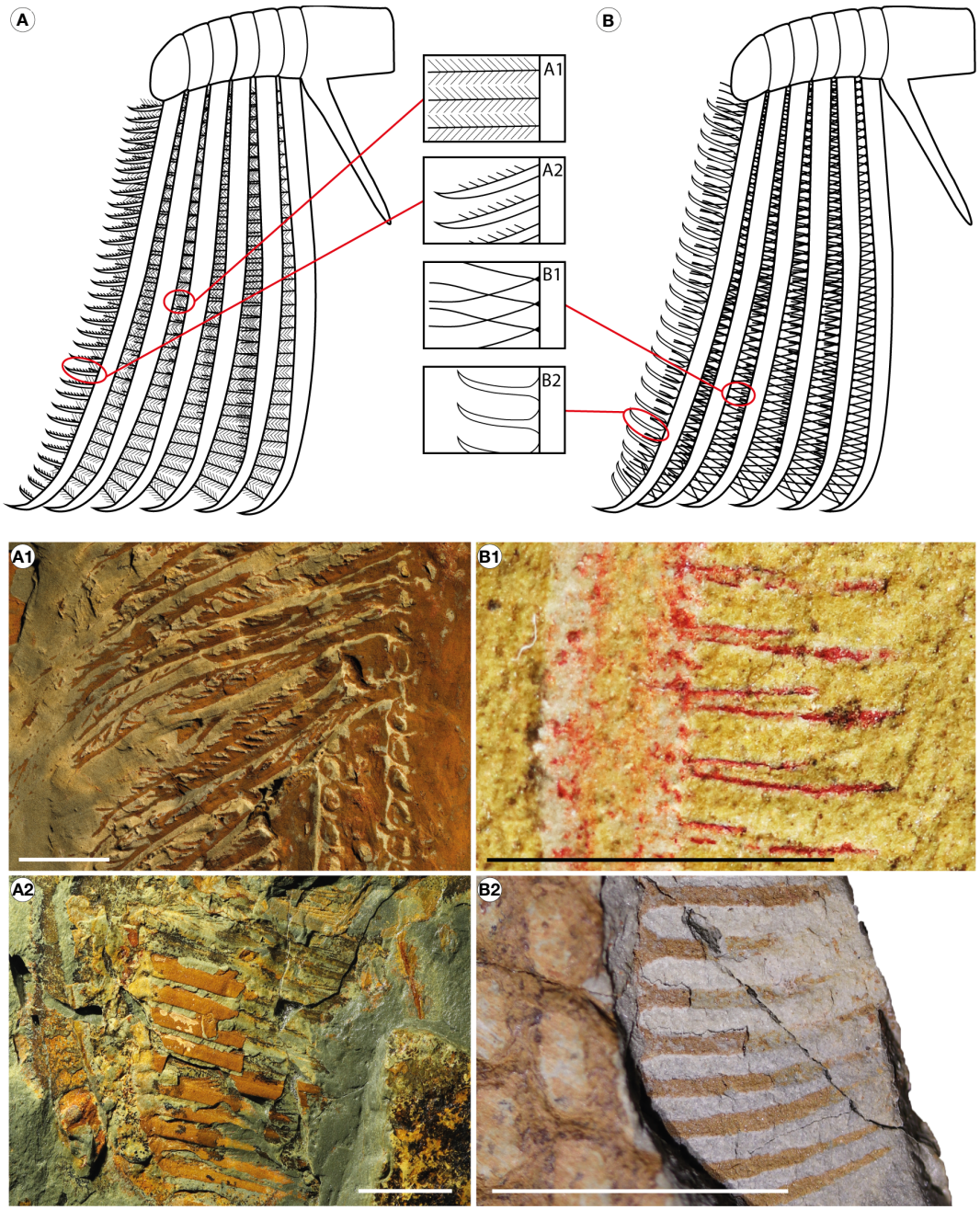

FIGURE 9
Reconstructions of Aegirocassisinae appendages with close-ups of the different setae morphologies. **(A)** *Aegirocassis benmoulai*. **(B)** *Pseudoangustidontus izdigua*. (A1) YPM IP 517125, *A benmoulai* setae from intermediate region endites 1 to 5. (A2) YPM IP 523428, *A benmoulai* setae from intermediate region endite 6. (B1) MGL 103603, *P. izdigua* setae from intermediate region endites 1 to 5. (B2) MGL 103606, *P. izdigua* setae from intermediate region endite 6. Scale bars: (A1, A2, B2): 1cm; (B1): 0.5cm. Images and drawings credit: (**A, B**, A2, B1, B2) G. Potin, (A1) A. Daley.

Moysiuk, 2021). For suspension-feeding radiodonts, auxiliary structures are called setae, because they are long and thin with a small interspace between them, and they can bear spinules (Caron and Moysiuk, 2021). The sediment sifter appendages have endites bearing auxiliary spines that are shorter and more robust with a wider interspace between them, forming a coarse, resistant mesh for sifting through sediment for infaunal prey. Endites are usually shorter in sediment-sifters as compared to suspension-feeders, to facilitate movement through the sediment and resist breakage (Caron and Moysiuk, 2021).

In the Fezouata Shale, radiodont frontal appendages have not yet been found fully articulated with all other body parts of the animal in place, but they have been found together in disarticulated assemblages with cephalic carapaces. The position and the role of the appendages in relation to the oral cone (mouthpart) remains unknown. Nonetheless, two hypotheses have been proposed

10.3389/fevo.2023.1214109

regarding food intake mechanics in suspension-feeders. First, if the appendages were positioned directly in front of the mouth, the fine mesh created by setae and spinules would play a passive role in feeding by letting particles pass through the appendages to directly enter the oral cone. In this case, the particles captured by the setae are not consumed and are later evacuated in the water. The second hypothesis proposes that the appendages are held out anterior to the head where they play an active role in feeding by capturing what will be eaten. The small particles that pass through the setae are not consumed, and the larger plankton caught in the mesh of the frontal appendages is moved to the oral cone for consumption. This is the hypothesis that has been proposed for the function of suspension-feeding in radiodonts so far (Vinther et al., 2014; Van Roy et al., 2015b; Lerosey-Aubril and Pates, 2018), and is followed in the present work. Consequently, measuring the appendage mesh size allows for an estimation of the minimum prey size that suspension-feeding animals can capture (Sieburth et al., 1978; Vinther et al., 2014; Van Roy et al., 2015b; Lerosey-Aubril and Pates, 2018).

Previously, among suspension-feeding radiodonts, mesh sizes in *Aegirocassis benmoulai* and *Tamisiocaris* have been estimated to ca. 0.5mm in average, enabling them to capture prey of about 1 mm (Figure 10) (Vinther et al., 2014; Lerosey-Aubril and Pates, 2018). With current alignment of prey and non-spheroidal prey shape, it is estimated that the maximum length of the prey that can be ingested is around three times the mesh width (see a similar calculation for Archaeocyathan filtration in Antcliffe et al. (2019). With the study of the new specimens, the average mesh size of *Aegirocassis benmoulai* is here re-evaluated to be 0.56mm. The average mesh size in *Pseudoangustidontus* is ca. 0.50mm, with 0.49mm and 0.51mm in *P. duplospineus* and *P. izdigua* sp. nov., respectively. The prey of these two genera fall into the category of mesoplankton (0.2-20mm), which consists of metazooplankton (small invertebrates) and some phytoplankton and protozooplankton (Sieburth et al., 1978; Vinther et al., 2014; Lerosey-Aubril and Pates, 2018; Antcliffe et al., 2019). Early Paleozoic metazooplankton was composed of trilobitomorphs (mostly larvae), ostracods, bradoriids, copepods, malacostracan and branchiopod arthropods, as well as graptolites and chitinozoans (Perrier et al., 2015; Servais et al., 2016). For the possible suspension-feeder *Pahvantia*, the mean mesh size was measured to be 0.7mm, which allowed it to capture smaller (>0.10mm) prey (Figure 10) (Lerosey-Aubril and Pates, 2018), including large microplankton (mainly phytoplankton and protozooplankton) and the smallest mesoplankton (Sieburth et al., 1978; Vinther et al., 2014; Lerosey-Aubril and Pates, 2018), which in the Early Paleozoic could include eggs, arthropod larvae and small specimens of acritarchs or chitinozoans (Perrier et al., 2015; Servais et al., 2016).

In the paratype of *Pseudoangustidontus izdigua* sp. nov. (MGL 103606), a unidentified shell or carapace is trapped by the setae of endites 4 and 5 (see Figure 7, abbreviated TO). The size of this carapace (ca. 3 mm in diameter) is larger than the size of the prey that has been estimated for this species (Figure 10). The presence of this captured prey highlights the fact that mesh size only provides an estimation of the minimum potential prey size. Such estimations have been made based on average values from extant organisms, so

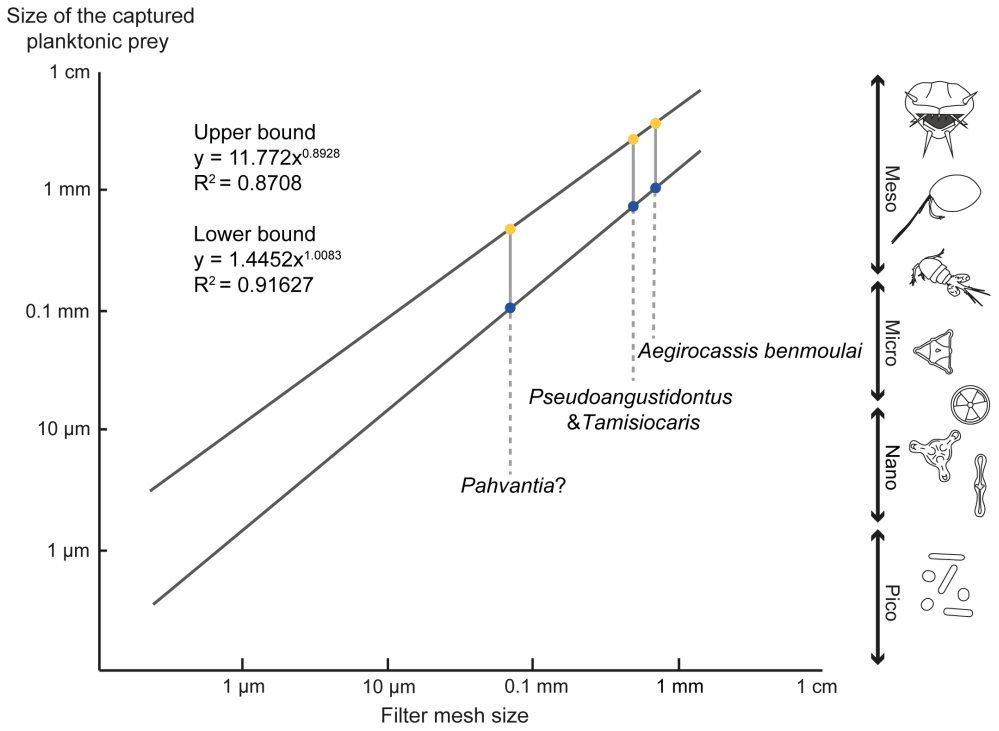

FIGURE 10
Size of captured particles by the suspension-feeding radiodonts. Data have been compiled from Vinther et al. (2014); Van Roy et al. (2015b) and Lerosey-Aubril and Pates (2018), and the graph modified from Vinther et al. (2014).

the range of the prey size can be larger than this average (Vinther et al., 2014).

The identification in this study of dimorphism in the appendages of *Aegirocassis* indicates that food intake was even more complex than previously described. The larger mesh size of the dimorphic endite (En6) has not been taken into account in calculations of estimated prey size because it has a coarser mesh size and would therefore not contribute to the minimum prey size estimation. Given that endite 6 is the most distal endite, it could have had a role as a coarse first filter, capturing large particles that would otherwise have the potential to damage the five other endites with their fine setae and spinules, and therefore had a protection role. It may also have had a strengthening role, acting as a more robust framework or scaffold to lend stability to the whole endite-bearing region of the frontal appendage. Additionally, if angled towards the mouth, it could have funnelled particles onto the other endites.

6.3 Diversity of suspension-feeding radiodonts

Only three suspension-feeding radiodonts had been described previously: *Aegirocassis*, *Tamisiocaris* and questionably *Pahvantia* (Vinther et al., 2014; Van Roy et al., 2015b; Lerosey-Aubril and Pates, 2018; Pates and Daley, 2019; Pates et al., 2019; Caron and Moysiuk, 2021). *Pseudoangustidontus* is herein described as the fourth genus of suspension-feeding radiodont. As the new subfamily Aegirocassisinae contains three species (*Aegirocassis benmoulai*, *Pseudoangustidontus duplospineus* and *Pseudoangustidontus izdigua* sp. nov.), the Ordovician Fezouata Shale is the locality with the highest known species diversity of suspension-feeding radiodonts, making the Tremadocian stage the most diverse time for suspension-feeding radiodonts (Figure 11). The only definitive suspension-feeding radiodont taxon described from the Cambrian is *Tamisiocaris borealis* Daley and Peel, 2010 and questionably *Pahvantia hastata* Robison and Richards, 1981, *Cambroraster falcatus* Moysiuk and Caron, 2019 and *Echidnacaris briggsi* Nedin, 1995 (Robison and Richards, 1981; Nedin, 1995; Daley and Peel, 2010; Daley et al., 2013b; Vinther et al., 2014; Lerosey-Aubril and Pates, 2018; Moysiuk and Caron, 2019; Pates and Daley, 2019; Pates et al., 2019; Potin and Daley, 2023; Paterson et al., 2023).

Tamisiocaris, the only definitive Cambrian suspension-feeding radiodont was found in the Cambrian Stage 3 and Stage 4 Kinzers Formation in Pennsylvania, and also in the Cambrian Series 2 Stage 3 Sirius Passet Formation in Greenland (Figure 11) (Daley and Peel, 2010; Vinther et al., 2014; Lerosey-Aubril and Pates, 2018; Pates and Daley, 2019; Pates et al., 2019). *Cambroraster* is also found in the Cambrian Stage 4 of the Chengjiang Biota (China), and in the Wuliuan at the Burgess Shale (Canada) and the Mantou Formation (China) (Moysiuk and Caron, 2019; Liu et al., 2020; Sun et al., 2020b; Paterson et al., 2023; Potin and Daley, 2023). *Echidnacaris briggsi* is exclusively found in the Emu Bay Shale in Australia, dated from the Cambrian Stage 4 (Daley et al., 2013b; Potin and Daley, 2023; Paterson et al., 2023). *Pahvantia* was reported from the Lower Drumian (middle Cambrian) Wheeler and Marjum Formations in Utah (Figure 11)

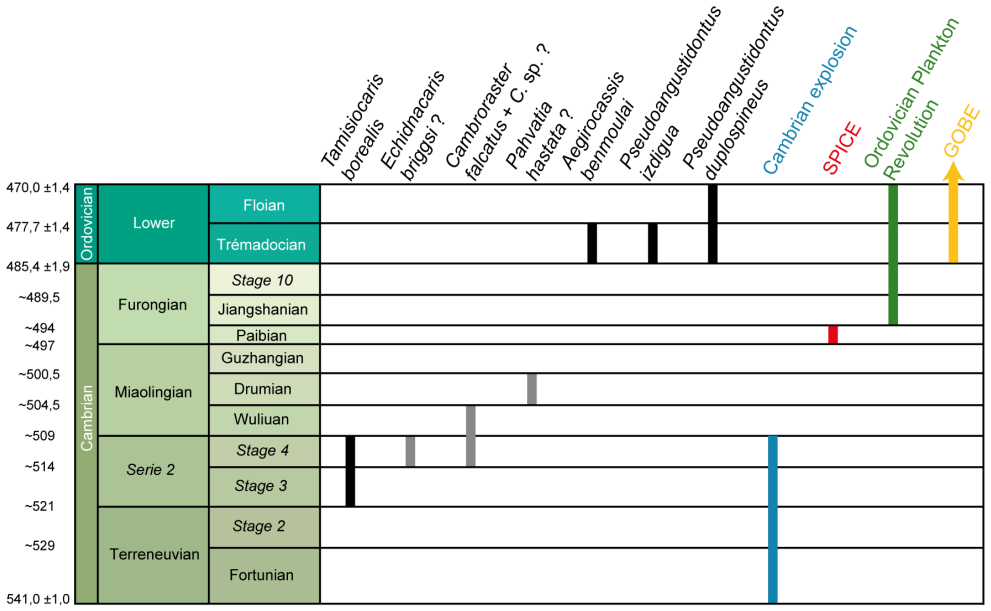

FIGURE 11
Stratigraphic distribution of suspension-feeding radiodonts species and major evolutionary events during the early Paleozoic. Grey bars represent taxa where suspension-feeding interpretations are debated. Data have been compiled from Robison and Richards (1981); Nedin (1995); Van Roy and Tetlie (2006); Daley and Budd (2010); Saltzman et al. (2011); Daley et al. (2013b); Vinther et al. (2014); Servais et al. (2016); Vaucher et al. (2016); Lerosey-Aubril and Pates (2018); Moysiuk and Caron (2019); Paterson et al. (2019); Pates and Daley (2019); Pates et al. (2019); Liu et al. (2020); Sun et al. (2020b). Modified from Cohen et al. (2013).

(Robison and Richards, 1981; Lerosey-Aubril and Pates, 2018; Pates et al., 2019; Pates et al., 2021b; Potin and Daley, 2023).

Tamisiocaris is not a hurdiid radiodont and has an appendage morphology characterised by having at least 18 podomeres each bearing a pair of long endites with densely packed setae (Daley and Peel, 2010; Vinther et al., 2014). In phylogenetic analyses, it typically forms a clade with *Echidnacaris briggsi*, which some authors has considered to be a suspension-feeder (Vinther et al., 2014; Paterson et al., 2020), though this ecological interpretation has been challenged (Daley et al., 2013b). The clade of these two taxa does not have a stable position in the radiodont phylogenetic tree, and has been retrieved as sister group to all other radiodont families depending on the matrix coding and methods used (e.g. see figure 8 in Potin and Daley, 2023). In all cases, it has never been retrieved together with *Aegirocassis* and so can be considered as a separate evolutionary innovation of suspension feeding that was restricted to the Cambrian and was not associated with a large body size.

6.4 Dominance of suspension-feeding radiodonts during the GOBE

In the Fezouata Shale collections examined in this study, suspension-feeding frontal appendages are domimant in terms of proportion among the studied specimens, with only eight out of 105 total known hurdiid appendages indicating a sediment-sifting mode of feeding rather than suspensions feeding (Figure 12). Two of these sediment-sifter frontal appendages (YPM 227644 and YPM 227646) have been reported in Van Roy and Briggs (2011), to which we add a further six from this study. Outside the Fezouata Biota, another Early Ordovician hurdiid appendage (NMW 2012.36G.90) from the Tremadocian Afon Gam Biota (Dol-cyn-Afon Formation) in Wales (Pates et al., 2020) shares anatomical similarities with sediment-sifter radiodonts rather than suspensions feeding radiodonts.

The strong dominance of suspension-feeding over sediment-sifting radiodonts in the Fezouata Shale, as well as the overall higher diversity of suspension-feeders during the Ordovician, could be related to the "Ordovician Plankton Revolution" that took place during the Upper Cambrian and Lower Ordovician (Servais et al., 2010; Servais et al., 2016). This event saw the rapid diversification of plankton within many groups such as acritarchs, graptolites, chitinozoans, radiolarians but also small planktonic arthropods (such as pelagic trilobites and phyllocarid crustaceans) and cephalopods (Servais et al., 2016). Although the origin(s) of the Ordovician Plankton Revolution remain extensively debated, it appears to be related to the "Steptoean Positive Carbon Isotope Excursion $\delta 13C_{carb}$" (SPICE) that took place during the Paibian (Furogian) (Servais et al., 2016). The SPICE is associated with an increase in atmospheric oxygen as well as an increase in nutrients available in the oceans (Servais et al., 2016). The Ordovician Plankton Revolution completely modified the structures of food chains allowing the diversification and abundance of suspension-feeding organisms during the early part of the Ordovician period (Servais et al., 2010; Van Roy et al., 2015b; Servais et al., 2016). Thus, the greater diversity of plankton may have incited diversification in suspension-feeding organisms, resulting in increased morphological diversity of radiodonts with frontal appendages specialised for feeding in the early Ordovician Fezouata Shale.

On the other hand, the associated decline in raptorial predator radiodonts is also estimated to have taken place around the early Ordovician period. This decline could be explained by an increase in competition with other predators such as cephalopods (Pates et al., 2020), which probably appeared during the early Cambrian (Hildenbrand et al., 2021) and were the top predators in the food chain during the Ordovician (Kröger and Zhang, 2009; Kröger et al., 2009). Cephalopods underwent a rapid diversification during the Ordovician radiation particularly in the pelagic domain during the Tremadocian (Kröger et al., 2009). The presence of cephalopods in the Ordovician of the Fezouata Shale is well known (Van Roy et al., 2010; Kröger and Lefebvre, 2012; Van Roy et al., 2015a). The competition between cephalopods and anomalocaridids may have been to the advantage of the cephalopods owing to their better adaptation and efficiency in swimming and thus predation (Klug et al., 2010; Whalen and Briggs, 2018). The emergence of other predatory taxa such as eurypterids, whose presence has been documented in the Fezouata Shale based on a few fragmentary remains (Van Roy et al., 2015a); note that this would predates the earliest-known, Darriwilian, eurypterids, Lamsdell et al. (2015) may have accentuated the decline of raptorial predator radiodonts.

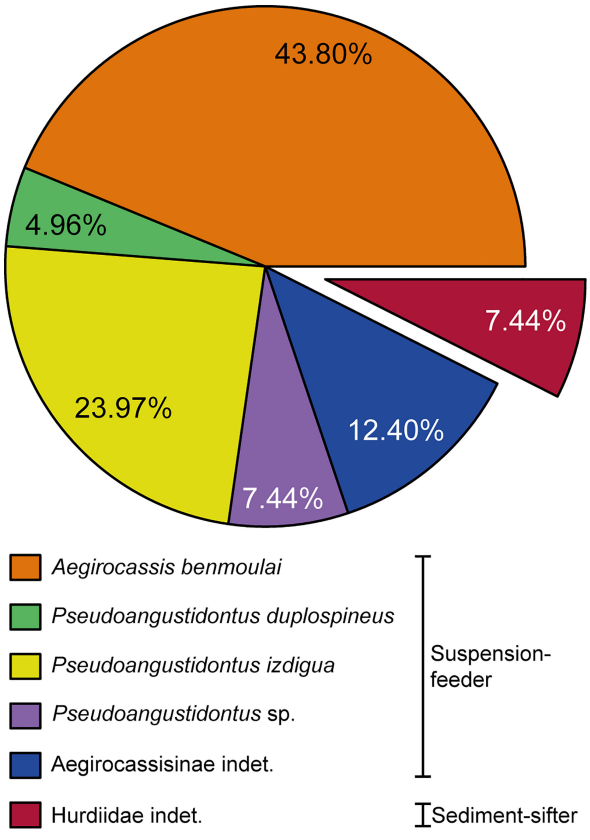

FIGURE 12
Proportion of the different frontal appendage radiodont taxa found in the Fezouata Shale. Data uncertainty is 0.1%. Data, n=121 frontal appendage specimens, have been compiled from new materials, Van Roy and Tetlie (2006); Van Roy and Briggs (2011); Van Roy et al. (2015b). Image credit: G. Potin.

7 Conclusion

The study of new specimens and new species of radiodonts from the Fezouata Shale Formation has clarified the diversity and ecology of Hurdiidae at this locality, and allowed for the erection of a new subfamily Aegirocassisinae. This new subfamily includes two species of *Pseudoangustidontus* and *Aegirocassis benmoulai*. The presence of dimorphic endites bearing long-thin setae in these taxa is particularly distinctive. This group contains all the suspension-feeding radiodonts from the Fezouata Shale. During the Lower Ordovician suspension-feeding radiodonts are the dominant form of the group, following the "Ordovician Plankton Revolution" that saw a major radiation in plankton diversity. Measurements of the mesh size of the different frontal appendages within Aegirocassisinae allowed us to estimate the size of the preys that they could have captured, revealing that they mostly ate mesoplankton. Finally, only two feeding strategies have been identified among Fezouata radiodonts: suspension-feeding and sediment sifting. We found, however, no evidence for any active apex predator similar *to Anomalocaris*, while they were common during the Cambrian. This highlights the high competition with other large active nektonic predators that rapidly evolved during the Lower Ordovician, such as cephalopods or eurypterid arthropods. As a result, the evolutionary and ecological plasticity of the radiodonts can be seen as they adapt to a rapidly changing Ordovician world.

Data availability statement

The original contributions presented in the study are included in the article/Supplementary Material. Further inquiries can be directed to the corresponding author.

Author contributions

AD and GP designed the project, and GP examined, photographed and drew the fossil material. Advanced imaging and analytical techniques were performed by PG and GP. Fossil interpretations were done together with all authors, who also all contributed to writing the manuscript. GP prepared the figures and Supplementary Material.

Funding

GP and this research were funded by the Canton de Vaud and the Swiss National Science Foundation, grant number 205321_179084 entitled "Arthropod Evolution during the Ordovician Radiation: Insights from the Fezouata Biota" and awarded to AD.

Acknowledgments

We are grateful to Lukáš Laibl (Czech Academy of Sciences), Susan Butts (Yale Peabody Museum) and Jessica Utrup (Yale Peabody Museum), Bertrand Lefebvre (University Claude Bernard Lyon 1) for access to the material from the collection of the University of Lausanne, the Yale Peabody Museum and the Marrakech Collections of the Cadi Ayyad University (stored in University Claude Bernard Lyon 1) respectively. Benita Putlitz (UNIL) ran µCT scanning, and Julien Alleon (UNIL) provided assistance with Raman microspectroscopy. We thank Jonathan B. Antcliffe (UNIL) for English language editing of the manuscript. We acknowledge the SOLEIL Synchrotron for provision of beamtime, and Cristian Mocuta, Dominique Thiaudière, Solenn Réguer and Philippe Joly (SOLEIL Synchrotron) for assistance at the DiffAbs beamline. We thank Pénélope Claisse, Lorenzo Lustri, Sinéad Lynch and Francesc Pérez-Peris (UNIL) for their help with the statistical analysis, Farid Saleh (Yunnan University) for discussion about taphonomy and preservation in the Fezouata Shale, and Peter Van Roy for discussion about Fezouata radiodonts. We thanks Ismail Khardali for the translation of the word "filter" in Tamazight language used to name the new species of *Pseudoangustidontus*.

Conflict of interest

The authors declare that the research was conducted in the absence of any commercial or financial relationships that could be construed as a potential conflict of interest.

Publisher's note

Supplementary material

The Supplementary Material for this article can be found online at: https://www.frontiersin.org/articles/10.3389/fevo.2023.1214109/full#supplementary-material

References

Antcliffe, J. B., Jessop, W., and Daley, A. C. (2019). Prey fractionation in the Archaeocyatha and its implication for the ecology of the first animal reef systems. *Paleobiology* 45 (4), 652–675. doi: 10.1017/pab.2019.32

Briggs, D. E. G. (1979). *Anomalocaris*, the largest known Cambrian arthropod. *Palaeontology* 22 (3), 631–664.

Caron, J.-B., Gaines, R. R., Mángano, M. G., Streng, M., and Daley, A. C. (2010). A new Burgess Shale–type assemblage from the "thin" Stephen Formation of the southern Canadian Rockies. *Geology* 38 (9), 811–814. doi: 10.1130/G31080.1

Caron, J.-B., and Moysiuk, J. (2021). A giant nektobenthic radiodont from the Burgess Shale and the significance of hurdiid carapace diversity. *R. Soc. Open Sci.* 8 (9), 210664. doi: 10.1098/rsos.210664

Cohen, K. M., Finney, S. C., Gibbard, P. L., and Fan, J. -X. (2013). *The ICS International Chronostratigraphic Chart. Episodes* 36:199–204.

Collins, D. (1996). The "evolution" of *Anomalocaris* and its classification in the arthropod class Dinocarida (nov.) and order Radiodonta (nov.). *J. Paleontol.* 70 (2), 280–293. doi: 10.1017/S0022336000023362

Cong, P. Y., Edgecombe, G. D., Daley, A. C., Guo, J., Pates, S., and Hou, X. G. (2018). New radiodonts with gnathobase-like structures from the Cambrian Chengjiang Biota and implications for the systematics of Radiodonta. *Papers Palaeontol.* 4 (4), 605–621. doi: 10.1002/spp2.1219

Conway Morris, S., and Whittington, H. B. (1979). The animals of the Burgess Shale. *Sci. Am.* 241 (1), 122–135. https://www.jstor.org/stable/24965247

Cooper, C. L. (1936). Actinopterygian jaws from the Mississippian black Shale of the Mississippi valley. *J. Paleontol.* 10 (2), 92–94. https://www.jstor.org/stable/1298344

Daley, A. C., and Budd, G. E. (2010). New anomalocaridid appendages from the Burgess Shale, Canada. *Palaeontology.* 53 (4), 721–738. doi: 10.1111/j.1475-4983.2010.00955.x

Daley, A. C., Budd, G. E., and Caron, J.-B. (2013a). Morphology and systematics of the anomalocaridid arthropod *Hurdia* from the middle Cambrian of British Columbia and Utah. *J. Syst. Palaeontol.* 11 (7), 743–787. doi: 10.1080/14772019.2012.732723

Daley, A. C., Paterson, J. R., Edgecombe, G. D., García-Bellido, D. C., and Jago, J. B. (2013b). New anatomical information on *Anomalocaris* from the Cambrian Emu Bay Shale of South Australia and a reassessment of its inferred predatory habits. *Palaeontology.* 56 (5), 971–990. doi: 10.1111/pala.12029

Daley, A. C., and Peel, J. S. (2010). A possible anomalocaridid from the Cambrian Sirius Passet Lagerstätten, North Greenland. *J. Paleontol.* 84 (2), 352–355. doi: 10.1666/09-136R1.1

De Vivo, G., Lautenschlager, S., and Vinther, J. (2021). Three-dimensional modelling, disparity and ecology of the first Cambrian apex predators. *Proc. R. Soc B* 288, 20211176. doi: 10.1098/rspb.2021.1176

Drage, H. B., Vandenbroucke, T. R. A., Van Roy, P., and Daley, A. C. (2019). Sequence of post-moult exoskeleton hardening preserved in a trilobite mass moult assemblage from the Lower Ordovician Fezouata Konservat-Lagerstatte, Morocco. *Acta Palaeontologica Polonica* 64 (2), 261–273. doi: 10.4202/app.00582.2018

Gaines, R. R., Briggs, D. E. G., Orr, P. J., and Van Roy, P. (2012). Preservation of giant anomalocaridids in silica-chlorite concretions from the Early Ordovician of Morocco. *Palaios* 27 (5), 317–325. doi: 10.2110/palo.2011.p11-093r

Gueriau, P., Charbonnier, S., and Clément, G. (2014). Angustidontid crustaceans from the Late Devonian of Strud (Namur Province, Belgium): insights into the origin of Decapoda. *Neues Jahrbuch für Geologie und Paläontologie* 273 (3), 327–337. doi: 10.1127/0077-7749/2014/0434

Guo, J., Pates, S., Cong, P., Daley, A. C., Edgecombe, G. D., Chen, T., et al. (2019). A new radiodont (stem Euarthropoda) frontal appendage with a mosaic of characters from the Cambrian (Series 2 Stage 3) Chengjiang Biota. *Papers Palaeontol* 5 (1), 99–110. doi: 10.1002/spp2.1231

Gutiérrez-Marco, J. C., García-Bellido, D. C., Rábano, I., and Sá, A. A. (2017). Digestive and appendicular soft-parts, with behavioural implications, in a large Ordovician trilobite from the Fezouata Lagerstätten, Morocco. *Sci. Rep.* 7 (1), 39728. doi: 10.1038/srep39728

Hammer, Ø., and Harper, D. A. T. (2008). *Paleontological data analysis* (New Jersey, USA: John Wiley & Sons).

Hammer, Ø., Harper, D. A. T., and Ryan, P. D. (2001). Paleontological statistics software package for education and data analysis. *Paleontologia Electronica* 4 (1), 4–9.

Hildenbrand, A., Austermann, G., Fuchs, D., Bengtson, P., and Stinnesbeck, W. (2021). A potential cephalopod from the early Cambrian of eastern Newfoundland, Canada. *Commun. Biol.* 4 (1), 388. doi: 10.1038/s42003-021-01885-w

Klug, C., Kröger, B., Kiessling, W., Mullins, G. L., Servais, T., Frýda, J., et al. (2010). The Devonian nekton revolution. *Lethaia* 43 (4), 465–477. doi: 10.1111/j.1502-3931.2009.00206.x

Kröger, B., and Lefebvre, B. (2012). Palaeogeography and palaeoecology of early Floian (Early Ordovician) cephalopods from the upper Fezouata formation, Anti-Atlas, Morocco. *Fossil Rec.* 15 (2), 61–75. doi: 10.1002/mmng.201200004

Kröger, B., Servais, T., and Zhang, Y. (2009). The origin and initial rise of pelagic cephalopods in the Ordovician. *PloS One* 4 (9), e7262. doi: 10.1371/journal.pone.0007262

Kröger, B., and Zhang, Y.-D. (2009). Pulsed cephalopod diversification during the Ordovician. *Palaeogeogr. Palaeoclimatol. Palaeoecol.* 273 (1-2), 174–183. doi: 10.1016/j.palaeo.2008.12.015

Kühl, G., Briggs, D. E. G., and Rust, J. (2009). A great-appendage arthropod with a radial mouth from the Lower Devonian Hunsrück Slate, Germany. *Science* 323 (5915), 771–773. doi: 10.1126/science.1166586

Lamsdell, J. C., Briggs, D. E. G., Liu, H. P., Witzke, B. J., and McKay, R. M. (2015). The oldest described eurypterid: a giant Middle Ordovician (Darriwilian) megalograptid from the Winneshiek Lagerstätten of Iowa. *BMC Evol. Biol.* 15 (1), 169. doi: 10.1186/s12862-015-0443-9

Lebrun, P. (2017). Le biotope de Fezouata: un gisement fossilifère d'exception de l'Ordovicien Inférieur du Maroc. *Fossiles Rev. française paléontologie* 31, 5–30.

Leclercq, N., Berthault, J., Langlois, F., Le, S., Poirier, S., Bisou, J., et al. (2015). "Flyscan: a fast and multi-technique data acquisition platform for the SOLEIL beamlines," in *Proceedings of the 15th International Conference on Accelerator and Large Experimental Physics Control Systems (ICALEPCS 2015)*, Melbourne, Australia, October 17-23, 2015. doi: 10.18429/JACoW-ICALEPCS2015-WEPGF056

Lefebvre, B., Gutiérrez-Marco, J. C., Lehnert, O., Martin, E. L. O., Nowak, H., Akodad, M., et al. (2018). Age calibration of the Lower Ordovician Fezouata Lagerstätten, Morocco. *Lethaia* 51 (2), 296–311. doi: 10.1111/let.12240

Lerosey-Aubril, R., and Pates, S. (2018). New suspension-feeding radiodont suggests evolution of microplanktivory in Cambrian macronekton. *Nat. Commun.* 9 (1), 3774. doi: 10.1038/s41467-018-06229-7

Liu, Y., Lerosey-Aubril, R., Audo, D., Zhai, D., Mai, H., and Ortega-Hernández, J. (2020). Occurrence of the eudemersal radiodont *Cambroraster* in the early Cambrian Chengjiang Lagerstätten and the diversity of hurdiid ecomorphotypes. *Geol. Mag.* 157 (7), 1200–1206. doi: 10.1017/S0016756820000187

Liu, J., Lerosey-Aubril, R., Steiner, M., Dunlop, J. A., Shu, D., and Paterson, J. R. (2018). Origin of raptorial feeding in juvenile euarthropods revealed by a Cambrian Radiodontan. *Natl. Sci. Rev.* 5 (6), 863–869. doi: 10.1093/nsr/nwy057

Martin, E. L. O., Lerosey-Aubril, R., and Vannier, J. (2016a). Palaeoscolecid worms from the Lower Ordovician Fezouata Lagerstätten, Morocco: palaeoecological and palaeogeographical implications. *Palaeogeogr. Palaeoclimatol. Palaeoecol.* 460, 130–141. doi: 10.1016/j.palaeo.2016.04.009

Martin, E. L. O., Pittet, B., Gutiérrez-Marco, J.-C., Vannier, J., El Hariri, K., Lerosey-Aubril, R., et al. (2016b). The Lower Ordovician Fezouata Konservat-Lagerstätten from Morocco: age, environment and evolutionary perspectives. *Gondwana Res.* 34, 274–283. doi: 10.1016/j.gr.2015.03.009

Martin, E. L. O., Vidal, M., Vizcaïno, D., Vaucher, R., Sansjofre, P., Lefebvre, B., et al. (2016c). Biostratigraphic and palaeoenvironmental controls on the trilobite associations from the Lower Ordovician Fezouata Shale of the central Anti-Atlas, Morocco. *Palaeogeogr. Palaeoclimatol. Palaeoecol.* 460, 142–154. doi: 10.1016/j.palaeo.2016.06.003

Moysiuk, J., and Caron, J.-B. (2019). A new hurdiid radiodont from the Burgess Shale evinces the exploitation of Cambrian infaunal food sources. *Proc. R. Soc. B* 286 (1908), 20191079. doi: 10.1098/rspb.2019.1079

Moysiuk, J., and Caron, J.-B. (2021). Exceptional multifunctionality in the feeding apparatus of a mid-Cambrian radiodont. *Paleobiology* 47 (4), 704–724. doi: 10.1017/pab.2021.19

Moysiuk, J., and Caron, J.-B. (2022). A three-eyed radiodont with fossilized neuroanatomy informs the origin of the arthropod head and segmentation. *Curr. Biol.* 32 (15), 3302–3316. e3302. doi: 10.1016/j.cub.2022.06.027

Nedin, C. (1995). The Emu Bay Shale, a lower Cambrian fossil Lagerstätten, Kangaroo Island, South Australia. *Memoirs Assoc. Australas. Palaeontologists* 18, 31–40.

Nedin, C. (1999). *Anomalocaris* predation on nonmineralized and mineralized trilobites. *Geology* 27 (11), 987–990. doi: 10.1130/0091-7613(1999)027<0987:APONAM>2.3.CO;2

Nielsen, C. (1995). *Animal evolution: interrelationships of the living phyla* (Oxford, United Kingdom, Oxford University Press).

Ortega-Hernández, J., Van Roy, P., and Lerosey-Aubril, R. (2016). A new aglaspidid euarthropod with a six-segmented trunk from the Lower Ordovician Fezouata Konservat-Lagerstätten, Morocco. *Geological Magazine* 153 (3), 524–536. doi: 10.1017/S0016756815000710

Paterson, J. R., Edgecombe, G. D., and García-Bellido, D. C. (2020). Disparate compound eyes of Cambrian radiodonts reveal their developmental growth mode and diverse visual ecology. *Sci. Adv.* 6 (49), eabc6721. doi: 10.1126/sciadv.abc6721

Paterson, J. R., Edgecombe, G. D., and Lee, M. S. Y. (2019). Trilobite evolutionary rates constrain the duration of the Cambrian explosion. *Proc. Natl. Acad. Sci.* 116 (10), 4394–4399. doi: 10.1073/pnas.1819366116

Paterson, J. R., García-Bellido, D. C., and Edgecombe, G. D. (2023). The early Cambrian Emu Bay Shale radiodonts revisited: morphology and systematics. *J. Syst. Palaeontol.* 21 (1), 2225066. doi: 10.1080/14772019.2023.2225066

Pates, S., Botting, J. P., McCobb, L. M. E., and Muir, L. A. (2020). A miniature Ordovician hurdiid from Wales demonstrates the adaptability of Radiodonta. *R. Soc. Open Sci.* 7 (6), 200459. doi: 10.1098/rsos.200459

Pates, S., and Daley, A. C. (2019). The Kinzers Formation (Pennsylvania, USA): the most diverse assemblage of Cambrian Stage 4 radiodonts. *Geological Magazine* 156 (7), 1233–1246. doi: 10.1017/S0016756818000547

Pates, S., Daley, A. C., and Butterfield, N. J. (2019). First report of paired ventral endites in a hurdiid radiodont. *Zoological Lett.* 5 (1), 18. doi: 10.1186/s40851-019-0132-4

Pates, S., Daley, A. C., Edgecombe, G. D., Cong, P., and Lieberman, B. S. (2021a). Systematics, preservation and biogeography of radiodonts from the Southern Great Bassin, USA, during the upper Dyeran (Cambrian Series 2, Stage 4). *Papers Palaeontol.* 7 (1), 235–262. doi: 10.1002/spp2.1277

Pates, S., Lerosey-Aubril, R., Daley, A. C., Kier, C., Bonino, E., and Ortega-Hernández, J. (2021b). The diverse radiodont fauna from the Marjum Formation of Utah, USA (Cambrian: Drumian). *PeerJ* 9, e10509. doi: 10.7717/peerj.10509

Pérez-Peris, F., Laibl, L., Lustri, L., Gueriau, P., Antcliffe, J. B., Bath Enright, O. G., et al. (2021a). A new nektaspid euarthropod from the Lower Ordovician strata of Morocco. *Geological Magazine* 158 (3), 509–517. doi: 10.1017/S001675682000062X

Pérez-Peris, F., Laibl, L., Vidal, M., and Daley, A. C. (2021b). Systematics, morphology, and appendages of an early Ordovician pilekiine trilobite *Anacheirurus* from Fezouata Shale and the early diversification of Cheiruridae. *Acta Palaeontologica Polonica* 66 (4), 857–877. doi: 10.4202/app.00902.2021

Perrier, V., Williams, M., and Siveter, D. J. (2015). The fossil record and palaeoenvironmental significance of marine arthropod zooplankton. *Earth-Science Rev.* 146, 146–162. doi: 10.1016/j.earscirev.2015.02.003

Potin, G. J.-M., and Daley, A. C. (2023). The significance of *Anomalocaris* and other Radiodonta for understanding paleoecology and evolution during the Cambrian explosion. *Front. Earth Sci.* 11. doi: 10.3389/feart.2023.1160285

Robison, R. A., and Richards, B. C. (1981). Larger bivalve arthropods from the middle Cambrian of Utah. *Kansas Paleontological Contributions* 106, 1–28. https://hdl.handle.net/1808/3757

Rolfe, W. D. I., and Dzik, J. (2006). *Angustidontus*, a Late Devonian pelagic predatory crustacean. *Trans. R. Soc. Edinburgh: Earth Sci.* 97 (1), 75–96. doi: 10.1017/S0263593300001413

Saleh, F., Antcliffe, J. B., Lefebvre, B., Pittet, B., Laibl, L., Pérez-Peris, F., et al. (2020a). Taphonomic bias in exceptionally preserved biotas. *Earth Planetary Sci. Lett.* 529, 115873. doi: 10.1016/j.epsl.2019.115873

Saleh, F., Bath-Enright, O. G., Daley, A. C., Lefebvre, B., Pittet, B., Vite, A., et al. (2021a). A novel tool to untangle the ecology and fossil preservation knot in exceptionally preserved biotas. *Earth Planetary Sci. Lett.* 569, 117061. doi: 10.1016/j.epsl.2021.117061

Saleh, F., Candela, Y., Harper, D. A. T., Polechová, M., Lefebvre, B., and Pittet, B. (2018). Storm-induced community dynamics in the Fezouata Biota (Lower Ordovician, Morocco). *Palaios* 33 (12), 535–541. doi: 10.2110/palo.2018.055

Saleh, F., Guenser, P., Gibert, C., Balseiro, D., Serra, F., Waisfeld, B. G., et al. (2022a). Contrasting Early Ordovician assembly patterns highlight the complex initial stages of the Ordovician radiation. *Sci. Rep.* 12 (1), 3852. doi: 10.1038/s41598-022-07822-z

Saleh, F., Lefebvre, B., Hunter, A. W., and Nohejlová, M. (2020b). Fossil weathering and preparation mimic soft tissues in eocrinoid and somasteroid echinoderms from the Lower Ordovician of Morocco. *Microscopy Today* 28 (1), 24–28. doi: 10.1017/S1551929519001238

Saleh, F., Ma, X., Guenser, P., Mángano, M. G., Buatois, L. A., and Antcliffe, J. B. (2022b). Probability-based preservational variations within the early Cambrian Chengjiang Biota (China). *PeerJ* 10, e13869. doi: 10.7717/peerj.13869

Saleh, F., Pittet, B., Perrillat, J.-P., and Lefebvre, B. (2019). Orbital control on exceptional fossil preservation. *Geology* 47 (2), 103–106. doi: 10.1130/G45598.1

Saleh, F., Pittet, B., Sansjofre, P., Gueriau, P., Lalonde, S., Perrillat, J.-P., et al. (2020c). Taphonomic pathway of exceptionally preserved fossils in the Lower Ordovician of Morocco. *Geobios* 60, 99–115. doi: 10.1016/j.geobios.2020.04.001

Saleh, F., Vaucher, R., Antcliffe, J. B., Daley, A. C., El Hariri, K., Kouraiss, K., et al. (2021b). Insights into soft-part preservation from the Early Ordovician Fezouata Biota. *Earth-Science Rev.* 213, 103464. doi: 10.1016/j.earscirev.2020.103464

Saleh, F., Vaucher, R., Vidal, M., Hariri, K. E., Laibl, L., Daley, A. C., et al. (2022c). New fossil assemblages from the Early Ordovician Fezouata Biota. *Sci. Rep.* 12 (1), 20773. doi: 10.1038/s41598-022-25000-z

Saleh, F., Vidal, M., Laibl, L., Sansjofre, P., Gueriau, P., Pérez-Peris, F., et al. (2021c). Large trilobites in a stress-free Early Ordovician environment. *Geological Magazine* 158 (2), 261–270. doi: 10.1017/S0016756820000448

Saltzman, M. R., Young, S. A., Kump, L. R., Gill, B. C., Lyons, T. W., and Runnegar, B. (2011). Pulse of atmospheric oxygen during the late Cambrian. *Proc. Natl. Acad. Sci.* 108 (10), 3876–3881. doi: 10.1073/pnas.1011836108

Servais, T., Owen, A. W., Harper, D. A. T., Kröger, B., and Munnecke, A. (2010). The Great Ordovician Biodiversification Event (GOBE): the palaeoecological dimension. *Palaeogeogr. Palaeoclimatol. Palaeoecol.* 294 (3-4), 99–119. doi: 10.1016/j.palaeo.2010.05.031

Servais, T., Perrier, V., Danelian, T., Klug, C., Martin, R., Munnecke, A., et al. (2016). The onset of the 'Ordovician plankton revolution'in the late Cambrian. *Palaeogeogr. Palaeoclimatol. Palaeoecol.* 458, 12–28. doi: 10.1016/j.palaeo.2015.11.003

Sieburth, J. M., Smetacek, V., and Lenz, J. (1978). Pelagic ecosystem structure: heterotrophic compartments of the plankton and their relationship to plankton size fractions 1. *Limnol. oceanography* 23 (6), 1256–1263. doi: 10.4319/lo.1978.23.6.1256

Solé, V. A., Papillon, E., Cotte, M., Walter, P., and Susini, J. (2007). A multiplatform code for the analysis of energy-dispersive X-ray fluorescence spectra. *Spectrochimica Acta Part B: Atomic Spectrosc.* 62 (1), 63–68. doi: 10.1016/j.sab.2006.12.002

Sun, Z., Zeng, H., and Zhao, F. (2020a). A new middle Cambrian radiodont from North China: implications for morphological disparity and spatial distribution of hurdiids. *Palaeogeogr. Palaeoclimatol. Palaeoecol.* 558, 109947. doi: 10.1016/j.palaeo.2020.109947

Sun, Z., Zeng, H., and Zhao, F. (2020b). Occurrence of the hurdiid radiodont *Cambroraster* in the middle Cambrian (Wuliuan) Mantou Formation of North China. *J. Paleontol.* 94 (5), 881–886. doi: 10.1017/jpa.2020.21

Vannier, J., Vidal, M., Marchant, R., El Hariri, K., Kouraiss, K., Pittet, B., et al. (2019). Collective behaviour in 480-million-year-old trilobite arthropods from Morocco. *Sci. Rep.* 9 (1), 14941. doi: 10.1038/s41598-019-51012-3

Van Roy, P., and Briggs, D. E. G. (2011). A giant Ordovician anomalocaridid. *Nature* 473 (7348), 510–513. doi: 10.1038/nature09920

Van Roy, P., Briggs, D. E. G., and Gaines, R. R. (2015a). The Fezouata fossils of Morocco; an extraordinary record of marine life in the Early Ordovician. *J. Geological Soc.* 172 (5), 541–549. doi: 10.1144/jgs2015-017

Van Roy, P., Daley, A. C., and Briggs, D. E. G. (2015b). Anomalocaridid trunk limb homology revealed by a giant filter-feeder with paired flaps. *Nature* 522 (7554), 77–80. doi: 10.1038/nature14256

Van Roy, P., Orr, P. J., Botting, J. P., Muir, L. A., Vinther, J., Lefebvre, B., et al. (2010). Ordovician Faunas of Burgess Shale type. *Nature* 465 (7295), 215–218. doi: 10.1038/nature09038

Van Roy, P., and Tetlie, O. E. (2006). A spinose appendage fragment of a problematic arthropod from the Early Ordovician of Morocco. *Acta Palaeontologica Polonica* 51 (2), 239–246.

Vaucher, R., Martin, E. L. O., Hormière, H., and Pittet, B. (2016). A genetic link between Konzentrat-and Konservat-Lagerstättenn in the Fezouata Shale (Lower Ordovician, Morocco). *Palaeogeogr. Palaeoclimatol. Palaeoecol.* 460, 24–34. doi: 10.1016/j.palaeo.2016.05.020

Vaucher, R., Pittet, B., Hormière, H., Martin, E. L. O., and Lefebvre, B. (2017). A wave-dominated, tide-modulated model for the Lower Ordovician of the Anti-Atlas, Morocco. *Sedimentology* 64 (3), 777–807. doi: 10.1111/sed.12327

Vidal, M. (1998). Le modèle des biofaciès à trilobites: un test dans l'Ordovicien Inférieur de l'Anti-Atlas, Maroc. *Comptes Rendus l'Académie Des. Sciences-Series IIA-Earth Planetary Sci.* 327 (5), 327–333. doi: 10.1016/S1251-8050(98)80051-7

Vinther, J., Stein, M., Longrich, N. R., and Harper, D. A. T. (2014). A suspension-feeding anomalocarid from the early Cambrian. *Nature* 507 (7493), 496–499. doi: 10.1038/nature13010

von Siebold, C. T. E. (1848). *Lehrbuch der vergleichenden anatomie* (Berlin, Germany, Veit).

Walcott, C. D. (1911). Cambrian Geology and paleontology II: middle Cambrian Holothurians and Medusae. *Smithsonian Miscellaneous Collections* 57 (3), 41–69.

Walcott, C. D. (1912). Middle Cambrian Branchiopoda, Malacostraca, Trilobita, and Merostomata. *Smithsonian Misc. Collect.* 57 (6), 145–228.

Whalen, C. D., and Briggs, D. E. G. (2018). The Palaeozoic colonization of the water column and the rise of global nekton. *Proc. R. Soc. B: Biol. Sci.* 285 (1883), 20180883. doi: 10.1098/rspb.2018.0883

Whittington, H. B. (1975). The enigmatic animal *Opabinia regalis*, middle Cambrian, Burgess Shale, British Columbia. *Philos. Trans. R. Soc. London. B Biol. Sci.* 271 (910), 1–43. doi: 10.1098/rstb.1975.0033

Wu, Y., Pates, S., Ma, J., Lin, W., Wu, Y., Zhang, X., et al. (2022). Addressing the Chengjiang conundrum: a palaeoecological view on the rarity of hurdiid radiodonts in this most diverse early Cambrian Lagerstätten. *Geosci. Front.* 13 (6), 101430. doi: 10.1016/j.gsf.2022.101430

Zeng, H., Zhao, F., Yin, Z., and Zhu, M. (2017). Morphology of diverse Radiodontan head sclerites from the early Cambrian Chengjiang Lagerstätten, South-West China. *J. Syst. Palaeontol.* 16 (1), 1–37. doi: 10.1080/14772019.2016.1263685

Zhu, X., Lerosey-Aubril, R., and Ortega-Hernández, J. (2021). Furongian (Jiangshanian) occurrences of radiodonts in Poland and South China and the fossil record of the Hurdiidae. *PeerJ* 9, e11800. doi: 10.7717/peerj.11800

frontiers | Frontiers in Ecology and Evolution

TYPE Original Research
PUBLISHED 21 August 2023
DOI 10.3389/fevo.2023.1226924

OPEN ACCESS

EDITED BY
Zhifei Zhang,
Northwest University, China

REVIEWED BY
Thomas Hegna,
State University of New York at Fredonia, United States
Li Tian,
China University of Geosciences Wuhan, China

*CORRESPONDENCE
Harriet B. Drage
harriet.drage@unil.ch

RECEIVED 22 May 2023
ACCEPTED 11 July 2023
PUBLISHED 21 August 2023

CITATION
Drage HB, Legg DA and Daley AC (2023) Novel marrellomorph moulting behaviour preserved in the Lower Ordovician Fezouata Shale, Morocco.
Front. Ecol. Evol. 11:1226924.
doi: 10.3389/fevo.2023.1226924

Novel marrellomorph moulting behaviour preserved in the Lower Ordovician Fezouata Shale, Morocco

Harriet B. Drage[1]*, David A. Legg[2] and Allison C. Daley[1]

[1]Institute of Earth Sciences, University of Lausanne, Lausanne, Switzerland, [2]School of Earth and Environmental Sciences, University of Manchester, Manchester, United Kingdom

Exoskeleton moulting is the process of shedding the old exoskeleton to enable growth, development and repair, representing a crucial recurrent event in the life histories of all euarthropods. The fossil record of moulting allows us to interpret the evolution of this important behaviour and its impact on the evolutionary trajectories of extinct and extant euarthropods. Current knowledge of Palaeozoic euarthropod moulting relates largely to trilobites, with fewer examples known for non-mineralised extinct taxa from early in euarthropod evolutionary history. We describe exuviae from a marrellid marrellomorph found abundantly in the Early Ordovician Fezouata Shale Lagerstätte of Morocco, which allow a novel reconstruction, the second ever, of marrellid moulting behaviours. We identify the moulting suture location, describe preserved moulting assemblages, and suggest how its moulting behaviours are adaptive to its morphology. Several specimens represent complete and nearly complete assemblages and additional disarticulated specimens confirm the suture line location. The suture line is located between the mediolateral and posterolateral spine pairs, dividing the cephalic shield into anterior and posterior parts. The Fezouata marrellid likely exited the exoskeleton during exuviation using posterior and upwards movements, analogous in terms of movement to lobster-like extant arthropods. The suture line is comparable in the closely related marrellid *Mimetaster*, and distinctive from that of another marrellid, *Marrella splendens*, which has an exuvial opening at the anterior of the cephalic shield and exited the exoskeleton anteriorly. This difference in moulting behaviour as compared to *Marrella* is likely adaptive to the greater complexity of the Fezouata marrellid, with upwards rather than forwards movement presumably providing a more favourable angle for the extraction of complex spines. This description of the moulting behaviours and related morphological features of marrellomorphs expands our understanding of this crucial characteristic in extinct euarthropods.

KEYWORDS

Euarthropoda, exoskeleton, exuviation, Fezouata Shale, Marrellida, moulting, Ordovician, palaeoecology

1 Introduction

Moulting is the process of shedding the exoskeleton, which all euarthropods must periodically do to grow and develop. Moulting is of central importance in the life histories of extinct and extant euarthropods, as all individuals must repeat this process multiple times, and they are particularly vulnerable to predation and parasitism during moulting and immediately after (Ewer, 2005). Evidence of moulting has been described for many extinct euarthropod groups, including some of the stratigraphically earliest representatives of the group from the lower Cambrian (see Daley and Drage, 2016, for a review of the pre-2016 literature on the fossil record of moulting). The majority of the fossil record of moulting pertains to crown-group Euarthropoda, with abundant data from the trilobites (e.g., Brandt, 2002; Drage et al., 2018; Drage, 2019; Corrales-García et al., 2020; Zong, 2020; Wang et al., 2021; Zong, 2021; Drage, 2022; Drage et al., 2023), as well as some data from eurypterids (e.g., Tetlie et al., 2008; Brandt, 2021) and other chelicerates (e.g., Selden et al., 1991; McCoy and Brandt, 2009), decapod crustaceans (e.g., Glaessner, 1969; Klompmaker and Fraaije, 2011), ostracods (Olempska, 2012), isopods (e.g., Hyžný et al., 2013), and hexapods (e.g., Kukalova, 1968; Rasnitsyn, 2002). Much less is known about moulting in other euarthropod groups, with clear moult assignments of only a few taxa, including a single marrellomorph specimen (García-Bellido and Collins, 2004), a fuxianhuiid (Yang et al., 2019), and mass moults of *Canadaspis* and *Alalcomenaeus* (Haug et al., 2013). These specimens suggest that moulting in stem-group euarthropods was likely comparable in biomechanics to extant crown-group representatives (Daley and Drage, 2016). However, with only sparse knowledge of moulting in euarthropod stem-groups, we have little basis with which to understand the early evolution of moulting as a behaviour, and the impacts this might have had on other evolutionary aspects such as morphology, physiology, ontogeny, and ecology.

The Marrellomorpha are an unusual group of euarthropods known only from the Cambrian to Devonian (*c.* 390–508 Ma), and best known by the characteristic and highly abundant *Marrella splendens* from the Burgess Shale (García-Bellido and Collins, 2006). The Marrellomorpha may represent a monophyletic grouping (though this is still in doubt; see Moysiuk et al., 2022), comprising two orders—Marrellida and Acercostraca—with the Marrellida having a cephalic shield supporting large lateral spines, and the Acercostraca having a large cordiform carapace covering more of the body (see Legg, 2015; Legg, 2016 on the Acercostraca). One putative marrellomorph species, the fragmentary *Austromarrella klausmuelleri* is unresolved within this taxonomic framework (Haug et al., 2012), though there is doubt over its marrellomorph assignment (Legg, 2016). However, the ancestral condition of the Marrellomorpha (spiny cephalic shield or carapace) remains uncertain, as does their phylogenetic position within Euarthropoda as a whole, being variously considered arachnomorphs, stem mandibulates, or stem-lineage euarthropods (e.g., Legg, 2016; Aris et al., 2017; Moysiuk et al., 2022, and references therein).

The Marrellida are currently represented by four genera: *Marrella* (Cambrian, Canada and China; Whittington, 1971; García-Bellido and Collins, 2006; Liu, 2013), *Furca* (Upper Ordovician, Czech Republic and suggested for Morocco, see Material and methods section; Van Roy, 2006; Van Roy et al., 2010; Rak et al., 2012), *Mimetaster* (Lower Ordovician, Argentina, and Lower Devonian, Germany; Kühl and Rust, 2010; Aris et al., 2017), and *Tomlinsonus* (Late Ordovician, Canada; Moysiuk et al., 2022). *Marrella* has a comparably simpler cephalic shield morphology, with two pairs of spines and no secondary spinosity (García-Bellido and Collins, 2006; Liu, 2013). *Furca, Mimetaster*, and potentially *Tomlinsonus*, all have three pairs of spines on the cephalic shield, and extensive secondary spinosity of the primary cephalic spines.

To date, the only described evidence of moulting in Marrellomorpha is a single specimen of *Marrella splendens* from the early Cambrian Burgess Shale, Canada (García-Bellido and Collins, 2004), that has been preserved during the act of exuviation (the actual process of exiting the old exoskeleton during moulting), which is sufficiently rare that no other euarthropod fossils have been described as in-the-act. Extant euarthropod representatives spend only minutes to hours (though this is variable between taxa) in the act of exuviation (Ewer, 2005), and therefore the likelihood of an individual being preserved and fossilised during this short period is presumably very low (Drage et al., 2019). This means that, to date, our knowledge of moulting in the Marrellomorpha is restricted to only an exceptional case of a single specimen of an abundant genus, which itself has a simpler cephalic shield morphology than other Marrellida (and differs greatly in morphology to the Acercostraca).

Specimens of a not-yet-formally described marrellid marrellomorph, putatively assigned to the '*Furca*' genus (Van Roy, 2006; Van Roy et al., 2010; see Material and methods section), are abundantly preserved in the Ordovician Fezouata Shale Lagerstätte, Morocco. The species has a complex cephalic shield morphology, with three pairs of elongate lateral spines and extensive secondary spinosity. Amongst these specimens are complete and nearly complete moult assemblages, as well as disarticulated isolated cephalic shield elements, all of which indicate a consistent moulting suture line location. These specimens allow for the second reconstruction ever of marrellomorph moulting behaviour, and conclusively show that there was variability in moulting within this clade that was likely linked to the complexity of the cephalic shield.

2 Geological setting

All specimens are from the Lower Ordovician Fezouata Shale Konservat-Lagerstätte of the central Anti-Atlas region of Morocco, which is renowned for its exceptional preservation of non-mineralised and lightly-sclerotised inhabitants of a highly diverse marine biota (Van Roy et al., 2010). In the Zagora region, from which all specimens of this study derive, a single unit is designated the Fezouata Shale, comprising a succession from the Tremadocian to Floian, with a regional transgressive contact at the base of the unit (Gutiérrez-Marco and Martin, 2016) and discontinuous, though well-understood, occurrences of exceptional preservation throughout

(Martin et al., 2016a; Martin et al., 2016b; Saleh et al., 2021a). The Fezouata Shale is a succession 900 m thick of blue-green to yellow-green siltstones (Destombes et al., 1985).

Several modes of exceptional preservation have been described from the Fezouata Shale Formation, including silica-chlorite concretions preserving radiodonts and trilobites in three-dimensions (Gaines et al., 2012; Van Roy et al., 2015b; Saleh et al., 2021b), and more two-dimensional compressed fossils within claystones preserved initially as carbonaceous films with authigenic minerals such as pyrite, but now found as iron oxide compressions after weathering leached carbon from the fossils (Van Roy et al., 2010; Martin et al., 2016a; Saleh et al., 2020; Pérez-Peris et al., 2021). This second mode of preservation comprises many of the exceptionally preserved fossils of the Fezouata Shale, including those studied herein, and is restricted to two intervals (Martin et al., 2016a). The lower interval is mainly within the *Araneograptus murrayi* zone and lower parts of the *Hunnegraptus copiosus* zone, corresponding to the late Tremadocian (Tr3; Gutiérrez-Marco and Martin, 2016; Lehnert et al., 2016; Nowak et al., 2016; Lefebvre et al., 2018). The upper interval is likely of Floian age, within the ? *Baltograptus jacksoni* zone (Lefebvre et al., 2018). A third interval shows the potential for exceptional preservation (Saleh et al., 2022), corresponding to the upper Floian. All specimens discussed herein originate from the *A. murrayi* zone of the late Tremadocian.

The depositional environment of the Fezouata Shale in general facilitated rapid burial of autochthonous communities in a shallow open marine environment (Martin et al., 2016a; Saleh et al., 2018; Saleh et al., 2020; Saleh et al., 2021b). This ranged from offshore to foreshore positioning, at a depth of *c.* 50–150 m (Vaucher et al., 2016). For the exceptionally preserved compressed specimens from the Zagora region, the environment was intermediate to distal open shelf, between the offshore and lower shoreface (Martin et al., 2016a), just below the storm wave base (Saleh et al., 2020).

3 Materials and methods

All specimens examined are from the lower interval of the Fezouata Shale (*A. murrayi* zone, upper Tremadocian, Lower Ordovician), from the Zagora region of the central Anti-Atlas. Two moult specimens accessioned at the Muséum cantonal des sciences naturelles, département de géologie, Lausanne, Switzerland (MGL; 103019_MGL, 104259_MGL) and one from the Yale Peabody Museum of Natural History, USA (YPM; YPM 532136) were examined. Several disarticulated specimens were also used for the description herein from the MGL and YPM (see Supplementary 1). Finally, complete carcasses from the Université Claude Bernard Lyon 1, France, were contrasted to the moult assemblages and disarticulated specimens (FSL AA.BIZ30.OI.1, FSL AA.BIZ31.OI.39). All specimens in the MGL and YPM collections were collected by authorised Moroccan collector Mohamed 'Ou Saïd' Ben Moula and his family during 2009 to 2015 (YPM) and 2015 to 2016 (MGL). These were purchased by the University of Lausanne and the Swiss National Science Foundation (MGL collection), or funds for acquisition of scientific collections of the Yale Peabody Museum (YPM), and in both cases the collections were subjected to export approval from the Ministry of Energy, Mines and the Environment of the federal government of the kingdom of Morocco, before being shipped by sea and land to the MGL and YPM. Export permits and exact GPS coordinates of the localities are curated with the materials. Lyon collection specimens are currently hosted within the Université Claude Bernard Lyon 1, but the Marrakech Collections of the Cadi Ayyad University retains ownership. See also Supplementary 1 for all specimen number and host collections information.

Specimens were photographed using a Canon EOS 800D camera with a Canon macro MP-E 65 mm 1:2.8 1-5X lens. Specimens were lit with long-angle NW lighting, or with full lighting. Photographs of each specimen were stacked in Adobe Photoshop CC to ensure good focus. Resulting images were processed in Adobe CC, in which brightness and contrast were altered to provide the best visibility. Line drawings were made from photographs using Adobe CC.

A morphological and taxonomic description of the Fezouata marrellid is not included herein. This falls outside the scope of this paper, which focuses solely on the novel moulting configuration preserved and relevant suture line location, and will no doubt be addressed independently of this work. Van Roy (2006), as well as subsequent papers to figure specimens of the Fezouata marrellid (Van Roy et al., 2015a; Lefebvre et al., 2016; Martin et al., 2016a; Vaucher et al., 2016; Saleh et al., 2021a), referred to the species as *'Furca' mauritanica*. However, the species has not been formally described, and we do not wish to further direct the prospective taxonomic assignment of this species without providing a valid description; as such, we refer to the species throughout as the 'Fezouata marrellid'. The general terminology used follows that of other marrellomorph descriptive literature, including Rak et al. (2012) and Aris et al. (2017).

4 Results

4.1 Suture line location

The Fezouata marrellid moult assemblages (Figure 1B, YPM 532136; Figure 1C, 104259_MGL; Figures 1D–F, 103019_MGL) show the existence of a suture line dividing the cephalic shield into two parts. This suture runs around the cephalic shield, from the posterior edges of the mediolateral spine pair, curving towards the posterior of the individual, and meeting to form a convex curved to squared posterior margin depending on whether it is on the dorsal or ventral side. The suture line thereby divides the cephalic shield into a larger anterior section, supporting the anterolateral and mediolateral pairs of spines, and a smaller posterior section, with the posterolateral pair of spines.

The suture line location is further supported by a number of disarticulated specimens, which consist of the anterior or posterior cephalic shield sections in isolation. In particular, 107796_MGL (Figures 2A, B) shows only the posterior section of the cephalic shield, with the posterolateral spine pair intact but no other material in association. This specimen clearly shows a clean disarticulation at the suture line described above, leaving a square-shaped recess into

10.3389/fevo.2023.1226924

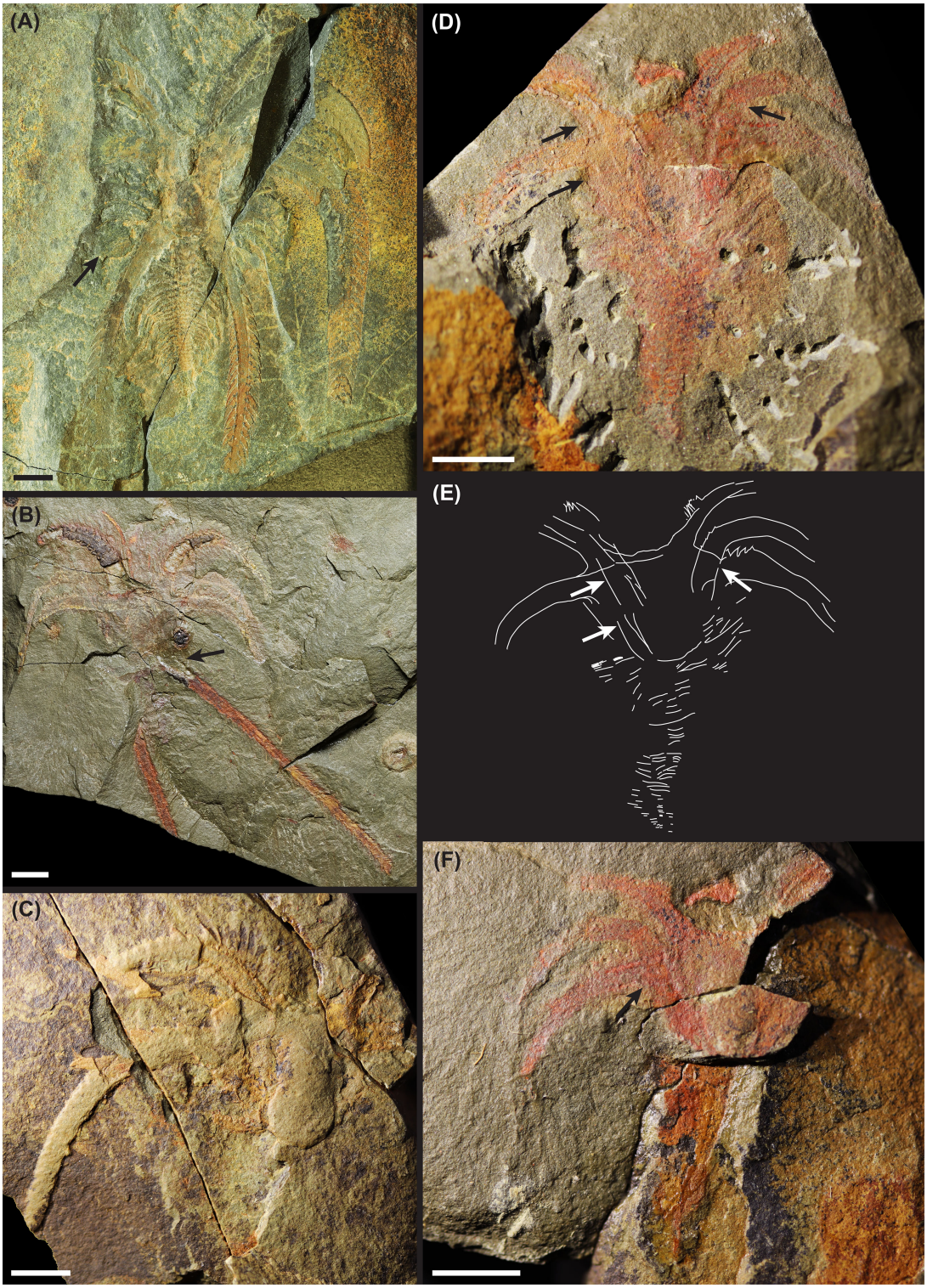

FIGURE 1
Photographs and drawing of putative moult assemblages of the Fezouata marrellid.: **(A)** photograph of intact carcass, FSL AA.BIZ.30.OI.1; **(B)** complete moult assemblage, YPM 532136b (counterpart comparable, not figured); **(C)** incomplete moult assemblage, 104259_MGL; **(D)** complete moult assemblage, 103019a_MGL (drawn in **E**); **(E)** interpretive drawing of complete moult assemblage, 103019a_MGL (specimen figured in **D**), drawing not morphologically descriptive; **(F)**, counterpart of **(D)**, 103019b_MGL. Black and white arrows in **(B, D–F)** point to disarticulated posterior cephalic shield sections, and in **(A)** to likely impressions of gill material. Scale bars = 5 mm.

the posterior cephalic shield section and two thin, anteriorly-directed, lateral projections. Additional specimens (103015_MGL, YPM 515771, YPM 517631, YPM 517634, YPM 519694, YPM 519905; e.g., Figures 2C, D), also show comparable isolated posterior sections. Eight specimens (YPM 520988, YPM 521588, YPM 522288, YPM 523536, YPM 525343, 102389_MGL, 104150_MGL, 107769_MGL) appear to represent the disarticulated anterior cephalic shield section (e.g., Figures 2E–G). Specimens YPM 530556 and YPM 530919 also seem to be isolated anterior cephalic shield sections with this suture line location, and are considered to be from juvenile individuals based on their small sizes.

Lastly, the suture line is also observable in many well-preserved complete specimens (presumably carcasses) of the Fezouata marrellid. For example, two large (3–4 cm long) complete specimens from Lyon (FSL AA.BIZ30.OI.1, FSL AA.BIZ31.OI.39) and two YPM specimens (YPM 525233, YPM 530594) show the suture line location particularly well, but it is apparent in many complete specimens in a dorsum-up orientation (e.g., Figures 2A, 3).

4.2 Description of moult assemblages

YPM 532136 (Figure 1B) is a complete moult assemblage of an adult individual, with all major exoskeleton parts visible. The anterior cephalic shield section appears mostly in place, but the posterior cephalic shield section is disarticulated, slightly displaced, and rotated approximately 20–30 degrees clockwise. Some anterior trunk tergites are clearly preserved *in situ*, and several appendages (including the enlarged appendage pair) and the antennae are also visible. Fully soft-tissue internal structures, and other soft-tissue aspects like the gills, are not visible.

Two further specimens represent disarticulated moult assemblages. Specimen 103019_MGL (Figures 1D–F) consists of the anterior cephalic shield section with an almost-complete trunk of tapering tergites, and poorly preserved appendage material. The posterior cephalic shield section is clearly disarticulated but appears to be associated with the rest of the assemblage, as an additional pair of primary spines fully overlaps the anterior cephalic shield section, potentially resulting from an anteriorly pointing posterior section. Specimen 104259_MGL is less well-preserved, and lacking evidence of the posterior cephalic shield section (Figure 1C). However, the anterior section remains with both pairs of primary spines, with some preservation of thoracic and appendage material.

Specimens consisting of only disarticulated anterior or posterior cephalic shield sections may or may not represent moulted exoskeletal material (e.g., 107796_MGL, 102389_MGL; Figure 2). It is impossible to determine whether they are moults without more associated material, as they may simply represent the remains of decayed and disarticulated material, as carcasses would presumably naturally open at the suture line due to it acting as a plane of weakness (see Daley and Drage, 2016). However, for this reason, though impossible to unambiguously assign as moult

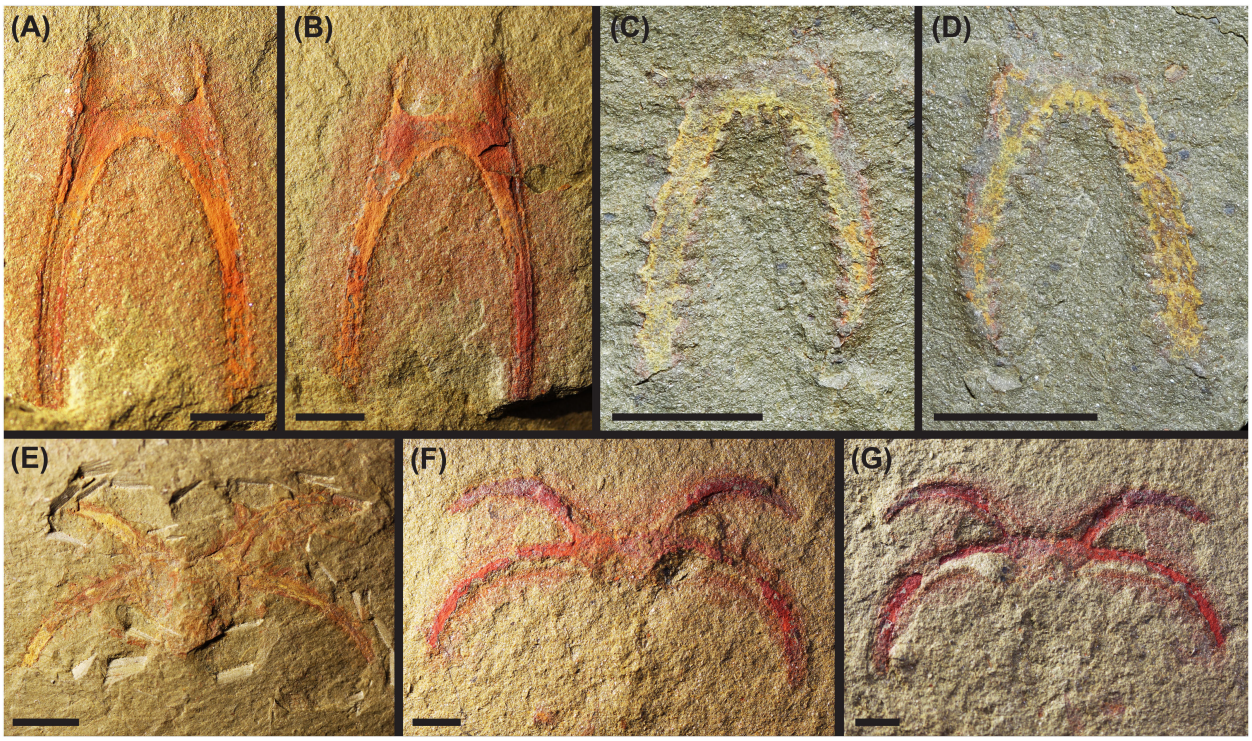

FIGURE 2
Photographs of disarticulated, isolated anterior and posterior cephalic shield sections of the Fezouata marrellid. **(A–D)** Posterior cephalic shield sections; **(A)** 107796b_MGL; **(B)** counterpart of **(A)** 107796a_MGL; **(C)** YPM 515771a; **(D)** counterpart of **(C)** YPM 515771b. **(E–G)** Anterior cephalic shield sections; **(E)** 104150_MGL; **(F)** 102389b_MGL; **(G)** counterpart of **(F)** 102389a_MGL. Scale bars = 5 mm.

or decayed carcass remains, these disarticulated cephalic shield fragments are useful in their support of the suture line location and morphology.

5 Discussion and conclusions

5.1 Marrellid suture line locations

The suture line location is alike that suggested for the, presumably carcass, specimen of '*Mimetaster*' *florestaensis* described by (Aris et al., 2017, Figure 2). They also suggest that the suture line curves posteriorly from the mediolateral spine pair to divide a posterior section supporting the posterolateral spine pair from the anterior section. However, this is unfortunately based on only one complete cephalic shield. *Mimetaster* species, which to date include '*Mi*'. *florestaensis* and *Mi. hexagonalis*, show similar morphologies to the Fezouata marrellid in terms of the cephalic shield shape and spines, and have been suggested to be closely related to the Fezouata marrellid (Mimetasteridae in Legg, 2016; Aris et al., 2017). '*Mi*'. *florestaensis*, in particular, is notably similar to the Fezouata marrellid and *Furca bohemica*, the latter of which also has three pairs of secondary spinose cephalic shield spines, which themselves have a similar length and shape (Rak et al., 2012). However, no suture line has been inferred for *Mi. hexagonalis* (Stürmer and Bergström, 1976; Kühl and Rust, 2010) or *F. bohemica* (Rak et al., 2012). In the latter case, a diagrammatic representation infers its possible existence in the same location as the Fezouata marrellid, although only discussed in the text is an 'inflated cephalic shield' so this is unclear (Rak et al., 2012, Figure 4A).

Tomlinsonus dimitrii is apparently also closely related to *Mimetaster* and *Furca*, as well as the Fezouata marrellid (Moysiuk et al., 2022). Again, no suture line has yet been identified for *T. dimitrii*, which was described from a single specimen. However, Moysiuk et al. (2022) note that the posterior margins of the cephalic shield have not been observed, resulting in no evidence of a potential posterolateral spine pair (e.g., their Figure 3, 4.1). Based on specimens of the Fezouata marrellid showing the anterior cephalic shield section with *in situ* trunk, but opened suture and consequently absent posterior section (e.g., Figure 1C), it is possible that the suture line of *T. dimitrii* is in a comparable location, and the posterior section is disarticulated and missing in the described *T. dimitrii* specimen, which may therefore represent a moult. Analysis of additional *T. dimitrii* specimens would be required to confirm or deny this.

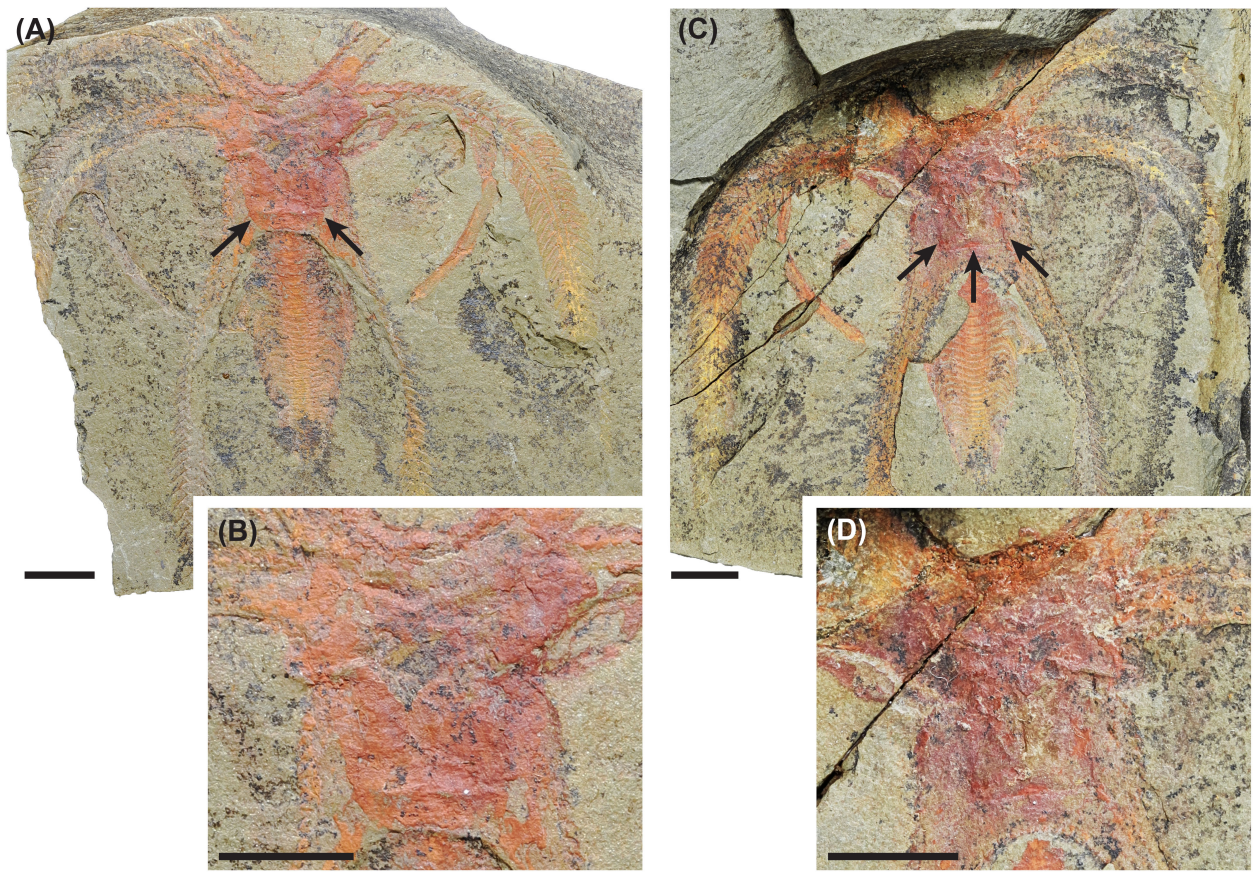

FIGURE 3
Photographs of part **(A)** with closeup of cephalic shield and suture line **(B)** and counterpart **(C)** also with closeup **(D)** of a complete Fezouata marrellid carcass (YPM 525233); suture line indicated by black arrows. Scale bars = 5 mm.

Other, probably more distantly related, marrellids must have had very different suture lines to that described here for the Fezouata marrellid. To produce the in-the-act moulting specimen described for *Marrella splendens* (García-Bellido and Collins, 2004), the suture line must track around the anterior margin of the cephalic shield, allowing for an exuvial gape to open at the anterior-most section of the shield. Thus, the suture line would be impossible to see in the vast majority of *M. splendens* specimens, which are preserved dorsum-up or ventrum-up rather than obliquely. This means that the actual suture line of *M. splendens* has not so-far been directly described or figured (neither in Whittington, 1971, nor in García-Bellido and Collins, 2006). Further, there is no apparent sign of a suture line, suggesting a marginal location, in specimens of *Marrella* sp. described from the Balang Formation, China (Liu, 2013).

The three moult assemblages described here are all presumed to represent adults, based on body size. However, two juvenile anterior cephalic shield sections were also observed (YPM 530556 and YPM 530919), based on their minute size. These juvenile specimens demonstrate that the suture line was seemingly in the same location as for adults (see ontogenetic sequence in Laibl et al., this volume), which suggests that moulting behaviour was also consistent across ontogenetic stages of the Fezouata marrellid. However, to conclusively determine consistent moulting behaviour with development more moult specimens or isolated elements would be required, particularly those at the earliest, most minute, life stages. Further, greater quantities of adult moult specimens would be necessary to determine whether marrellid individuals continued moulting into adulthood or halted following attainment of an adult morphology or certain size.

5.2 Preservation of moult assemblages

All contextual information supports the putative assignments of the three specimens here as moults (see Daley and Drage, 2016; Drage and Daley, 2016), including the completeness of the assemblages (particularly Figures 2C, E), lack of obvious biostratinomic effects (no alignment, no fragmentation of exoskeleton parts), characteristic and consistent disarticulation at the suture line location, and lack of softer external structures (e.g., gills, which are occasionally present in carcasses; see Figure 1A) and internal tissues. The moult assemblages described here thereby greatly differ to similarly well-preserved specimens of marrellid from the Fezouata and other Konservat-Lagerstätten (García-Bellido and Collins, 2006). Internal tissues can be confidently considered to designate specimens as carcasses (Daley and Drage, 2016), though there was significant decay before burial in the Fezouata Shale, often preventing preservation of soft tissue (Saleh et al., 2021a), and so this alone cannot be used to differentiate moults and carcasses from this Konservat-Lagerstätte. Evidence of appendages, and likely antennae, are to be expected in well-preserved moult specimens, as these are exoskeleton components that must necessarily be moulted. Isolated anterior and posterior cephalic shield elements (Figure 2) are impossible to assign as either moults or carcasses, due to the lack of contextual information relayed above; however, they remain important for conclusively demonstrating the suture line location.

5.3 Inferred mode of moulting

The previously described suture line and moult assemblages of the Fezouata marrellid suggest a newly observed mode of moulting behaviour for this group, which is highly divergent from that described for *M. splendens* (García-Bellido and Collins, 2004). Due to the mediolateral location of the suture, the Fezouata marrellid may have moved upwards and perhaps posteriorly when extracting the body out of the old exoskeleton. Firstly, this direction of movement would have fully opened an exuvial gape at the suture line between the mediolateral and posterolateral spine pairs owing to pressure put on this plane of weakness. The animal would then have moved upwards and/or backwards away from the old exoskeleton, pulling its body free with the large cephalic shield spines coming out afterwards (Figure 4). In comparison, *M. splendens*, with an exuvial gape at the anterior margin of the

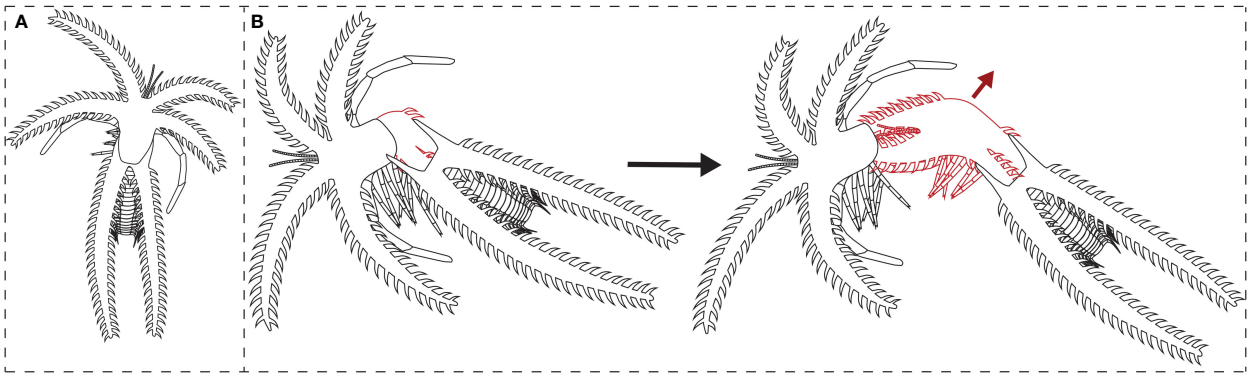

FIGURE 4
Interpretive drawing of a complete carcass of the Fezouata marrellid, and its suggested moulting process: **(A)** complete carcass; **(B)** moulting individual (red lines) opening the exoskeleton at the suture line and withdrawing from the old exoskeleton (black lines) in an upwards and backwards movement (red arrow).

cephalic shield, moved forwards to exit the old exoskeleton during moulting. This movement caused severe bending of the cephalic shield spines for *M. splendens* (see García-Bellido and Collins, 2004, Figure 1). It is worth noting that some extinct arthropod groups, particularly trilobites, show intraspecific variability in the moulting behaviours they employed, even producing exuvial gapes in multiple places, likely due to the specific movements carried out during the traumatic moulting process (e.g., see Drage, 2019; Drage, 2022). It is therefore possible that marrellomorphs also varied in moulting behaviours intraspecifically, though we have no evidence to date that supports this idea.

The differences in morphology between the Fezouata marrellid and *M. splendens* likely explain their dissimilar moulting movements, largely reflecting the greater complexity of the former compared to the latter. The Fezouata marrellid (and *Mimetaster* and *Furca* species; Rak et al., 2012; Aris et al., 2017) had an additional pair of cephalic shield spines, all three spine pairs were of greater lengths, and all spines had extensive secondary spinosity, compared to *M. splendens*. These complex cephalic shield spines may have been correspondingly more difficult to extract during moulting. Perhaps this upwards rather than forwards movement during exuviation provided a more favourable angle for the spines, requiring less bending, and therefore a lower risk of sustaining moulting injuries. This is supported by the angular orientations of the secondary spines; they are pointed distally at a *c.* 45-degree angle, rather than perpendicular to the primary spine direction. This means that the secondary spines would be at a favourable angle to slide out of the old exoskeleton without much bending (see Figure 4), whereas moulting injuries from the spines bending and catching would be more likely if the secondary spines were perpendicular or proximally orientated. Additionally, the cephalic shield in adult individuals was both physically and proportionally larger in the Fezouata marrellid than *M. splendens*, which may have also benefitted from a mediolateral exuvial gape the full width of the cephalic shield.

Mechanically, an upwards and/or posterior body movement during moulting for the Fezouata marrellid is more similar to the moulting movements of several other arthropod clades, than those of *M. splendens*. For example, this movement is overall analogous to the moulting of arthropod clades with lobster-like bodyplans. Lobsters, shrimp, and similar decapods produce a medial split in the dorsal side of the carapace, and the animal then emerges from the old exoskeleton up and backwards, pulling out the appendages after the body (Glaessner, 1969; Daley and Drage, 2016). This produces fossil moults preserved in the characteristic 'Open Moult Position'. Moulting spiders and crabs also move similarly, disarticulating the dorsal part of the carapace to produce a large exuvial gape, exiting backwards and pulling their appendages after the body (Petrunkevitch, 1942; Glaessner, 1969; Daley and Drage, 2016).

5.4 The marrellomorph moult record

It is remarkable that only one in-the-act-of-moulting specimen (García-Bellido and Collins, 2004) and potentially five isolated cephalic shields (Whittington, 1971) of *M. splendens*, one of the most abundant animals in the Cambrian Burgess Shale (Whittington, 1971; Conway Morris, 1979; García-Bellido and Collins, 2006), and the three probable moult assemblages of the Fezouata marrellid figured herein, have been described for the entirety of the marrellomorph fossil record. Whittington (1971) notes that almost all *M. splendens* individuals discovered at that time, numbering thousands of individuals, represent carcasses due to the presence of soft tissue and associated organic material. They consider only five specimens of isolated cephalic shield to be potential moults due to the lack of soft material (Whittington, 1971, plate XVIII, Figure 5) which is a reasonable interpretation based on their notably different preservation to all other individuals from the Burgess Shale. The moult status of the singular *M. splendens* individual described by García-Bellido and Collins (2004) is indisputable, as are the assignments of several specimens presented here (see discussion above), though it is difficult to consider isolated cephalic shields as moults with absolute certainty and additional moulted exoskeleton material (e.g., of the appendages, thorax) would be expected for well-preserved moult assemblages (see Daley and Drage, 2016). Many researchers have hypothesised that the fossil records of various euarthropod groups are likely to be biased towards more numerous moults than carcasses, based on both arguments of preservation (e.g., moults are less attractive to scavengers) and ontogeny (an individual moults many times during its life, but produces only one carcass) (Braddy, 2001; Daley and Drage, 2016). However, some arthropod groups regularly consume their moults (e.g., in myriapods; Shear and Edgecombe, 2010), or reabsorb materials from the moult, and this may contrastingly lead to a bias towards carcasses in the fossil record, though this is extremely difficult to test in extinct groups and no conclusive evidence of this has so far been advanced for extinct arthropods (Daley and Drage, 2016). On balance, it is almost certain that many more moult assemblages exist in the marrellomorph fossil record, yet await identification and description as such.

Neither empty moults, nor additional in-the-act of moulting specimens have been described for any other marrellomorph (including acercostracans). The paucity of moulting evidence for Marrellomorpha may be related to their preservation potential, which was presumably lower than some other euarthropod groups, like trilobites, because marrellomorphs lacked biomineralised exoskeletons. However, in locations of exceptional preservation, like the Burgess Shale, carcasses of *M. splendens* seemingly preserve well, given their abundance (see Whittington, 1971), which suggests something else must be responsible for the lack of identified marrellomorph moults. As discussed, it is possible that moulted exoskeletons of marrellids with anterior marginal suture locations, as inferred for *Marrella*, are more common than realised, and are miscategorised as carcasses because the suture line is almost impossible to observe in the fossil record. This would be a similar scenario to horseshoe crabs and some morphologically-derived trilobites, for example harpetids, both of which have a suture line and exuvial gape around the anterior margin of the cephalon, which tends to mostly close after exuviation, leaving an empty exoskeleton that outwardly appears to be a normal carcass (Babcock et al., 2000; Tetlie et al., 2008; Daley and Drage, 2016; Drage, 2019). However, the

exuvial gape described here for the Fezouata marrellid, and potentially *Furca, Mimetaster* and *Tomlinsonus*, would not lead to this preservational issue, and would presumably leave recognisable moults, suggesting a reassessment of marrellid museum collections is a worthwhile endeavour. Researchers working on marrellomorphs should aim to distinguish moults from carcasses by looking for specimens lacking obvious soft tissue preservation, with all exoskeleton parts present in association, and disarticulation at described, or potential new, suture line locations. This work may be aided through the application of modern visualisation techniques, such as UV reflected photography and micro-XRF elemental mapping. Through these efforts, we can greatly expand our understanding of moulting in Marrellomorpha, and how their varied behaviours relate to their captivating morphologies.

Data availability statement

The original contributions presented in the study are included in the article/Supplementary Material. Further inquiries can be directed to the corresponding author.

Author contributions

HD: conceptualisation, investigation, writing – original draft, writing – review and editing, visualisation. DL: investigation, writing – review and editing. AD: conceptualisation, writing – review and editing. All authors contributed to the article and approved the submitted version.

Funding

HD and AD wish to acknowledge funding from a Swiss National Science Foundation Sinergia grant (198691).

Acknowledgments

B. Lefebvre and E. Robert at the Lyon 1 University, G. Potin and F. Saleh at the University of Lausanne, and J. Utrup, S. Butts and D.E.G. Briggs at the Yale Peabody Museum of Natural History are thanked for their collections access facilitation. We thank two reviewers, the editor Z. Zhang, B. Lieberman, and the managing editors of this special volume for their comments and publishing assistance with this manuscript. We acknowledge P. Van Roy for discussions on marrellomorph moult material during 2015–16. This work would be impossible without the years of intense collecting efforts of all researchers and fossil collectors involved.

Conflict of interest

The authors declare that the research was conducted in the absence of any commercial or financial relationships that could be construed as a potential conflict of interest.

Publisher's note

Supplementary material

The Supplementary Material for this article can be found online at: https://www.frontiersin.org/articles/10.3389/fevo.2023.1226924/full#supplementary-material

References

Aris, M. J., Corronca, J. A., Quinteros, S., and Pardo, P. L. (2017). A new marrellomorph euarthropod from the Early Ordovician of Argentina. *Acta Palaeontol. Pol.* 62, 1–8. doi: 10.4202/app.00240.2016

Babcock, L. E., Merriam, D. F., and West, R. R. (2000). *Paleolimulus*, an early limuline (Xiphosurida), from Pennsylvanian-Permian Lagerstätten of Kansas and taphonomic comparison with modern *Limulus*. *Lethaia* 33, 129–141. doi: 10.1080/00241160025100017

Braddy, S. J. (2001). Eurypterid palaeoecology: palaeobiological, ichnological and comparative evidence for a 'mass-moult-mate' hypothesis. *Palaeogeogr. Palaeoclimatol. Palaeoecol.* 172, 115–132. doi: 10.1016/s0031-0182(01)00274-7

Brandt, D. S. (2002). Ecdysial efficiency and evolutionary efficacy among marine arthropods: implications for trilobite survivorship. *Alcheringa* 26, 399–421. doi: 10.1080/03115510208619264

Brandt, D. S. (2021). Eurypterid morphology and implications for ecdysis and evolutionary longevity. *Lethaia* 54, 711–722. doi: 10.1111/let.12434

Conway Morris, S. (1979). The Burgess Shale (middle Cambrian) fauna. *Ann. Rev. Ecol. Syst.* 10, 327–349. doi: 10.1146/annurev.es.10.110179.001551

Corrales-García, A., Esteve, J., Zhao, Y., and Yang, X. (2020). Synchonized moulting behaviour in trilobites from the Cambrian Series 2 of South China. *Sci. Rep.* 10, 14099. doi: 10.1038/s41598-020-70883-5

Daley, A. C., and Drage, H. B. (2016). The fossil record of ecdysis, and trends in the moulting behaviour of trilobites. *Arthropod Struct. Dev.* 45, 71–96. doi: 10.1016/j.asd.2015.09.004

Destombes, R. R., Hollard, D. E. G., and Willefert, P. J. (1985). 'Lower Palaeozoic rocks of Morocco,' in *Lower Palaeozoic rocks of the world 4*. Ed. C. H. Holland (Wiley, New York), 91–336.

Drage, H. B. (2019). Quantifying intra- and interspecific variability in trilobite moulting behaviour across the Palaeozoic. *Palaeontol. Electron.* 22.2.34A, 1–39. doi: 10.26879/940

Drage, H. B. (2022). Trilobite moulting variability had little association with morphometry. *bioRxiv preprint*, 1–33. doi: 10.1101/2022.12.12.520015

Drage, H. B., and Daley, A. C. (2016). Recognising moulting behaviour in trilobites by examining morphology, development and preservation: Comment on Błażejowski et al., 2015. *BioEssays* 38, 981–990. doi: 10.1002/bies.201600027

Drage, H. B., Holmes, J. D., García-Bellido, D. C., and Daley, A. C. (2018). An exceptional record of Cambrian trilobite moulting behaviour preserved in the Emu Bay Shale, South Australia. *Lethaia* 51, 473–492. doi: 10.1111/let.12266

Drage, H. B., Holmes, J. D., García-Bellido, D. C., and Paterson, J. R. (2023). Associations between trilobite intraspecific moulting variability and body proportions:

Estaingia bilobata from the Cambrian Emu Bay Shale, Australia. *Palaeontology* 66, e12651. doi: 10.1111/pala.12651

Drage, H. B., Vandenbroucke, T. R. A., Van Roy, P., and Daley, A. C. (2019). Sequence of post-moult exoskeleton hardening preserved in a trilobite mass moult assemblage from the Lower Ordovician Fezouata Konservat-Lagerstätte, Morocco. *Acta Palaeontol. Pol.* 64, 261–273. doi: 10.4202/app.00582.2018

Ewer, J. (2005). How the ecdysozoan changed its coat. *PloS Biol.* 3, e349. doi: 10.1371/journal.pbio.0030349

Gaines, R. R., Briggs, D. E. G., Orr, P. J., and Van Roy, P (2012). Preservation of giant anomalocaridids in silica-chlorite concretions from the Early Ordovician of Morocco. *Palaios* 27, 317–325. doi: 10.2110/palo.2011.p11-093r

García-Bellido, D. C., and Collins, D. H. (2004). Moulting arthropod caught in the act. *Nature* 429, 40. doi: 10.1038/429040a

García-Bellido, D. C., and Collins, D. H. (2006). A new study of *Marrella splendens* (Arthropoda, Marrellomorpha) from the Middle Cambrian Burgess Shale, British Columbia, Canada. *Can. J. Earth Sci.* 43, 721–742. doi: 10.1139/e06-012

Glaessner, M. F. (1969). 'Decapoda,' in *Treatise on invertebrate paleontology*, vol. Pt R 4. Ed. R. C. Moore (Lawrence: Geological Society of America and University of Kansas Press), R400–R533. doi: 10.17161/dt.v0i0.5629

Gutiérrez-Marco, J. C., and Martin, E. L. O. (2016). Biostratigraphy and palaeoecology of Lower Ordovician graptolites from the Fezouata Shale (Moroccan Anti-Atlas). *Palaeogeogr. Palaeoclimatol. Palaeoecol.* 460, 35–49. doi: 10.1016/j.palaeo.2016.07.026

Haug, J. T., Caron, J.-B., and Haug, C. (2013). Demecology in the Cambrian: synchronized molting in arthropods from the Burgess Shale. *BMC Biol.* 11, 1–10. doi: 10.1186/1741-7007-11-64

Haug, J. T., Castellani, C., Haug, C., Waloszek, D., and Maas, A. (2012). A *Marrella*-like arthropod from the Cambrian of Australia: A new link between 'Orsten'-type and Burgess Shale assemblages. *Acta Palaeontol. Pol.* 58, 629–639. doi: 10.4202/app.2011.0120

Hyžný, M., Bruce, N. L., and Schlögl, J. (2013). An appraisal of the fossil record for the Cirolanidae (Malacostraca: Pericarida: Isopoda: Cymothoida), with a description of a new cirolanid isopod crustacean from the early Miocene of the Vienna Basin (western Carpathians). *Palaeontology* 56, 615–630. doi: 10.1111/pala.12006

Klompmaker, A. A., and Fraaije, R. H. B. (2011). The oldest (Middle Triassic, Anisian) lobsters from the Netherlands: taxonomy, taphonomy, paleoenvironment, and paleoecology. *Palaeontol. Electron.* 14, 1–15. Available at: https://palaeo-electronica.org/2011_1/220/220.pdf.

Kühl, G., and Rust, J. (2010). Re-investigation of *Mimetaster hexagonalis*: a marrellomorph arthropod from the Lower Devonian Hunsrück Slate (Germany). *Palaeontol. Z.* 84, 397–411. doi: 10.1007/s12542-009-0049-x

Kukalova, J. (1968). Permian mayfly nymphs. *Psyche* 75, 310–327. doi: 10.1155/1968/904597

Lefebvre, B., El Hariri, K., Lerosey-Aubril, R., Servais, T., and Van Roy, P. (2016). The Fezouata Shale (Lower Ordovician, Anti-Atlas, Morocco): A historical review. *Palaeogeogr. Palaeoclimatol. Palaeoecol.* 460, 7–23. doi: 10.1016/j.palaeo.2015.10.048

Lefebvre, B., Gutiérrez-Marco, J. C., Lehnert, O., Martin, E. L. O., Nowak, H., Akodad, M., et al. (2018). Age calibration of the Lower Ordovician Fezouata Lagerstätte, Morocco. *Lethaia* 51, 296–311. doi: 10.1111/let.12240

Legg, D. A. (2015). The morphology and affinities of *Skania fragilis* (Arthropoda) from the middle Cambrian Burgess Shale. *Bull. Geosci.* 90, 509–518. doi: 10.3140/bull.geosci.1532

Legg, D. A. (2016). An acercostracan marrellomorph (Euarthropoda) from the Lower Ordovician of Morocco. *Sci. Nat.* 103, 1–7. doi: 10.1007/s00114-016-1352-5

Lehnert, O., Nowak, H., Sarmiento, G. N., Gutiérrez-Marco, J. C., Akodad, M., and Servais, T. (2016). Conodonts from the Lower Ordovician of Morocco – Contributions to age and faunal diversity of the Fezouata Lagerstätte and peri-Gondwana biogeography. *Palaeogeogr. Palaeoclimatol. Palaeoecol.* 460, 50–61. doi: 10.1016/j.palaeo.2016.03.023

Liu, Q. (2013). The first discovery of *Marrella* (Arthropoda, Marrellomorpha) from the Balang Formation (Cambrian Series 2) in Hunan, China. *J. Paleontol.* 87, 391–394. doi: 10.1666/12-118.1

Martin, E. L. O., Pittet, B., Gutiérrez-Marco, J. C., Vannier, J., El Hariri, K., Lerosey-Aubril, R., et al. (2016a). The Lower Ordovician Fezouata Konservat-Lagerstätte from Morocco: Age, environment and evolutionary perspectives. *Gondwana Res.* 34, 274–283. doi: 10.1016/j.gr.2015.03.009

Martin, E. L. O., Vidal, M., Vizcaïno, D., Vaucher, R., Sansjofre, P., Lefebvre, B., et al. (2016b). Biostratigraphic and palaeoenvironmental controls on the trilobite associations from the Lower Ordovician Fezouata Shale of the central Anti-Atlas, Morocco. *Palaeogeogr. Palaeoclimatol. Palaeoecol.* 460, 142–154. doi: 10.1016/j.palaeo.2016.06.003

McCoy, V. E., and Brandt, D. S. (2009). Scorpion taphonomy: criteria for distinguishing fossil scorpion molts and carcasses. *J. Arachnol.* 37, 312–320. doi: 10.1636/sh09-07.1

Moysiuk, J., Izquierdo-López, A., Kampouris, G. E., and Caron, J.-B. (2022). A new marrellomorph arthropod from southern Ontario: a rare case of soft-tissue preservation on a Late Ordovician open marine shelf. *J. Paleontol.* 96, 859–874. doi: 10.1017/jpa.2022.11

Nowak, H., Servais, T., Pittet, B., Vaucher, R., Akodad, M., Gaines, R. R., et al. (2016). Palynomorphs of the Fezouata Shale (Lower Ordovician, Morocco): Age and environmental constraints of the Fezouata Biota. *Palaeogeogr. Palaeoclimatol. Palaeoecol.* 460, 62–74. doi: 10.1016/j.palaeo.2016.03.007

Olempska, E. (2012). Morphology and affinities of Eridostracina: Palaeozoic ostracods with moult retention. *Hydrobiologia* 688, 139–165. doi: 10.1007/s10750-011-0659-7

Pérez-Peris, F., Laibl, L., Vidal, M., and Daley, A. C. (2021). Systematics, morphology, and appendages of an Early Ordovician pilekiine trilobite *Anacheirurus* from Fezouata Shale and the early diversification of Cheiruridae. *Acta Palaeontol. Pol.* 66, 857–877. doi: 10.4202/app.00902.2021

Petrunkevitch, A. I. (1942). A study of amber spiders. *Trans. Conn. Acad. Arts Sci.* 34, 119–464.

Rak, S., Ortega-Hernández, J., and Legg, D. A. (2012). A revision of the Late Ordovician marrellomorph arthropod *Furca bohemica* from Czech Republic. *Acta Palaeontol. Pol.* 58, 615–528. doi: 10.4202/app.2011.0038

Rasnitsyn, A. P. (2002). 'Introduction to palaeoentomology,' in *History of insects*. Eds. A. P. Rasnitsyn and D. L. J. Quicke (Dordrecht, The Netherlands: Kluwer Academic Publishers), 19–20.

Saleh, F., Candela, Y., Harper, D. A. T., Polechovà, M., Pittet, B., and Lefebvre, B. (2018). Storm-induced community dynamics in the Fezouata Biota (Lower Ordovician, Morocco). *Palaios* 33, 535–541. doi: 10.2110/palo.2018.055

Saleh, F., Pittet, B., Sansjofre, P., Guériau, P., Lalonde, S., Perrillat, J.-P., et al. (2020). Taphonomic pathway of exceptionally preserved fossils in the Lower Ordovician of Morocco. *Geobios* 60, 99–115. doi: 10.1016/j.geobios.2020.04.001

Saleh, F., Vaucher, R., Anticliffe, J. B., Daley, A. C., El Hariri, K., Kouraiss, K., et al. (2021a). Insights into soft-part preservation from the Early Ordovician Fezouata Biota. *Earth-Sci. Rev.* 213, 1–12. doi: 10.1016/j.earscirev.2020.103464

Saleh, F., Vaucher, R., Vidal, M., El Hariri, K., Laibl, L., Daley, A. C., et al. (2022). New fossil assemblages from the early Ordovician Fezouata Biota. *Sci. Rep.* 12, 20773. doi: 10.1038/s41598-022-25000-z

Saleh, F., Vidal, M., Laibl, L., Sansjofre, P., Gueriau, P., Pérez-Peris, F., et al. (2021b). Large trilobites in a stress-free Early Ordovician environment. *Geol. Mag.* 158, 261–270. doi: 10.1017/s0016756820000448

Selden, P. A., Shear, W. A., and Bonamo, P. M. (1991). A spider and other arachnids from the Devonian of New York, and reinterpretation of Devonian Araneae. *Palaeontology* 34, 241–281. Available at: http://hdl.handle.net/1808/8336.

Shear, W. A., and Edgecombe, G. D. (2010). The geological record and phylogeny of the Myriapoda. *Arthropod Struct. Dev.* 39, 174–190. doi: 10.1016/j.asd.2009.11.002

Stürmer, W., and Bergström, J. (1976). The arthropods *Mimetaster* and *Vachonisia* from the Devonian Hunsrück Shale. *Palaeontol. Z.* 50, 78–111. doi: 10.1007/bf03001974

Tetlie, O. E., Brandt, D. S., and Briggs, D. E. G. (2008). Ecdysis in sea scorpions (Chelicerata: Eurypterida). *Palaeogeogr. Palaeoclimatol. Palaeoecol.* 265, 182–194. doi: 10.1016/j.palaeo.2008.05.008

Van Roy, P. (2006). *Non-trilobite arthropods from the Ordovician of Morocco* (Belgium: University of Ghent), 232.

Van Roy, P., Briggs, D. E. G., and Gaines, R. R. (2015a). The Fezouata fossils of Morocco; an extraordinary record of marine life in the Early Ordovician. *J. Geol. Soc* 172, 541–549. doi: 10.1144/jgs2015-017

Van Roy, P., Daley, A. C., and Briggs, D. E. G. (2015b). Anomalocaridid trunk limb homology revealed by a giant filter-feeder with paired flaps. *Nature* 522, 77–80. doi: 10.1038/nature14256

Van Roy, P., Orr, P. J., Botting, J. P., Muir, L. A., Vinther, J., Lefebvre, B., et al. (2010). Ordovician faunas of Burgess Shale type. *Nature* 465, 215–218. doi: 10.1038/nature09038

Vaucher, R., Martin, E. L. O., Hormière, H., and Pittet, B. (2016). A genetic link between Konzentrat- and Konservat-Lagerstätten in the Fezouata Shale (Lower Ordovician, Morocco). *Palaeogeogr. Palaeoclimatol. Palaeoecol.* 460, 24–34. doi: 10.1016/j.palaeo.2016.05.020

Wang, Y., Peng, J., Wang, D., Zhang, H., Luo, X., Shao, Y., et al. (2021). Ontogenetic moulting behavior of the Cambrian oryctocephalid trilobite *Arthricocephalites xinzhaiheensis*. *PeerJ* 9, e12217. doi: 10.7717/peerj.12217

Whittington, H. B. (1971). Redescription of *Marrella splendens* (Trilobitoidea) from the Burgess Shale, middle Cambrian, British Columbia. *Geol. Sur. Can. Bull.* 209, 1–24. doi: 10.4095/102427

Yang, J., Ortega-Hernández, J., Drage, H. B., Du, K.-S., and Zhang, X.-G. (2019). Ecdysis in a stem-group euarthropod from the early Cambrian of China. *Sci. Rep.* 9:5709, 1–9. doi: 10.1038/s41598-019-41911-w

Zong, R. (2020). Coupled exuviae of the Ordovician *Ovalocephalis* (Pliomeridae, Trilobita) in South China and its behavioral implications. *PeerJ* 8, e10166. doi: 10.7717/peerj.10166

Zong, R. (2021). Injuries and molting interference in a trilobite from the Cambrian (Furongian) of South China. *PeerJ* 9, e11201. doi: 10.7717/2Fpeerj.11201

frontiers | Frontiers in Ecology and Evolution

TYPE Original Research
PUBLISHED 25 September 2023
DOI 10.3389/fevo.2023.1232612

OPEN ACCESS

EDITED BY
Tae-Yoon Park,
Korea Polar Research Institute,
Republic of Korea

REVIEWED BY
Dongjing Fu,
Northwest University, China
James Holmes,
University of New England, Australia

*CORRESPONDENCE
Lukáš Laibl
lukaslaibl@gmail.com
Allison C. Daley
allison.daley@unil.ch

RECEIVED 31 May 2023
ACCEPTED 25 August 2023
PUBLISHED 25 September 2023

CITATION
Laibl L, Gueriau P, Saleh F, Pérez-Peris F, Lustri L, Drage HB, Bath Enright OG, Potin GJ-M and Daley AC (2023) Early developmental stages of a Lower Ordovician marrellid from Morocco suggest simple ontogenetic niche differentiation in early euarthropods. *Front. Ecol. Evol.* 11:1232612. doi: 10.3389/fevo.2023.1232612

Early developmental stages of a Lower Ordovician marrellid from Morocco suggest simple ontogenetic niche differentiation in early euarthropods

Lukáš Laibl[1,2]*, Pierre Gueriau[3,4], Farid Saleh[3], Francesc Pérez-Peris[5], Lorenzo Lustri[3], Harriet B. Drage[3], Orla G. Bath Enright[6], Gaëtan J.-M. Potin[3] and Allison C. Daley[3]*

[1]Czech Academy of Sciences, Institute of Geology, Prague, Czechia, [2]Institute of Geology and Palaeontology, Faculty of Science, Charles University, Prague, Czechia, [3]Institute of Earth Sciences, University of Lausanne, Lausanne, Switzerland, [4]Université Paris-Saclay, CNRS, Ministère de la Culture, UVSQ, MNHN, Institut photonique d'analyse non-destructive européen des matériaux anciens, Saint-Aubin, France, [5]Department of Earth and Environmental Sciences, The University of Iowa, Iowa, IA, United States, [6]Department of Palaeontology, Staatliches Museum für Naturkunde, Stuttgart, Germany

Early developmental stages of euarthropods are exceptionally rare in the fossil record. This hampers our understanding of the biology, phylogeny, and development of this extremely diverse metazoan group. Herein, we use classical paleontological methods in combination with synchrotron X-ray microtomography to explore the morphology in ca. 480 million-year-old early developmental stages of the Lower Ordovician Fezouata Shale marrellid euarthropod. These stages range between 3.8 and 5.3 mm in length and are characterized by three distinct pairs of gently curved spines that projects from the head shield. The first pair of cephalic appendages are represented by uniramous antenullae of a sensory function. The second pair of cephalic appendages is robust, and had an anchoring or stabilizing function. The third cephalic appendage pair is composed of long cylindrical podomeres and was used for walking. The trunk appendages are biramous and consist of an endopod and a lamellate exopod. Two anterior trunk endopods are composed of long slender podomeres and were used for walking, while the more posterior trunk endopods bear robust endites and associated setae and were used for food gathering. The trunk of the earliest developmental stages is composed of thirteen segments, in contrast to more than 22 segments in the adult trunk. The similar appendage morphology and differentiation along the body is evident in adult individuals of the Fezouata marrellid, suggesting these different developmental stages shared similar methods of locomotion and food processing. Given that adults and juveniles are often preserved in the same or nearby sites, the niche differentiation between these life stages would be the result of the absolute smaller appendage size in immature stages compared to larger adults, effectively differentiating the size of food resources consumed by each. In addition, the

delicate setae present in the posterior trunk appendages of early developmental stages might have been used to capture smaller food particles. This simple mode of ontogenetic niche differentiation might have been common in the early diverging euarthropod groups.

KEYWORDS

Euarthropoda, development, niche differentiation, Ordovician, Morocco, marrellida

1 Introduction

The early post-embryonic stages of various metazoans are important constituents of both recent and past marine ecosystems. This is especially the case for euarthropods – a clade that comprises most metazoans on Earth, both in terms of diversity (Zhang, 2011) and biomass (Bar-On et al., 2018). Extant euarthropods show immensely diverse post-embryonic development, and the same was likely the case for extinct groups, although, in the latter case, limited data is available. The only extinct euarthropod group with a well-documented developmental fossil record are trilobites because they biomineralized their dorsal exoskeleton soon after hatching (Chatterton and Speyer, 1997; Hopkins, 2017; Lerosey-Aubril and Laibl, 2021). Trilobites had hemianamorphic development (i.e., they added segments in their early post-embryonic stages, while later stages show segment stability, Minelli and Fusco, 2013). Trilobites also show both direct and indirect development, with or without distinct metamorphosis (Chatterton and Speyer, 1997; Park et al., 2016; Laibl et al., 2018; Laibl et al., 2021; Laibl et al., 2023), and various modes of feeding in their earliest stages (e.g., Chatterton and Speyer, 1989; Laibl et al., 2017).

In contrast to the rich developmental record of trilobites, early developmental stages of other extinct early Paleozoic euarthropods are rare (Lerosey-Aubril and Laibl, 2021). This is striking, considering that adult euarthropods represent a large part of Paleozoic marine ecosystems (Caron and Jackson, 2008; Caron et al., 2014; Zhao et al., 2014; Van Roy et al., 2015; Paterson et al., 2016; Lerosey-Aubril et al., 2018; Fu et al., 2019; Saleh et al., 2020a). Even within the famous Cambrian Burgess Shale-type (BST) deposits, including the iconic Burgess Shale of Canada and Chengjiang Biota of China, where preservation of soft tissues and lightly sclerotized taxa occur, small euarthropod specimens are an exception and fossils are biased towards later developmental stages and adults, except for the recently discovered Haiyan locality (Yang et al., 2021). Correspondingly, larval or juvenile stages have been described for only a handful of species (e.g., García-Bellido and Collins, 2006; Haug et al., 2013; Fu et al., 2014; Liu et al., 2014; Liu et al., 2016; Fu et al., 2018; Liu et al., 2018; Zhai et al., 2019).

Contrary to BST deposits, Orsten-type (OT) deposits preserve secondarily phosphatized body envelopes of tiny stages of various euarthropods but do not contain samples larger than 2 mm (Maas et al., 2006). OT deposits are thus biased toward small species or early developmental stages, whilst adults are generally absent (Maas et al., 2006). Opposing biases in BST and OT deposits mean that two extreme scenarios exist in the fossil record. Some sites provide extensive data on euarthropod adult morphology, with only limited information on their early developmental stages. In other sites, early developmental stages are exquisitely preserved, but no adults are found. Preservational inconsistencies such as this hamper our understanding of the biology, phylogeny, and development of extinct euarthropods.

Bridging these two extremes, rare Konservat-Lagerstätten contain both early and late developmental stages, as is the case for Haiyan (Yang et al., 2021) and the Fezouata Shale Lagerstätte (Van Roy et al., 2010; Saleh et al., 2021b). Recent discoveries from this Lower Ordovician formation in Morocco have revealed numerous early developmental stages of several euarthropods, such as marrellids (herein), xiphosurans (Lustri and Laibl, personal observation 2018–2023) and trilobites (Laibl et al., in press), in addition to other metazoans (Saleh et al., 2018). The Fezouata Shale therefore appears pivotal to partially fill the gap in knowledge of Paleozoic euarthropod development. In this contribution, we describe exquisitely preserved minute early post-embryonic stages of a formally undescribed marrellid euarthropod from the Fezouata Shale.

Marrellids are exclusively Paleozoic euarthropods whose name derives from *Marrella splendens*, a rather small (up to 25 mm long) but extremely abundant taxon in the Burgess Shale (Whittington, 1971; García-Bellido and Collins, 2006). Marrellids are characterized by a prominent cephalic shield with two or three pairs of primary spines, a pair of uniramous antennulae, and one or two pairs of cephalic appendages (Whittington, 1971; García-Bellido and Collins, 2006; Kühl and Rust, 2010; Rak et al., 2013; Aris et al., 2017; Moysiuk et al., 2022). Their trunk is composed of numerous cylindrical segments, each associated with a pair of biramous appendages (Whittington, 1971; Stürmer and Bergström, 1976; García-Bellido and Collins, 2006; Kühl and Rust, 2010). Trunk appendages are composed of a six-podomere endopod and a multi-annulated exopod with associated lamellae (García-Bellido and Collins, 2006; Haug et al., 2013). The group is known from Cambrian strata of Canada (Whittington, 1971), China (Zhao et al., 2003; Liu, 2013) and Australia (Haug et al., 2013); and from Ordovician strata of Czechia (Chlupáč, 1999), Morocco (Van Roy et al., 2010), Argentina (Aris et al., 2017), Canada (Moysiuk et al., 2022) and the UK (Legg, 2016); as well as from Devonian strata of Germany (Kühl and Rust, 2010).

While rare minute stages of marrellids have been described earlier, they generally do not show any details of the appendages (García-Bellido and Collins, 2006; Kühl and Rust, 2010) or are

represented by a single isolated appendage fragment (Haug et al., 2013). The early developmental stages of the Fezouata marrellid described herein show exquisitely preserved appendages, revealed using synchrotron X-ray microtomography. Immature stages of the Fezouata marrellid have a lower number of trunk segments and a slightly different morphology of the cephalic shield when compared to adults of the same species. However, immature and adult stages share many similarities in the appendage differentiation and similar morphology of individual appendage pairs, suggesting that these developmental stages shared the same locomotion and food processing method. We further discuss the development of Marrellida and its ecological and evolutionary significance.

2 Material and methods

2.1 Geologic, stratigraphic, and environmental context

The Lower Ordovician Fezouata Shale crops out in many sites of southeastern Morocco (Martin et al., 2016a; Lefebvre et al., 2018). In the Ternata plain, north of Zagora, this formation reaches a thickness between 900 and 1000 m (Vaucher et al., 2016) and is formed of blue-green to yellow-green mudstones and siltstones (Destombes et al., 1985; Vaucher et al., 2016). It was deposited in a shallow sea dominated by storms and modulated by tides in very high latitudes of the southern hemisphere (Martin et al., 2016a; Vaucher et al., 2017; Cocks and Torsvik, 2021). Its biota encompasses numerous taxa (at least 183 genera; Van Roy et al., 2015; Saleh et al., 2020a; Saleh et al., 2021b), including a considerable diversity of non-mineralized, sclerotized, or cuticularized organisms (Saleh et al., 2020a; Saleh et al., 2021b), and abundant euarthropods (Van Roy et al., 2010; Van Roy et al., 2015; Martin et al., 2016b; Ortega-Hernández et al., 2016; Pérez-Peris et al., 2021a; Potin and Daley, 2023; Potin et al., 2023).

The soft-bodied preservation is known from three stratigraphic intervals within the succession (Lefebvre et al., 2018; Saleh et al., 2022); the lower interval belongs to the *Sagenograptus murrayi* graptolite biozone (Tremadocian; Lefebvre et al., 2018; Figure 1A), the middle one is in the ?*Baltograptus jacksoni* biozone (Floian; Lefebvre et al., 2018) and the upper interval approximately belongs to the *Baltograptus minutus* biozone–'*Azygograptus* interval' (upper Floian, Saleh et al., 2022). Mineralized animals (e.g., trilobites, brachiopods, bivalves) colonized a large part of the proximal–distal axis of the environment (i.e., from around the fair-weather base (FWB) to below the storm-weather base (SWB); Saleh et al., 2018; Saleh et al., 2021a; Saleh et al., 2021c) and are distributed discontinuously throughout the entire succession (Saleh et al., 2021c). On the other hand, soft-bodied preservation occurs mainly *in situ* in the lower and middle intervals, predominantly in one facies, deposited right under the SWB (Figure 1B), although sclerotized organisms may occur on some occasions in more proximal settings (Saleh et al., 2020d). The depositional setting of the Fezouata Shale is corroborated by normally graded, storm-

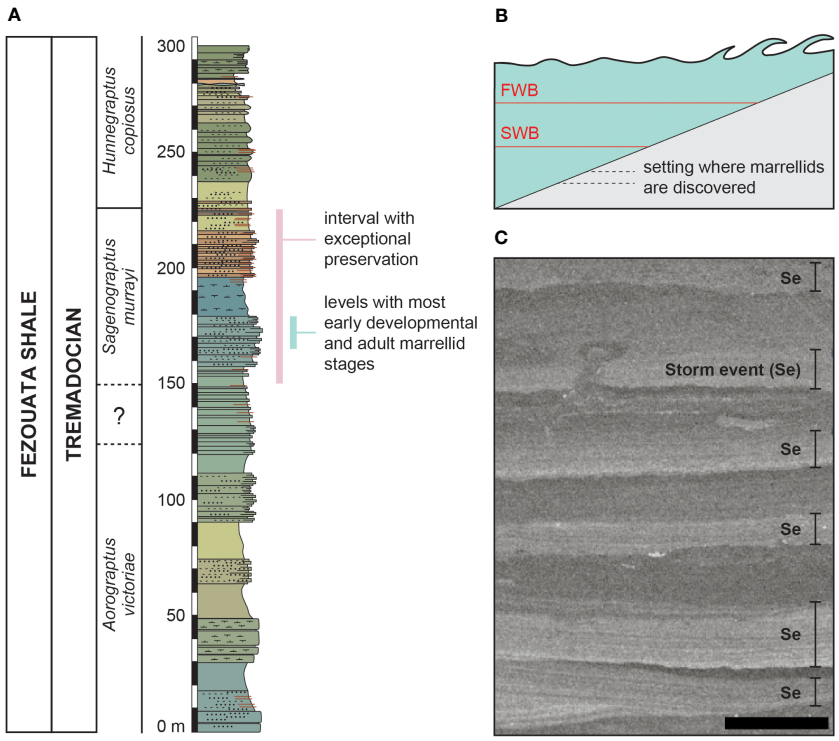

FIGURE 1
Stratigraphic **(A)** and environmental **(B)** settings of the Tremadocian levels of Fezouata Shale with a particular focus on the levels with exceptional preservation. The drill core section **(C)** shows repeated storm events within the *Sagenograptus murrayi* Zone. Scale bar in C represents 1 cm. FWB, fair wave base; SWB, storm wave base.

induced deposits covering organisms (Figure 1C), and most of the exceptional fossil preservation occurs under rather than within these beds (Saleh et al., 2020d). These soft-bodied taxa were often originally preserved in minute details (Van Roy et al., 2015; Saleh et al., 2019) as carbonaceous compressions with authigenic minerals such as pyrite (Saleh et al., 2020c; Saleh et al., 2020d). However, most of the pyrite was oxidized into iron oxides and oxyhydroxides (Saleh et al., 2020b; Saleh et al., 2020d; Potin et al., 2023), and the carbonaceous remains were leached by processes of modern weathering, such as precipitation.

The majority of marrellid specimens studied herein were collected from the facies deposited right below the SWB from the lower interval with exceptional preservation and are Tremadocian in age (Figure 1A). The immature and adult marrellids co-occur in the same excavation sites/collection pits, or come from localities separated by tens of meters on the same hill in nearly equivalent levels with similar lithology and facies.

2.2 Material and institutional repositories

In total, 16 immature specimens of the Fezouata marrellid were studied. Three adult specimens were studied for comparative purposes and are also figured. The studied material is housed and accessioned in public collections, namely in the Muséum cantonal des sciences naturelles, Département de géologie, Lausanne, Switzerland (MGL, 16 specimens) and in the Yale Peabody Museum of Natural History, New Haven, CT, USA (YPM, 3 specimens). All material of Fezouata marrellid used in this study was collected by authorized and academically recognized avocational Moroccan collector Mohamed Ben Moula and his family from 2015 to 2016 (MGL collection), and between 2009 and 2014 (YPM collection); two of the authors (AD and LuL) and Peter Van Roy worked in collaboration with them to produce the metadata associated with the collected fossils.

Mohamed Ben Moula has a long-standing working relationship with several academics, has received the Mary Anning Award from the Palaeontological Association in 2017, and has a radiodont fossil (*Aegirocassis benmoulai*) named after him in honor of his great contribution to the field of paleontology. The MGL fossil collection was purchased with funds from the University of Lausanne and the Swiss National Science Foundation, following all regulations for purchases. The fossil collection was transported to Casablanca and subjected to export approval by the Ministry of Energy, Mines, and the Environment of the federal government of the Kingdom of Morocco and approved for shipment to Switzerland on 11.05.2017 (export permits curated with the collection). Fossils were shipped by sea and land to the University of Lausanne, where they are curated as part of the collection of the Muséum cantonal des sciences naturelles, Département de géologie. The collections of the Yale Peabody Museum of Natural History were obtained both through direct collection of specimens by Peter Van Roy during fieldwork, and through purchase using dedicated museum funds for the acquisition of scientific collections. Export permits were obtained through the Moroccan Ministry of Energy, Mines, and the Environment, with specimens being transported from Casablanca by sea. For the list of studied immature specimens with details of their preservation and locality data see Supplementary data.

2.3 Taxonomic remarks

The specimens studied herein belong to a marrellid marrellomorph provisionally described by Van Roy (2006) as a new species, *Furca mauretanica (nomen nudum)*. Subsequent papers to figure specimens of the Fezouata marrellid (Van Roy et al., 2010; Van Roy et al., 2015; Lefebvre et al., 2016; Martin et al., 2016a; Vaucher et al., 2016; Saleh et al., 2021a) continued to refer to the species either as *Furca* sp., or as a marrellomorph arthropod, probably belonging to the genus *Furca*, yet these fossils have not been formally described. A formal taxonomic description and naming of the Fezouata marrellid falls outside the scope of this paper, which focuses on its ontogeny, and particularly the morphology of its early developmental stages, and will no doubt be addressed independently of this work. As such, we refer to the species throughout this work as the 'Fezouata marrellid'.

2.4 Preparation and documentation of material

Specimens were mechanically prepared with a Micro-Jack 4 pneumatic air scribe equipped with a pointed stylus. Photographs were taken using a digital camera Canon EOS 800D coupled with a Canon MP-E 65-mm 1:2.8 1-5X macro lens. A polarizing filter was attached to the lens and the light source to reduce reflections and enhance the contrast between the rock and the specimen. To further increase the contrast, all specimens were immersed in diluted ethanol. The images were subsequently processed in Adobe Lightroom 4.3, to enrich brightness, contrast, shadows, highlights, colors, and saturation. Line drawings as well as all reconstructions and diagrams were made in Adobe Illustrator 25.3.1.

The immature specimens were measured using the optical image analyzer TpsDig2 2.31 (Rohlf, 2006). Eight dimensions of the immature specimens were measured, namely the maximal length and width of the cephalic shield (both including and excluding the cephalic spines), the lengths of the anterolateral, mediolateral, and posterolateral cephalic spines, and the observed length of the trunk (see Supplementary data). The measured length and width of the cephalic shield (excl. spines) of 15 specimens were plotted on bivariate plots (Figure 2) using PAST 4.02 (Hammer et al., 2001).

2.5 Synchrotron imaging

The ventrally projected anatomical features such as the hypostome and appendages are rarely exposed on the surface of the fossil samples. For that reason, one specimen (MGL 102399) was imaged using synchrotron X-ray microtomography at the X02DA TOMCAT beamline of the Swiss Light Source, Paul Scherrer Institut, Villigen, Switzerland. Acquisitions were

10.3389/fevo.2023.1232612

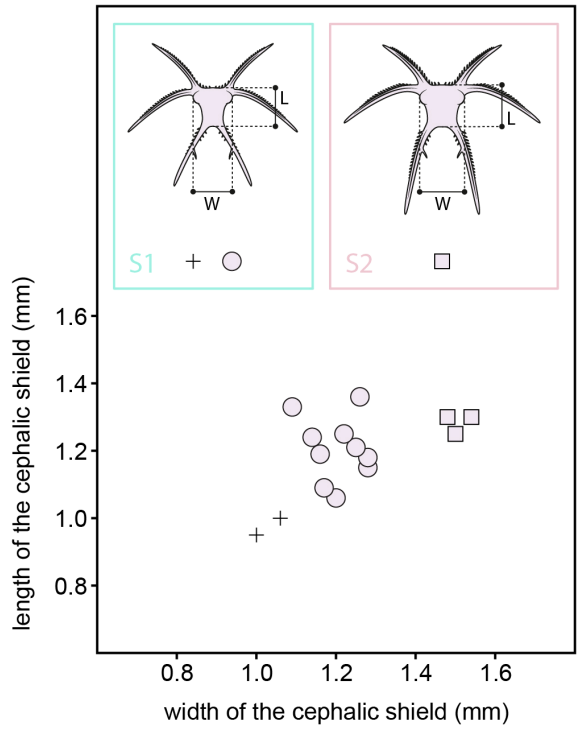

FIGURE 2
Cephalic shield width vs. length plot of the early developmental stages of Fezouata marrellid. L, cephalic shield length; S1-2 early developmental stages 1 and 2; W, cephalic shield width.

performed using a monochromatic beam of 38 keV, a single propagation distance of 250 mm, a 100 µm LuAg : Ce scintillator, and a 4× objective, yielding reconstructed tomographic data with a voxel size of 1.75 µm. 1501 projections were recorded over 180° with exposure of 1000 ms. Reconstruction was performed on a 60-core Linux PC farm using a Fourier transform routine and a regrinding procedure (Marone et al., 2010). Manual segmentation using level tracing and three-dimensional rendering were performed using 3D Slicer (https://www.slicer.org/). A selection of tomograms, as well as sum intensity projections of several (30 to 110) tomograms processed using ImageJ, are presented in Figure 3.

3 Results

3.1 Description of the early developmental stages of the Fezouata marrellid

Plotted dimensions of the cephalic shields (excluding spines) of the 15 smallest measured immature specimens reveal three separate clusters (Figure 2). The cluster with the smallest specimens contains only two samples, 1.00 mm and 1.06 mm wide, and 0.95 mm and 1.00 mm long, respectively. The middle cluster contains ten specimens that range from 1.16 mm to 1.28 mm in width, and from 1.06 mm to 1.36 mm in length. The last cluster is composed of three individuals that range from 1.48 mm to 1.54 mm in width and 1.25 mm to 1.30 mm in length. The smallest and middle cluster individuals share cephalic shields that are morphologically indistinguishable from each other. In contrast, the cephalic shield of the largest cluster individuals differs from that of the smaller individuals in several aspects (see below). For that reason, we interpret the smallest and middle cluster individuals as belonging to early developmental stage 1 (S1), and the largest cluster individuals as belonging to the early developmental stage 2 (S2). This numbering only refers to observed early developmental stages and does not implie that the stages smaller than S1 were not present in the ontogeny of Fezouata marrellid.

The S1 cephalic shields are 3.8–4.6 mm long and 4.8–5.1 mm wide, including the cephalic spines. The shield is sub-trapezoidal in outline, narrowing posteriorly (Figures 4A, B). Three pairs of long cephalic spines project from the cephalic shield (*als*, *mls* and *pls* in Figure 4A). The anterolateral spines (*als*) are gently curved, 1.28–2.05 mm long, and diverge forward at an angle about 70° near their base. The mediolateral spines (*mls*) are the longest spine pair in these early stages, with a total length of 1.88–2.35 mm. They are directed laterally and slightly posteriorly, each diverging from the transversal axis about 10–15° in their proximal parts and curving slightly backwards. The anterior margin of the cephalic shield, anterolateral, mediolateral, and posterolateral spines bear numerous small secondary spines (*ss* in Figures 3A, 4B) developed along their anterior (or outer) margins. In addition, the posterolateral spines bear one elongated secondary spine (*ess* in Figure 3A), developed on the inner edge approximately at the midpoint of the primary spine. There is a distinct bulge near the posterior base of the mediolateral spines on both sides of the cephalic shield (*eb* in Figures 4A, B); these bulges are interpreted as a dorsal exoskeletal protrusion that might accommodate ventrally-situated eyes. The posterolateral spines (*pls*) are straight, 2.07–2.40 mm long, and diverge posteriorly at an angle of 50–60°.

The S2 cephalic shields are 4.5–5.3 mm long and 4.6–5.6 mm wide, including spines. Morphologically, the S2 cephalic shields are similar to those of the S1. The major difference between them is the morphology of the posterolateral cephalic spines (cf. Figures 4, 5). These spines are proportionally the longest spine pair in the S2 (Figures 5A, C), and diverge at an angle of about 35–40°. The secondary spines are developed both on the outer and inner edges of the posterior spines. The enlarged secondary spine is located on the inner edge, ca. one-third of the distance from the posterolateral spine base (Figure 5B).

The hypostome of early developmental stages is developed ventrally from the cephalic shield (*hy* in Figures 3A, F, G). It is a prominent elongated structure, generally ovoid in outline, covers most of the ventral part of the cephalic shield, and posteriorly reaches to the final cephalic appendages.

The first pair of cephalic appendages are in the form of uniramous antennulae (*an* in Figure 3A). They are elongated (ca. 1.5 mm long in the smallest recorded specimen) and circular in cross-section. Each antennula is composed of numerous short articles (Figure 3G). Although these are not always easily discernible, it seems that the proximal and distal parts are composed of proportionally longer articles than the middle part of the antennula, which is composed of rather short articles (cf. arrowheads in Figure 3G), though this might also be caused by the orientation of the antennula in sediment. The antennulae insert into the cephalon laterally from the hypostome

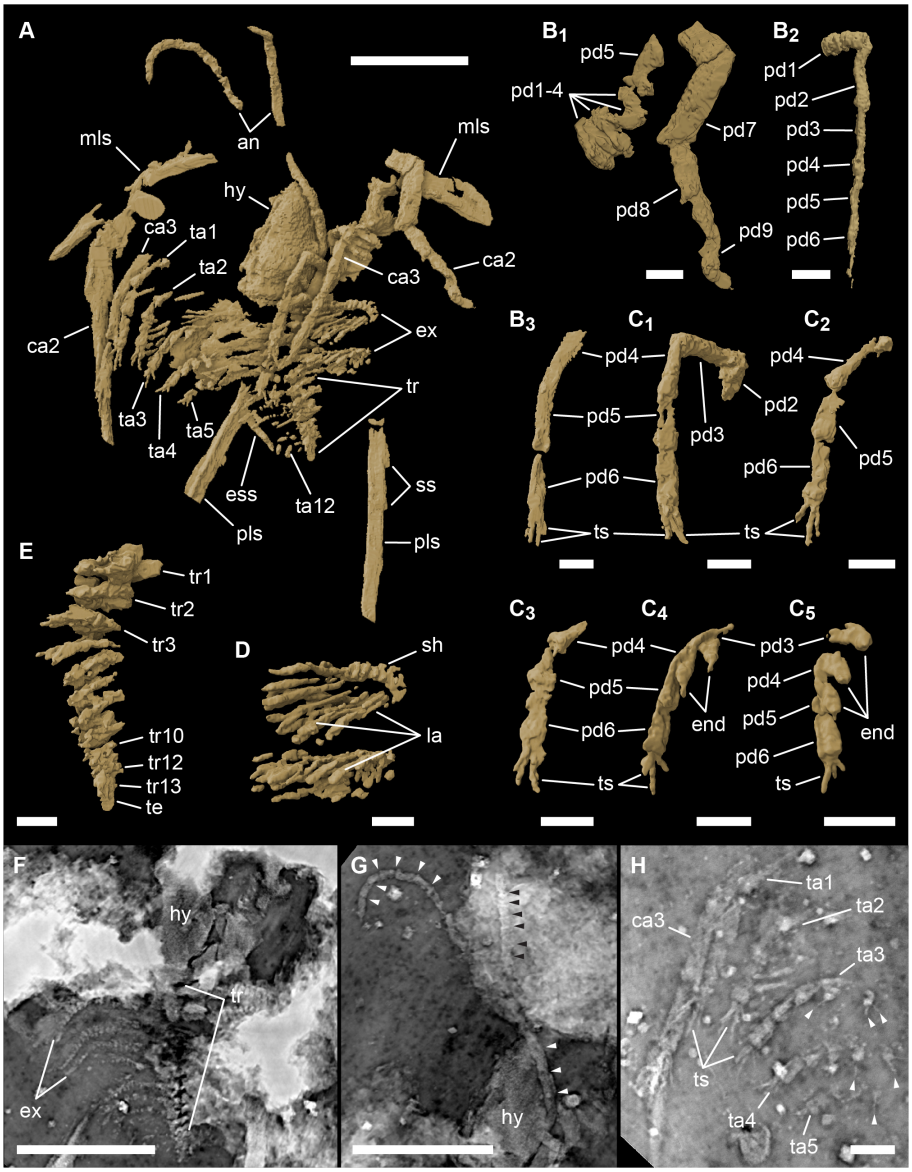

FIGURE 3
3D rendering of the early developmental stage (S1) of Fezouata marrellid based on synchrotron X-ray tomography, Fezouata Shale, Lower Ordovician, Morocco. **(A)** oblique ventral 3D rendering of the entire specimen no. MGL 102399. **(B)** details of cephalic appendages: **(B_1)** second cephalic appendage; **(B_2)** third left cephalic appendage; **(B_3)** third right cephalic appendage. **(C)** details of trunk appendages: **(C_1)** first left trunk appendage; **(C_2)** first right trunk appendage; **(C_3)** second right trunk appendage; **(C_4)** third right trunk appendage; **(C_5)** fourth right trunk appendage. **(D)** detail of the trunk exopods. **(E)** detail of trunk segments. **(F–H)** sum intensity projections of 30 tomograms through the trunk **(F)** 75 tomograms through the antennulae **(G)**, and 110 tomograms through right appendages **(H)**. Scale bars represent 500 µm in **(A)**, **(F)**, and **(G)**, and 100 µm in **(B–E)** and **(H)**. an, antennula; ca2–ca3, cephalic appendage 2 and 3; end, endites; ess, enlarged secondary spine; ex, exopods; hy, hypostome; la, lamellae; mls, mediolateral spine; pd1–pd9, podomere 1 to 9; pls, posterolateral spine; sh, shaft; ss, secondary spines; ta1–ta12, trunk appendage 1 to 12; te, terminal piece; tr, trunk; tr1–tr13, trunk segments 1 to 13; ts, terminal spines. Arrows in G point to article boundaries, in H to setae.

(Figures 3A, G), posterior to the base of the mediolateral spine, that is, in the area that would be behind the eye bulge, implying their deutocerebral origin.

The second cephalic appendage is robust, uniramous, and seemingly homologous to the second cephalic appendage of *Marrella*, *Mimetaster*, and *Tomlinsonus* based on its similar morphology and topological position (cf., García-Bellido and Collins, 2006; Kühl and Rust, 2010; Moysiuk et al., 2022). This appendage is the longest one (total length 2.3 mm in specimen MGL 102143, Figure 4C) and consists of nine podomeres (*pd1–9* in Figure 3B$_1$). The four most proximal podomeres are stout, short, and densely packed, resembling their homologs in *Mimetaster* and *Tomlinsonus* (cf., Stürmer and Bergström, 1976; Moysiuk et al., 2022). Podomere five is comparatively long (about 0.4 mm long in specimen MGL 102143), with the width being about 45% of the podomere length. Podomeres six and seven are medium-sized (about 0.3 mm long in specimen MGL 102143), their width/length proportions being 35–45%. Both the sixth and seventh podomeres are narrowest proximally and gently widen distally. Podomere eight is the longest one (0.45 mm long in specimen MGL

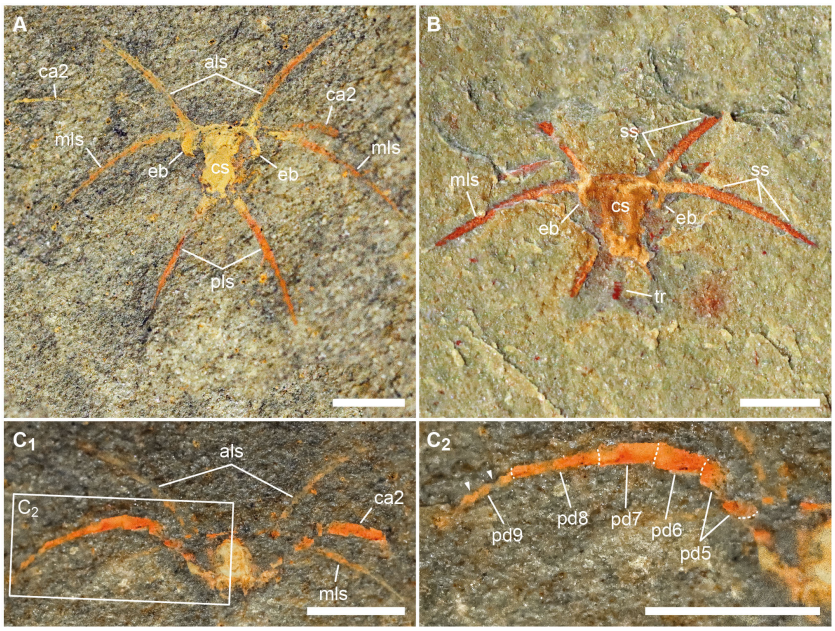

FIGURE 4
Early developmental stages (S1) of Fezouata marrellid, Fezouata Shale, Lower Ordovician, Morocco. **(A)** specimen no. MGL 102141; **(B)** specimen no. MGL 102188; **(C_1)** specimen no. MGL 102143; **(C_2)** detail of second cephalic appendage in the specimen no. MGL 102143. Scale bars represent 1 mm. als, anterolateral spines; ca2, cephalic appendage 2; cs, cephalic shield; eb, eye bulge; mls, mediolateral spine; pd5–pd9, podomere 5 to 9; pls, posterolateral spine; ss, secondary spines; tr, trunk.

102143) and is shaped like a long, slender cylinder (width being only 15% of its length). The nature of the last podomere is somewhat obscured, and it is not clear if it is composed of one segment (as in *Marrella* and *Tomlinsonus*, cf., Whittington, 1971; Moysiuk et al., 2022) or tarsus-like annuli (as in *Mimetaster*, cf., Stürmer and Bergström, 1976; Kühl and Rust, 2010). Both the synchrotron data and the microscopic observation of exposed specimens are ambiguous in this respect, although the contraction in specimen MGL 102143 (arrowheads in Figure $4C_2$) and the slightly flexed tip in specimen MGL 102399 (Figure $3B_1$) favor the latter morphology.

The third cephalic appendage is long, slender, and composed of six elongated cylindrical podomeres (Figures $3B_2$, $_3$), with their width/length proportions being about 25–30%. The individual podomeres are of similar lengths, with only the most proximal and two distal-most podomeres being slightly shorter than the rest. This appendage terminates with four rather long, tightly-packed terminal spines (*ts* in Figures $3B_3$, H). The third cephalic appendage inserts just posteriorly to the second one and bears no exopod.

The trunk projects from under the cephalic shield between the posterolateral spines (Figures 3A, 5A, B). In both S1 and S2, the entire length of the trunk never exceeds the length of the posterolateral spines. The length of the trunk is about 0.6 mm in the S1, while in the S2 the trunk ranges between 1.14–1.37 mm. In the S1, the trunk reaches up to the enlarged secondary spine of the posterolateral spines and is composed of 13 segments and a terminal piece (*te* in Figure 3E). The trunk segments are cylindrical, wider transversely than sagittally, each bearing one pair of post-cephalic appendages. In the S2, the number of segments in the trunk is unknown.

The trunk appendages (*ta* in Figure 3A) are biramous and consistent in general morphology. The endopods of trunk appendages 1 and 2 are each composed of six elongated cylindrical podomeres (the proximal ones are poorly preserved) with their width/length proportions being 25–40% (Figures $3C_1$, $_3$). The individual podomeres are of similar length, with podomeres five and six being just slightly shorter than podomeres two to four. The distal tips of the endopods each bear four tightly-packed terminal spines (*ts* in Figures $3C_1$, $_3$, H). The exopod is composed of the central shaft (*sh* in Figure 3D) and comparatively long lamellar setae (*la* in Figure 3D), similar to those in *Austromarrella* (Haug et al., 2013).

From the third trunk appendage posteriorly, endopod morphology changes considerably. The podomeres are short (width to length ratio of around 80%) and at least podomeres two to five bear stout sub-triangular endites (*end* in Figures $3C_4$, $_5$). These endites are sharp and project from the endopod medioventrally. The endites are nearly as long as the diameter of the corresponding podomere and some appear to bear delicate setae (arrowheads in Figure 3H). Podomere six lacks the endite and bears four terminal spines on its distal tip (*ts* in Figures $3C_4$, $_5$, H). The endopods of appendage that is posterior to trunk appendage 6 are poorly preserved in specimen MGL 102399, but they diminish in size rapidly, resulting in the minute size of the thirteenth trunk appendage (Figure 3A).

3.2 Description of adults of the Fezouata marrellid

Despite lacking a formal description, the Fezouata marrellid was identified and preliminarily described by Peter Van Roy in his Ph.D.

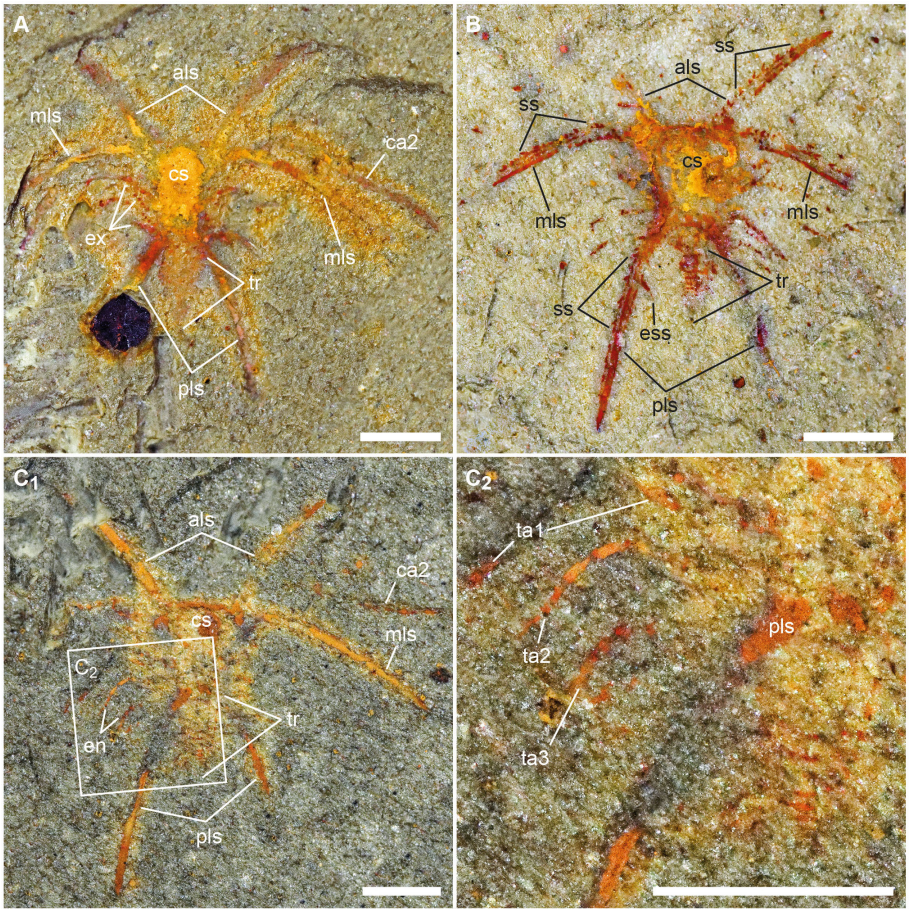

FIGURE 5
Early developmental stages (S2) of Fezouata marrellid, Fezouata Shale, Lower Ordovician, Morocco. **(A)** specimen no. MGL 102187; **(B)** specimen no. MGL 102382; **(C_1)** specimen no. MGL 102140; **(C_2)** detail of the specimen no. MGL 102140. Scale bars represent 1 mm. als, anterolateral spines; ca2, cephalic appendage 2; cs, cephalic shield; en, endopods; ess, enlarged secondary spine; ex, exopods; mls, mediolateral spine; pls, posterolateral spine; ss, secondary spines; ta1–ta3, trunk appendage 1 to 3; tr, trunk.

thesis as *Furca mauretanica* (*nomen nudum*). The adults of this species have been figured in numerous papers (Van Roy et al., 2010; Van Roy et al., 2015; Lefebvre et al., 2016; Martin et al., 2016a; Vaucher et al., 2016; Saleh et al., 2020a; Saleh et al., 2020d; Saleh et al., 2021b; Drage et al., 2023). Sufficient data exist on the adult specimens to allow for a comparison with the immature material, which is the focus of this study. We therefore describe the adult specimens only briefly, and where appropriate refer to already published figures. In addition, we figure three adult specimens to illustrate the morphological characters discussed and to allow for direct comparison to the immature material.

The adult stages of the Fezouata marrellid have an elongated subtrapezoidal cephalic shield, which bears three pairs of cephalic spines (*als*, *mls*, and *pls* in Figures $6A_1$, B_1). The size of the adult cephalic shield exceeds 5 mm in width and 6 mm in length (excluding spines). The anterolateral cephalic spines project from the anterolateral corners of the cephalic shield and are strongly curved out and backwards. The mediolateral cephalic spines are positioned just posteriorly from the bases of the anterolateral spine pair. They run sub-laterally initially and then curve backwards. The eye bulge is developed near the posterior base of the mediolateral spine, on both sides of the cephalic shield (*eb* in Figure $6A_1$). The posterolateral spines project from the posterior margin of the cephalic shield, point posteriorly and can vary from nearly straight to curved towards the medial axis. All pairs of cephalic spines bear comparatively long falcate secondary spines (*ss* in Figure $6A_1$) that are developed on both the external and internal edges of the primary spines. There is no evidence of an enlarged secondary spine on the inner edge of the posterolateral spines.

The first pair of appendages comprise uniramous antennulae (*an* in Figures $6A_1$, B_1) that are comparatively long and composed of short cylindrical podomeres. The second cephalic appendage is robust, composed of long cylindrical podomeres similar in structure to the second cephalic appendage of early developmental stages (Figure $6B_2$, see also Martin et al., 2016a, Figure 3C). The third cephalic appendage is composed of very long cylindrical podomeres (Figure $6B_3$)

The trunk is composed of cylindrical segments that progressively diminish in size posteriorly (Figure $6B_4$). The total number of trunk segments is over 22 (Figures $6A_1$, B_4). Each trunk segment bears one pair of biramous appendages. The endopods of anterior trunk appendages (at least up to the fourth trunk

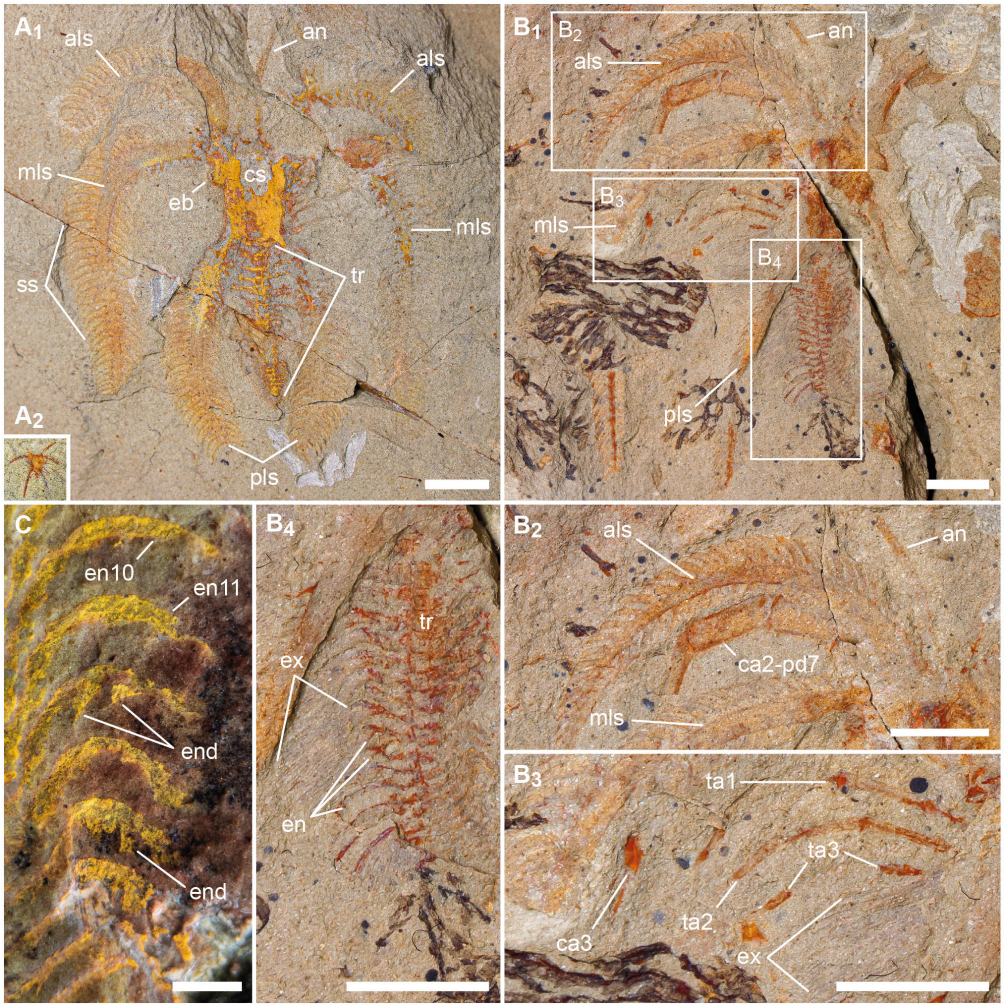

FIGURE 6
Adult and early developmental stages of Fezouata marrellid, Fezouata Shale, Lower Ordovician, Morocco. **(A_1)** adult specimen no. MGL 102397; **(A_2)** immature specimen (S2) no. MGL 102382 in the same scale as **(A_1)**; **(B_1)** adult specimen no. MGL 102390; **(B_2)** detail of the second cephalic appendage of the specimen no. MGL 102390; **(B_3)** detail of trunk appendages of the specimen no. MGL 102390; **(B_4)** detail of the trunk of the specimen no. MGL 102390; **(C)** detail of the trunk endopods of the adult specimen no. MGL 102392. Scale bars represent 1 cm in A and B, and 1 mm in C. als, anterolateral spines; an, antennula; ca2–ca3, cephalic appendage 2 and 3; cs, cephalic shield; eb, eye bulge; en, endopods; en10–11, endopods 10 and 11; end, endites; ex, exopods; mls, mediolateral spine; pd7, podomere 7; pls, posterolateral spine; ss, secondary spines; ta1–ta3, trunk appendage 1 to 3; tr, trunk.

appendage pair) are composed of long cylindrical podomeres, with a width-to-length ratio of about 20%, and lacking endites (Figure $6B_3$). The posterior trunk endopods are usually preserved in a curved position. They have comparatively short podomeres (width/length of 50–60%) with pointed endites (Figure 6C). The exopods are composed of a slender shaft and bear long lamellar setae all along the trunk (Figure $6B_4$).

4 Discussion

4.1 Developmental stage assignment and comparisons

All immature specimens described and figured herein are considered to represent early post-embryonic stages of the undescribed marrellid from the Fezouata Shale. This assignment is based on three lines of evidence. Firstly, the overall morphology of early developmental stage (S1 and S2) and adult cephalic shields is very similar, both bearing three pairs of spines projecting anterolaterally, laterally, and posteriorly fringed with secondary spines, and both with prominent eye bulges on the cephalic shield. Secondly, both early developmental and adult stages have similar appendage differentiation, subdivided from the anterior to the posterior part into antennula, a robust second cephalic appendage, a third cephalic appendage, and a series of biramous trunk appendages of similar composition (see Section 3). Finally, early developmental and adult individuals co-occur in the same stratigraphic levels and facies (Figure 1A), and generally within the same fossiliferous localities in the Fezouata Shale.

The minute size of immature individuals suggests that they represent comparatively early developmental stages; with their

whole-body length (excluding spines) ranging between 1.6–2.6 mm (= cephalic shiled + trunk lengths) they are about ten times smaller than the average adult specimens (Figures 6A$_1$, $_2$). The size of the early developmental stages of Fezouata marrellid is comparable to the size of the larval stage of *Leanchoilia illecebrosa* (length ca. 2 mm) from the Cambrian Series 2 Chiungchussu Formation of China (Liu et al., 2016), and with larvae of *Misszhouia*, *Leanchoilia*, and *Isoxys* (2.5–3.8 mm) recently reported by Yang et al. (2021) from the same formation. A similar length (2.4 mm) was also reported for the smallest stages of *Marrella splendens* from the Miaolingian Burgess Shale of Canada (García-Bellido and Collins, 2006; Haug et al., 2013, Figure 3E therein). The size of immature Fezouata marrellids is also comparable to early meraspid stages of various early-diverging Cambrian trilobites (e.g., Dai and Zhang, 2013; Hou et al., 2017; Laibl et al., 2021). Further, the sizes of the early developmental Fezouata marrellid specimens are similar to some Recent marine euarthropods such as the lecithotrophic metanauplii of remipedes (Koenemann et al., 2007), the juvenile stages of cephalocarids (Sanders and Hessler, 1964), the furciliae of euphausiaceans (Mauchline, 1971), and some decapod protozoeae and zoeae (Anger, 2006).

The smallest specimen of the Fezouata marrellid possesses about 13 trunk segments, which would equate to 17 segments plus a terminal piece in total, assuming a four-segmented head. In terms of segmentation, this specimen thereby likely represents an earlier developmental stage than the smallest known specimens of other marrellids, such as *Mimetaster hexagonalis* (the smallest known specimen has about 19 trunk segments, Kühl and Rust, 2010) and *M. splendens* (the smallest known specimen has 17 trunk segments, García-Bellido and Collins, 2006; a similar number is plausible for the specimen in Haug et al., 2013, Figure 3E). By the total number of appendages (16 pairs of appendages, derived from 3 cephalic pairs plus 13 trunk pairs), the immature Fezouata marrellid is also comparable to the larva of *L. illecebrosa* with 14 pairs of appendages. Additionally, the appendages posterior to the fourth appendage pair in the larva of *L. illecebrosa* have the form of tiny buds (cf., Liu et al., 2016, Figure 4), while in the smallest known specimen of the Fezouata marrellid twelve pairs of anterior appendages are already well developed (Figure 3).

The size and number of segments in the smallest individuals of the Fezouata marrellid suggest they do not represent the earliest post-embryonic developmental stages of the species. However, it is possible that the Fezouata marrellid produced large eggs, like Recent xiphosurans (Shuster and Sekiguchi, 2003) or some anomuran decapods (Lovrich and Vinuesa, 1999), and the immature stages hatched into reasonably advanced forms (i.e., abbreviated development, cf. Rabalais and Gore, 1985). It is equally possible that the Fezouata marrellid hatched into earlier post-embryonic stages than presented here, but that their minute dimensions and fragile exoskeletons might prevent their fossilization. The absence of earlier developmental stages might also result from a collection bias, due to their incredibly small sizes. Similarly, the intermediate developmental stages (i.e., larger than S2 but smaller than adults) with cephalic shield lengths from 1.3 mm to 6 mm are rare in both the MGL (one specimen recorded) and YPM collections (two specimens recorded). Their rarity means that these intermediate stages do not seem to co-occur with adults and early developmental stages (S1 and S2). On the contrary, early post-embryonic stages (S1 and S2) and adults frequently co-occur at the same levels. This latter co-occurrence might be explained by seasonal breeding, and so early developmental stages (S1 and S2) could represent one brood, that lived alongside adults from previous seasons. This might explain why adults and early developmental stages (S1 and S2) are found in association, but without the intermediate stages, though it doesn't explain why the intermediate size juveniles are generally rarer in the Fezouata Shale.

From a terminological perspective, the immature individuals of the Fezouata marrellid can be characterized as morpho-larva s.l. *sensu* Haug (2020), as they show morphological differences in the cephalic shield and the number of trunk segments compared to the adults. The immature individuals, however, do not seem to significantly differ in their ecological niches from the adults (see Section 4.4). As such, they do not fulfill the criteria to be characterized as eco-larva (*sensu* Haug, 2020).

4.2 Morphological comparison of early developmental and adult stages

Despite the numerous similarities between the early developmental and adult stages of Fezouata marrellids, there are several, generally minor, differences (cf., Figures 6–8). The anterolateral and mediolateral cephalic spines are strongly curved in adult specimens, while they are gently curved in juveniles. Such changes in the curvature of primary spines during ontogeny may have been reflected later in marrellid evolution. *Mi. hexagonalis*, for example, has straight primary cephalic spines (Stürmer and Bergström, 1976; Kühl and Rust, 2010) that resemble those of the immature stages of Fezouata marrellid. The derived marrellids such as *Mi. hexagonalis* might have acquired their straight cephalic spines via paedomorphic heterochrony.

The secondary spines in adults of Fezouata marrellid are long and strongly developed along both the inner and outer edges of the primary cephalic spines. In immature stages, these secondary spines are minute, developed only along the outer edges of the anterolateral and mediolateral spines, and each posterolateral spine also bears a single elongated secondary spine on the inner margin. These morphological differences between juveniles and adults indicate an allometric growth of both primary and secondary spines in this species.

The differences in the trunk region are related to the lower number of segments and, consequently, the lower number of trunk appendages in immature individuals. The smallest recorded specimen shows 13 trunk segments, while the adults have over 22 trunk segments. It can therefore be reasonably assumed that the Fezouata marrellid grew by anamorphosis, where segments are added during development. Anamorphic development has been suggested in some other marrellids, such as *M. splendens* (García-Bellido and Collins, 2006) and *Mi. hexagonalis* (Kühl and Rust, 2010), demonstrating this was a common developmental pattern in Marrellida. Moreover, the anamorphic development was likely a plesiomorphic trait in Marrellida, given this type of development

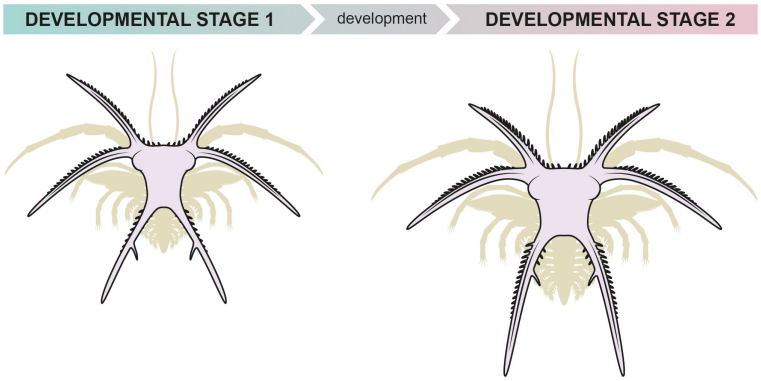

FIGURE 7
Reconstruction of the early developmental stages 1 and 2 of the Fezouata marrellid.

has been suggested to be an ancestral condition for euarthropods (Hughes et al., 2006; Moysiuk and Caron, 2023).

Both early developmental and adult stages share comparatively slender uniramous antennulae, followed by a pair of robust second cephalic appendages and a third pair of cephalic appendages composed of long cylindrical podomeres (Figure 8). The trunk appendages are biramous in both adults and early developmental stages. The exopods have a slender shaft with numerous lamellar setae that differ between the life stages in only their sizes. The immature exopods are also similar to exopods of mature *M. splendens* (Haug et al., 2013, Figure 3). In the early developmental stages of the Fezouata marrellid, the endopods of the two anterior-most trunk appendages are composed of long cylindrical podomeres, while the more posterior ones have short podomeres with pointed endites (Figure 8). The endites of the posterior endopods also bear delicate setae, while these setae are absent in adults. A similar pattern of appendage differentiation is apparent in adult individuals, although the trunk differentiation is shifted posteriorly (Figure 8). Consequently, in adults the endopods of trunk appendages 1 to 4 are composed of long cylindrical podomeres, while the more posterior trunk appendages have short endite-bearing podomeres. This posterior shift of the trunk appendage differentiation also indicates that some endopod podomeres went through profound allometric changes. For

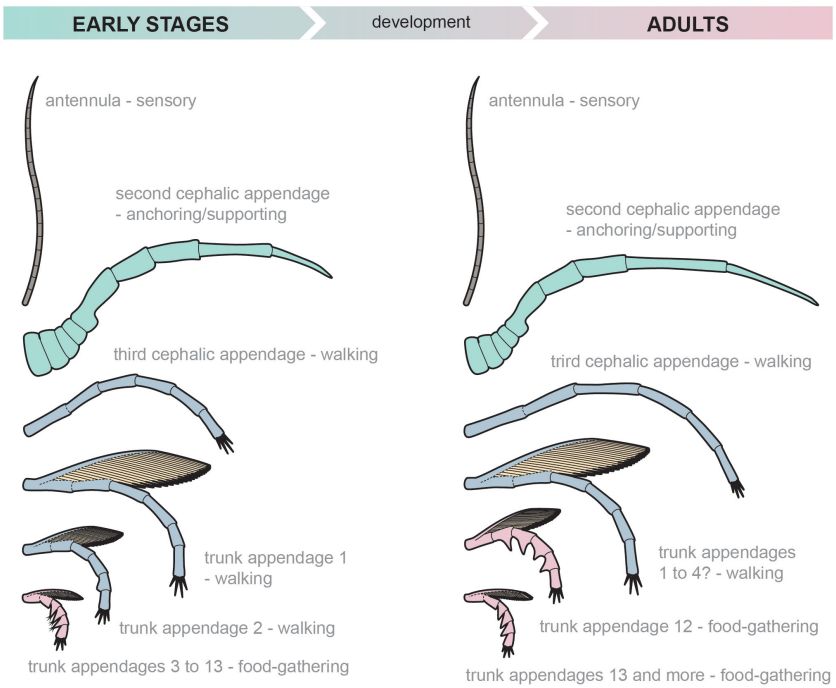

FIGURE 8
Reconstruction of the appendages of early developmental stages and adults of the Fezouata marrelid. Note the virtually identical appendage differentiation, the posterior shift of the trunk appendage differentiation, and the lack of setae in the posterior trunk appendages of adults. Appendages of the early developmental and adult stages are not to scale.

example, the immature endopod of trunk appendage 3 is composed of short endite-bearing podomeres, whereas the homologous endopod in adults is composed of long cylindrical podomeres (Figure 8) meaning the podomeres must have prolonged and lost their endites during development.

4.3 Mode of life of early developmental stages of the Fezouata marrellid

Fezouata marrellids were living in high-latitude seasonal seas along the western margin of Gondwana (Saleh et al., 2019; Cocks and Torsvik, 2021; Laibl et al., in press). Considering the morphological similarity in the cephalic shield and appendages of the Fezouata marrellid with those of other marrellids (Whittington, 1971; García-Bellido and Collins, 2006; Kühl and Rust, 2010), it is very likely that the Fezouata species had a benthic or nektobenthic mode of life as proposed for *Marrella*, *Mimetaster*, *Tomlinsonus*, and *Furca* (Whittington, 1971; Stürmer and Bergström, 1976; Briggs and Whittington, 1985; Conway Morris, 1986; García-Bellido and Collins, 2006; Kühl and Rust, 2010; Rak et al., 2013; Moysiuk et al., 2022). Living close to or on the seafloor, the Fezouata marrellids would have inhabited an offshore environment (Vaucher et al., 2016) with minimal physical disturbance, as evidenced by their deposition below the storm wave base (Saleh et al., 2020a; Saleh et al., 2021b).

The appendages of the immature Fezouata marrellids are morphologically differentiated along the sagittal axis of the body into the antennulae, the second cephalic appendage, the third cephalic appendage, the anterior portion of trunk appendages, and the posterior portion of trunk appendages (Figure 8). The deutocerebral antennulae were likely sensory, as this is their function in many extant mandibulates (Sombke et al., 2012) and as has been suggested for marrellomorphs (Whittington, 1971; Siveter et al., 2007; Kühl and Rust, 2010). However, recent reinvestigation of *M. splendens* suggests they might have been also used in food gathering (J. Haug, personal communication 2021). The second cephalic appendage might have been used for anchoring, or supporting the animal on the seafloor, given its similarity to the second cephalic appendage of *Mi. hexagonalis* and *Tomlinsonus dimitrii*, where it has been interpreted to fulfil this function (cf., Stürmer and Bergström, 1976; Moysiuk et al., 2022). This interpretation is supported by the robust morphology of this appendage, which indicates strong musculature that might have helped to support the cephalic shield and move it above the seafloor. It is unlikely that this appendage was used for swimming, as suggested for *M. splendens* by García-Bellido and Collins (2006), as, in comparison, *M. splendens* has a thinner and paddle-like second cephalic appendage with setose fringes.

The last cephalic appendage pair as well as the first two trunk appendage pairs of the early developmental stages of Fezouata marrellid were most likely used for walking on the seafloor. This function is supported by the rather long tightly packed terminal spines in their distal ends. These spines resemble, to some extent, the processes and apoteles of the horseshoe crab pushing legs (Bicknell et al., 2018) or, even more, spines in the prosomal appendages of *Weinbergina opitzi* (cf., Moore et al., 2005, Figure 6). Such terminal spines in the last cephalic appendage and first trunk appendages of Fezouata marrellid could have pushed the animal over the muddy seafloor in a similar way as in xiphosurans or *Weinbergina*.

The trunk appendages of the Fezouata marrellid show anteroposterior differentiation into two portions, similar to that observed in adult specimens of *M. splendens*. The anterior endopods of the latter species are composed of long cylindrical podomeres whereas the posterior endopod podomeres are short and bear prominent endites (cf., Whittington, 1971, p. 13, text – Figure 8; García-Bellido and Collins, 2006, Figure 15C). Whittington (1971) and Briggs and Whittington (1985) argued that this anteroposterior appendage differentiation reflects the mode of life of adult *M. splendens*. These authors suggested that the long anterior endopods of trunk appendages 1 to 9, with cylindrical podomeres, were used for walking on the seafloor, while the endopods of the posterior appendages were used for food gathering. When *Marrella* walked on the seafloor, the posterior part of the trunk was curved down, with the posterior endopods forming an arc shape (Whittington, 1971). In this way, the pointed endites on the posterior podomeres formed a network to trap and filter food particles (Whittington, 1971, p. 18; Briggs and Whittington, 1985, p. 156). García-Bellido and Collins (2006) agreed with this interpretation, though they hypothesized that this food capture took place while the animal was swimming. The food gathering function has been also suggested for endites of the trunk endopods of the Silurian marrellomorph *Xylokorys chledophilia* (Siveter et al., 2007) and for *Mi. hexagonalis* (Kühl and Rust, 2010), though in these two species, the endites seem to be developed on nearly all trunk appendages. A similar feeding mode might have been also plausible for some trilobites that bear endites in posterior appendages (e.g., Whittington and Almond, 1987; Pérez-Peris et al., 2021b). Consequently, we suggest that appendages posteriorly to the second trunk appendage that shares pointed endites were in the immature stages of Fezouata marrellid employed in food gathering (Figure 8), similar to *M. splendens*. The network created by pointed endites was likely quite efficient in particle feeding, given the endites were associated with delicate setae. As such, early developmental stages of the Fezouata marrellid were likely able to feed on detritus and/or on the diverse assemblage of unicellular algae found in the Fezouata Shale (Nowak et al., 2016). The function of the trunk exopods in the Fezouata marrellid is less clear, but they likely had a respiratory function as has been suggested for other marrellomorph taxa (Whittington, 1971; Siveter et al., 2007).

4.4 Ecological and evolutionary implications

Both adult and early developmental individuals of the Fezouata marrellid inhabited the same environment, as is evident from their co-occurrence in certain localities and facies. As discussed above (Section 4.2), both adult and immature stages also share the same general appendage differentiation along the body axis (although with different ratios of the walking/food-gathering appendages), showing only minor changes in podomere morphologies and, as expected, differing in overall body size and segment number. It

seems reasonable to therefore assume that the minute early developmental stages shared nearly the same modes of locomotion and food processing as the adults (Section 4.3). The smaller size of the immature appendages, the smaller endites on the posterior appendages, as well as the associated setae, suggest the early developmental stages were presumably feeding on smaller particles than the adults. The size differentiation of the food particles would mean that individual developmental phases were not directly competing for food resources, despite similarities in their appendage morphologies and living within the same environments. The posterior shift in trunk appendage differentiation between immature and adult stages (Figure 8, Section 4.2) also suggests that adults had more walking appendages and might have been more mobile than the immature stages. On the contrary, the immature stages likely benefitted from having a higher ratio of the food-gathering limbs, which might have been an adaptation to more efficient nutrient intake.

Ontogenetic niche differentiation is a well-recognized evolutionary strategy that prevents intraspecific competition between juveniles and adults and allows different phases of a life cycle to be subject to different selective forces (Werner and Gilliam, 1984; Ebenman, 1987; Ebenman, 1992; Moran, 1994). It is therefore not surprising that we can observe distinct ontogenetic niche differentiation in the life cycles of many euarthropods. In fossil taxa, this strategy has been reported for the megacheirans *Leanchoilia illecebrosa* (Liu et al., 2014) and possibly also for *Yohoia tenuis* (Haug et al., 2012), as well as for the trilobitomorph *Naraoia spinosa* (Zhai et al., 2019). In all these taxa, the appendages show different morphologies between the immature and adult stages, allowing them to occupy different ecological niches. Similar niche differentiation likely also occurred in trilobites that passed through metamorphoses, such as asaphids, trinucleids, and proetids (cf., Chatterton and Speyer, 1997; Lerosey-Aubril and Feist, 2005; Laibl et al., 2023). In marrellids, this ontogenetic niche differentiation appears to have been driven by the absolute differences in the size between individual developmental stages, by the presence of fine setae on food-gathering appendages, and by the ratio of the walking/food-gathering appendages, rather than by the development of vastly different morphologies, or structures with specific functions. A similar ontogenetic niche differentiation has been demonstrated for the *Leanchoilia illecebrosa*, which have lost a series of fine setae during the development from larva to adult (cf., Liu et al., 2014).

The phylogenetic position of Marrellida is currently in flux. Marrellids have been resolved within stem-mandibulates (Legg et al., 2013; Legg, 2015; Aria and Caron, 2017a), stem-chelicerates (Aria and Caron, 2017b), close to crustaceans (Chen et al., 2019; Du et al., 2019), or even close to pycnogonids (Vannier et al., 2018; Moysiuk et al., 2022). In any of these scenarios, they tend to occupy an early diverging position within a particular clade. Thus, such a simple mode of ontogenetic niche differentiation might have been common in the early diverging euarthropod groups.

Data availability statement

The datasets presented in this study can be found in online repositories. The names of the repository/repositories and accession number(s) can be found in the article/Supplementary Material.

Author contributions

LuL and PG designed the project under the supervision of AD. LuL photographed the material and measured the specimens. PG collected the synchrotron data and rendered the images. LuL, PG, and FS wrote the original draft. HD, FP-P, LoL, OB, GP, and AD helped to interpret and discuss the results and contributed to the writing of the final version of the manuscript. All authors contributed to the article and approved the submitted version.

Funding

LuL's research was funded by the Czech Science Foundation (project no. 20-23550Y), and the Center for Geosphere Dynamics (UNCE/SCI/006), and was conducted within institutional support RVO 67985831 of the Institute of Geology of the Czech Academy of Sciences. This research was also funded by the Swiss National Science Foundation, grant number 205321_179084 entitled 'Arthropod Evolution during the Ordovician Radiation: Insights from the Fezouata Biota' and awarded to AD. FS work is funded by an SNF Ambizione Grant (no. PZ00P2_209102) and by the Postdoctoral Fellowship of the Faculty of Geosciences and Environment at the University of Lausanne. HD was funded by a Swiss Natural Science Foundation Sinergia Grant (198691).

Acknowledgments

We thank Imran Rahman for beamtime on the X02DA TOMCAT beamline at the Swiss Light Source, and Christian Schlepütz and Federica Marone for assistance at the beamline. Many thanks to Joachim Haug, Carolin Haug, Peter Van Roy, and Javier Ortega-Hernández for inspiring discussions related to Marrellida, Euarthropoda, and their development. The manuscript has benefitted from constructive reviews by James Holmes and Dongjing Fu, as well as from comments by editor Tae-Yoon Park. This work would not be possible without Peter Van Roy's work on the Fezouata Shale and his detailed field notes. Mark Florence is thanked for access to the comparative material from the Smithsonian collections, and Susan Butts and Jessica Utrup are thanked for providing access to specimens at the Yale Peabody Museum.

Conflict of interest

The authors declare that the research was conducted in the absence of any commercial or financial relationships that could be construed as a potential conflict of interest.

The reviewer JH declared a past co-authorship with the author HD to the handling editor.

Publisher's note

All claims expressed in this article are solely those of the authors and do not necessarily represent those of their affiliated organizations, or those of the publisher, the editors and the reviewers. Any product that may be evaluated in this article, or claim that may be made by its manufacturer, is not guaranteed or endorsed by the publisher.

Supplementary material

The Supplementary Material for this article can be found online at: https://www.frontiersin.org/articles/10.3389/fevo.2023.1232612/full#supplementary-material

References

Anger, K. (2006). Contributions of larval biology to crustacean research: a review. *Invertebr. Reproduction. Dev.* 49, 175–205. doi: 10.1080/07924259.2006.9652207

Aria, C., and Caron, J.-B. (2017a). Burgess Shale fossils illustrate the origin of the mandibulate body plan. *Nature* 545, 89–92. doi: 10.1038/nature22080

Aria, C., and Caron, J.-B. (2017b). Mandibulate convergence in an armoured Cambrian stem chelicerate. *BMC Evol. Biol.* 17, 261. doi: 10.1186/s12862-017-1088-7

Aris, M. J., Corronca, J. A., Quinteros, S., and Pardo, P. L. (2017). A new marrellomorph euarthropod from the Early Ordovician of Argentina. *Acta Palaeontol. Pol.* 62, 1–8. doi: 10.4202/app.00240.2016

Bar-On, Y. M., Phillips, R., and Milo, R. (2018). The biomass distribution on Earth. *PNAS* 115, 6506–6511. doi: 10.1073/pnas.1711842115

Bicknell, R. D. C., Klinkhamer, A. J., Flavel, R. J., Wroe, S., and Paterson, J. R. (2018). A 3D anatomical atlas of appendage musculature in the chelicerate arthropod *Limulus polyphemus*. *PloS One* 13, e0191400. doi: 10.1371/journal

Briggs, D. E. G., and Whittington, H. B. (1985). Modes of life of arthropods from the Burgess Shale, British Columbia. *Trans. R. Soc Edinburgh. Earth Environ. Sci.* 76, 149–160. doi: 10.1017/S0263593300010415

Caron, J. B., Gaines, R. R., Aria, C., Mángano, M. G., and Streng, M. (2014). A new phyllopod bed-like assemblage from the Burgess Shale of the Canadian Rockies. *Nat. Commun.* 5, 3210. doi: 10.1038/ncomms4210

Caron, J. B., and Jackson, D. A. (2008). Paleoecology of the greater phyllopod bed community, Burgess Shale. *Palaeogeogr. Palaeoclimatol. Palaeoecol.* 258, 222–256. doi: 10.1016/j.palaeo.2007.05.023

Chatterton, B. D. E., and Speyer, S. E. (1989). Larval ecology, life history strategies, and patterns of extinction and survivorship among Ordovician trilobites. *Paleobiology* 15, 118–132. doi: 10.1017/S0094837300009313

Chatterton, B. D. E., and Speyer, S. E. (1997). 'Ontogeny,' in *Treatise on invertebrate paleontology, part O, arthropoda 1, trilobita, revised, volume 1: introduction, order agnostida, order redlichiida*. Ed. R. L. Kaesler (Boulder, Colorado and Lawrence, Kansas: The Geological Society of America, Inc. and The University of Kansas), 173–248.

Chen, X., Ortega-Hernández, J., Wolfe, J. M., Zhai, D., Hou, X., Chen, A., et al. (2019). The appendicular morphology of *Sinoburius lunaris* and the evolution of the artiopodan clade Xandarellida (Euarthropoda, early Cambrian) from South China. *BMC Evol. Biol.* 19, 165. doi: 10.1186/s12862-019-1491-3

Chlupáč, I. (1999). Some problematical arthropods from the Upper Ordovician Letná Formation of Bohemia. *J. Czech. Geol. Soc* 44, 79–87.

Cocks, L. R. M., and Torsvik, T. H. (2021). Ordovician palaeogeography and climate change. *Gondwana. Res.* 100, 53–72. doi: 10.1016/j.gr.2020.09.008

Conway Morris, S. (1986). The community structure of the Middle Cambrian Phyllopod Bed (Burgess Shale). *Palaeontology* 29, 423–467.

Dai, T., and Zhang, X. (2013). Ontogeny of the redlichiid trilobite *Eoredlichia intermediata* from the Chengjiang Lagerstätte, lower Cambrian, southwest China. *Lethaia* 46, 262–273. doi: 10.1111/let.12002

Destombes, J., Hollard, H., and Willefert, S. (1985). 'Lower Palaeozoic rocks of Morocco,' in *Lower Palaeozoic rocks of the world 4*. Ed. C. H. Holland (New York: Wiley), 91–336.

Drage, H. B., Legg, D. A., and Daley, A. C. (2023). Novel marrellomorph moulting behaviour preserved in the Lower Ordovician Fezouata Shale, Morocco. *Front. Ecol. Evol.* 11. doi: 10.3389/fevo.2023.1226924

Du, K., Ortega-Hernández, J., Yang, J., and Zhang, X. (2019). A soft-bodied euarthropod from the early Cambrian Xiaoshiba Lagerstätte of China supports a new clade of basal artiopodans with dorsal ecdysial sutures. *Cladistics* 35, 269–281. doi: 10.1111/cla.12344

Ebenman, B. (1987). Niche differences between age classes and intraspecific competition in age-structured populations. *J. Theor. Biol.* 124, 25–33. doi: 10.1016/S0022-5193(87)80249-7

Ebenman, B. (1992). Evolution in organisms that change their niches during the life cycle. *Am. Nat.* 139, 990–1021. doi: 10.1086/285370

Fu, D., Ortega-Hernández, J., Daley, A. C., Zhang, X., and Shu, D. (2018). Anamorphic development and extended parental care in a 520 million-year-old stem-group euarthropod from China. *BMC Evol. Biol.* 18, 147. doi: 10.1186/s12862-018-1262-6

Fu, D., Tong, G., Dai, T., Liu, W., Yang, Y., Zhang, Y., et al. (2019). The Qingjiang biota—A Burgess Shale–type fossil Lagerstätte from the early Cambrian of South China. *Sci. (80-.)* 363, 1338–1342. doi: 10.1126/science.aau8800

Fu, D., Zhang, X., Budd, G. E., Liu, W., and Pan, X. (2014). Ontogeny and dimorphism of *Isoxys auritus* (Arthropoda) from the Early Cambrian Chengjiang biota, South China. *Gondwana. Res.* 25, 975–982. doi: 10.1016/j.gr.2013.06.007

García-Bellido, D. C., and Collins, D. H. (2006). A new study of *Marrella splendens* (Arthropoda, Marrellomorpha) from the Middle Cambrian Burgess Shale, British Columbia, Canada. *Can. J. Earth Sci.* 43, 721–742. doi: 10.1139/e06-012

Hammer, Ø., Harper, D. A. T., and Ryan, P. D. (2001). Past: paleontological statistics software package for education and data analysis. *Palaeontol. Electron.* 4, 1–9.

Haug, J. T. (2020). Why the term 'larva' is ambiguous, or what makes a larva? *Acta Zool.* 101, 167–188. doi: 10.1111/azo.12283

Haug, J. T., Castellani, C., Haug, C., Waloszek, D., and Maas, A. (2013). A *Marrella*-like arthropod from the Cambrian of Australia: A new link between 'Orsten'-type and Burgess Shale assemblages. *Acta Palaeontol. Pol.* 58, 629–639. doi: 10.4202/app.2011.0120

Haug, J. T., Waloszek, D., Maas, A., Liu, Y., and Haug, C. (2012). Functional morphology, ontogeny and evolution of mantis shrimp-like predators in the Cambrian. *Palaeontology* 55, 369–399. doi: 10.1111/j.1475-4983.2011.01124.x

Hopkins, M. J. (2017). Development, trait evolution, and the evolution of development in trilobites. *Integr. Comp. Biol.* 57, 488–498. doi: 10.1093/icb/icx033

Hou, J. B., Hughes, N. C., Yang, J., Lan, T., Zhang, X. G., and Dominguez, C. (2017). Ontogeny of the articulated yiliangellinine trilobite *Zhangshania typica* from the lower Cambrian (Series 2, Stage 3) of southern China. *J. Paleontol.* 91, 86–99. doi: 10.1017/jpa.2016.118

Hughes, N. C., Minelli, A., and Fusco, G. (2006). The ontogeny of trilobite segmentation: a comparative approach. *Paleobiology* 32, 602–627. doi: 10.1666/06017.1

Koenemann, S., Schram, F. R., Bloechl, A., Iliffe, T. M., Hoenemann, M., and Held, C. (2007). Post-embryonic development of remipede crustaceans. *Evol. Dev.* 9, 117–121. doi: 10.1111/j.1525-142X.2007.00142.x

Kühl, G., and Rust, J. (2010). Re-investigation of *Mimetaster hexagonalis*: a marrellomorph arthropod from the Lower Devonian Hunsrück Slate (Germany). *Paläontologische. Z.* 84, 397–411. doi: 10.1007/s12542-009-0049-x

Laibl, L., Cederström, P., and Ahlberg, P. (2018). Early post-embryonic development in *Ellipsostrenua* (Trilobita, Cambrian, Sweden) and the developmental patterns in Ellipsocephaloidea. *J. Paleontol.* 92, 1018–1027. doi: 10.1017/jpa.2018.25

Laibl, L., Drage, H. B., Pérez-Peris, F., Schöder, S., Saleh, F., and Daley, A. C. (in press). Babies from the Fezouata Biota: Early developmental trilobite stages and their adaptation to high latitudes. *Geobios*. doi: 10.1016/j.geobios.2023.06.005

Laibl, L., Esteve, J., and Fatka, O. (2017). Giant postembryonic stages of *Hydrocephalus* and *Eccaparadoxides* and the origin of lecithotrophy in Cambrian trilobites. *Palaeogeogr. Palaeoclimatol. Palaeoecol.* 470, 109–115. doi: 10.1016/j.palaeo.2017.01.023

Laibl, L., Maletz, J., and Olschewski, P. (2021). Post-embryonic development of *Fritzolenellus* suggests the ancestral morphology of the early developmental stages in Trilobita. *Pap. Palaeontol.* 7, 839–859. doi: 10.1002/spp2.1324

Laibl, L., Saleh, F., and Pérez-Peris, F. (2023). Drifting with trilobites: The invasion of early post-embryonic trilobite stages to the pelagic realm. *Palaeogeogr. Palaeoclimatol. Palaeoecol.* 613, 111403. doi: 10.1016/j.palaeo.2023.111403

Lefebvre, B., El Hariri, K., Lerosey-Aubril, R., Servais, T., and Van Roy, P. (2016). The Fezouata Shale (Lower Ordovician, Anti-Atlas, Morocco): A historical review. *Palaeogeogr. Palaeoclimatol. Palaeoecol.* 460, 7–23. doi: 10.1016/j.palaeo.2015.10.048

Lefebvre, B., Gutiérrez-Marco, J. C., Lehnert, O., Martin, E. L. O., Nowak, H., Akodad, M., et al. (2018). Age calibration of the lower Ordovician Fezouata Lagerstätte, Morocco. *Lethaia* 51, 296–311. doi: 10.1111/LET.12240

Legg, D. A. (2015). The morphology and affinities of *Skania fragilis* (Arthropoda) from the middle Cambrian Burgess Shale. *Bull. Geosci.* 90, 509–518. doi: 10.3140/bull.geosci.1532

Legg, D. A. (2016). A new marrellid arthropod from the Ordovician of Wales. *Acta Palaeontol. Pol.* 61, 617–619. doi: 10.4202/app.00246.2016

Legg, D. A., Sutton, M. D., and Edgecombe, G. D. (2013). Arthropod fossil data increase congruence of morphological and molecular phylogenies. *Nat. Commun.* 4, 2485. doi: 10.1038/ncomms3485

Lerosey-Aubril, R., and Feist, R. (2005). Ontogeny of a new cyrtosymboline trilobite from the Famennian of Morocco. *Acta Palaeontol. Pol.* 50, 449–464.

Lerosey-Aubril, R., Gaines, R. R., Hegna, T. A., Ortega-Hernández, J., Van Roy, P., Kier, C., et al. (2018). The Weeks Formation Konservat-Lagerstätte and the evolutionary transition of Cambrian marine life. *J. Geol. Soc London.* 175, 705–715. doi: 10.1144/jgs2018-042

Lerosey-Aubril, R., and Laibl, L. (2021). Protaspid larvae are unique to trilobites. *Arthropod. Struct. Dev.* 63, 101059. doi: 10.1016/j.asd.2021.101059

Liu, Q. (2013). The first discovery of *Marrella* (Arthropoda, Marrellomorpha) from the Balang Formation (Cambrian Series 2) in Hunan, China. *J. Paleontol.* 87, 391–394. doi: 10.1666/12-118.1

Liu, Y., Haug, J. T., Haug, C., Briggs, D. E. G., and Hou, X. (2014). A 520 million-year-old chelicerate larva. *Nat. Commun.* 5, 4440. doi: 10.1038/ncomms5440

Liu, J., Lerosey-Aubril, R., Steiner, M., Dunlop, J. A., Shu, D., and Paterson, J. R. (2018). Origin of raptorial feeding in juvenile euarthropods revealed by a Cambrian radiodontan. *Natl. Sci. Rev.* 5, 863–869. doi: 10.1093/nsr/nwy057

Liu, Y., Melzer, R. R., Haug, J. T., Haug, C., Briggs, D. E. G., Hörnig, M. K., et al. (2016). Three-dimensionally preserved minute larva of a great-appendage arthropod from the early Cambrian Chengjiang biota. *PNAS* 113, 5542–5546. doi: 10.1073/pnas.1522899113

Lovrich, G. A., and Vinuesa, J. H. (1999). Reproductive potential of the lithodids *Lithodes santolla* and *Paralomis granulosa* (Anomura, Decapoda) in the Beagle Channel, Argentina. *Sci. Mar.* 63, 355–360. doi: 10.3989/scimar.1999.63s1355

Maas, A., Braun, A., Dong, X.-P., Donoghue, P. C. J., Müller, K. J., Olempska, E., et al. (2006). The 'Orsten'—More than a Cambrian Konservat-Lagerstätte yielding exceptional preservation. *Palaeoworld* 15, 266–282. doi: 10.1016/j.palwor.2006.10.005

Marone, F., Münch, B., and Stampanoni, M. (2010). Fast reconstruction algorithm dealing with tomography artifacts. *Proc. Vol. 7804. Dev. X-Ray. Tomogr. VII.* 7804, 292–302. doi: 10.1117/12.859703

Martin, E. L. O., Pittet, B., Gutiérrez-Marco, J. C., Vannier, J., El Hariri, K., Lerosey-Aubril, R., et al. (2016a). The Lower Ordovician Fezouata Konservat-Lagerstätte from Morocco: Age, environment and evolutionary perspectives. *Gondwana. Res.* 34, 274–283. doi: 10.1016/J.GR.2015.03.009

Martin, E. L. O., Vidal, M., Vizcaïno, D., Vaucher, R., Sansjofre, P., Lefebvre, B., et al. (2016b). Biostratigraphic and palaeoenvironmental controls on the trilobite associations from the Lower Ordovician Fezouata Shale of the central Anti-Atlas, Morocco. *Palaeogeogr. Palaeoclimatol. Palaeoecol.* 460, 142–154. doi: 10.1016/J.PALAEO.2016.06.003

Mauchline, J. (1971). *Euphausiacea larvae* (Copenhagen: Conseil International pour l'Exploration de la Mer).

Minelli, A., and Fusco, G. (2013). 'Arthropod post-embryonic development,' in *Arthropod biology and evolution*. Eds. A. Minelli, G. Boxshall and G. Fusco (Berlin, Heidelberg: Springer-Verlag), 91–122. doi: 10.1007/978-3-642-36160-9_5

Moore, R. A., Briggs, D. E. G., and Bartels, C. (2005). A new specimen of *Weinbergina opitzi* (Chelicerata: Xiphosura) from the Lower Devonian Hunsrück Slate, Germany. *Paläontologische. Z.* 79, 399–408. doi: 10.1007/BF02991931

Moran, N. A. (1994). Adaptation and constraint in the complex life cycles of animals. *Annu. Rev. Ecol. Syst.* 25, 573–600. doi: 10.1146/annurev.es.25.110194.003041

Moysiuk, J., and Caron, J. B. (2023). A quantitative assessment of ontogeny and molting in a Cambrian radiodont and the evolution of arthropod development. *Paleobiology*, 1–16. doi: 10.1017/pab.2023.18

Moysiuk, J., Izquierdo-López, A., Kampouris, G. E., and Caron, J. B. (2022). A new marrellomorph arthropod from southern Ontario: a rare case of soft-tissue preservation on a Late Ordovician open marine shelf. *J. Paleontol.* 96, 859–874. doi: 10.1017/jpa.2022.11

Nowak, H., Servais, T., Pittet, B., Vaucher, R., Akodad, M., Gaines, R. R., et al. (2016). Palynomorphs of the Fezouata Shale (Lower Ordovician, Morocco): Age and environmental constraints of the Fezouata Biota. *Palaeogeogr. Palaeoclimatol. Palaeoecol.* 460, 62–74. doi: 10.1016/j.palaeo.2016.03.007

Ortega-Hernández, J., Van Roy, P., and Lerosey-Aubril, R. (2016). A new aglaspidid euarthropod with a six-segmented trunk from the Lower Ordovician Fezouata Konservat-Lagerstätte, Morocco. *Geol. Mag.* 153, 524–536. doi: 10.1017/S0016756815000710

Park, T.-Y. S., Kihm, J.-H., Woo, J., Kim, Y. H. G., and Lee, J. I. (2016). Ontogeny of the Furongian (late Cambrian) trilobite *Proceratopyge* cf. *P. lata* Whitehouse from northern Victoria Land, Antarctica, and the evolution of metamorphosis in trilobites. *Palaeontology* 59, 657–670. doi: 10.1111/pala.12251

Paterson, J. R., García-Bellido, D. C., Jago, J. B., Gehling, J. G., Lee, M. S. Y., and Edgecombe, G. D. (2016). The Emu Bay Shale Konservat-Lagerstätte: a view of Cambrian life from East Gondwana. *J. Geol. Soc London.* 173, 1–11. doi: 10.1144/jgs2015-083

Pérez-Peris, F., Laibl, L., Lustri, L., Gueriau, P., Antcliffe, J. B., Bath Enright, O. G., et al. (2021a). A new nektaspid euarthropod from the Lower Ordovician strata of Morocco. *Geol. Mag.* 158, 509–517. doi: 10.1017/S001675682000062X

Pérez-Peris, F., Laibl, L., Vidal, M., and Daley, A. C. (2021b). Systematics, morphology, and appendages of an Early Ordovician pilekiine trilobite *Anacheirurus* from Fezouata Shale and the early diversification of Cheiruridae. *Acta Palaeontol. Pol.* 66, 857–877. doi: 10.4202/app.00902.2021

Potin, G. J.-M., and Daley, A. C. (2023). The significance of *Anomalocaris* and other Radiodonta for understanding paleoecology and evolution during the Cambrian explosion. *Front. Earth Sci.* 11. doi: 10.3389/feart.2023.1160285

Potin, G. J.-M., Gueriau, P., and Daley, A. C. (2023). Radiodont frontal appendages from the Fezouata Biota (Morocco) reveal high diversity and ecological adaptations to suspension-feeding during the Early Ordovician. *Front. Ecol. Evol.* 11. doi: 10.3389/fevo.2023.1214109

Rabalais, N. N., and Gore, R. H. (1985). 'Abbreviated development in decapods,' in *Crustacean issues 2: larval growth* (Rotterdam: A.A. Balkema), 67–126.

Rak, Š., Ortega-Hernández, J., and Legg, D. A. (2013). A revision of the Late Ordovician marrellomorph arthropod *Furca bohemica* from Czech Republic. *Acta Palaeontol. Pol.* 58, 615–628. doi: 10.4202/app.2011.0038

Rohlf, F. J. (2006). *TpsDig2, digitize landmarks and outlines, version 2.10*. Available at: http://life.bio.sunysb.edu/morph/.

Saleh, F., Antcliffe, J. B., Lefebvre, B., Pittet, B., Laibl, L., Perez Peris, F., et al. (2020a). Taphonomic bias in exceptionally preserved biotas. *Earth Planet. Sci. Lett.* 529, 115873. doi: 10.1016/j.epsl.2019.115873

Saleh, F., Bath-Enright, O. G., Daley, A. C., Lefebvre, B., Pittet, B., Vite, A., et al. (2021a). A novel tool to untangle the ecology and fossil preservation knot in exceptionally preserved biotas. *Earth Planet. Sci. Lett.* 569, 117061. doi: 10.1016/J.EPSL.2021.117061

Saleh, F., Candela, Y., Harper, D. A. T., Polechová, M., Lefebvre, B., and Pittet, B. (2018). Storm-induced community dynamics in the Fezouata Biota (Lower Ordovician, Morocco). *Palaios* 33, 535–541. doi: 10.2110/PALO.2018.055

Saleh, F., Daley, A. C., Lefebvre, B., Pittet, B., and Perrillat, J. P. (2020b). Biogenic iron preserves structures during fossilization: A hypothesis. *BioEssays* 42, 1900243. doi: 10.1002/BIES.201900243

Saleh, F., Lefebvre, B., Hunter, A. W., and Nohejlová, M. (2020c). Fossil weathering and preparation mimic soft tissues in eocrinoid and somasteroid echinoderms from the Lower Ordovician of Morocco. *Micros. Today* 28, 24–28. doi: 10.1017/S1551929519001238

Saleh, F., Pittet, B., Perrillat, J. P., and Lefebvre, B. (2019). Orbital control on exceptional fossil preservation. *Geology* 47, 103–106. doi: 10.1130/G45598.1

Saleh, F., Pittet, B., Sansjofre, P., Gueriau, P., Lalonde, S., Perrillat, J. P., et al. (2020d). Taphonomic pathway of exceptionally preserved fossils in the Lower Ordovician of Morocco. *Geobios* 60, 99–115. doi: 10.1016/J.GEOBIOS.2020.04.001

Saleh, F., Vaucher, R., Antcliffe, J. B., Daley, A. C., El Hariri, K., Kouraiss, K., et al. (2021b). Insights into soft-part preservation from the Early Ordovician Fezouata Biota. *Earth-Sci. Rev.* 213, 103464. doi: 10.1016/j.earscirev.2020.103464

Saleh, F., Vaucher, R., Vidal, M., El Hariri, K., Laibl, L., Daley, A. C., et al. (2022). New fossil assemblages from the Early Ordovician Fezouata Biota. *Sci. Rep.* 12, 20773. doi: 10.1038/s41598-022-25000-z

Saleh, F., Vidal, M., Laibl, L., Sansjofre, P., Gueriau, P., Pérez-Peris, F., et al. (2021c). Large trilobites in a stress-free Early Ordovician environment. *Geol. Mag.* 158, 261–270. doi: 10.1017/s0016756820000448

Sanders, H. L., and Hessler, R. R. (1964). The larval development of *Lightiella incisa* Gooding (Cephalocarida). *Crustaceana* 7, 81–97. doi: 10.1163/156854064X00326

Shuster, C. N., and Sekiguchi, K. (2003). 'Growing up takes about ten years and eighteen stages,' in *The American horseshoe crab*. Eds. C. N. Shuster, R. B. Barlow and H. J. Brockmann (Cambridge: Harvard University Press), 103–132.

Siveter, D. J., Fortey, R. A., Sutton, M. D., Briggs, D. E. G., and Siveter, D. J. (2007). A silurian 'marrellomorph' arthropod. *Proc. R. Soc B. Biol. Sci.* 274, 2223–2229. doi: 10.1098/rspb.2007.0712

Sombke, A., Lipke, E., Kenning, M., Müller, C. H. G., Hansson, B. S., and Harzsch, S. (2012). Comparative analysis of deutocerebral neuropils in Chilopoda (Myriapoda): implications for the evolution of the arthropod olfactory system and support for the Mandibulata concept. *BMC Neurosci.* 13, 1. doi: 10.1186/1471-2202-13-1

Stürmer, W., and Bergström, J. (1976). The arthropods *Mimetaster* and *Vachonisia* from the Devonian HunsrüCk Shale. *Paläontologische. Z.* 50, 78–111. doi: 10.1007/BF03001974

Vannier, J., Aria, C., Taylor, R. S., and Caron, J.-B. (2018). *Waptia fieldensis* Walcott, a mandibulate arthropod from the middle Cambrian Burgess Shale. *R. Soc Open Sci.* 5, 172206. doi: 10.1098/rsos.172206

Van Roy, P. (2006). *Non-trilobite arthropods from the ordovician of Morocco*. (PhD dissertation. Ghent: Ghent University).

Van Roy, P., Briggs, D. E. G., and Gaines, R. R. (2015). The Fezouata fossils of Morocco; an extraordinary record of marine life in the Early Ordovician. *J. Geol. Soc London.* 172, 541–549. doi: 10.1144/jgs2015-017

Van Roy, P., Orr, P. J., Botting, J. P., Muir, L. A., Vinther, J., Lefebvre, B., et al. (2010). Ordovician faunas of Burgess Shale type. *Nature* 465, 215–218. doi: 10.1038/nature09038

Vaucher, R., Martin, E. L. O., Hormière, H., and Pittet, B. (2016). A genetic link between Konzentrat- and Konservat-Lagerstätten in the Fezouata Shale (Lower Ordovician, Morocco). *Palaeogeogr. Palaeoclimatol. Palaeoecol.* 460, 24–34. doi: 10.1016/J.PALAEO.2016.05.020

Vaucher, R., Pittet, B., Hormière, H., Martin, E. L. O., and Lefebvre, B. (2017). A wave-dominated, tide-modulated model for the Lower Ordovician of the Anti-Atlas, Morocco. *Sedimentology* 64, 777–807. doi: 10.1111/SED.12327

Werner, E. E., and Gilliam, J. F. (1984). The ontogenetic niche and species interactions in size-structured populations. *Annu. Rev. Ecol. Syst.* 15, 393–425. doi: 10.1146/annurev.es.15.110184.002141

Whittington, H. B. (1971). Redescription of *Marrella splendens* (Trilobitoidea) from the Burgess Shale, Middle Cambrian, British Columbia. *Bull. Geol. Surv. Canada.* 209, 1–24.

Whittington, H. B., and Almond, J. E. (1987). Appendages and habits of the Upper Ordovician trilobite *Triarthrus eatoni*. *Philos. Trans. R. Soc London. B. Biol. Sci.* 317, 1–46. doi: 10.1098/RSTB.1987.0046

Yang, X., Kimmig, J., Zhai, D., Liu, Y., Kimmig, S. R., and Peng, S. (2021). A juvenile-rich palaeocommunity of the lower Cambrian Chengjiang biota sheds light on palaeo-boom or palaeo-bust environments. *Nat. Ecol. Evol.* 5, 1082–1090. doi: 10.1038/s41559-021-01490-4

Zhai, D., Edgecombe, G. D., Bond, A. D., Mai, H., Hou, X., and Liu, Y. (2019). Fine-scale appendage structure of the Cambrian trilobitomorph *Naraoia spinosa* and its ontogenetic and ecological implications. *Proc. R. Soc B. Biol. Sci.* 286, 20192371. doi: 10.1098/rspb.2019.2371

Zhang, Z.-Q. (2011). Phylum Arthropoda von Siebold 1848. *Zootaxa* 3148, 99–103. doi: 10.11646/zootaxa.3148.1.14

Zhao, F., Caron, J. B., Bottjer, D. J., Hu, S., Yin, Z., and Zhu, M. (2014). Diversity and species abundance patterns of the Early Cambrian (Series 2, Stage 3) Chengjiang Biota from China. *Paleobiology* 40, 50–69. doi: 10.1666/12056

Zhao, Y., Yuan, J., Zhu, M., Yang, X., and Peng, J. (2003). The occurrence of the genus *Marrella* (Trilobitoidea) in Asia. *Prog. Nat. Sci.* 13, 708–711. doi: 10.1080/10020070312331344280

frontiers | Frontiers in Ecology and Evolution

TYPE Original Research
PUBLISHED 03 October 2023
DOI 10.3389/fevo.2023.1270429

OPEN ACCESS

EDITED BY
Sylvain Charbonnier,
Muséum National d'Histoire Naturelle, France

REVIEWED BY
Paul Antony Selden,
University of Kansas, United States
James Lamsdell,
West Virginia University, United States

*CORRESPONDENCE
Lorenzo Lustri
lorenzo.lustri90@gmail.com
Allison C. Daley
allison.daley@unil.ch

RECEIVED 31 July 2023
ACCEPTED 30 August 2023
PUBLISHED 03 October 2023

CITATION
Lustri L, Antcliffe JB, Saleh F, Haug C, Laibl L, Garwood RJ, Haug JT and Daley AC (2023) New perspectives on the evolutionary history of xiphosuran development through comparison with other fossil euchelicerates. *Front. Ecol. Evol.* 11:1270429. doi: 10.3389/fevo.2023.1270429

New perspectives on the evolutionary history of xiphosuran development through comparison with other fossil euchelicerates

Lorenzo Lustri[1]*, Jonathan B. Antcliffe[1], Farid Saleh[1], Carolin Haug[2], Lukáš Laibl[3], Russell J. Garwood[4,5], Joachim T. Haug[2] and Allison C. Daley[1]*

[1]Institute of Earth Sciences, University of Lausanne, Lausanne, Switzerland, [2]Biocenter, Faculty of Biology, Ludwig Maximilian University of Munich (LMU), Munich, Germany, [3]Czech Academy of Sciences, Institute of Geology, Prague, Czechia, [4]Department of Earth and Environmental Sciences, University of Manchester, Manchester, United Kingdom, [5]The Natural History Museum, London, United Kingdom

Introduction: Euchelicerata is a diverse group encompassing Xiphosura, Chasmataspidida, Eurypterida, and Arachnida. Xiphosura represents an extant group with a rich fossil record dating back to the Ordovician period. Xiphosurans are often referred to as "living fossils" due to their seemingly unchanged morphology over millions of years. Numerous studies have contributed to the understanding of xiphosuran development, revealing changes in the timing and rate of their growth. These changes have been mainly associated with the freshwater invasion of early xiphosuran forms. However, limited research has been conducted to compare the developmental patterns of xiphosurans with other euchelicerates inhabiting aquatic environments.

Methods: This study compares the developmental patterns of xiphosurans with that of the fossil clades of eurypterids and chasmataspidids. By incorporating environmental and phylogenetic information within ancestral state reconstruction analyses, and then testing different evolutionary scenarios, the influence of the environment on the evolution of developmental patterns of euchelicerates is examined.

Results: The results confirm that the developmental changes in Xiphosura throughout their evolutionary history are correlated with the exploitation of different environments. However, the inclusion of eurypterids and chasmataspidids indicates that the entirety of changes seen for Xiphosura represent only a small portion of the total variability recovered for euchelicerates.

Discussion: Our results emphasize the importance of considering phylogenetic relationships and outgroup comparisons to understand the evolutionary dynamics of Xiphosura.

KEYWORDS

Euchelicerata, Xiphosura, stasis, ontogeny, evolutionary rate, ancestral state

Introduction

Euchelicerata is a successful clade of arthropods including Xiphosura, Chasmataspidida, Eurypterida, and Arachnida. Xiphosura is a group with extant representatives, which has an extensive fossil record dating back to the Ordovician (Rudkin et al., 2008; van Roy et al., 2015; Lamsdell et al., 2023). The earliest described xiphosuran fossil remains come from the Williams member of the Stone Mountain formation of Manitoba, Canada which dates to the latest Ordovician at c. 443Ma (Rudkin et al., 2008), but recent fossil discoveries suggest they first evolved in the early Ordovician (van Roy et al., 2015). Molecular clock estimates suggest a late Cambrian origin for the group (Lozano-Fernandez et al., 2020). Representatives of Xiphosura have long been referred to as "living fossils" (Stoermer, 1952) with major morphological traits seemingly unaltered by the ravages of time over hundreds of millions of years. Even recently, they have been cited as an example of extreme morphological conservatism (Bicknell and Pates, 2020). The term "living fossils" is somewhat problematic as the subtext of the term implies a lack of evolution taking place in the group, whereas it is well established that broad-scale evolutionary stasis results from gradual evolutionary changes around a relatively static morphological average position through time (Simpson, 1944; Eldredge et al., 2005; Tëmkin and Eldredge, 2015) (Figure 1). While a certain degree of morphological conservatism is recognized in Xiphosura (Bennett et al., 2018), especially in late Mesozoic and Cenozoic forms (Avise et al., 1994; Rudkin and Young, 2009; Kin and Błażejowski, 2014; Lamsdell and McKenzie, 2015; Bicknell et al., 2019b), most late Paleozoic and early Mesozoic forms are considered to go through a much more pronounced evolutionary exploration of morphological space (Lamsdell, 2016; Bicknell, 2019; Bicknell et al., 2019a; Bicknell et al., 2020; Lamsdell, 2021a; Lamsdell, 2021b; Lustri et al., 2021; Bicknell et al., 2022). Freshwater colonization during the late Paleozoic resulted in xiphosurans adapting to many new habitats, possibly on multiple occasions, and is associated with the first record of remarkable radiation of the group in the fossil record (Lamsdell, 2016; Lamsdell, 2021a; Bicknell et al., 2022).

Heterochrony has been proposed as the main pattern to described the freshwater invasion of early xiphosuran forms (Lamsdell, 2021a; Lamsdell, 2021b). To understand these developmental patterns the following Paleozoic taxa are key: *Alanops magnifica* (Racheboeuf et al., 2002) and the *Euproops* complex, including the species nicknamed "*Piesproops*" (more formally *Andersoniella* sp.) (Lamsdell, 2020), *Euproops danae* and *Euproops rotundatus* (Haug et al., 2012; Haug and Rötzer, 2018b; Tashman et al., 2019; Haug and Haug, 2020). Insights provided by these taxa, alongside studies of the development of extant species (Scholl, 1977; Jegla and Costlow, 1982; Sekiguchi et al., 1988; Shuster and Sekiguchi, 2003; Haug and Rötzer, 2018a), has allowed the recognition of peramorphic and paedomorphic patterns in two of the four main clades of Xiphosura, Austrolimulidae and Belinuridae (Bicknell, 2019; Lamsdell, 2021a; Bicknell et al., 2021b; Lustri et al., 2021). Those studies critically enhanced our understanding of evolution and development, but less has been done to compare the developmental patterns of xiphosurans with other euchelicerates inhabiting the same aquatic realm.

Arthropods are generally characterized by an extreme specialization of their different life stages (Minelli et al., 2016). However, this is usually not the case for euchelicerates including xiphosurans (Haug and Rötzer, 2018a; Kaiser and Schoppe, 2018). Euchelicerates are characterized by a gradual, direct and usually epimorphic development, where there is no addition of segments after hatching (Sekiguchi et al., 1988; Braddy, 2001; Lamsdell and Selden, 2013; Haug, 2019; Lamsdell et al., 2019; Fusco and Minelli, 2021).

In order to provide a phylogenetic context to the study of xiphosuran development, it is essential to compare them with other euchelicerate groups. Modeling of evolutionary scenarios needs to account for the phylogenetic relationships between organisms as this is the only independent way to estimate rates of evolution (Garamszegi, 2014). "Stasis is generally defined as little or no net accrued species-wide morphological change during a species-lineage's existence up to millions of years" (Eldredge et al., 2005, p. 133), yet, it is important to define what exactly "little or no" means (Eldredge et al., 2005). The only way to do so is to compare xiphosurans with other, related groups inhabiting the same environment. It is certainly very clear that the time scale matters here as what may appear to be static over millions of years may disguise a great deal of change around a mean when viewed at higher temporal resolution. Conversely, stasis at high temporal resolution may miss larger and gradual temporal trends only observable when a longer view is taken. To understand the evolutionary dynamics of any lineage, a diversity

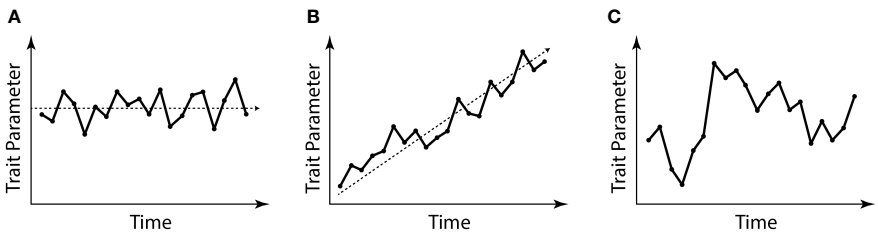

FIGURE 1
Graphical explanation of the evolutionary stasis often attributed to Xiphosurida. **(A)** Example of stationary morphological evolution around a middle trait parameter; **(B)** example of morphological evolution with a trait parameter diverging through time; **(C)** example of a "random walk". Edited from Tëmkin and Eldredge (2015).

of temporal views must be taken and then contrasted to related lineages.

The inclusion of other euchelicerate groups such as eurypterids and chasmataspidids in the analyses helps to refine not only the estimation of developmental parameters at the root of Xiphosura but also the possible correlations of different evolutionary scenarios with the paleoenvironment independently from the phylogeny. Eurypterids and chasmataspidids shared similar environments with the horseshoe crabs during the Paleozoic (Dunlop, 2010; Howard et al., 2020). The development of xiphosurans has been recently explored by meta-analyses (Lamsdell, 2016; Lamsdell, 2021a; Bicknell et al., 2022), but the development of eurypterids and chasmataspidids has never been incorporated in such analyses. Data for eurypterids and chasmataspidids are also available, and research has focused on fine detailed analyses of the development of single species such as *Hoplitaspis hiawathai* (Lamsdell et al., 2019) and *Eurypterus lacustris* (Ruebenstahl et al., 2021).

In this work, a meta-analysis is presented of morphometric developmental data from eight species of Xiphosura, combined with data from one species of Eurypterida and one species of Chasmataspidida. These data have been utilized alongside environmental and phylogenetic information to perform an ancestral state reconstruction analysis for the allometric growth patterns and environment of Xiphosura. The influence of different environments on the evolution of development are then tested within a phylogenetic framework.

Materials and methods

Studied specimens

The specimens used in this study belong to eight different species of Xiphosura, including two extant and six extinct taxa,

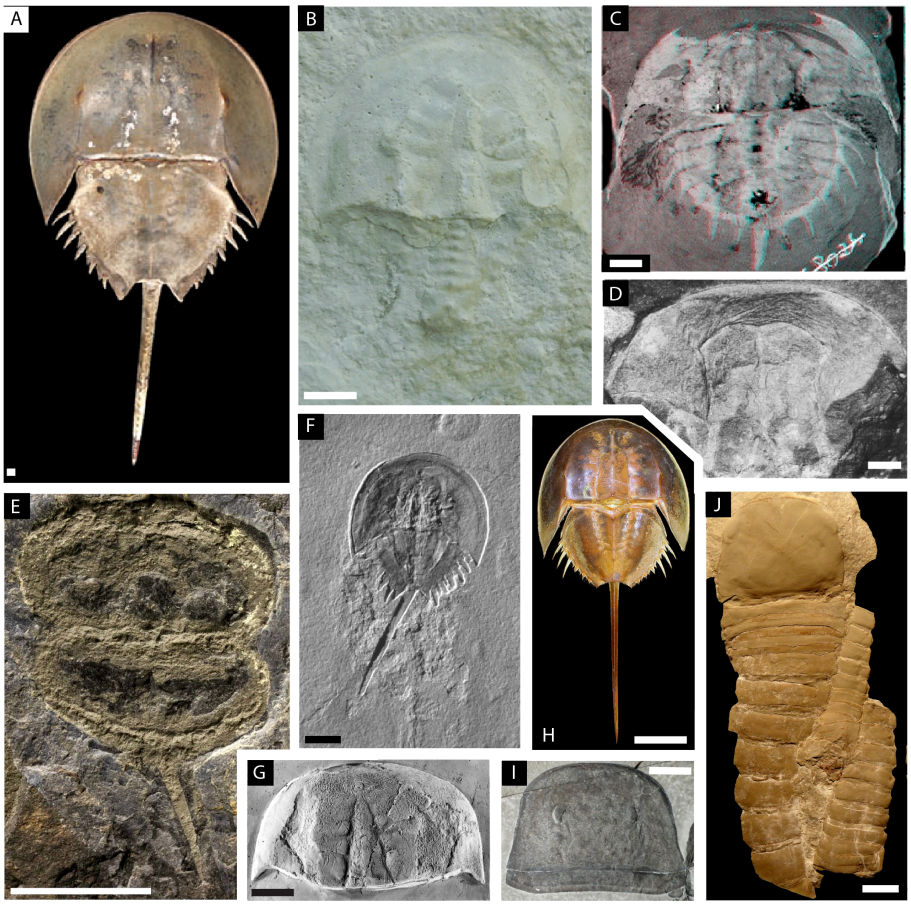

FIGURE 2
Illustration plate of the euchelicerates species used in the study with focus on showing the prosomal shield (carapace). **(A–H)** Xiphosurans. **(A)** *Limulus polyphemus* modified from Lamsdell (2021a). **(B)** *Paleolimulus kunguricus* modified from Naugolnykh and Bicknell (2022). **(C)** *Euproops danae*, stereo image, modified from Haug and Rötzer (2018b). **(D)** *Euproops sp* modified from Schultka (2000). **(E)** *Prolimulus woodwardi* modified from Lustri et al. (2021). **(F)** *Mesolimulus walchi* modified from Briggs et al. (2005). **(G)** *Paleolimulus signatus* modified from Babcock et al. (2000). **(H)** *Tachypleus tridentatus* modified from Bicknell et al. (2021a). **(I)** The eurypterid *Eurypterus lacustris* modified from Ruebenstahl et al. (2021). **(J)** The chasmataspidid *Hoplitaspis hiawathai* modified from Lamsdell et al. (2019). Scale bars represent 1 mm in **(A)**; 5 mm in **(C)**; 10 mm in **(B, D, E, G, J)**; 20 mm in **(F, I)**; and 40 mm in **(H)**.

together with two outgroups consisting of one species of Eurypterida and one species of Chasmataspidida (Figure 2). Morphometric developmental data, summarized by the slope of the linear regression for the prosomal shield (carapace) width and length through their ontogeny, has been collected for each taxon (Figure 3). The raw measurement of 171 specimens of *Eurypterus lacustris* (Eurypterida), hosted at Yale Peabody Museum of Natural History, New Haven, USA (YPM IP) were taken from Ruebenstahl et al. (2021). The raw measurement for the prosomal shield of 18 specimens of *Hoplitaspis hiawathai* (Chasmataspidida), hosted at University of Wisconsin Geology Museum, Wisconsin, USA (UWGM) were taken from Lamsdell et al. (2019). Four specimens of *Hoplitaspis hiawathai* have been excluded as they are preserved in lateral view, leaving 14 specimens to include in the analyses. The raw measurements of 10 specimens of *Paleolimulus kunguricus*, curated at the Paleontological Museum of the Perm State University, Perm, Russia (PSU) and the Geological Institute of the Russian Academy of Sciences, Moscow, Russia (GIN), were personally communicated to the authors by R.D.C. Bicknell. The 18 specimens used for *Prolimulus woodwardi* are all figured in Lustri et al. (2021). For *Euproops* sp., raw measurements were collected from photographs taken by C. Haug from 15 specimens curated at Yale Peabody Museum of Natural History, New Haven, USA (YPM IP). None of the fossil specimens measured showed or has been reported to show evidence of deformation. Data for *Limulus polyphemus* were collected from a single ontogenetic series of 15 stages from hatch to the 14th moult (Lamsdell, 2021a) (Figures 3C, D). Fossil measurements were collected from photographs of the specimens using ImageJ and the program tpsDig2 2.31. Raw data are available in Table 1.

Regressions of morphometric measurements during ontogeny

When the slope of the linear regression for the prosomal shield (carapace) width and length was not directly available in the literature, it was calculated. Prior to performing the linear regression, the natural log of all datasets was taken to reduce the skewness. Linear regression analyses were then conducted for prosomal shield lengths vs. prosomal shield widths for the following species: *Eurypterus lacustris, Hoplitaspis hiawathai, Prolimulus woodwardi, Euproops* sp., *Paleolimulus kunguricus* and *Limulus polyphemus*. The regression slopes for *Paleolimulus signatus*, *Euproops danae*, *Mesolimulus walchi*, and *Tachypleus tridentatus* were taken from Bicknell et al. (2022). Therefore, at least one representative of three of the four taxa of Xiphosura (Paleolimulidae, Bellinurina, and Limulidae) were considered, alongside two non-xiphosuran euchelicerates. Linear regressions of the measurements of *Eurypterus lacustris, Hoplitaspis hiawathai, Prolimulus woodwardi, Euproops* sp., *Paleolimulus kunguricus and Limulus polyphemus* were performed with the function "lm" in RStudio 2021.09.0 + 351 "Ghost Orchid". The plots of the linear regressions were made using the function "plot" in RStudio 2021.09.0 + 351 "Ghost Orchid" and subsequently edited with Adobe Illustrator (R script in Supplementary Datasheet S1). All the linear regression slopes are reported in Table 2.

Phylogenetic analyses

Bayesian phylogenetic analyses were performed using the matrix from Lamsdell (2020), with the addition of *Hoplitaspis hiawathai* and *Prolimulus woodwardi*. The character coding for *Hoplitaspis hiawathai* was based on Lamsdell et al. (2019), and character coding for *Prolimulus woodwardi* was based on Lustri et al. (2021). *Eurypterus lacustris* was not present in this matrix and has not been coded. Instead, *Eurypterus tetragonophthalmus* was used as a proxy representing the relative phylogenetic position of *Eurypterus lacustris* as the utilized matrix is expected to be coded identically for them both (in Figure 4, *Eurypterus lacustris* would have appeared as a sister species to *Eurypterus tetragonophthalmus* highlighted in red). The methods are the same as in the original work from Lamsdell (2020), using MrBayes ver. 3.2.7a (Huelsenbeck and Ronquist, 2001). The final data matrix includes 162 taxa and 259 discrete characters. The analyses consisted of four independent runs of 10,000,000 generations and four chains each, under the maximum likelihood model with gamma-distributed rate variation among sites (Mkv + Γ:) (Lewis, 2001). Characters were unordered and given equal weighting (Congreve and Lamsdell, 2016). Trees were sampled every 100 generations. The resulting trees per run is 1,000,000 and the first 25,000 sampled trees of each run were discarded as burn-in. Extended majority rule tree obtained was used for the subsequent analyses (Figure 4). The matrix used for the phylogenetic analyses and the mrBayes code are available in Supplementary Datasheet S2.

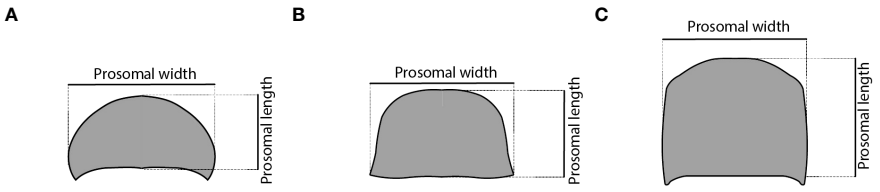

FIGURE 3
Schemes of different euchelicerate prosomal shield (carapace) shapes showing how the measurements were made. **(A)** xiphosurid, **(B)** eurypterid, and **(C)** chasmataspidid.

10.3389/fevo.2023.1270429

TABLE 1 List of the measurements for *Hoplitaspis hiawathai*, *Limulus polyphemus*, *Paleolimulus kunguricus*, *Prolimulus woodwardi*, *Euproops* sp. (*Andersoniella*) and *Eurypterus lacustris* used for the morphometric analyses.

Hoplitaspis hiawathai		
Measurement credits James Lamsdell		
Specimen no.	Prosomal shield length	Prosomal shield width
UWGM_1840B	13	15
UWGM _1863	14	10
UWGM_1873A	29	37
UWGM_1875	23	32
UWGM_1877	23	26
UWGM_1880	11	12
UWGM_2041	15	17
UWGM_2044A	11	12
UWGM_2044B	12	13
UWGM_2069B	18	18
UWGM_2268	25	33
UWGM_2273A	11	17
UWGM_2273D	13	5
UWGM_2279A	15	9
UWGM_2279B	15	18
UWGM_2279C	15	16
UWGM_2700	21	24
Limulus polyphemus		
Photo credits James Lamsdell		
Stage	Prosomal shield length	Prosomal shield width
Hatch	2	4.4
1th	2.2	4.8
2nd	2.2	4.1
3rd	2.8	4.1
4th	3	5.2
5th	3.3	5.9
6th	3.9	7.8
7th	4.4	7.8
8th	5.1	8.6
9th	4.4	8.8
10th	5.1	10.1
11th	7	10.7
12th	8.2	14.2
13th	8.1	16.3
14th	31	52.4
Paleolimulus kunguricus		
Photo credits Russell Bicknell		
Specimen no.	Prosomal shield length	Prosomal shield width
PSU	36.8	65.3
GIN PH_9	69	106
GIN PH_11	-	-
GIN PH_12	-	-
GIN PH_18	27.2	44.68
GIN PH_19	-	-
GIN PH_22	60.5	88.9
GIN PH_31	3.27	4.36
GIN PH_32	9.14	10.8
GIN PH_37	71.4	95
Prolimulus woodwardi		
Photo credits Russell Bicknell		
Specimen no.	Prosomal shield length	Prosomal shield width
NMM1031	11.9	20
NMMe146	8.5	11.5
NMMe39	7.5	10.5
NMMe142	6.8	12.6
NMMe145	8	13.3
NMM1038	10.8	19
NMM1045	7.5	11.6
NMMe141	11	19.4
NMMe109	5.9	10.3
NMMe139	15	20
NMMe143	6.7	10
NMMe140	9	15.3
NMMe144	6.5	8.8
NMMe138	6.9	10.4
NHMUKPIIn18588	7	14
NHMUKPII3395	10	15.1

(Continued)

(Continued)

TABLE 1 Continued

Prolimulus woodwardi		
Photo credits Russell Bicknell		
Specimen no.	Prosomal shield length	Prosomal shield width
MCZ109537	8	10.8
MBA1989	9.9	13.9
Euproops sp. (*Andersoniella*)		
Photo credits Carolin Haug		
Specimen no.	Prosomal shield length	Prosomal shield width
YPM_IP_000125	-	46.8
YPM_IP_16910	17.8	43.9
YPM_IP_25590	10.4	21.4
Euproops sp. (*Andersoniella*)		
Photo credits Carolin Haug		
Specimen no.	Prosomal shield length	Prosomal shield width
YPM_IP_28514	16.1	39.2
YPM_IP_035153	-	44.4
YPM_IP_50519	19.9	43.2
YPM_IP_50570	14.2	33.6
YPM_IP_50574	9.8	22.9
YPM_IP_050644	18.1	42.5
YPM_IP_50689	3.3	7.3
YPM_IP_050733	6.7	15.9
YPM_IP_050735	-	-
YPM_IP_050754	16.9	38.5
YPM_IP_050835	-	25.5
YPM_IP_050935	6.7	15.7
YPM_IP_168026	15.4	35.5
YPM_IP_168040	7.4	15.4
YPM_IP_016909	17.6	42.9
YPM_IP_50472	12	21.6
YPM_IP_50502	-	36.1
YPM_IP_50687	-	17.6
Eurypterus lacustris		
Measurement credits James Lamsdell		
Specimen no.	Prosomal shield length	Prosomal shield width
186707	38	57
YPM_IP_207952	43	64

(Continued)

TABLE 1 Continued

Eurypterus lacustris		
Measurement credits James Lamsdell		
Specimen no.	Prosomal shield length	Prosomal shield width
YPM_IP_208085	38.5	55
YPM_IP_209979	35	54
YPM_IP_209981	24	34
YPM_IP_212841	23.5	34.5
YPM_IP_212842	24.5	34
YPM_IP_212846	36.5	56
YPM_IP_212857	25.5	43
YPM_IP_212860	27	41.5
YPM_IP_212861	32	48.5
YPM_IP_212862	28	37.5
YPM_IP_212863	42	64.5
YPM_IP_212864	18	26
YPM_IP_212867	26	40
YPM_IP_212869	35	52
Eurypterus lacustris		
Measurement credits James Lamsdell		
Specimen no.	Prosomal shield length	Prosomal shield width
YPM_IP_212871	27	40
YPM_IP_212872	26	40.5
YPM_IP_212881	24	34
YPM_IP_212886	32.5	59
YPM_IP_212893	37	54.5
YPM_IP_212896	23	34
YPM_IP_212996	38	53
YPM_IP_213007	38.5	42
YPM_IP_213053	24	38
YPM_IP_213067	19.5	31
YPM_IP_213204	32	47
YPM_IP_213539	39.2	75
YPM_IP_214132	27.5	40
YPM_IP_216514	23.5	36
YPM_IP_216518	30	44.5
YPM_IP_216519	24	38
YPM_IP_216526	22	30
YPM_IP_216528	37.5	51

(Continued)

10.3389/fevo.2023.1270429

TABLE 1 Continued

Eurypterus lacustris		
Measurement credits James Lamsdell		
Specimen no.	Prosomal shield length	Prosomal shield width
YPM_IP_216531	41	61.5
YPM_IP_216534	38	55
YPM_IP_216537	40	62.5
YPM_IP_216541	29.5	41
YPM_IP_216544	26	40
YPM_IP_216554	36.5	54
YPM_IP_216555	26	39.5
YPM_IP_216557	35	52
YPM_IP_216558	34	55
YPM_IP_216560	37	54
YPM_IP_216561	36	53
YPM_IP_216565	27.5	40.5
YPM_IP_216566	37.5	54
YPM_IP_216568	33	47
YPM_IP_216573	37	55
YPM_IP_216578	20	30
YPM_IP_216584	37	53
YPM_IP_216585	29	43
YPM_IP_216586	29	44
Eurypterus lacustris		
Measurement credits James Lamsdell		
Specimen no.	Prosomal shield length	Prosomal shield width
YPM_IP_216588	22.5	35.5
YPM_IP_216595	8	11.5
YPM_IP_216596	7	9
YPM_IP_216604	31	55
YPM_IP_216609	30	46
YPM_IP_216610	24.5	38
YPM_IP_216614	33.5	
YPM_IP_216624	32.5	50
YPM_IP_216636	32	53.5
YPM_IP_216644	26	40
YPM_IP_216647	34	51
YPM_IP_216652	30	44.5
YPM_IP_216660	27	40.5

(Continued)

TABLE 1 Continued

Eurypterus lacustris		
Measurement credits James Lamsdell		
Specimen no.	Prosomal shield length	Prosomal shield width
YPM_IP_216661	28.5	41.5
YPM_IP_216662	29	44
YPM_IP_216666	19	30
YPM_IP_216670	31	44
YPM_IP_216679	30	44
YPM_IP_216682	42	62.5
YPM_IP_216683	32.5	49
YPM_IP_216687	25	35
YPM_IP_216695	20	29.5
YPM_IP_216699	20	30
YPM_IP_216703	19.5	26.5
YPM_IP_216704	31	49
YPM_IP_216707	24	39
YPM_IP_216713	39.5	55
YPM_IP_216715	43	67
YPM_IP_216716	21	32
YPM_IP_216717	23	33
YPM_IP_216718	34	47
YPM_IP_216723	41	59
YPM_IP_216724	34	55
YPM_IP_216725	13	17.5
YPM_IP_216727	30	53
YPM_IP_216728	35	52
YPM_IP_216729	36	56
Eurypterus lacustris		
Measurement credits James Lamsdell		
Specimen no.	Prosomal shield length	Prosomal shield width
YPM_IP_216730	26	44
YPM_IP_216733	40	58.5
YPM_IP_216734	49	70
YPM_IP_217694	24	35
YPM_IP_217696	11	16
YPM_IP_217700	36	55
YPM_IP_217712	24	37.5
YPM_IP_217713	31	47

(Continued)

TABLE 1 Continued

Eurypterus lacustris		
Measurement credits James Lamsdell		
Specimen no.	Prosomal shield length	Prosomal shield width
YPM_IP_217714	32	51
YPM_IP_217715	25.5	39
YPM_IP_217722	44	66
YPM_IP_217723	33	49
YPM_IP_217724	32	47
YPM_IP_217725	43	64
YPM_IP_217726	29.5	46
YPM_IP_217727	36.5	56
YPM_IP_217729	31	47
YPM_IP_217730	32	48.5
YPM_IP_217732	8	10
YPM_IP_217736	25.5	37
YPM_IP_217739	27	40.5
YPM_IP_217743	40	65
YPM_IP_217750	38	61
YPM_IP_217751	25.5	38.5
YPM_IP_217755	27	42
YPM_IP_217756	56	84.5
YPM_IP_217761	24.5	38
YPM_IP_217762	22.5	34
YPM_IP_217763	33	54.5
YPM_IP_217764	41	63.5
YPM_IP_217766	23	34.5
YPM_IP_217770	19	26
YPM_IP_217775	19.5	32
YPM_IP_217777	23.5	36
YPM_IP_217780	27	39.5
YPM_IP_217790	21	32.5
YPM_IP_223420	25	36.5
Eurypterus lacustris		
Measurement credits James Lamsdell		
Specimen no.	Prosomal shield length	Prosomal shield width
YPM_IP_223423	33	50
YPM_IP_288014	21.5	37.5

(Continued)

TABLE 1 Continued

Eurypterus lacustris		
Measurement credits James Lamsdell		
Specimen no.	Prosomal shield length	Prosomal shield width
YPM_IP_288044	45	63
YPM_IP_388026	21.5	37
YPM_IP_403855	35	54
YPM_IP_403865	23	36
YPM_IP_403867	24.5	34
YPM_IP_403882	24	36
YPM_IP_403885	39	61
YPM_IP_403889	58	83
YPM_IP_403890	31	54
YPM_IP_403891	19	29
YPM_IP_403892	36.5	55.5
YPM_IP_426065	33.5	50
YPM_IP_426066	35	51.5
YPM_IP_426067	44.5	70
YPM_IP_426068	29	40
YPM_IP_426076	23	34
YPM_IP_426078	40	61
YPM_IP_426090	34	50
YPM_IP_426096	11.5	17
YPM_IP_426100	30	48
YPM_IP_426101	19.5	32
YPM_IP_426140	39	58
YPM_IP_426141	24	39
YPM_IP_426142	26	40
YPM_IP_426143	27	40
YPM_IP_426151	38.5	61
YPM_IP_426164	40	58
YPM_IP_426200	24	35.5
YPM_IP_426282	36.5	56
YPM_IP_426283	26.5	40
YPM_IP_426285	45	65
YPM_IP_426286	37.5	53
YPM_IP_426297	23	39
YPM_IP_426298	25	38
YPM_IP_426299	7.5	12

(Continued)

TABLE 1 Continued

Eurypterus lacustris		
Measurement credits James Lamsdell		
Specimen no.	Prosomal shield length	Prosomal shield width
YPM_IP_426300	23	35
YPM_IP_426313	20.5	31
YPM_IP_426314	9	12.5
YPM_IP_426393	28.5	44
YPM_IP_426394	26	37.5
YPM_IP_427341	26	38.5
YPM_IP_545059	16	26

All measurements are in mm.

Ancestral state reconstruction and the estimation of evolutionary rates

The phylogenetic tree obtained with the Bayesian phylogenetic analyses was pruned with the "ape" (Paradis and Schliep, 2019) function "drop.tip" in RStudio 2021.09.0 + 351 "Ghost Orchid". Two different pruned trees were obtained. The first tree retained the branch length and node positions for xiphosurans species with known growth-pattern data (prosomal shield length and width ratio along the growth), resulting in a tree with 8 tips and 7 internal nodes. The second tree retained the branch length and the node positions for all euchelicerate species with known growth-pattern data (prosomal shield length and width ratio along the growth), resulting in a tree of 10 tips and 9 internal nodes. The branch lengths of the trees are based on morphological character distance. Using the packages "mvMORPH" (Clavel et al., 2015), "ape"

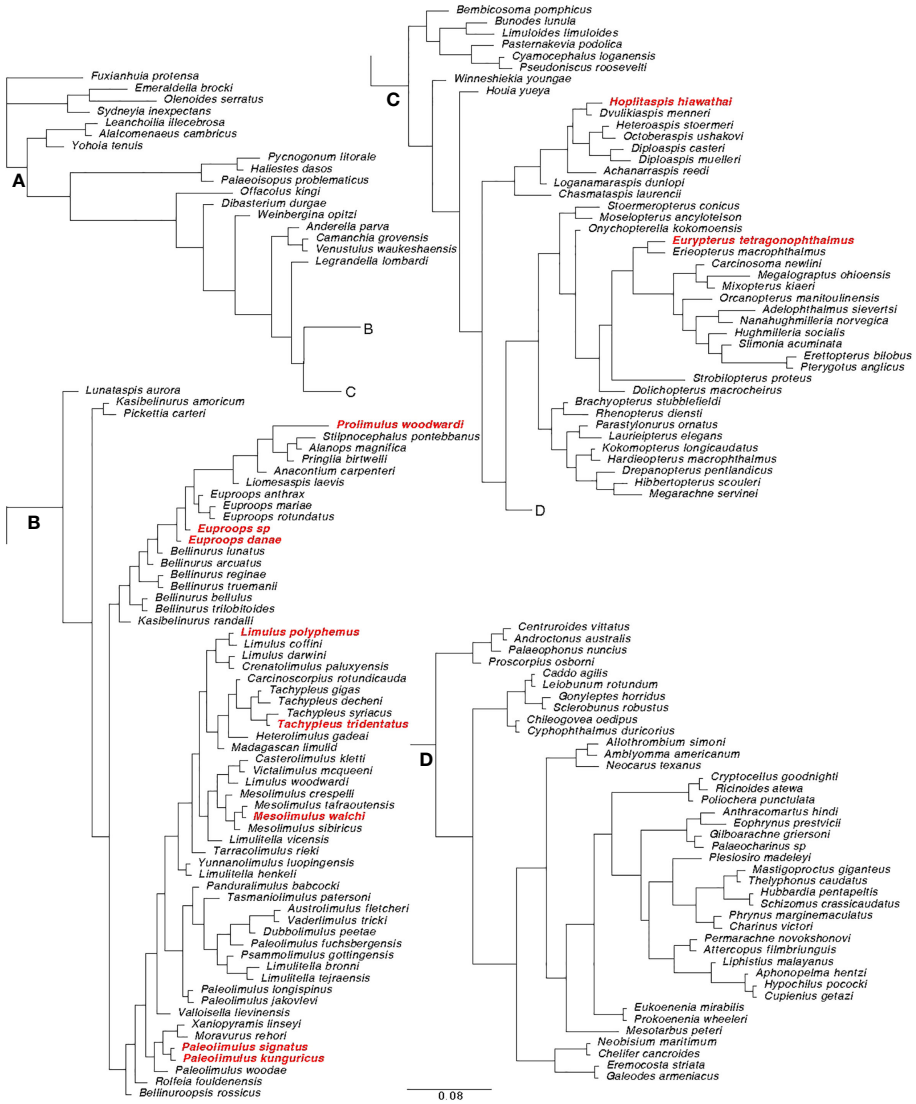

FIGURE 4
Extended majority rule tree of the Bayesian analysis performed on the matrix modified from Lamsdell (2020). **(A)** Root section of the tree; **(B)** Xiphosura section of the tree; **(C)** Eurypterida and Chasmataspidida section of the tree. **(D)** Arachnida section of the tree. The species used in the analyses of this paper are highlighted in red. The tree is based on a matrix composed of 162 taxa and 259 characters.

TABLE 2 Linear regression slopes of all the taxa examined in the study.

Species	Prosomal shield slope	Host museum	Reference slope
Hoplitaspis hiawathai	0.719	UWGM	Present work
Limulus polyphemus	0.965	YPM IP	Present work
Paleolimulus kunguricus	0.92	GIN, PSU	Present work
Euproops danae	0.888	YPM IP	Present work
Prolimulus woodwardi	0.959	NM, NHMUK PI, MCZ, MBA	Present work
Euproops sp.	1.02	MAS Pal.	Bicknell et al., 2022; Haug et al., 2012
Mesolimulus walchi	0.978	CM, JME SOS, MCZ, MNHN, NM, SMNS, SNSB-BSPG, USNM, YPM IP	Bicknell et al., 2022
Eurypterus lacustris	0.936	YPM IP	Present work
Paleolimulus signatus	1.02	KUMIP, USNM, YMP IP	Bicknell et al., 2022
Tachypleus tridentatus	0.99	N/A	Bicknell et al., 2022; Kaiser and Schoppe, 2018

(Paradis and Schliep, 2019) and "phytools" (Revell, 2012), ancestral state analyses have been performed on both trees, incorporating the discrete environmental data of Lamsdell (2021), here divided between marginal (not fully marine) and marine settings following Bicknell et al. (2022). The ML function was used for a maximum likelihood estimation of the ancestral state under Brownian motion models. Subsequently, two evolutionary models were tested on the ancestral states recovered from both pruned phylogenetic trees: a Multivariate Brownian motion process (BM), and a Multi-rate Brownian motion process (BMM). The BM is a model in which a single path of evolution is simulated under Brownian motion processes while the BMM is a model in which multiple paths of evolution are simulated under Brownian motion processes. The models were used to test the null hypothesis where an absence of correlation between environmental (in our case two variables marginal and marine) and development would result in the BM model (allowing only one evolutionary path) outperforming the BMM model (allowing two different evolutionary paths). The evolutionary rates of marginal and marine species were calculated under both models using the "mvBM" command to investigate the possible correlation between the environment and the evolution of ontogenetic characters over time. The ontogenetic variation investigated is the change in shape of the prosomal shield (carapace) during ontogeny. The fit of these different evolutionary models was assessed by calculating the Akaike weight with the command "aicw". All the aforementioned analyses were made using RStudio 2021.09.0 + 351 "Ghost Orchid" (R script in Supplementary Datasheet S3).

Results

The slopes of the prosomal shield length and width of *Eurypterus lacustris, Hoplitaspis hiawathai, Prolimulus woodwardi, Euproops* sp., *Paleolimulus kunguricus* and *Limulus polyphemus* are available together with the slopes gathered from the literature of *Paleolimulus signatus*, *Euproops danae*, *Mesolimulus walchi*, *Tachypleus tridentatus* in Table 2. Gradient values greater than 1 represent a preferential growth of length over width, with higher numbers representing a more extreme allometry. A gradient of exactly 1 represents ontogenetic isometry (inflationary growth), while a gradient of less than 1 represents width increasing quicker than length during ontogeny with lower numbers representing more extreme allometry. The prosomal shield slopes range from 0.719 in *Hoplitaspis hiawathai* to 1.02 in *Euproops* sp and *Paleolimulus signatus*. Between these extremes, *Eurypterus lacustris*, *Euproops danae*, *Prolimulus woodwardi, Paleolimulus kunguricus*, *Limulus polyphemus, Mesolimulus walchi* and *Tachypleus tridentatus* range from 0.888 in *Euproops danae* to 0.99 in *Tachypleus tridentatus*. All performed regressions are shown in Figure 5.

The results for the reconstructed ancestral state of the allometric growth of the prosomal shield, partitioned by environment, are summarized in the phylogenetic trees shown in Figures 6 and 7. Figure 6 represents the tree that includes only Xiphosura, while Figure 7 includes both Xiphosura and additional euchelicerate species (*Eurypterus lacustris* and *Hoplitaspis hiawathai*). In both trees, the lowest values of the slope (indicating width increasing quicker than length) are found in species associated with marginal environments, such as *Hoplitaspis hiawathai* and *Euproops danae*, while values closer to 1 are more commonly associated with marine settings.

The two evolutionary models tested on the two different phylogenetic trees (xiphosurans-only and euchelicerate trees) with the reconstructed character history show differences in fitting the data and different statistical support. For the xiphosurans-only tree the BM model, which does not account for environmental differences, outperforms the BMM model, which considers environmental effects (BM AICw = 0.676; and BMM AICw = 0.324, see also Table 3). The Log-likelihood Ratio Test for this model yields a p-value of 0.89. For the euchelicerates tree, the BMM model, which accounts for environmental differences, outperforms

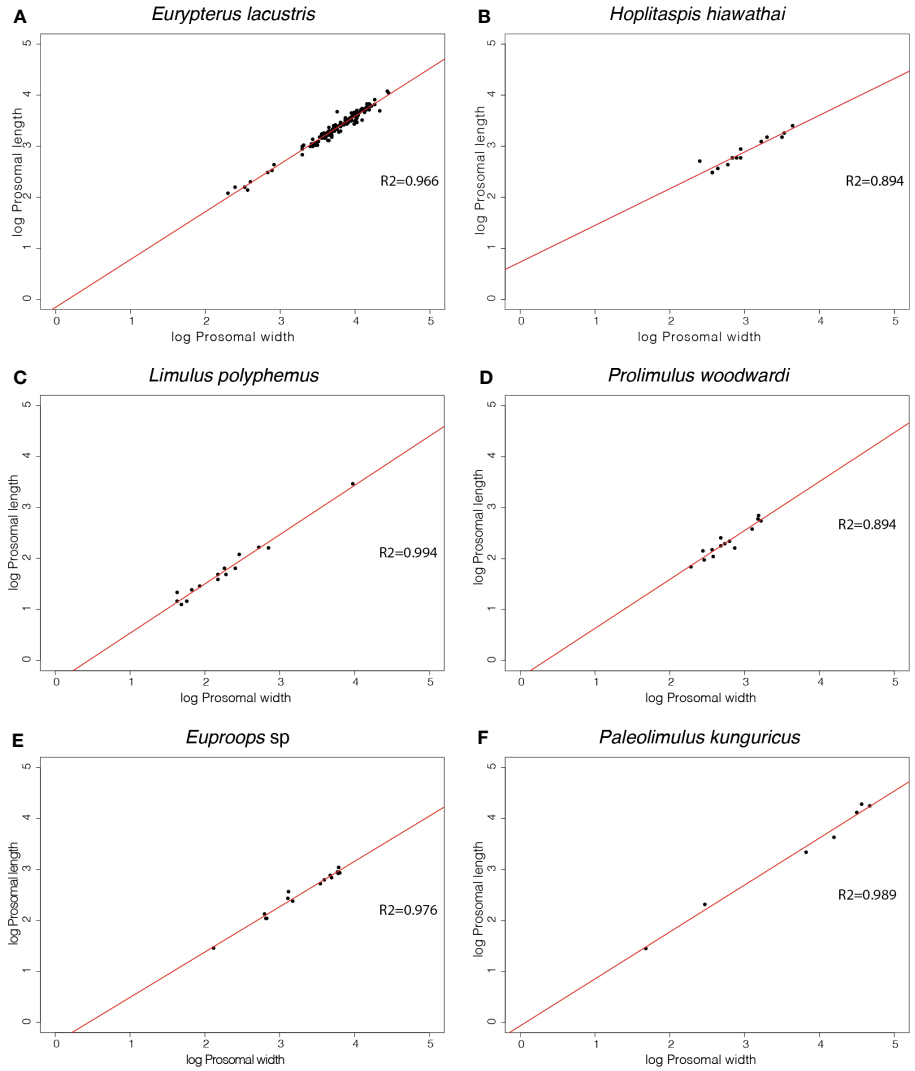

FIGURE 5
Linear regressions of morphometric measurements of the prosomal shield length and width of 6 different euchelicerate species. Slope values resulting from the regressions are available in Table 2 alongside slopes taken from the literature.

the BM model (BM AICw = 0.027; and BMM AICw = 0.973, see also Table 4). The Log-likelihood Ratio Test for this model shows a p-value of 0.00246. When accounting for environmental affinities, the evolutionary rate recovered for marginal species is higher than in marine species for both xiphosurans-only and all-euchelicerates analyses. However, this pattern is much more evident in the all-euchelicerates tree. Full data regarding the comparison of the two models alongside evolutionary rates recovered in marine and marginal environments are presented in Tables 3, 4.

Discussion

Several patterns are present in the reconstructed ancestral state for the growth pattern of the prosomal shield (carapace) compared across different environments and systematic levels (Figures 6 and 7). The obtained regression slopes represent how much the carapace length increases in comparison to its width. A lower slope value indicates a smaller growth of the carapace length in comparison to its width. In the reconstruction of ancestral states performed on the xiphosurans-only dataset and tree, higher slope values are found on average in limulid species from marine environments. Isolated species of Paleolimulidae and Bellinuridae from marginal environments also exhibit high slope values (specifically *Paleolimulus signatus* and *Euproops* sp.) (Figure 6). On the other hand, lower slope values are found in the marginal environment with *Euproops danae*. This may reflect a certain degree of morphological plasticity associated with species inhabiting the marginal environment, as supported by previous research (Lamsdell, 2016; Lamsdell 2021a; Bicknell et al., 2022). It is further supported by a higher estimated evolutionary rate for the marginal environment (Table 3). However, when comparing the BMM, which includes the environmental variable as a potential correlate to evolutionary rates, with the BM that does not account for this, there is no significant support for the BMM over the BM (Table 3). Instead, a single Brownian motion model for all the

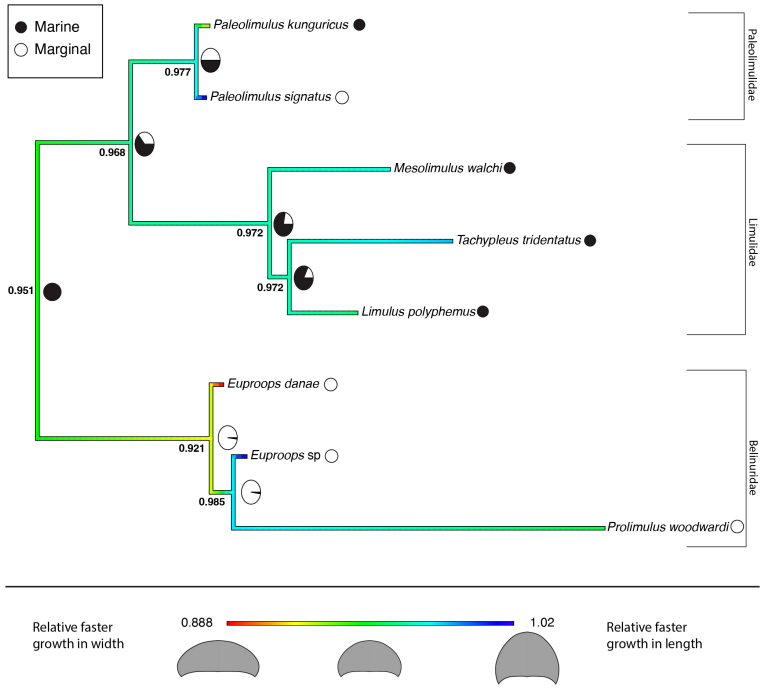

FIGURE 6
Ancestral state reconstruction of the prosomal shield allometric growth and environments of Xiphosura. Numbers at the nodes are the reconstructed ancestral state for the prosomal shield slope. Pie charts express the probability of a marginal or marine environment at the node. 0.888 is the lowest slope value and 1.02 is the highest slope value. Results of the evolutionary models (BM and BMM) tested on the tree are available in Table 3.

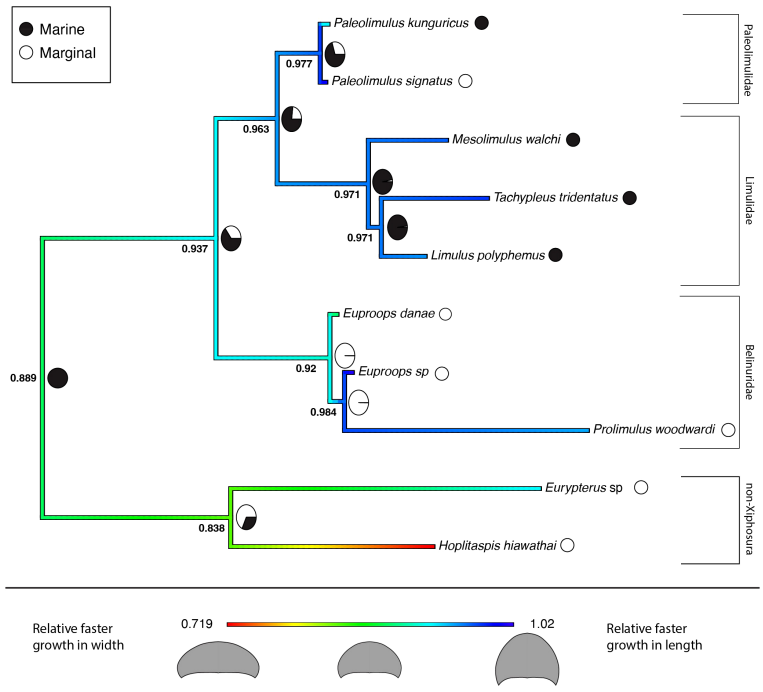

FIGURE 7
Ancestral state reconstruction of the prosomal shield allometric growth and environments of Xiphosura, Eurypterida and Chasmataspidida. Numbers at the nodes are the reconstructed ancestral state for the prosomal shield slope. Pie charts express the probability of a marginal or marine environment at the node. 0.478 is the lowest slope value and 1.02 is the highest slope value. Results of the evolutionary models (BM and BMM) tested on the tree available are in Table 4.

10.3389/fevo.2023.1270429

TABLE 3 AIC supports and estimated rate of evolution for the BM and BMM models that include only the xiphosurans.

Model including only Xiphosurida	
Multivariate Brownian motion process (BM)	
LogLikelihood:	5.490783
AIC:	−6.981566
AICc:	−4.581566
Estimated rate of evolution	
pL/pW slop	0.3174505
Multi-rate Brownian motion process (BMM)	
LogLikelihood:	5.500164
AIC:	−5.000327
AICc:	0.9996729
Estimated rate of evolution marginal environment	
pL/pW slop	0.3390649
Estimated rate of evolution marine environment	
pL/pW slop	0.2859732
Akaike weights for the two models	
BMM versus BM	
	AIC diff / AICw
BM	−6.98 / 0.676
BMM	−5.51 / 0.324
Log-likelihood Ratio Test for the two models	
LRT statistic: 0.0187614 p-value: 0.8910527	

TABLE 4 AIC supports and estimated rate of evolution for the BM and BMM models that include Xiphosurida, Eurypterida and Chasmataspidida.

Model including Xiphosurida, Eurypterids and Chasmataspidida	
Multivariate Brownian motion process (BM)	
LogLikelihood:	2.430013
AIC:	−0.8600268
AICc:	0.8542589
Estimated rate of evolution	
pL/pW slop	0.4916194
Multi-rate Brownian motion process (BMM)	
LogLikelihood:	7.013268
AIC:	−8.026537
AICc:	−4.026537
Estimated rate of evolution marginal environment	
pL/pW slop	0.5915447
Estimated rate of evolution marine environment	
pL/pW slop	0.002031127
Akaike weights for the two models	
BMM versus BM	
	AIC diff / AICw
BM	−0.86 / 0.027
BMM	−8.03 / 0.973
Log-likelihood Ratio Test for the two models	
LRT statistic: 9.16651 p-value: 0.00246	

xiphosurans included in the analyses fits the data better than two different Brownian models associated with the marginal and marine environments. This analysis yields a high p-value (Table 3), weakening the assumption that the evolution of xiphosuran development can be inferred solely considering the internal relationships of the group. While these results may be due to the absence of correlation between evolutionary rates and environments for the Xiphosura, other hypotheses can also explain this outcome. The sample size used for the analyses may have been too small, reflecting a lack of available fossil data. Another factor that may have contributed to the results of this analysis is the difficulty in discriminating between coastal, estuarian or freshwater environments for fossil specimens. This becomes clearer when examining the results obtained from the same analyses performed on a tree and dataset that includes the non-xiphosuran euchelicerates: *Eurypterus lacustris* and *Hoplitaspis hiawathai*. The inclusion of other euchelicerates increases the variability in carapace allometric growth, and provides a new perspective on the intra-xiphosurans differences recovered from the previous analyses (Figure 7). At this systematic scale, the differences among xiphosurans appear more subtle (Figure 7). This conclusion is also supported by a higher estimated evolutionary rate for the marginal environment in the second analysis compared to the previous one (Table 4). However, it is important to note some limitations of this second approach as well. In the second analyses, *Hoplitaspis hiawathai* represents a significant portion of the total variability. This may not reflect the average status in Chasmataspidida. Another important factor limiting our study is a possible error in environmental assignment introduced by the ethological aspect of several of the examined taxa. It is well known that aquatic euchelicerates possessed gregarious behaviors, often associated with group molting events (Daley and Drage, 2016; Bicknell et al., 2019b; Lamsdell et al., 2019; Lustri et al., 2021) that took place in shallow waters. This may have affected our environmental classification for species such as *Hoplitaspis hiawathai* (Lamsdell et al., 2019), *Eurypterus lacustris* (Ruebenstahl et al., 2021) and *Prolimulus woodwardi* (Lustri et al., 2021) for which gregarious behaviors are reported and specimens were moults, meaning we cannot exclude this to be the case for other taxa involved in the study.

In the all-euchelicerates analysis, stronger support for the BMM over the BM is demonstrated, suggesting the presence of two different evolutionary rates for the two different environments.

This signal was not recoverable when using the dataset that relies on only xiphosurans. The all-euchelicerates analysis reinforces the results of the xiphosurans-only analysis and gives a phylogenetic perspective to the evolutionary patterns of xiphosurans. Both analyses show an increase in morphological plasticity, independent of phylogeny but associated with the colonization of new environments. Furthermore, the second analysis shows that while these changes happened and are likely related to different environments within Xiphosura, they are much less pronounced than in the absence of outgroups. Body proportions in adulthood are generally stereotypical for any given species, and ontogenetic development is the process leading to their establishment. This implies that growth and form are related, but not by a simple relationship of cause and effect, because the starting point of body proportions at hatching/birth plays an important role too. Nevertheless, in light of the highest evolutionary rates of allometric growth recovered from our analyses associated with the freshwater environment, is still important to note extreme proportions of the prosomal shield even when they occur in species known from only one or few specimens where developmental data are lacking. Extremes in the proportions of the prosomal shield are often recovered in Mesozoic freshwater taxa, several of which have been excluded by our analyses owing to the lack of data about the development. This is the case for the radiation of Austrolimulidae. Austrolimulidae such as *Austrolimulus fletcher* (Riek, 1955) and *Dubbolimulus peetae* (Pickett, 1984) for example, shows an exploration of extreme prosomal shield proportions at least at a single point in their development (Bicknell et al., 2022). Other examples are present among the grade belinurines of Belinuridae. *Belinurus bellulus* (König, 1825), *Parabelinurus lunatus* (Lamsdell, 2020) and *Macrobelinurus arcuatus* (Lamsdell, 2020), to name a few are all freshwater species with a prosomal shield with a relative width greater than the length resulting in a crescentic moon shape of the carapace. Even if information about the evolution of development is not available for these species, their wide prosomal shield proportion provides support for the hypothesis of freshwater environments being positively correlated with higher evolutionary rates in xiphosurans. The exploration of different prosomal shield proportions took place during an anatomical radiation as the group invaded freshwater environments (Lamsdell, 2016; Lamsdell 2021a).

The evolutionary scenario for the development of xiphosurans, depicted by the analyses accounting only for the intra-xiphosuran variability, shows a similar pattern to a random walk scenario of evolution (Figure 1C) or even a trend (Figure 1B) towards isometric growth. This is especially true in the case of Limulidae (Figure 6). However, this is not the case for Belinuridae, which appear to have had explored a wide range of allometric patterns, neither is it the case for Paleolimulidae, which, even if at a lower degree, did experience different developmental patterns (Figure 6). On the other hand, in the case of Limulidae, a broader phylogenetic perspective finds a general accordance with stasis (Figure 7), showing gradual evolutionary change around a relatively static average morphological position through time (Figure 1A). A broader phylogenetic perspective also reduces the perceived variability in the families Belinuridae and Paleolimulidae. This second analysis provides the appropriate systematic level for the study of developmental evolution in xiphosurans and their related aquatic euchelicerates. In other words, changes in the allometric growth of xiphosuran species are associated with different environments, but they are relatively minor compared to the different allometric patterns found in their closest relatives (Figure 7).

Uniting knowledge of non-Xiphosura euchelicerates with knowledge of Xiphosura development has improved the understanding of the evolution of Xiphosura allometric growth patterns. While this study supports the idea that the colonization of new environments has led to increased evolutionary rates for allometric growth in xiphosurans, the wider phylogenetic framework of our analyses suggest that the entirety of those changes were still somewhat limited when compared to changes seen more broadly in euchelicerates, as it represents a small portion of the total variability observed for euchelicerates. It appears clear that the evolution of xiphosurans cannot be pigeonholed into simplistic terminology such as "living fossils". Less impactful but more concrete definitions such as "gradual morphological evolution around a middle trait parameter" may better explain the observed pattern, at least regarding allometric growth. Furthermore, this research compares phylogeny-based evolutionary modelling without and with outgroups, emphasizing the importance of the latter to contextualize and to properly interpret the evolution for the target group.

Conclusion

The results show that the evolutionary rates of development of Xiphosura undergoes significant changes throughout the evolutionary history of the group, in concert with the adaptive radiation of the group as they exploit different environments through evolutionary time, and independently from their phylogenetic position. They also highlight the importance of considering outgroups when attributing evolutionary trends to a specific group. The magnitude of allometric growth among Xiphosurais was lower than in other euchelicerates with similar environmental affinities, which flattens what might otherwise appear as an explosion in diversity based solely on the observation of Xiphosura.

Data availability statement

The original contributions presented in the study are included in the article/Supplementary Material. Further inquiries can be directed to the corresponding authors.

Author contributions

LLu: Conceptualization, Data curation, Formal Analysis, Investigation, Methodology, Writing – original draft, Writing – review & editing. JA: Methodology, Supervision, Writing – review & editing. FS: Writing – review & editing. CH: Conceptualization,

Data curation, Supervision, Writing – review & editing. LLa: Conceptualization, Methodology, Writing – review & editing. RG: Conceptualization, Methodology, Writing – review & editing. JH: Supervision, Writing – review & editing, Conceptualization, Data curation. AD: Funding acquisition, Resources, Supervision, Writing – review & editing, Conceptualization.

Funding

LLu and this research were funded by the Swiss National Science Foundation, grant number 205321_179084 entitled "Arthropod Evolution during the Ordovician Radiation: Insights from the Fezouata Biota" awarded to AD and the additional Swiss National Science Foundation Mobility Grant awarded to LLu and AD. FS's work is funded by an SNF Ambizione Grant (no. PZ00P2_209102). LLa's research was financed by the Czech Science Foundation (project no. 20-23550Y) and was conducted with institutional support RVO 67985831 of the Institute of Geology of the Czech Academy of Sciences. RG was supported by NERC standard grant NE/T000813/1.

Acknowledgments

We thank Julien Clavel and his course at "Transmitting Science" for instruction and help with the R package mvMORPH, Claudia Baumgartner for revising this manuscript in an early stage as part of Lorenzo Lustri's PhD thesis, and Russell Bicknell for kindly providing data. Finally, we thank Paul Antony Selden and James Lamsdell for their insightful and informative reviews, which helped direct and improve the text.

Conflict of interest

The authors declare that the research was conducted in the absence of any commercial or financial relationships that could be construed as a potential conflict of interest.

The authors declared that they were an editorial board member of Frontiers, at the time of submission. This had no impact on the peer review process and the final decision.

Publisher's note

Supplementary material

The Supplementary Material for this article can be found online at: https://www.frontiersin.org/articles/10.3389/fevo.2023.1270429/full#supplementary-material

References

Avise, J. C., Nelson, W. S., and Sugita, H. (1994). A speciational history of "living fossils": molecular evolutionary patterns in horseshoe crabs. *Evolution* 48, 1986–2001. doi: 10.1111/j.1558-5646.1994.tb02228.x

Babcock, L. E., Merriam, D. F., and West, R. R. (2000). Paleolimulus, an early limuline (Xiphosurida), from Pennsylvanian-Permian Lagerst tten of Kansas and taphonomic comparison with modern Limulus. *Lethaia* 33, 129–141. doi: 10.1080/00241160025100017

Bennett, D. J., Sutton, M. D., and Turvey, S. T. (2018). Quantifying the living fossil concept. *Palaeontologia Electronica* 21 (1), 14A. doi: 10.26879/750

Bicknell, R. D. (2019). Xiphosurid from the Upper Permian of Tasmania confirms Palaeozoic origin of Austrolimulidae. *Palaeontologia Electronica* 22, 1–13. doi: 10.26879/1005

Bicknell, R. D., Amati, L., and Ortega-Hernández, J. (2019a). New insights into the evolution of lateral compound eyes in Palaeozoic horseshoe crabs. *Zoological J. Linn. Soc.* 187, 1061–1077. doi: 10.1093/zoolinnean/zlz065

Bicknell, R. D., Błażejowski, B., Wings, O., Hitij, T., and Botton, M. L. (2021a). Critical re-evaluation of Limulidae uncovers limited Limulus diversity. *Papers Palaeontology* 7, 1525–1556. doi: 10.1002/spp2.1352

Bicknell, R. D., Hecker, A., and Heyng, A. M. (2021b). New horseshoe crab fossil from Germany demonstrates post-Triassic extinction of Austrolimulidae. *Geological Magazine* 158, 1461–1471. doi: 10.1017/S0016756820001478

Bicknell, R. D., Kimmig, J., Budd, G. E., Legg, D. A., Bader, K. S., Haug, C., et al. (2022). Habitat and developmental constraints drove 330 million years of horseshoe crab evolution. *Biol. J. Linn. Soc.* 136, 155–172. doi: 10.1093/biolinnean/blab173

Bicknell, R. D., Naugolnykh, S. V., and Brougham, T. (2020). A reappraisal of Paleozoic horseshoe crabs from Russia and Ukraine. *Sci. Nat.* 107, 1–17. doi: 10.1007/s00114-020-01701-1

Bicknell, R. D., and Pates, S. (2020). Pictorial atlas of fossil and extant horseshoe crabs, with focus on Xiphosurida. *Front. Earth Sci.* 8, 98. doi: 10.3389/feart.2020.00098

Bicknell, R. D., Pates, S., and Botton, M. L. (2019ba). Euproops danae (Belinuridae) cluster confirms deep origin of gregarious behaviour in xiphosurids. *Arthropoda Selecta. Русский артроподологический журнал* 28 (4), 549–555. doi: 10.15298/arthsel.28.4.07

Bicknell, R. D., Žalohar, J., Miklavc, P., Celarc, B., Križnar, M., and Hitij, T. (2019b). A new limulid genus from the Strelovec Formation (Middle Triassic, Anisian) of northern Slovenia. *Geological Magazine* 156, 2017–2030. doi: 10.1017/S0016756819000323

Braddy, S. J. (2001). Eurypterid palaeoecology: palaeobiological, ichnological and comparative evidence for a "mass–moult–mate" hypothesis. *Palaeogeography Palaeoclimatology Palaeoecol.* 172, 115–132. doi: 10.1016/S0031-0182(01)00274-7

Briggs, D. E., Moore, R. A., Shultz, J. W., and Schweigert, G. (2005). Mineralization of soft-part anatomy and invading microbes in the horseshoe crab Mesolimulus from the Upper Jurassic Lagerstätte of Nusplingen, Germany. *Proc. R. Soc. B: Biol. Sci.* 272, 627–632. doi: 10.1098/rspb.2004.3006

Clavel, J., Escarguel, G., and Merceron, G. (2015). mvMORPH: an R package for fitting multivariate evolutionary models to morphometric data. *Methods Ecol. Evol.* 6 (11), 1311–1319.

Congreve, C. R., and Lamsdell, J. C. (2016). Implied weighting and its utility in palaeontological datasets: a study using modelled phylogenetic matrices. *Palaeontology* 59, 447–462. doi: 10.1111/pala.12236

Daley, A. C., and Drage, H. B. (2016). The fossil record of ecdysis, and trends in the moulting behaviour of trilobites. *Arthropod structure Dev.* 45 (2), 71–96. doi: 10.1016/j.asd.2015.09.004

Dunlop, J. A. (2010). Geological history and phylogeny of Chelicerata. *Arthropod structure Dev.* 39, 124–142. doi: 10.1016/j.asd.2010.01.003

Eldredge, N., Thompson, J. N., Brakefield, P. M., Gavrilets, S., Jablonski, D., Jackson, J. B., et al. (2005). The dynamics of evolutionary stasis. *Paleobiology* 31, 133–145. doi: 10.1666/0094-8373(2005)031[0133:TDOES]2.0.CO;2

Fusco, G., and Minelli, A. (2021). The development of arthropod segmentation across the embryonic/post-embryonic divide–an evolutionary perspective. *Front. Ecol. Evol.* 9, 622482. doi: 10.3389/fevo.2021.622482

Garamszegi, L. Z. (2014). *Modern phylogenetic comparative methods and their application in evolutionary biology: concepts and practice* (Berlin Heidelberg: Springer-Verlag).

Haug, J. T. (2019). Categories of developmental biology: Examples of ambiguities and how to deal with them. In: G. Fusco (ed), *Perspectives on Evolutionary and Developmental Biology. Essays for Alessandro Minelli. Festschrift 2.* (Padova: Padova University Press), 93–102.

Haug, C., and Haug, J. T. (2020). Untangling the Gordian knot—further resolving the super-species complex of 300-million-year-old xiphosurids by reconstructing their ontogeny. *Dev. Genes Evol.* 230, 13–26. doi: 10.1007/s00427-020-00648-7

Haug, C., and Rötzer, M. A. (2018a). The ontogeny of *Limulus polyphemus* (Xiphosura s. str., Eucheliceratа) revised: looking "under the skin". *Dev. Genes Evol.* 228, 49–61. doi: 10.1007/s00427-018-0603-1

Haug, C., and Rötzer, M. A. (2018b). The ontogeny of the 300 million year old xiphosuran *Euproops danae* (Eucheliceratа) and implications for resolving the *Euproops* species complex. *Dev. Genes Evol.* 228, 63–74. doi: 10.1007/s00427-018-0604-0

Haug, C., van Roy, P., Leipner, A., Funch, P., Rudkin, D. M., Schöllmann, L., et al. (2012). A holomorph approach to xiphosuran evolution—a case study on the ontogeny of *Euproops*. *Dev. Genes Evol.* 222, 253–268. doi: 10.1007/s00427-012-0407-7

Howard, R. J., Puttick, M. N., Edgecombe, G. D., and Lozano-Fernandez, J. (2020). Arachnid monophyly: Morphological, palaeontological and molecular support for a single terrestrialization within Chelicerata. *Arthropod Structure Dev.* 59, 100997. doi: 10.1016/j.asd.2020.100997

Huelsenbeck, J. P., and Ronquist, F. (2001). MRBAYES: Bayesian inference of phylogenetic trees. *Bioinformatics* 17, 754–755. doi: 10.1093/bioinformatics/17.8.754

Jegla, T. C., and Costlow, J. D. (1982). Temperature and salinity effects on developmental and early posthatch Limulus. In: J. Bonaventura, C. Bonaventura and S. Tesh (eds), *Physiology and Biology of Horseshoe Crabs*. Alan R. Liss, New York. pp 103–113.

Kaiser, D., and Schoppe, S. (2018). Postembryonic development of the Tri-spine Horseshoe Crab *Tachypleus tridentatus* (Merostomata: Xiphosura) in a nursery habitat in the Philippines. *J. Threatened Taxa* 10, 12916–12932. doi: 10.11609/jott.4125.10.15.12916-12932

Kin, A., and Błażejowski, B. (2014). The horseshoe crab of the genus *Limulus*: living fossil or stabilomorph? *PLoS One* 9, e108036. doi: 10.1371/journal.pone.0108036

König, C. D. E. (1825). *Icones fossilium sectiles*. Ed. G. B. Sowerby (London). 19 pp.

Lamsdell, J. C. (2016). Horseshoe crab phylogeny and independent colonizations of fresh water: ecological invasion as a driver for morphological innovation. *Palaeontology* 59, 181–194. doi: 10.1111/pala.12220

Lamsdell, J. C. (2021a). A new method for quantifying heterochrony in evolutionary lineages. *Paleobiology* 47, 1–22. doi: 10.7934/P2606

Lamsdell, J. C. (2020). The phylogeny and systematics of Xiphosura. *PeerJ* 8, e10431. doi: 10.7717/peerj.10431

Lamsdell, J. C. (2021b). The conquest of spaces: exploring drivers of morphological shifts through phylogenetic palaeoecology. *Palaeogeography Palaeoclimatology Palaeoecol.* 583, 110672. doi: 10.1016/j.palaeo.2021.110672

Lamsdell, J. C., Gunderson, G. O., and Meyer, R. C. (2019). A common arthropod from the Late Ordovician Big Hill Lagerstätte (Michigan) reveals an unexpected ecological diversity within Chasmataspidida. *BMC Evolutionary Biol.* 19, 1–24. doi: 10.1186/s12862-018-1329-4

Lamsdell, J. C., Isotalo, P. A., Rudkin, D. M., and Martin, M. J. (2023). A new species of the Ordovician horseshoe crab Lunataspis. *Geological Magazine* 160 (1), 167–171. doi: 10.1017/S0016756822000875

Lamsdell, J. C., and McKenzie, S. C. (2015). Tachypleus Syriacus (Woodward)—a sexually dimorphic Cretaceous crown limulid reveals underestimated horseshoe crab divergence times. *Organisms Diversity Evol.* 15, 681–693. doi: 10.1007/s13127-015-0229-3

Lamsdell, J. C., and Selden, P. A. (2013). Babes in the wood–a unique window into sea scorpion ontogeny. *BMC Evolutionary Biol.* 13, 1–46. doi: 10.1186/1471-2148-13-98

Lewis, P. O. (2001). A likelihood approach to estimating phylogeny from discrete morphological character data. *Systematic Biol.* 50, 913–925. doi: 10.1080/106351501753462876

Lozano-Fernandez, J., Tanner, A. R., Puttick, M. N., Vinther, J., Edgecombe, G. D., and Pisani, D. (2020). A Cambrian–Ordovician terrestrialization of arachnids. *Front. Genet.* 182. doi: 10.3389/fgene.2020.00182

Lustri, L., Laibl, L., and Bicknell, R. D. (2021). A revision of Prolimulus woodwardi Fritsch 1899 with comparison to other highly paedomorphic belinurids. *PeerJ* 9, e10980. doi: 10.7717/peerj.10980

Minelli, A., Boxshall, G., and Fusco, G. (2016). *Arthropod biology and evolution* (Berlin Heidelberg: Springer-Verlag).

Naugolnykh, S. V., and Bicknell, R. D. (2022). Ecology, morphology and ontogeny of Paleolimulus kunguricus—a horseshoe crab from the Kungurian (Cisuralian) of the Cis-Urals, Russia. *LETHAIA* 55, 1–13. doi: 10.1111/let.12451

Paradis, E., and Schliep, K. (2019). ape 5.0: an environment for modern phylogenetics and evolutionary analyses in R. *Bioinformatics* 35(3), 526–528.

Pickett, J. W. (1984). A new freshwater Limuloid from the Middle Triassic of the New South Wales. *Palaeontology* 27 (3), 609–621.

Racheboeuf, P. R., Vannier, J., and Anderson, L. I. (2002). A new three-dimensionally preserved xiphosuran chelicerate from the Montceau-Les-Mines Lagerstätte (Carboniferous, France). *Palaeontology* 45, 125–147. doi: 10.1111/1475-4983.00230

Revell, L. J. (2012). phytools: an R package for phylogenetic comparative biology (and other things). *Methods Ecol. Evol.* (2), 217–223.

Riek, E. F. (1955). A new xiphosuran from the Triassic sediments at Brookvale. *New South Wales. Records Aust. Museum* 23 (5), 281–282. doi: 10.3853/j.0067-1975.23.1955.637

Rudkin, D., and Young, G. (2009). "Horseshoe crabs–an ancient ancestry revealed," in *Biology and conservation of horseshoe crabs*, vol. 25-44. (New York: Springer), Custom 7.

Rudkin, D. M., Young, G. A., and Nowlan, G. S. (2008). The oldest horseshoe crab: a new xiphosurid from Late Ordovician Konservat-Lagerstätten deposits, Manitoba, Canada. *Palaeontology* 51, 1–9. doi: 10.1111/j.1475-4983.2007.00746.x

Ruebenstahl, A., Ciurca, J. S.J., and Briggs, D. E. (2021). A giant *Eurypterus* from the silurian (Pridoli) bertie group of North America. *Bull. Peabody Museum Natural History* 62, 3–13.

Scholl, G. (1977). Beiträge zur Embryonalentwicklung von Limulus polyphemus L.(Chelicerata, Xiphosura). *Zoomorphologie* 86, 99–154. doi: 10.1007/BF00995521

Schultka, S. (2000). Zur Palökologie der Euproopiden im Nordwestdeutschen Oberkarbon. *Fossil Rec.* 3, 87–98. doi: 10.5194/fr-3-87-2000

Sekiguchi, K., Seshimo, H., and Sugita, H. (1988). Post-embryonic development of the horseshoe crab. *Biol. Bull.* 174, 337–345. doi: 10.2307/1541959

Shuster, J. C. N., and Sekiguchi, K. (2003). Growing up takes about ten years and eighteen stages. In: C. N. Shuster Jr, R. B. Barlow and H. J. Brockmann, eds. *The American Horseshoe Crab*, Harvard University Press, Cambridge, pp. 103–132.

Simpson, G. G. (1944). *Tempo and mode in evolution* (New York: Columbia University Press).

Stoermer, L. (1952). Phylogeny and taxonomy of fossil horseshoe crabs. *J. Paleontology* 26, 630–640.

Tashman, J. N., Feldmann, R. M., and Schweitzer, C. E. (2019). Morphological variation in the Pennsylvanian horseshoe crab *Euproops danae* (Meek & Worthen 1865)(Xiphosurida, Euproopidae) from the lower Mercer Shale, Windber, Pennsylvania, USA. *J. Crustacean Biol.* 39, 396–406. doi: 10.1093/jcbiol/ruz030

Tëmkin, I., and Eldredge, N. (2015). "Networks and hierarchies: Approaching complexity in evolutionary theory," in *Macroevolution*, vol. 183-226. (Switzerland: Springer International Publishing), Custom 7.

van Roy, P., Briggs, D. E., and Gaines, R. R. (2015). The Fezouata fossils of Morocco; an extraordinary record of marine life in the Early Ordovician. *J. Geological Soc.* 172, 541–549. doi: 10.1144/jgs2015-017

frontiers | Frontiers in Ecology and Evolution

TYPE Original Research
PUBLISHED 23 October 2023
DOI 10.3389/fevo.2023.1290063

OPEN ACCESS

EDITED BY
Haijun Song,
China University of Geosciences Wuhan, China

REVIEWED BY
Przemyslaw Gorzelak,
Polish Academy of Sciences, Poland
James Thomka,
State University of New York College at Plattsburgh, United States

*CORRESPONDENCE
Christophe Dupichaud
c.dupichaud@gmail.com
Farid Saleh
farid.saleh@unil.ch

RECEIVED 06 September 2023
ACCEPTED 04 October 2023
PUBLISHED 23 October 2023

CITATION
Dupichaud C, Lefebvre B, Milne CH, Mooi R, Nohejlová M, Roch R, Saleh F and Zamora S (2023) Solutan echinoderms from the Fezouata Shale Lagerstätte (Lower Ordovician, Morocco): diversity, exceptional preservation, and palaeoecological implications. *Front. Ecol. Evol.* 11:1290063. doi: 10.3389/fevo.2023.1290063

Solutan echinoderms from the Fezouata Shale Lagerstätte (Lower Ordovician, Morocco): diversity, exceptional preservation, and palaeoecological implications

Christophe Dupichaud[1]*, Bertrand Lefebvre[1], Claire H. Milne[2], Rich Mooi[3], Martina Nohejlová[4], Renaud Roch[5], Farid Saleh[6]* and Samuel Zamora[7,8]

[1]Unité Mixte de Recherche (UMR) 5276 Laboratoire de Géologie de Lyon, Terre, Planétes, Environnement (LGLTPE), Univ Lyon, Univ Lyon 1, Ecole Normale Supérieure de Lyon (ENSL), Centre National de la Recherche Scientifique (CNRS), Villeurbanne, France, [2]Department of Classics, University of California, Berkeley, Berkeley, CA, United States, [3]Department of Invertebrate Zoology and Geology, California Academy of Sciences, San Francisco, CA, United States, [4]Czech Geological Survey, Prague, Czechia, [5]Jurassica Museum, Porrentruy, Switzerland, [6]Institute of Earth Sciences (ISTE), University of Lausanne, Geopolis, Lausanne, Switzerland, [7]Instituto Geológico y Minero de Espana (IGME-CSIC), Zaragoza, Spain, [8]Grupo Aragosaurus-Instituto Universitario de Investigación en Ciencias Ambientales de Aragón (IUCA), Universidad de Zaragoza, Zaragoza, Spain

In the Lower Ordovician of Morocco, solutan echinoderms are relatively common, locally abundant, geographically widespread (Central and Eastern Anti-Atlas), and biostratigraphically long-ranging (late Tremadocian–mid Floian) components of the Fezouata Biota. The lower part of the Fezouata Shale (late Tremadocian) yielded one specimen, here tentatively identified as a *Castericystis*-like syringocrinid, with exceptionally preserved internal soft parts presumably corresponding to the distal region of the gut. Most solutan remains from the Fezouata Shale are assigned to *Plasiacystis mobilis*, which was already known from the late Tremadocian of France and the Darriwilian of the Czech Republic and United Kingdom. Several isolated dististeles provisionally identified as *Plasiacystis* sp. may belong to large individuals of *P. mobilis* or a new taxon. Several specimens of late Tremadocian solutans from the Fezouata Shale, morphologically intermediate between *Minervaecystis vidali* (late Tremadocian, France) and *Plasiacystis mobilis*, are assigned to *Nimchacystis agterbosi* gen. et sp. nov. The diagnosis of the syringocrinid family Minervaecystidae is modified to include the four genera *Minervaecystis*, *Nimchacystis*, *Pahvanticystis*, and *Plasiacystis*, all characterised by an ovoid theca, a laterally inserted feeding appendage, and a twisted, flattened dististele. Minervaecystids are interpreted as active epibenthic *detritus feeders*, using their dististele to crawl on soft substrates. The newly described solutan taxa highlight that the benthic communities of Fezouata Biota are more diverse than what was previously described.

KEYWORDS

Echinodermata, Soluta, Fezouata Shale, Morocco, Ordovician, systematics

Introduction

The Early Ordovician represents a critical interval in the diversification of echinoderms, with the transition from low diversity, relatively cosmopolitan assemblages dominated by eocrinoids, glyptocystitid rhombiferans, and stylophorans (Furongian–mid Tremadocian), to more diverse faunas (late Tremadocian and onwards) characterised by the onset of new classes, typical of Sepkoski's Palaeozoic Evolutionary Fauna (e.g., asteroids, crinoids, diploporitans, and ophiuroids) (Sumrall et al., 1997; Lefebvre et al., 2013). Morocco (Anti-Atlas), along with France (Montagne Noire) and western USA (Nevada, Utah), is one of the few places in the world yielding abundant echinoderm faunas documenting this major evolutionary transition (Sprinkle and Guensburg, 2004; Lefebvre et al., 2013; Lefebvre et al., 2016). While faunas from North America (Laurentia) occur in carbonate-dominated substrates from low latitudes, France and Morocco (Gondwana) offer a good opportunity to understand such transitions at higher latitudes in siliciclastic-dominated substrates. The Anti-Atlas is also the only region known so far where exceptionally preserved soft parts (ambulacral system and gut) were documented in Early Ordovician echinoderms (Lefebvre et al., 2019; Saleh et al., 2021; Dupichaud and Lefebvre, 2022). Exceptionally preserved soft parts can be particularly important in the case of extinct classes, such as solutans, whose anatomy and phylogenetic positions within the phylum Echinodermata are debated (see, e.g., David et al., 2000; Smith, 2005; Zamora and Rahman, 2014; Lefebvre et al., 2019). Solutans are considered either basal, pre-radial echinoderms (Smith, 2005; Rahman and Lintz, 2012; Zamora and Rahman, 2014) or regular blastozoans, closely related to gogiid eocrinoids (e.g., David et al., 2000; Lefebvre and Lerosey-Aubril, 2018; Nohejlová and Lefebvre, 2022).

The class Soluta is a small, long-lived clade of echinoderms (Drumian–Emsian) characterised by a single feeding appendage, a more or less flattened theca, and a stem-like appendage (homoiostele) used for permanent attachment to the sea floor in plesiomorphic forms (e.g., *Coleicarpus*; Ubaghs and Robison, 1988; Daley, 1996) but generally modified into a locomotory device in most taxa (e.g., Sprinkle and Guensburg, 1997; Rahman and Lintz, 2012; Noailles et al., 2014). The fossil record suggests a Laurentian origin for solutans, with all their earliest occurrences so far documented exclusively in North America (Lefebvre and Lerosey-Aubril, 2018). During the Furongian–Tremadocian interval, solutans expanded to South China (Zamora et al., 2013) and high-latitude Gondwanan regions, such as the Anti-Atlas (Lefebvre et al., 2016; Dupichaud and Lefebvre, 2022) and the Montagne Noire (Thoral, 1935; Ubaghs, 1970; Dupichaud et al., 2023).

In the Anti-Atlas, the Fezouata Shale (Tremadocian–Floian) yielded extremely abundant remains of solutans (Lefebvre et al., 2016; Saleh et al., 2022a), some of which had putative soft parts preserved (Saleh et al., 2021; Dupichaud and Lefebvre, 2022). However, while the morphology and systematics of solutans from the Montagne Noire have been thoroughly investigated (Ubaghs, 1970; Dupichaud et al., 2023), no comparable work has been performed so far on those from the Fezouata Shale. Consequently, the aim of this paper is to present the first detailed systematic overview of solutans from the Fezouata Biota and to discuss their taphonomy, palaeoecology, and palaeobiogeographic affinities.

Geological setting

In the Anti-Atlas, remains of Early Ordovician solutans were found in distinct stratigraphic levels of the Fezouata Shale in several localities belonging to three distinct geographic areas (Figures 1B, C, D). Most solutan occurrences are situated in the Ternata Plain, north of Zagora, in the Central Anti-Atlas. In this area, the Fezouata Shale corresponds to a *ca* 900-m-thick, relatively monotonous siliciclastic sequence consisting mainly of siltstones, but with intercalated sandstone levels towards the top, near the transition with the overlying Zini Formation (Destombes et al., 1985; Vaucher et al., 2017). In the Zagora area, the Fezouata Shale corresponds to a storm-dominated, tide-modulated succession deposited on a relatively shallow shelf that dipped gently to the North West (in modern orientation) (Vaucher et al., 2017; Saleh et al., 2020). In the Ternata plain, the stratigraphic position of each solutan-bearing locality could be determined based on a precise biostratigraphic scheme using acritarchs, chitinozoans, conodonts, and graptolites (Lefebvre et al., 2018).

In the Zagora area, the stratigraphically oldest solutan remains (*Sagenograptus murrayi* Zone, late Tremadocian) were found in green micaceous siltstones exposed at Oued Beni Zoli (Z-F5; Figures 1A, D, 2D) and the nearby locality of Tinzouline (Z-F5[2]; Figures 1A, D). Both sites yielded a particularly abundant and diverse fauna dominated by gastropods (*Pelecyogyra*), rhombiferans (*Macrocystella*), and trilobites (*Ampyx*, *Asaphellus*, *Ceraurinella*, *Colpocoryphe*, *Euloma*, *Parabathycheilus*, and *Toletanaspis*) (Ebbestad, 2016; Martin et al., 2016; Kouraïss et al., 2019). Bivalves (*Redonia*), brachiopods, cephalopods (*Polymeres*), conulariids, eocrinoids (*Balantiocystis*), graptolites, hyolithids, solutans, somasteroids, and stylophorans are minor elements of the assemblage (Kröger and Lefebvre, 2012; Lefebvre et al., 2016). Solutans, like most other organisms from Z-F5, are preserved intact or slightly disarticulated, suggesting *in-situ* burial by storm deposits at or slightly below the storm wave base (Martin et al., 2016; Kouraïss et al., 2019).

In recent years, several fully articulated specimens of solutans were found in fine beige siltstones at Tignit (Z-F17b), associated with a low-diversity assemblage comprising the enigmatic fossil *Webbyites felix* Muir and Gutiérrez-Marco, 2023. This level is probably laterally equivalent to the nearby Z-F6 locality (Oued Ouaoufraout), which similarly yielded several specimens of *Webbyites*, and was assigned to the uppermost part of the *S. murrayi* Zone (late Tremadocian) (Muir and Gutiérrez-Marco, 2023). The preservation of fully articulated specimens of solutans and *Webbyites* implies that they were buried by distal storm deposits in an otherwise quiet, relatively distal setting, below the storm wave base (Saleh et al., 2020; Saleh et al., 2021). The precise

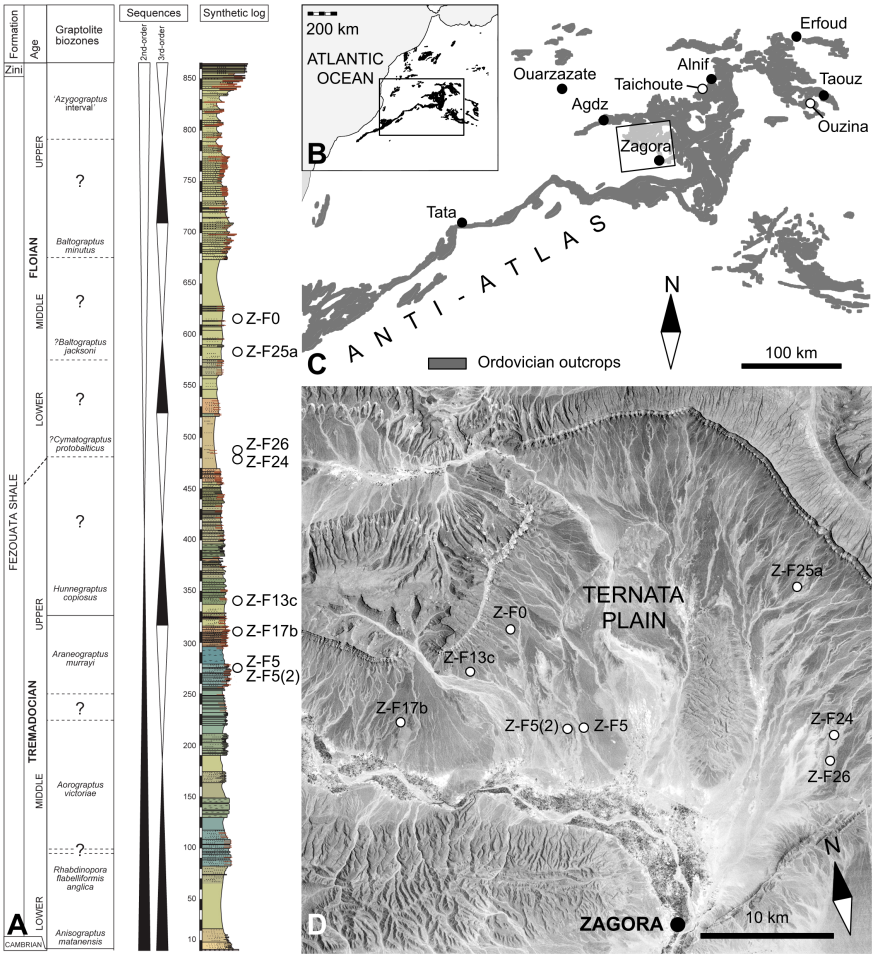

FIGURE 1
Stratigraphic and geographic occurrences of solutan echinoderms in the Fezouata Shale (Lower Ordovician), Anti-Atlas, Morocco. **(A)** Stratigraphic position of solutan localities in the Ternata plain (Zagora area, Central Anti-Atlas). Graptolite biozonation, eustatic sequences, and synthetic log (left columns) are based on Lefebvre et al. (2016); Lefebvre et al. (2018). Colours on the log correspond to those of the rocks on the outcrop. **(B)** Simplified geological map of northwestern Africa showing the distribution of Ordovician rocks and the location of the Anti-Atlas. **(C)** Simplified geological map of the Anti-Atlas showing the distribution of Ordovician rocks and the location of the three main areas yielding Early Ordovician solutan remains: Ternata plain (Zagora area), western Maïder (Taichoute), and Taouz Massif (Ouzina). **(D)** Landsat view of the Ternata plain (Zagora area, Central Anti-Atlas) showing the location of all main Early Ordovician solutan localities mentioned in the text and specified on the log; photograph courtesy of the U.S. Geological Survey.

locality and stratigraphic position of the single known specimen of solutan with exceptionally preserved soft parts (Figure 3) are unknown. However, the associated lithology (fine beige siltstones, Figure 2C) strongly suggests that it was found in the same stratigraphic interval as Z-F6 and Z-F17b, i.e., in the uppermost part of the lower interval with exceptional preservation identified by Lefebvre et al. (2018).

Disarticulated remains of solutans (dististeles and isolated thecal plates) are relatively common at locality Z-F13c, which is situated in the same area as Z-F6 and Z-F17b (western part of the Ternata plain; Figures 1A, D), but in stratigraphically younger levels belonging to the *Hunnegraptus copiosus* Zone (latest Tremadocian) (Lefebvre et al., 2016). The pistachio micaceous siltstones of Z-F13c also yielded a relatively diverse benthic assemblage consisting of disarticulated skeletal remains belonging to bivalves, brachiopods, conulariids (*Eoconularia*), and trilobites (*Ampyx*, *Asaphellus*, and *Geragnostus*). Taphonomic features suggest relatively proximal, well-oxygenated environmental conditions at, or more likely above, the storm wave base (Martin et al., 2016).

The next two solutan localities, Z-F24 and Z-F26, are geographically (southeastern part of the Ternata plain) and stratigraphically (*Cymatograptus*? *protobalticus* Zone, early Floian) very close to each other (Figures 1A, D). However, these localities have yielded distinct assemblages, probably reflecting different environmental conditions. In Z-F24, solutan remains (mostly isolated dististeles) are abundant in beige micaceous siltstones, associated with a relatively low diversity assemblage comprising mostly cephalopod phragmocones (*Destombesiceras*, *Rioceras*)? and large trilobite elements (cephalons and pygidiums), along with some rare bivalves (*Ekaterodonta* and *Redonia*), crinoids (*Iocrinus*), edrioasteroids (*Argodiscus*), eocrinoids, gastropods (*Carcassonnella*), hyolithids, and mitrates (*Anatifopsis*) (Kröger and Lefebvre, 2012; Lefebvre et al., 2016; Figure 2A). The strong disarticulation and sometimes fragmentation of most skeletal

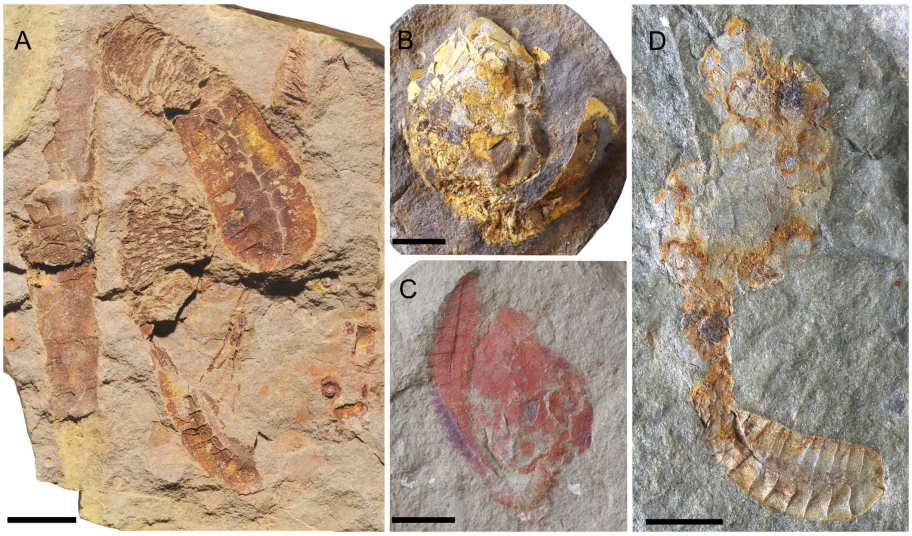

FIGURE 2
Diversity of preservation. **(A)** MHNM.15690.216, *Plasiacystis* sp. from the Z-F24 locality (early Floian), preserved in storm-generated accumulations. **(B)** MPZ.2022.927, *Plasiacystis mobilis* from the Taichoute locality (middle Floian), preserved in a silico-aluminous concretion. **(C)** UCBL-FSL.713058, *Nimchacystis agterbosi* from the Z-F17b locality (late Tremadocian), preserved in fine beige siltstones. **(D)** MHNM.15690.200, *Plasiacystis mobilis* from the Z-F5 locality (late Tremadocian), preserved in green micaceous siltstones. Scale bars = 10 mm. Photographs by Vincent Perrier.

remains, as well as their occurrence in lenticular levels, are indicative of storm-generated accumulations generated in relatively proximal settings. This interpretation is further supported by the frequent current-induced orientation of cephalopod and hyolithid conchs (Kröger and Lefebvre, 2012). In contrast, the extremely fine, micaceous beige siltstones of Z-F26 (Toumiat) have yielded a particularly diverse benthic assemblage dominated by bivalves (e.g., *Babinka*, *Coxiconchia*, *Ekaterodonta*, *Praenucula*, and *Redonia*), gastropods (*Lesueurilla*), tergomyans (*Carcassonnella*), and trilobites (e.g., *Ampyx*, *Asaphellus*, *Parabathycheilus*, and *Toletanaspis*) (Ebbestad, 2016; Martin et al., 2016; Polechová, 2016). Other faunal elements comprise relatively common cephalopods (*Destombesiceras*), eocrinoids (*Balantiocystis*), and cornutes (*Sokkaejaecystis*) associated with rare asterozoans, brachiopods, conulariids, crinoids (*Ramseyocrinus*)?, edrioasteroids (*Argodiscus*), graptolites, mitrates (*Balanocystites*), and solutans (Kröger and Lefebvre, 2012; Lefebvre et al., 2016). Most skeletal remains are fully articulated, with some bivalves preserved in a butterfly position (Polechová, 2016). These taphonomic features are suggestive of quiet environmental conditions, below the storm wave base.

Rare, isolated dististeles of *Plasiacystis* collected in the beige micaceous siltstones of Z-F0 (Jbel Bou Zeroual; Figures 1A, D) and Z-F25a (Bou Chrebeb; Figures 1A, D) represent the youngest known occurrences of solutans in the Ternata plain (? *Baltograptus jacksoni* Zone, middle Floian). These two sites have yielded relatively similar, extremely abundant, and very diverse benthic assemblages dominated by bivalves (e.g., *Babinka*, *Coxiconchia*, and *Redonia*), gastropods (*Lesueurilla* and *Sinuites*), tergomyans (*Carcassonnella* and *Thoralispira*), and trilobites (*Agerina*, *Ampyx*, *Asaphellus*, *Colpocoryphe*, *Euloma*, *Parabathycheilus*, *Prionocheilus*, and *Toletanaspis*) (Ebbestad, 2016; Martin et al., 2016; Polechová, 2016). The associated fauna includes relatively common brachiopods, cephalopods (*Polymeres*), conulariids (*Archaeoconularia* and *Eoconularia*), cornutes (*Sokkaejaecystis*), eocrinoids (*Balantiocystis*), graptolites, and hyolithids, as well as rare demosponges (*Pirania*), edrioasteroids (*Argodiscus*), anomalocystitid mitrates, and possibly also the pterobranch()? *W. felix* (Kröger and Lefebvre, 2012; Botting, 2016; Lefebvre et al., 2016; Muir and Gutiérrez-Marco, 2023). In both sites, the occurrence of exceptionally preserved organisms (e.g., demosponges and *Webbyites*) associated with articulated remains of skeletonised taxa (e.g., trilobites) suggests relatively quiet environmental conditions at or slightly below the storm wave base (Martin et al., 2016).

In the Anti-Atlas, Early Ordovician solutan remains were also found in two other areas outside of the Ternata plain. In the western Maïder, at Taichoute (approximately 18 km SW of Alnif; Figure 1C), a concretion-bearing level (i.e., assemblage a1 in Saleh et al., 2022a) yielded a *Plasiacystis*-dominated assemblage (Figure 2B) that could be assigned to the middle Floian based on the presence of the graptolite *Baltograptus deflexus* (Saleh et al., 2022a). Other faunal elements include brachiopods, cephalopods (*Bathmoceras*), gastropods (*Lesueurilla*), mitrates (*Anatifopsis*), glyptocystitid rhombiferans (*Macrocystella*), somasteroids, and trilobites. Contrary to the situation in localities from the Ternata plain (see above), fossil remains in Taichoute are preserved three-dimensionally in silico-aluminous concretions. Most solutans are intact and complete (feeding appendage, theca, and homoiostele), though frequently slightly disarticulated and collapsed. Their preservation suggests that concretions were probably initiated around decaying carcasses exposed on the sea floor in relatively quiet, distal environments, below the storm wave base (Loi and Dabard, 1999; Loi and Dabard, 2002; Saleh et al., 2022a).

FIGURE 3
Photograph of CASG 72938 showing preserved soft tissues as dark masses. **(A)** Part. **(B)** Counterpart. Scale bar = 10 mm. Photographs by Vincent Perrier.

Similarly preserved solutan remains were found in the Taouz Massif (eastern Anti-Atlas) at Destombes' locality 1540 (Figure 1C; Ouzina, in Havlíček, 1971). Destombes (2006) proposed an early Floian age for this concretion-bearing level. However, contrary to the situation in Taichoute, the Ouzina assemblage is largely dominated by the glyptocystitid rhombiferan *Macrocystella bohemica*, while *Plasiacystis mobilis* is relatively rare (Lefebvre et al., 2016). Other members of the Ouzina assemblage include brachiopods (*Plectorthis*), cephalopods, conulariids, hyolithids (*Cavernolites* and *Elegantilites*), mitrates (*Anatifopsis*), somasteroids, tergomyans (*Thoralispira*), and trilobites (e.g., *Ampyx* and Asaphidae) (Havlíček, 1971; Marek, 1983; Destombes, 2006; Lefebvre et al., 2016). As in Taichoute, it is very likely that this assemblage was autochthonous and associated with relatively distal environmental conditions below the storm wave base.

Materials and methods

Due to preservation as external and internal moulds (imprints) in the rock, fossils were cast with latex to reveal their original aspect. Latex casts were whitened with ammonium chloride (NH_4Cl)

sublimated for observation and imaging purposes. Fossils and latex casts were photographed using a Canon EOS 5SD R equipped with a Canon 100-mm macro lens and a Canon EOS 70D equipped with an EF-S 60-mm macro lens. Latex casts were observed and drawn with a stereomicroscope Zeiss Discovery.V8 equipped with a camera lucida for drawings. Drawings were reworked digitally with the software Krita v5.1.5. Measurements were made with the software ImageJ.

Over 150 specimens were observed based on material belonging to the following public institutions: Cadi-Ayyad University, Marrakesh, Morocco (AA); Natural History Museum, London, UK (BMNHUK); geological collections of the California Academy of Sciences, San Francisco, USA (CASG); Muséum d'Histoire Naturelle, Marseille, France (MHNM); Muséum d'Histoire Naturelle, Nantes, France (MHNN); Musée des Confluences, Lyon, France (ML); Museo de Ciencias Naturales de la Universidad de Zaragoza, Zaragoza, Spain (MPZ); Senckenberg Museum, Frankfurt, Germany (SMF); palaeontological collections of Lyon 1 University, Villeurbanne, France (UCBL-FSL); and Yale Peabody Museum, New Haven, USA (YPM). For comparative purposes, additional material belonging to the National Museum, Prague, Czech Republic (NMP), and several private collections in the Czech Republic, France, and Morocco was also considered.

Systematic palaeontology

Phylum **Echinodermata** Klein, 1778

Class **Soluta** Jaekel, 1901

Remarks: The systematic subdivision of solutans into two main orders (Dendrocystitida and Syringocrinida) based on the morphology of their homoiostele follows Noailles et al. (2014). Similarly, descriptive morphological terms used below are those used in all recent descriptions of solutans (e.g., Lefebvre et al., 2012; Rahman and Lintz, 2012; Noailles et al., 2014; Lefebvre and Lerosey-Aubril, 2018; Dupichaud and Lefebvre, 2022; Nohejlová and Lefebvre, 2022; Rozhnov, 2022; Dupichaud et al., 2023; Zamora and Gutiérrez-Marco, 2023). Discussion of the phylogenetic position of solutans within the phylum Echinodermata is beyond the scope of this paper.

Order **Syringocrinida** Noailles et al. 2014

Family **Minervaecystidae** Ubaghs, 1970

Emended diagnosis: Family of syringocrinids with ovoid theca lacking lobation or marginal frame. No visible differentiation between the lower and upper thecal sides. Thecal plates thin, smooth, polygonal, tesselated, and irregular in both shape and size. Feeding appendage emerging abruptly on the lateral side of the theca, relatively far from the apex. Small, cone-shaped anal pyramid on opposite, lateral edge of the theca, close to homoiostele insertion.

Remarks: The family Minervaecystidae was originally erected by Ubaghs (1970) to include *Minervaecystis vidali* (Thoral, 1935), from the Saint-Chinian Formation (late Tremadocian, Montagne Noire, France), as well as isolated homoiosteles from the Whipple Cave Formation (Cambrian Stage 10, Nevada, USA; Ubaghs, 1963). The diagnosis of this family is emended here to include all syringocrinids (i.e., solutans with a flattened, oblique dististele) possessing a large ovoid theca with a laterally inserted feeding appendage. In this expanded definition, the family Minervaecystidae includes the four genera *Minervaecystis* Ubaghs, 1970, *Nimchacystis* gen. nov., *Pahvanticystis* Lefebvre and Lerosey-Aubril, 2018, and *Plasiacystis* Prokop and Petr, 2003.

The morphology of the earliest known member of the family, *Pahvanticystis utahensis* (Weeks Formation, Guzhangian, Utah, USA), suggests that minervaecystids probably originated from a *Castericystis*-like ancestor. *Pahvanticystis* differs from other minervaecystids in the more anterior insertion of its feeding appendage along the antanal thecal side (Lefebvre and Lerosey-Aubril, 2018). The morphology of the isolated minervaecystid homoiosteles from the late Cambrian of Utah is very close to that of *Minervaecystis* (i.e., similar proxistele consisting of over 20, regular tetramerous rings; Ubaghs, 1963; Sumrall et al., 1997). However, the absence of thecal remains and precise information on the location of the feeding appendage prevents any identification at generic level. Similarly, as yet undescribed putative minervaecystids have been also reported from the Wah Wah Formation (late Floian) of Utah, a more precise taxonomic assignment is so far impossible due to the absence of information concerning their morphology (Sprinkle and Guensburg, 1993; Dupichaud et al., 2023).

The three minervaecystid genera *Minervaecystis*, *Nimchacystis* gen. nov., and *Plasiacystis* have almost identical thecae and feeding appendages, but they differ strongly in the morphology of their homoiosteles. In *Minervaecystis*, the proxistele is elongate and consists of numerous (over 20) regular telescopic rings, each made of four plates (Thoral, 1935; Ubaghs, 1970). Its long, flattened dististele is relatively narrow, stem-like, markedly curved, and bears several comb-like spikes along its keeled, concave (right) margin (Ubaghs, 1970; Dupichaud et al., 2023). *Plasiacystis* is a long-lived genus known from the Saint-Chinian Formation (late Tremadocian, France), the Fezouata Shale (late Tremadocian–middle Floian, Morocco), the Hope Shale (Darriwilian, UK), and the Šarká Formation (Darriwilian, Czech Republic) (Jaekel, 1918; Prokop and Petr, 2003; Lefebvre et al., 2012; Lefebvre et al., 2016; Dupichaud and Lefebvre, 2022; Dupichaud et al., 2023). Its proxistele is not organised into regular rings, being a flexible cylindrical structure made of numerous, imbricate scale-like elements. In *Plasiacystis*, the dististele corresponds to a short, broad, paddle-like structure, with a wide, rounded distal extremity (Prokop and Petr, 2003; Lefebvre et al., 2012; Dupichaud and Lefebvre, 2022; Dupichaud et al., 2023). Because of the unusual "beaver-tailed" morphology of its dististele, *Plasiacystis* was originally placed in a distinct family, Plasiacystidae (Prokop and Petr, 2003; Lefebvre et al., 2012). However, the discovery of syringocrinids (*Nimchacystis* gen. nov.) with a homoiostele morphologically intermediate between those of *Minervaecystis* and *Plasiacystis* (see below) suggests instead that they all belong to the same clade. Consequently, *Nimchacystis* gen. nov. and *Plasiacystis* are here assigned to the family Minervaecystidae.

The reevaluation of the morphology of *Dehmicystis* Caster, 1968, based on new material from the lower Ludlow (Silurian) of the Central Iberian Zone (Spain; Zamora and Gutiérrez-Marco, 2023)

questions its systematic position within the class Soluta. *Dehmicystis* was originally described based on a few poorly preserved, strongly flattened, and tectonically distorted specimens from the Hunsrück Shale (Emsian) of Germany (Dehm, 1934; Rahman and Lintz, 2012). *Dehmicystis* has usually been considered a typical dendrocystitid solutan (see, e.g., Caster, 1968; Rahman and Lintz, 2012; Noailles et al., 2014; Zamora and Gutiérrez-Marco, 2023). However, new morphological data (e.g., large ovoid, non-lobate theca; laterally inserted feeding appendage; keeled dististele; Rahman and Lintz, 2012; Zamora and Gutiérrez-Marco, 2023) suggest either syringocrinid affinities or a morphological convergence of some Siluro-Devonian dendrocystitids with Cambro-Ordovician syringocrinids, possibly resulting from similar modes of life.

Genus ***Plasiacystis*** Prokop and Petr, 2003

Type species: *Plasiacystis mobilis* Prokop and Petr, 2003, by monotypy.

Emended diagnosis. Genus of syringocrinid solutan with very flexible, cylindrical proxistele composed of numerous, unorganised, imbricate, scale-like elements. Proxistele and dististele of nearly equal lengths. Dististele comprising two series of large, opposite plates forming short, wide, rigid, flattened paddle with rounded distal extremity. One side of dististele frequently ornamented with single spike-shaped knob placed on the convex half.

Remarks: The genus *Plasiacystis* was originally described as a very unusual solutan with a large, polyplated, flattened theca, conspicuously elongate proxistele made of numerous scale-like elements, a short paddle-like dististele, and, possibly, no feeding appendage (Prokop and Petr, 2003). This initial reconstruction was based on relatively abundant material preserved in siliceous concretions from the Šarká and Dobrotivá formations (Darriwilian) of the Prague Basin, Czech Republic. However, the reevaluation of this material showed that it was a mixture of at least three different echinoderm taxa (Lefebvre et al., 2012). The generic name *Plasiacystis* was retained for the holotype and some other specimens, all from the Šarká Formation and corresponding to regular solutans with a feeding appendage, relatively ovoid theca, and distinctive paddle-like dististele (Lefebvre et al., 2012). Other portions of the original reconstruction of *Plasiacystis* were assigned to another, yet undescribed solutan (theca only) and to a rhenopyrgid edrioasteroid (proxistele only) (Lefebvre et al., 2012).

Plasiacystis mobilis Prokop and Petr, 2003

Figures 2B, D, 4–7

Holotype: NMP.L.13216.

Type level: Šarká Formation, early–middle Darriwilian (Middle Ordovician).

Type locality: Osek, near Rokycany, Prague Basin, Czech Republic.

Additional new material, localities, and horizons: The studied material from the Fezouata Shale, Anti-Atlas (Morocco), includes three specimens from Oued Beni Zoli (Z-F5; Figures 1A, D), *S. murrayi* Zone, late Tremadocian (MHNM.15690.200 and ML20.269401–402), 12 specimens from the hill N of Ouaoufraout (Z-F13c; Figures 1A, D), *H. copiosus* Zone, late Tremadocian

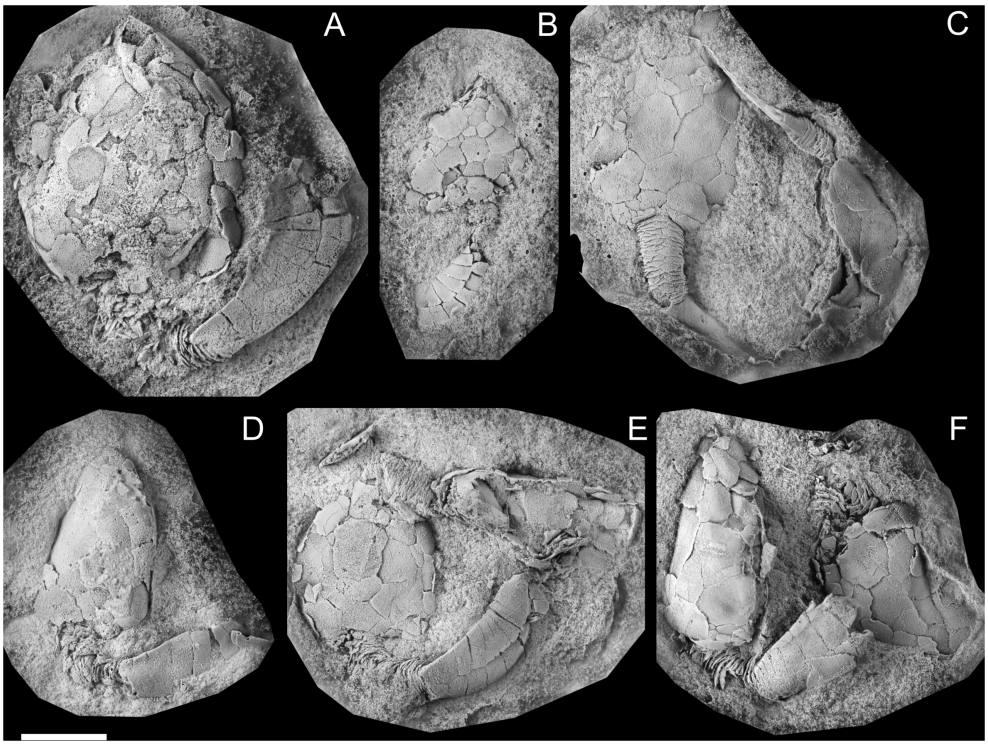

FIGURE 4
Whitened casts of *Plasiacystis mobilis* occurring in concretions from Taichoute (middle Floian). **(A)** MPZ.2022.927. **(B)** MPZ.2023.251. **(C)** ML20.269363 showing two specimens in the same concretion. **(D)** ML20.269394. **(E)** ML20.269360 showing two specimens in the same concretion. **(F)** ML20.269308 showing two specimens in the same concretion. Scale bar = 10 mm. Photographs by Vincent Perrier.

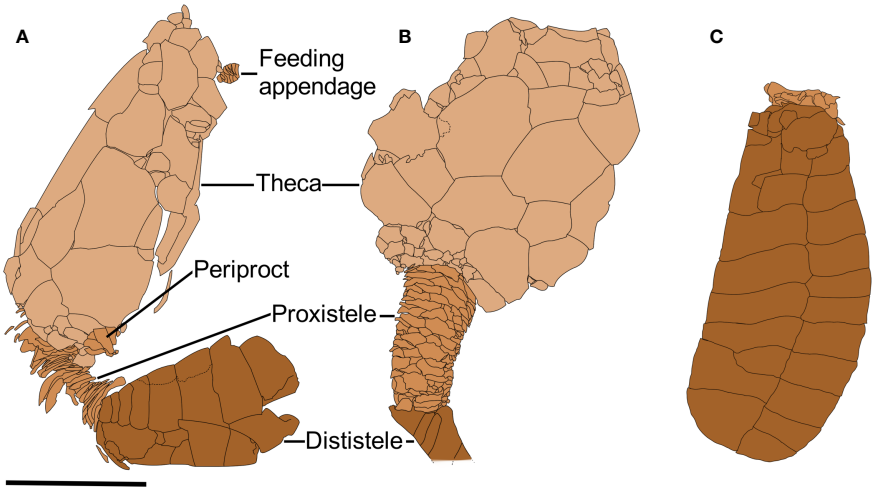

FIGURE 5
Observation drawings of *Plasiacystis mobilis* preserved in concretions from Taichoute (middle Floian). **(A)** ML20.269306 showing a specimen with both its periproct and a part of its feeding appendage. **(B)** ML20.269363 showing a nearly intact proxistele. **(C)** ML20.269402 showing an isolated dististele. Scale bar = 10 mm.

(AA.CNOc.OI.5–6, AA.CNOc.OI.9, AA.CNOc.OI.12, AA.CNOc.OI.14, AA.CNOc.OI.18–20, AA.CNOc.OI.22, AA.CNOc.OI.24, AA.CNOc.OI.31, and AA.CNOc.OI.45), two specimens from Toumiat (Z-F26; Figures 1A, D), *C.*? *protobalticus* Zone, early Floian (AA.TMT.OI.78–79), five specimens from Ouzina (Taouz Massif; Figure 1C), *C.*? *protobalticus* Zone, early Floian (UCBL-FSL.711645, UCBL-FSL.711648–649, ML20.268923, and ML20.269072), one specimen from Bou Chrebeb (Z-F25a; Figures 1A, D),?*B. jacksoni* Zone, middle Floian (UCBL-FSL.712446), eight specimens from Jbel Bou Zeroual (Z-F0; Figures 1A, D),?*B. jacksoni* Zone, middle Floian (AA.JBZ.OI.137, AA.JBZ.OI.141, AA.JBZ.OI.145–147, AA.JBZ.OI.202, ML20.269378, and YPM.IP.520778), 90 specimens from Taichoute (Western Maïder; Figure 1C),?*B. jacksoni* Zone, middle Floian (AA.TAI2.OI.1, UCBL-FSL.712954, UCBL-FSL.712956, UCBL-FSL.712958–959, UCBL-FSL.713593, ML20.269255, ML20.269265, ML20.269267, ML20.269271, ML20.269275–277, ML20.269283, ML20.269301–309, ML20.269311–360, ML20.269362–375, MPZ.2022.926–927, and MPZ.2023.251), and three specimens from unknown localities of the Ternata Plain (BMNHUK.EE.8727, MHNN.P.045588, and YPM.IP.371).

Diagnosis: As for genus, by monotypy.

Description: On average, specimens *ca* 50 mm long from the apex of the theca to the tip of dististele. Homoiostele approximately half the total length of the body, *ca* 28 mm long on average. Dististele representing approximately 60% of homoiostele length, *ca* 18 mm long on average.

Theca ovoid, slightly elongate, lacking lobes or a marginal frame (Figure 4). No visible differentiation between the upper and lower sides. Thecal plates numerous, irregular, polygonal, tesselate, almost smooth, flat or slightly convex, generally larger around the middle part of theca, and smaller around homoiostele insertion (Figures 4, 5B).

Feeding appendage stemming laterally, at an approximately one-third distance to the apex, along the antanal thecal side (Figures 4F, 5A; Type specimen NMP.L.29120). Apical tip and cover plates not observed.

Gonopore and hydropore situated on one or two plates, near insertion of feeding appendage (see, e.g., specimens UCBL-FSL.711949, ML20.269319, ML20.269324, and ML20.269337). Right of homoiostele insertion, small cone-shaped periproct, slightly bulging outward, made of thin, elongate plates arranged in a circle around the anal opening (Figures 4E, F, 5A).

Homoiostele inserted in the middle part of the posterior margin (i.e., opposite thecal apex) and divided into two distinct parts. Proxistele cylindrical, made of many thin, scale-shaped, imbricate elements of irregular sizes (Figures 4C, 5B). Dististele short, flattened, bean-shaped, with rounded tip (Figures 4A, D, E, 5C). Paddle-like portion of homoiostele made of two rows of opposite, tightly sutured, polygonal plates of irregular size. Dististele transversely thicker along longitudinal contact between opposite rows and thinner abaxially along its sharp lateral edges (Figures 4A, D, E, 5C). Longitudinal thickening of dististele enclosing narrow cylindrical lumen (see, e.g., specimens ML20.269321 and ML20.269325). In approximately 75% of observed specimens, short, smooth, spike-shaped knob borne by one plate of convex half of dististele (Figures 4B, 6). Knob highly variable in position.

Remarks: The particularly abundant material collected in the Fezouata Shale can be assigned to solutans (single feeding appendage) and more precisely to syringocrinids (flattened, oblique dististele). Moreover, the lateral insertion of the feeding appendage on the antanal thecal side and the morphology of the periproct (small, cone-shaped anal pyramid) both support a placement within the family Minervaecystidae. The possession of an unorganised proxistele made of numerous imbricate platelets and the possession of a dististele modified into a short, wide, bean-

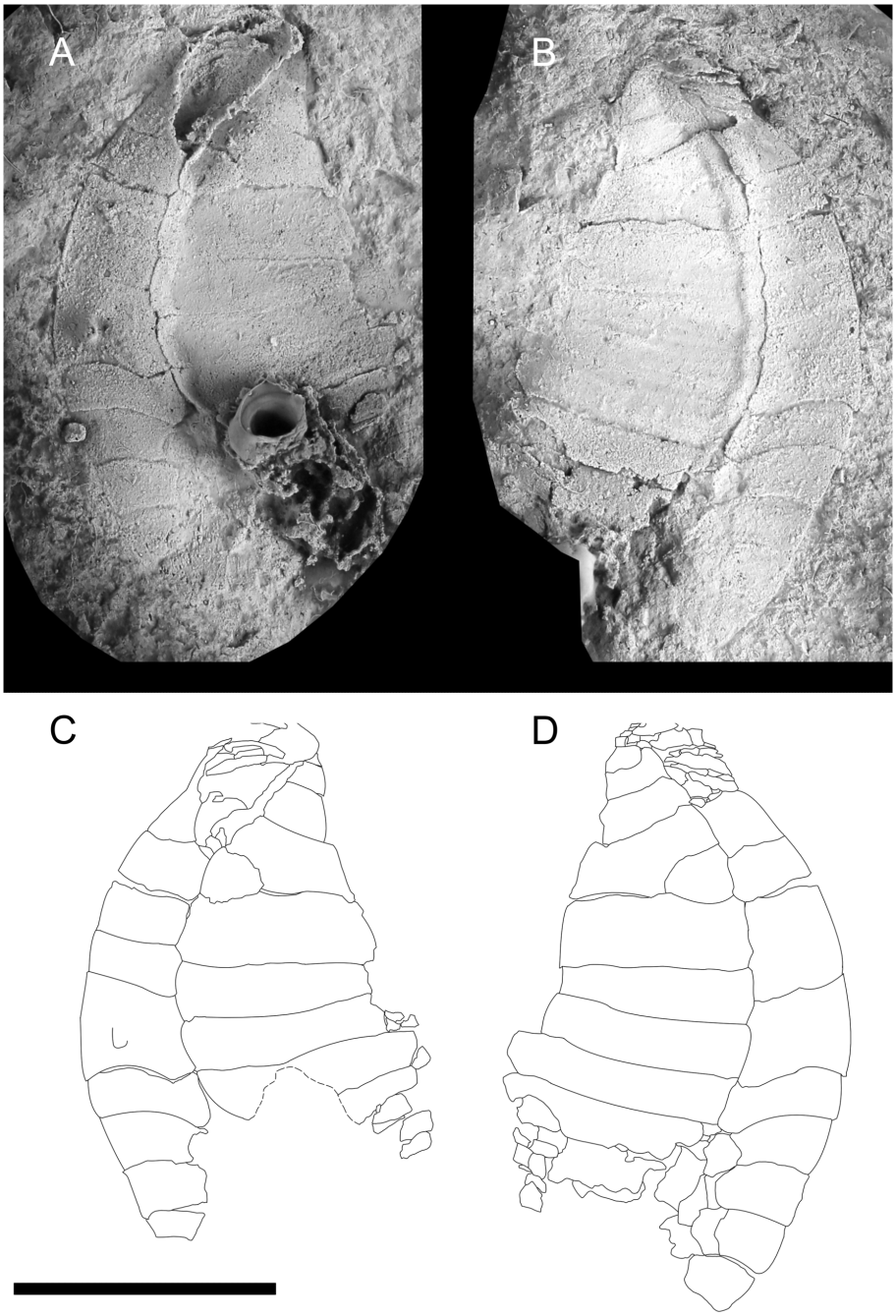

FIGURE 6
The only specimen of *Plasiacystis mobilis* found so far in France (Montagne Noire, late Tremadocian). **(A)** Whitened cast of the UCBL-FSL.711925 counterpart showing the ornamental knob. **(B)** Whitened cast of the UCBL-FSL.711925 part. **(C)** Observation drawing of the UCBL-FSL.711925 counterpart showing the ornamental knob. **(D)** Observation drawing of the UCBL-FSL.711925 part. Scale bar = 10 mm. Photographs by Vincent Perrier.

shaped paddle are diagnostic features of the genus *Plasiacystis*. Comparison of the Fezouata specimens of *Plasiacystis* with the original type material of *P. mobilis* did not reveal any significant morphological differences. Consequently, the Moroccan material is here assigned to *P. mobilis*, thus confirming the particularly long stratigraphic range of this taxon (late Tremadocian–middle Darriwilian; see Lefebvre et al., 2012; Lefebvre et al., 2016; Dupichaud et al., 2023). Moreover, the particularly abundant and well-preserved material from the Anti-Atlas brings new data on previously undocumented (e.g., gonopore and hydropore) or poorly known morphological features of *P. mobilis* (e.g., anal pyramid and feeding appendage) (see Lefebvre et al., 2012). The Moroccan material also makes it possible to document the occurrence of intraspecific variability with respect to the presence and position of the ornamentation (spike-shaped knob) on the dististele.

***Plasiacystis* sp.**

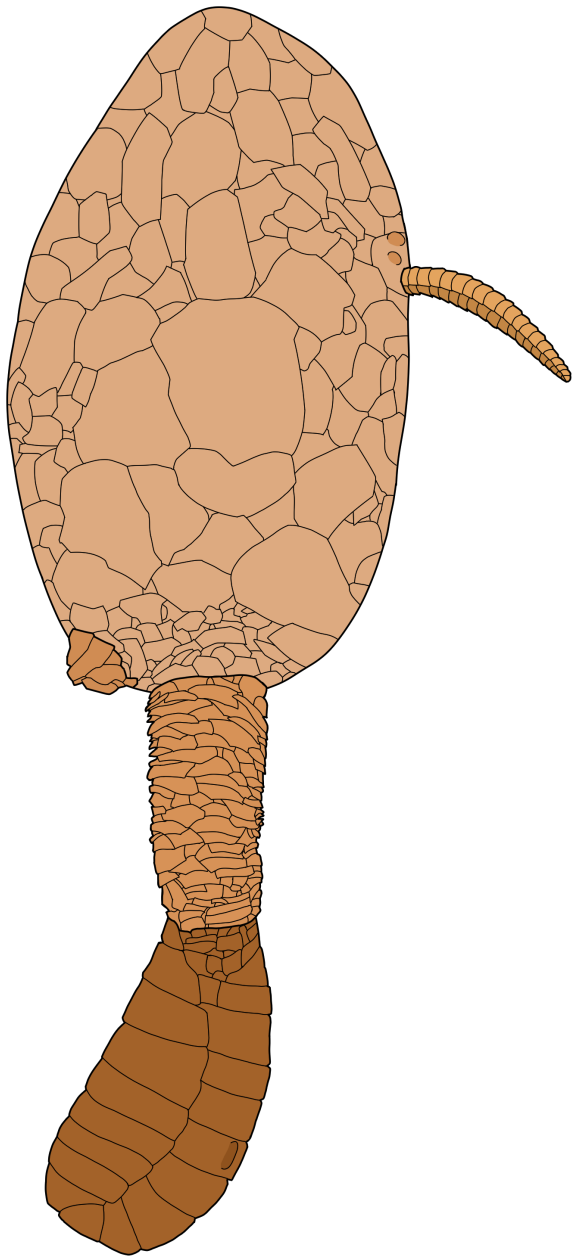

FIGURE 7
Reconstruction of the underside of *Plasiacystis mobilis*.

Figures 2A, 8, 9

Material, localities, and horizons: Included material from the Fezouata Shale (Anti-Atlas, Morocco) comprises 16 specimens from the hill North of Toumiat (Z-F24; Figures 1A, D), *C.*? *protobalticus* Zone, early Floian (AA.ONT.OI.10, MHNM.15690.211–215, and MHNM.15690.217–226) and one specimen (MHNN.P.045587) from an unknown locality (possibly Taichoute)? preserved in a concretion.

Description: Theca of numerous, irregular, tesselate, smooth, polygonal plates. Thecal outlines and size unknown; only three incomplete, disarticulated thecae could be observed (Figure 8A; specimens MHNM.15690.212, MHNM.15690.224, and MHNM.15690.226). Thecal orifices (anus, gonopore, and hydropore) not observed. Two originally connected portions of the same feeding appendage preserved in one specimen (MHNM.15690.224): one part still inserted into disarticulated theca, and the other in contact with dististele. Proxistele consisting of numerous, irregularly arranged, scale-like imbricate elements (Figures 8B, D). Dististele approximately twice as long as proxistele: on average, proxistele *ca* 14 mm long, dististele *ca* 30 mm long (Figure 8). Dististele made of two lateral rows of opposite, rectangular, tightly sutured plates forming flat, straight paddle, with broad and rounded tip (Figure 8).

Remarks: In locality Z-F24, a single storm-generated lens yielded numerous, remarkably large paddle-shaped dististeles, sometimes still in contact with proxisteles, and seldom associated with strongly disarticulated thecae. All available morphological features (theca consisting of numerous, smooth, polyplated plates, unorganised proxistele made of imbricate elements, broad, paddle-shaped dististele with a rounded posterior extremity) strongly support the assignment of these solutans to the genus *Plasiacystis*. However, their dististeles appear morphologically different from those of *P. mobilis*: they are proportionately longer (compared to the length of the proxistele), their outlines are straight (instead of bean-shaped as in *P. mobilis*), and their distal extremity is markedly wider than their anterior margin (whereas both margins are of approximately the same width in *P. mobilis*). Moreover, no ornamentation is present on the numerous observed dististeles from Z-F24, while most specimens of *P. mobilis* display a strong spike-shaped knob on their distal paddle. The same morphological features are present in a single large, three-dimensionally preserved, fully articulated incomplete specimen from an unknown concretion-bearing locality (MHNN.P.045587).

A first possible interpretation is to consider that all features departing from the standard morphology of *P. mobilis* result from allometry and can be explained by the unusually large size of specimens from Z-F24 (Dupichaud and Lefebvre, 2022). The occurrence of morphologically distinct, successive ontogenetic stages has already been seen in some solutans (see, e.g., Noailles et al., 2014). Comparable allometries have been also documented in other Palaeozoic echinoderms, such as eocrinoids (Parsley, 2012; Nohejlová and Fatka, 2016) and stylophorans (Lefebvre et al., 2022). In this interpretation, the unusual morphology of the Z-F24 solutans simply results from their larger size, and all specimens can be assigned to *P. mobilis*. However, the possibility that these solutans correspond to a distinct, endemic species of *Plasiacystis*, characterised by a morphologically distinct dististele, cannot be excluded.

Nimchacystis gen. nov.

Derivation of name: From *nimcha*, a Moroccan curved sword, referring to the shape of the dististele, and the suffix *-cystis* (ancient Greek), meaning "bag", commonly used for solutan generic names.

Type species: *Nimchacystis agterbosi* sp. nov., by monotypy.

Diagnosis: Genus of syringocrinid solutan with very flexible, distally tapering proxistele, composed of more than 20 telescopic cylindrical hexamerous rings, and rigid dististele comprising two sets of large, opposite plates forming elongate, relatively narrow, smooth (unornamented), scimitar-shaped paddle with blunt distal extremity.

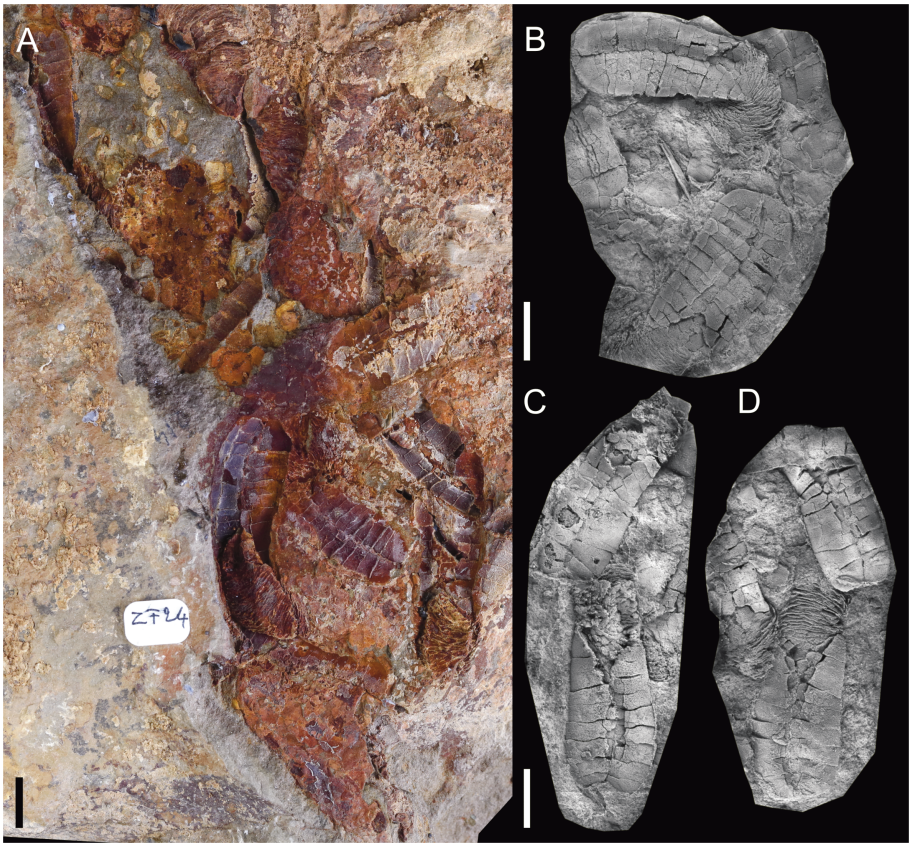

FIGURE 8
Plasiacystis of the Z-F24 locality; storm-generated accumulations (early Floian). **(A)** Photograph of MHNM.15690.224 showing the accumulation of disarticulated steles and thecae. **(B)** Whitened cast of MHNM.15690.214. **(C)** Whitened cast of MHNM.15690.222 part. **(D)** Whitened cast of MHNM.15690.222 counterpart. Scale bars = 10 mm. Photographs by Vincent Perrier.

Remarks. *Minervaecystis*, *Nimchacystis*, and *Plasiacystis* have almost identical ovoid thecae and laterally inserted feeding appendages, but very different homoiosteles. *Nimchacystis* shares with *Minervaecystis* the possession of a well-organised proxistele consisting of more than 20 regular rings, and of a relatively narrow, elongate, curved dististele. For this reason, the first observed specimens of *Nimchacystis* were assigned to *Minervaecystis* by Lefebvre and Fatka (2003). However, proximal rings are generally tetramerous in *Minervaecystis*, while they are hexamerous in *Nimchacystis*. In *Minervaecystis*, the width of the stem-like dististele remains more or less constant along its length, while in *Nimchacystis*, this region forms a broad, elongate blade, tapering both anteriorly and posteriorly. *Nimchacystis* shares with *Plasiacystis* the possession of a dististele modified into a stiff paddle-like structure. However, this region is short and broad and with a large, rounded distal extremity in *Plasiacystis*, whereas it is more elongate and narrower and with a blunt tip in *Nimchacystis*. In many aspects, the homoiostele of *Nimchacystis* appears morphologically intermediate between those of *Minervaecystis* and *Plasiacystis* (Dupichaud and Lefebvre, 2022). This observation is a strong argument supporting placement of these taxa in the same clade (Minervaecystidae).

Nimchacystis agterbosi sp. nov.
Figures 2C, 10–13

Derivation of name: The name refers to the non-academic Dutch palaeontologist Ton Agterbos, who collected and made available for study the most complete available specimen (herein designated as holotype) of the new species.

Holotype: UCBL-FSL.713120 (Figures 10A, 11A).

Type level: Fezouata Shale, *S. murrayi* Zone, late Tremadocian (Lower Ordovician).

Type locality: Tignit (Z-F17b; Figures 1A, D), approximately 26 km NW of Zagora, Ternata plain, Central Anti-Atlas (Morocco).

Additional material, localities, and horizons: Six specimens are from Tinzouline (Z-F5[2]; Figures 1A, D), *S. murrayi* Zone, late Tremadocian (YPM.IP.520227–231 and YPM.IP.520370). Three other specimens were collected in the lower part of the Fezouata Shale (*S. murrayi* Zone, late Tremadocian), but from an unknown locality in the Zagora area (SMF.89671–672 and UCBL-FSL.713058). Over 20 additional specimens were observed in private collections, most of them originating either from Tignit (Z-F17b) or from Tinzouline (Z-F5[2]).

Description: On average, specimens *ca* 73 mm long from thecal apex to the tip of dististele. Theca ovoid, slightly elongated, without evidence of anal lobe or marginal frame. No obvious difference in plating between the lower and upper thecal sides, both made of many polygonal, smooth, tesselate plates of different sizes

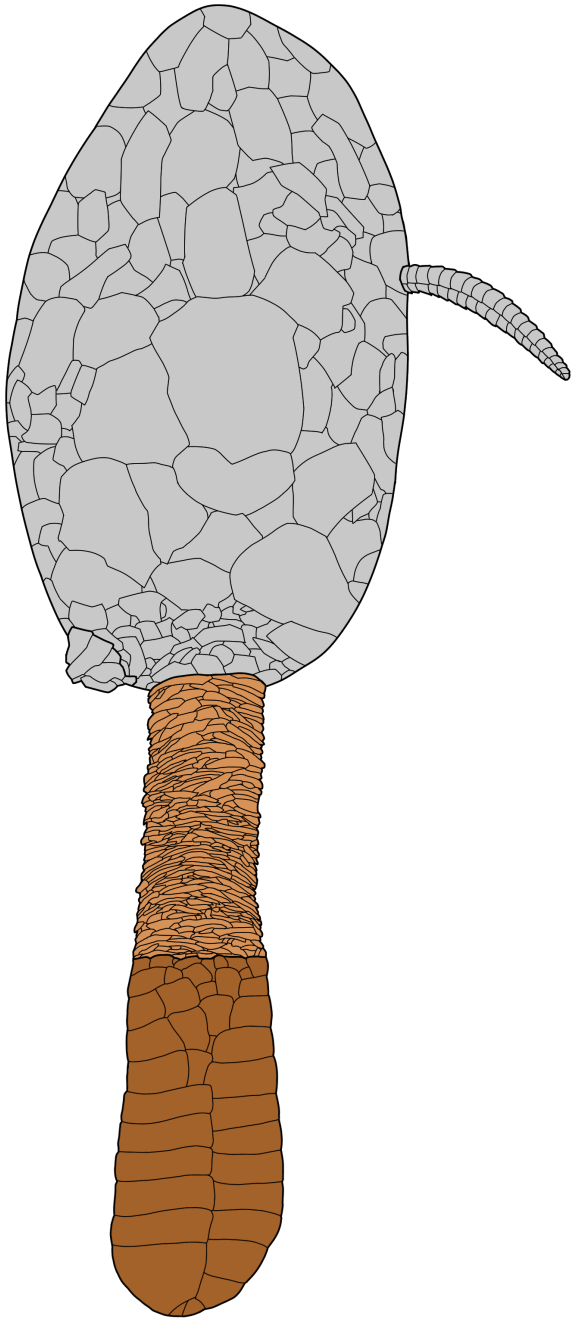

FIGURE 9
Reconstruction of the underside of *Plasiacystis* sp. Grey areas extrapolated from *Plasiacystis mobilis*.

(Figures 2C, 10A–C). Thecal orifices (anus, gonopore, hydropore) not observed.

Long, distally tapering feeding appendage inserted on left (antanal) thecal side. Feeding appendage 14 mm long in holotype (Figures 10A, 11A), 26 mm long and 3.5 mm wide at contact with theca in YPM.IP.520229 (Figure 10C). Feeding appendage consisting of at least 25 (holotype) and over 50 (YPM.IP.520229) pairs of alternating rectangular flooring plates, and two sets of smaller, opposite rectangular cover plates (Figures 10A, C, 11A).

Homoiostele inserted opposite to thecal apex and representing *ca* 60% of total body length; homoiostele *ca* 48 mm long on average. Cylindrical, distally tapering proxistele made of over 20 well-defined, regular telescopic rings, each consisting of six rectangular plates (Figures 10A, B, D–F, 11C). Elongate, curved dististele forming flat, rigid paddle tapering both anteriorly and posteriorly (Figures 2C, 10A, C, 11B, C). Distal paddle *ca* 30 mm long on average, and forming *ca* 65% of homoiostele length. Dististele consisting of two opposite rows of plates, each made of approximately 20 smooth (unornamented), rectangular elements (Figures 2C, 10A, C, 11B, C).

Family indet.

Syringocrinid gen. and sp. indet.

Figure 3

Material, locality, and horizon: The single known specimen (CASG 72938; Figure 3) is from an unknown locality of the Ternata plain, Zagora area (Central Anti-Atlas, Morocco). Associated lithology (fine beige siltstones) and preservation (occurrence of pyritised soft tissues within the theca) suggest that the specimen was collected at the top of the lower interval with exceptional preservation of the Fezouata Shale (*S. murrayi* Zone, late Tremadocian; Lefebvre et al., 2018).

Description: Specimen *ca* 66 mm long, from feeding appendage distal extremity to tip of dististele (feeding appendage: 6 mm; theca: 16 mm; homoiostele: 44 mm). Theca and associated feeding appendage preserved as extremely faint colourful (oxidised) impressions on rock (Figure 3).

Small, non-lobate theca with regularly convex, ellipsoid outlines. Narrow, elongate (9 mm long), dark, pyritised, three-dimensional intrathecal structure, extending anteriorly from the central part of theca (*ca* 6 mm away from the insertion of feeding appendage) into small, cone-shaped pyramid posteriorly, next to homoiostele insertion (Figure 3).

Short, poorly preserved portion of wide, segmented feeding arm inserted at the thecal apex (Figure 3).

Homoiostele long, narrow, proximally straight, slightly curved towards sharp tip (Figure 3). Details of homoiostele obscured by preservation as thin, oxidised crust.

Remarks: In spite of the very poor preservation of its skeletal elements, this specimen can be readily identified as a solutan echinoderm, based on the occurrence of a single, stout feeding appendage, a distinct theca, and an elongate stem-like structure (Lefebvre et al., 2016; Saleh et al., 2021; Dupichaud and Lefebvre, 2022). In the lower part of the Fezouata Shale, this type of preservation is typical for echinoderms occurring in levels with exceptional preservation (Lefebvre et al., 2019). Their original calcite skeletons are largely dissolved away, with only their outlines appearing as faint, oxidised impressions on the rock. In contrast, echinoderm soft tissues (ambulacral system and gut) can be preserved as three-dimensionally pyritised structures (Lefebvre et al., 2019; Saleh et al., 2021). In this context, it is very likely that the elongate structure preserved in specimen CASG 72938 represents exceptionally preserved soft parts. Its morphology, position, and posterior connection with a small pyramid (very likely

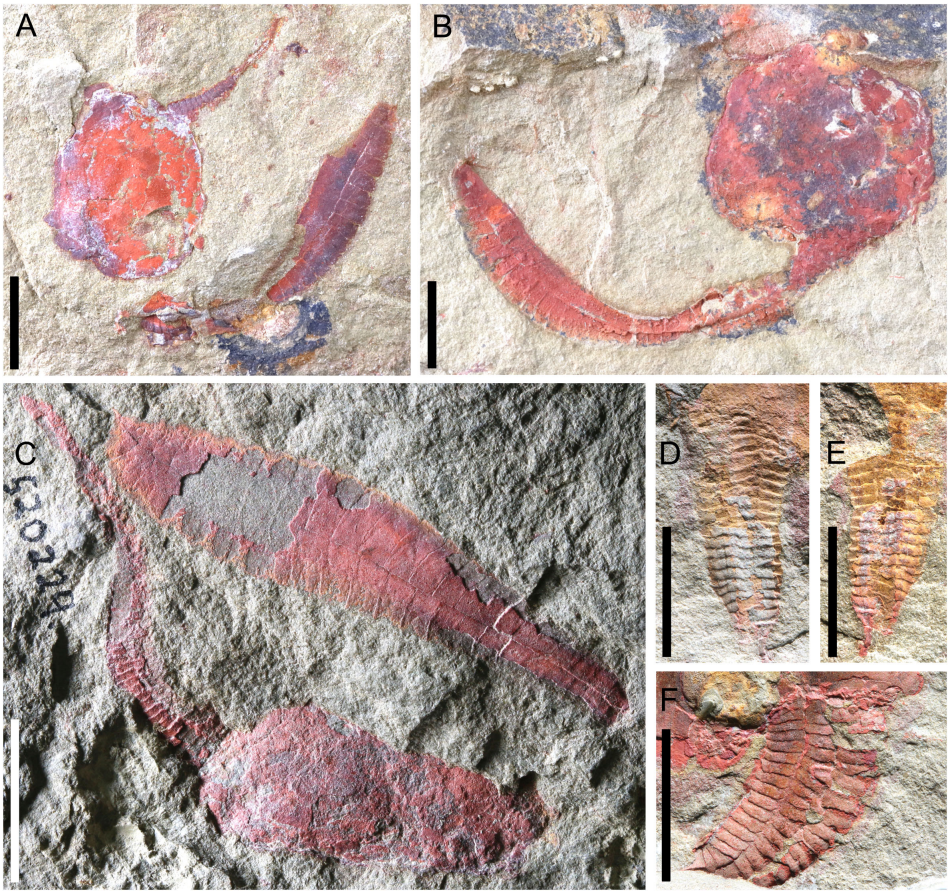

FIGURE 10
Photographs of *Nimchacystis agterbosi* from the Z-F17b locality (late Tremadocian). **(A)** Holotype UCBL-FSL.713120 showing theca, feeding appendage, proxistele, and dististele in near anatomical connectivity as in life. **(B)** SMF.89671 showing theca and stele in anatomical connection. **(C)** YPM.IP.520029 showing a large specimen with an apparently complete feeding appendage and dististele. **(D)** YPM.IP.520031 part showing a complete and well-preserved proxistele. **(E)** YPM.IP.520031 counterpart showing a complete and well-preserved proxistele. **(F)** YPM.IP.520370 showing a complete and well-preserved proxistele. Scale bars = 10 mm. Photographs **(A)** and **(B)** by Vincent Perrier. Photographs **(C)** to **(F)** by Jessica Utrup

corresponding to the periproct) suggest that this elongate structure corresponds to the hind gut (Saleh et al., 2021; Dupichaud and Lefebvre, 2022). In this specimen, the preferential preservation of the posterior part of the digestive system (the anterior part of the gut is missing) possibly results from its infilling by sediment.

The overall morphology of specimen CASG 72938 (e.g., large, flattened homoiostele) suggests probable syringocrinid affinities. The apical insertion of the feeding appendage excludes its assignment to the family Minervaecystidae, instead supporting affinities with Cambrian-like taxa such as *Coleicarpus* and

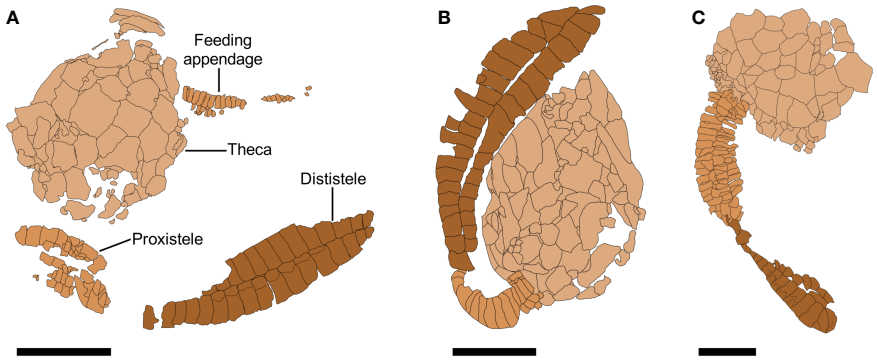

FIGURE 11
Camera lucida drawings of *Nimchacystis agterbosi*. **(A)** Holotype UCBL-FSL.713120 showing theca, feeding appendage, proxistele, and dististele almost in near anatomical connectivity as in life. **(B)** UCBL-FSL.713058 showing an almost complete dististele. **(C)** SMF.89671 showing theca and stele in anatomical connection. Scale bars = 10 mm.

10.3389/fevo.2023.1290063

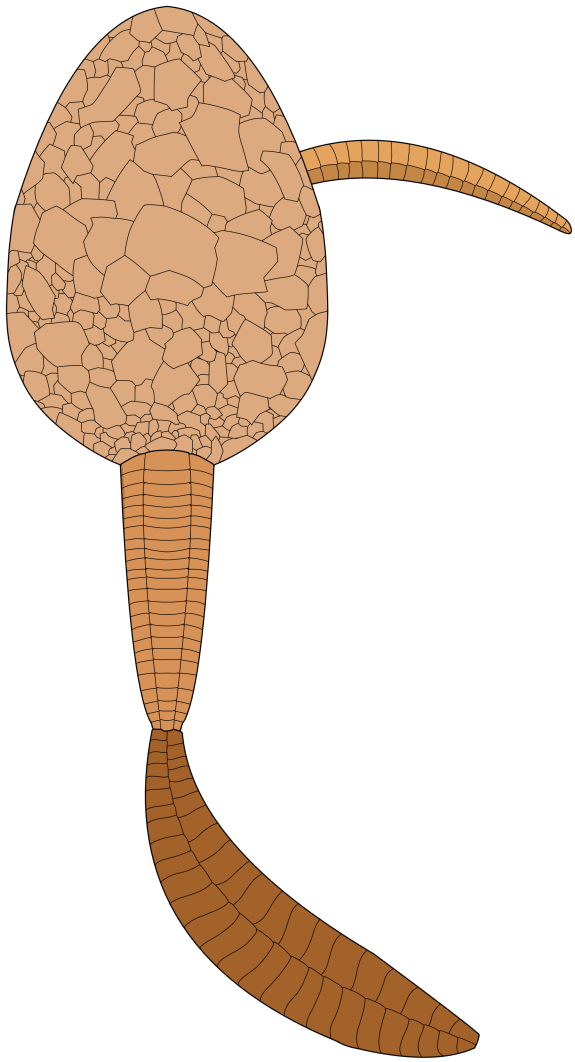

FIGURE 12
Reconstruction of the underside of *Nimchacystis agterbosi*.

Castericystis (Lefebvre et al., 2016; Dupichaud and Lefebvre, 2022). The overall morphology of CASG 72938 strongly recalls that of *Castericystis vali* Ubaghs and Robison, 1985: similar ellipsoid theca, slightly offset feeding appendage insertion, and long homoiostele with a sharp distal extremity. However, given the poor preservation of the single known specimen from the Fezouata Shale, it is untenable to assign it to the genus *Castericystis*, which was originally described from the Marjum Formation (Drumian) of Utah (Ubaghs and Robison, 1985; Daley, 1995). However, as yet undescribed *Castericystis*-like solutans were recently discovered in the Neuville Formation (lower Katian, Upper Ordovician) of Québec, Canada (R. Mooi, pers. obs., 2023). This suggests the persistence through time (at least up to the Late Ordovician) of solutans with Cambrian-like morphologies.

Discussion

Taphonomy

The main indicator for echinoderm taphonomy is the integrity of the calcite skeleton (Ausich, 2001). Fossil echinoderms have been arranged into taphonomic groups, based on experimental analyses of taphonomy conducted on extant taxa (e.g., Meyer, 1971; Kidwell and Baumiller, 1990; Donovan, 1991; Nebelsick, 1995; Kerr and Twitchett, 2004). These taphonomic groups are defined by how resistant their skeletal remains are to *post mortem* transport and disarticulation (Brett et al., 1997). Following this taphonomic classification, solutans are generally assigned to the "type 1" category, meaning that their skeleton is made of weakly sutured plates that quickly disarticulate after the death of the organism (a few days to a few weeks; Gorzelak and Salamon, 2013) by analogy to modern "type 1" echinoderms such as asteroids and ophiuroids (Lefebvre, 2007; Nohejlová and Lefebvre, 2022). In this context, uncovering extensively contiguous solutan endoskeletal remains implies not only a relatively rapid burial by obrution deposits (e.g., distal storm sediments) soon after or before death but also little or no transport and low bioturbation rates once buried. In the Lower Ordovician of the Anti-Atlas, such taphonomic conditions probably prevailed in most solutan-bearing localities that are generally associated with relatively distal environmental conditions at or below the storm wave base: Z-F0 (Jbel Bou Zeroual), Z-F5 (Oued Beni Zoli), Z-F5(2) (Tinzouline), Z-F17b (Tignit), Z-F26 (Toumiat), Ouzina, and Taichoute. All these localities, in which fully articulated solutans are preserved, can be considered "echinoderm Lagerstätten" *sensu* Smith (1988).

In contrast, some other localities (e.g., Z-F13c and Z-F24) have yielded solutan dististeles almost exclusively. Associated proxisteles are sometimes preserved, but thecae are generally totally disarticulated into hundreds of isolated plates. Such levels usually occur in more proximal, higher energy, storm-generated accumulation deposits, along with fragments of other invertebrates (e.g., cephalopods and trilobites). Such accumulations are particularly informative because they suggest that different parts of the same individual could follow distinct taphonomic pathways. Clearly, the solutan feeding appendage was the most fragile part of the organism and the most likely to be disarticulated. The more frequent preservation of large portions of proxisteles indicates that this part of the animal was a bit more resistant to disarticulation. However, the storm-generated accumulations of distal paddles of *Plasiacystis*-like solutans demonstrate that the dististele was the most taphonomically resistant module of the organism. This implies that the dististele of *Plasiacystis* was a particularly rigid structure made of tightly sutured plates. Following the taphonomic classification of Brett et al. (1997), solutans are assigned to the "type 1" category. However, *Plasiacystis*-like solutans possess more rigid, decay-

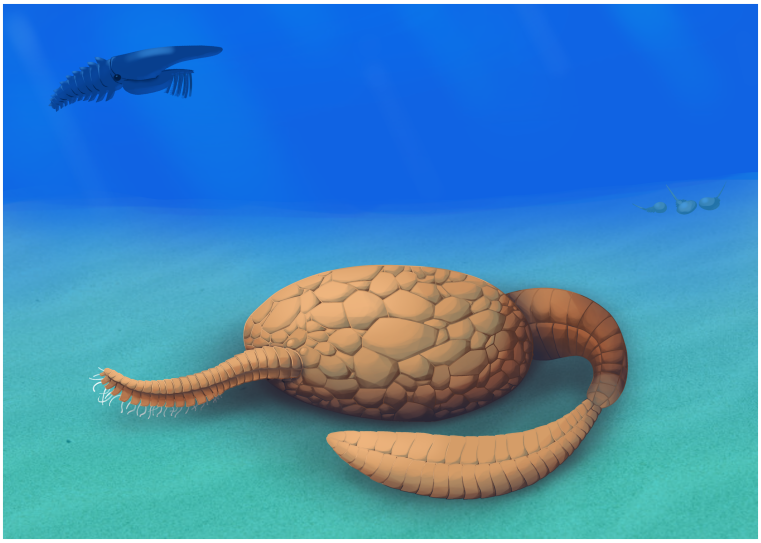

FIGURE 13
Artistic reconstruction of *Nimchacystis agterbosi* by Christophe Dupichaud.

resistant modules (e.g., dististele), so part of their anatomy could be assigned to the "type 2" category.

Palaeoecology

The earliest known solutans were permanently sessile (*Coleicarpus sprinklei*, Wheeler Shale, Drumian) or attached during juvenile stages (*C. vali*, Marjum Formation, Drumian) (Ubaghs and Robison, 1985; Ubaghs and Robison, 1988; Daley, 1995; Daley, 1996; Zamora et al., 2013; Zamora et al., 2017; Lefebvre and Lerosey-Aubril, 2018). All later solutans are generally considered vagile organisms, even if the presence of a hook at the tip of the homoiostele in some taxa might be related to the persistence of an attached juvenile stage. In this context, minervaecystids provide a remarkable example of an evolutionary trend towards more active mobility, with the transition from long, flattened stem-like appendages (*Minervaecystis*) towards short, broad, and rigid paddle-like structures (*Plasiacystis*). The slightly oblique dististele of *P. mobilis* was the stiffest and most resistant part of the organism (see above). It was thus perfectly designed for crawling (probably backwards, i.e., appendage first) on soft siliciclastic substrates. Its rounded posterior margin suggests the total absence of any attachment structure at juvenile stages (e.g., distal hook or blunt tip) and a permanently free mode of life.

The ovoid theca of minervaecystids is a plesiomorphic feature, inherited from permanently attached solutans (e.g., *Coleicarpus*). Such a morphology was possibly retained in minervaecystids because it also turned out to be well-suited for active backward crawling on soft substrates by significantly reducing the contact and therefore the resistance to traction exerted by the sediment on smooth, rounded, undifferentiated thecal walls. In contrast, markedly flattened solutan thecae, with contrasting morphologies on their lower and upper sides, possibly represent adaptations to less active epibenthic modes of life (e.g., solutan indet., gen. and sp. nov. in Lefebvre et al., 2012). Such flattened thecal morphologies provide indirect clues that fuel the ongoing debate on the life orientation and feeding posture of solutans (see, e.g., Noailles et al., 2014, and references therein). Direct comparison with other epibenthic organisms suggests that in such solutans, the flat side of their theca was very likely in contact with the substrate, whereas the opposite, convex surface was facing the water column.

Such a comparison is not possible in the case of minervaecystids: their globose, ovoid thecal morphology provides no clues to identify which surface was originally in contact with the substrate. The lack of a flat thecal face in minervaecystids may imply a degree of difference in feeding behaviour with more flattened solutans. As such, minervaecystids could be interpreted as having shown a mixed mode of feeding, allowed by the flexibility of their feeding appendage, being able to switch between bottom-feeding and suspension-feeding. However, their life orientation can be deduced indirectly based on the ornamentation occurring on the homoistele of *Minervaecystis*. In *M. vidali*, the concave portion of the dististele bears several comb-like lateral projections (Bather, 1913; Ubaghs, 1970; Dupichaud et al., 2023). Ubaghs (1970) suggested that these structures were originally directed upwards. He interpreted them as fin- or wing-like processes that could help *Minervaecystis* to swim forward (i.e., theca first; Ubaghs, 1970). This orientation of the comb-like structures (on the left side of the dististele) implies that the periproct was situated left of the homoiostele, and the feeding appendage was inserted, on the opposite, right thecal side (Ubaghs, 1970). In such an

orientation, the cover plates (and the underlying ambulacral food groove) are facing away from the substrate, which implies a suspension-feeding mode of life for *Minervaecystis* (Ubaghs, 1970).

However, the possession of an ovoid theca, a very flexible proxistele that likely housed powerful musculature (by analogy with stylophorans and pleurocystitid rhombiferans; see, e.g., Gorzelak and Zamora, 2016; Lefebvre et al., 2019), and a flattened, oblique dististele, sometimes modified into a rigid paddle (*Plasiacystis*), suggests that the morphology of minervaecystids was better designed for active backward crawling on soft substrates than for swimming (Prokop and Petr, 2003; Lefebvre and Lerosey-Aubril, 2018). In this interpretation, the comb-like structures occurring on the dististele of *Minervaecystis* were more likely directed downwards, acting as gripping devices to increase the contact surface between the dististele and the substrate. If this orientation is correct, then the comb-like structures of *Minervaecystis* were located on the right side of its dististele. In minervaecystids, the anus is therefore situated on the right side of the homoiostele, while the feeding appendage is inserted on the opposite (left) side of the theca. In such an orientation, the cover plates (and the ambulacral food groove) are facing downwards, implying that minervaecystids were *detritus feeder*s. This interpretation is compatible with the exceptional preservation of the hind gut (possibly full of ingested sediment) in the *Castericystis*-like specimen from the Fezouata Shale (see above; Figure 3). This gut also appears to be partially pyritised (see also Lefebvre et al., 2019). The ingested Fe-rich sediments could have aided the preservation of the hind gut by reducing bacterial activities under oxic conditions (Saleh et al., 2019) and by contributing to the seeding of pyrite precipitation once sulphate-reducing conditions were established (Saleh et al., 2020).

In the Lower Ordovician of the Anti-Atlas, minervaecystids (and in particular, *Plasiacystis*) are geographically widespread (Ternata plain, western Maïder, Taouz Massif), occurring in a large range of environmental conditions (from proximal, storm-influenced settings to more distal, quiet environments) and through a relatively long time interval (late Tremadocian–middle Floian). However, in most localities (e.g., Bou Chrebeb, Jbel Bou Zeroual, Oued Beni Zoli, Tinzouline, and Toumiat) solutans are a minor component of taxonomically diverse assemblages dominated by molluscs (bivalves, cephalopods, gastropods, and tergomyans) and trilobites (Lefebvre et al., 2016). In Ouzina, minervaecystids are also rare, but they are associated with a low diversity, almost monospecific fauna dominated by the glyptocystitid rhombiferan *M. bohemica* (Lefebvre et al., 2016).

In the Lower Ordovician of the Anti-Atlas, Taichoute (Figure 1C) stands out as the only locality yielding a low-diversity, solutan-dominated assemblage. Taphonomic features of Taichoute solutans (i.e., three-dimensionally preserved, complete, slightly disarticulated or collapsed individuals) suggest that most of them were very likely dead and already decaying on the sea floor when burial occurred (i.e., assemblage a1 in Saleh et al., 2022a). Comparable solutan-dominated assemblages have been described in the middle Cambrian of Utah, USA (Ubaghs and Robison, 1985; Ubaghs and Robison, 1988; Daley, 1995; Daley, 1996) and the Upper Ordovician of the Prague Basin, Czech Republic (Noailles et al., 2014; Nohejlová et al., 2019) and Tafilalt, Morocco (Hunter et al., 2010; Nohejlová and Lefebvre, 2022). The Taichoute echinoderm Lagerstätte provides the first example of a nearly monospecific, dense solutan bed in the Early Ordovician. As is frequently the case in echinoderm dense beds (see Lefebvre, 2007 and references therein), it is possible that the rarity and low diversity of associated benthic invertebrates (e.g., brachiopods, molluscs, and trilobites) result from unfavourable (oligotrophic)? environmental conditions leading to the opportunistic colonisation of the sea floor by gregarious, high-density populations of *Plasiacystis* (Taichoute) or *Macrocystella* (Ouzina). The oligotrophic interpretation does not contradict the presence of abundant large carcasses of filter-feeding arthropods in the a2 assemblage of Taichoute (see Saleh et al., 2022a). The a2 assemblage is younger and consists of transported material from more proximal sites, unlike the in-situ, non-transported solutans that colonised the Taichoute seafloor.

Palaeobiogeography

Castericystis, from the Marjum Formation (Drumian, Utah), represents the earliest known syringocrinid solutan (Noailles et al., 2014; Lefebvre and Lerosey-Aubril, 2018). The occurrence of *Pahvanticystis* in the Weeks Formation (late Guzhangian, Utah; Lefebvre and Lerosey-Aubril, 2018) and of minervaecystid remains in the Whipple Cave (Cambrian Stage 10, Nevada; Ubaghs, 1963; Sumrall et al., 1997) and Wah Wah (late Floian, Utah; Sprinkle and Guensburg, 1993) formations suggests a probable Laurentian origin for minervaecystids.

The onset of relatively cosmopolitan, undifferentiated low-diversity echinoderm faunas in the Furongian–Tremadocian interval probably explains the expansion of minervaecystids into Gondwanan regions, where they are documented as early as the late Tremadocian (*S. murrayi* Zone) in the Saint-Chinian Formation, Montagne Noire (France: *Minervaecystis* and *Plasiacystis*; Thoral, 1935; Ubaghs, 1970; Dupichaud et al., 2023) and the Fezouata Shale, Anti-Atlas (Morocco: *Nimchacystis* and *Plasiacystis*; Lefebvre et al., 2012; Lefebvre et al., 2016; Dupichaud and Lefebvre, 2022). The occurrence of closely related minervaecystid taxa, including one shared species (*P. mobilis*) in the Montagne Noire and the Anti-Atlas, confirms the existence of strong faunal links between these two regions during the Early Ordovician (e.g., Lefebvre et al., 2016; Saleh et al., 2022b). However, *Minervaecystis* has not so far been documented in Morocco, while this genus is relatively common in coeval deposits from France. Conversely, *Nimchacystis* is apparently endemic to the Central Anti-Atlas. In the Montagne Noire, *Plasiacystis* is known from a single isolated dististele, whereas it is geographically widespread and locally abundant in the Anti-Atlas.

Beyond these differences, possibly related to preservational biases and/or subtle differences in environmental conditions, Early Ordovician solutan faunas from the Anti-Atlas and the Montagne Noire make it possible to record a key evolutionary transition within minervaecystids. Within a relatively short time

interval (late Tremadocian), their long, flattened, stem-like dististele with lateral comb-like projections (*Minervaecystis*) was modified into an elongate (*Nimchacystis*) and then a short, rigid distal paddle (*Plasiacystis*). This new morphotype, probably triggered by the adoption of a more active, crawling mode of life on soft substrates, persisted at least until the middle Darriwilian: *Plasiacystis* was documented in the Šarká Formation of the Prague Basin (Czech Republic; Prokop and Petr, 2003; Lefebvre et al., 2012) and the Hope Shale of Shropshire (UK; K. Derstler in Lefebvre et al., 2012). The occurrence of *P. mobilis* in the Darriwilian of Bohemia confirms the strong faunal links between this region and other high-latitude (peri)Gondwanan areas (Anti-Atlas, Montagne Noire) belonging to the same Mediterranean Province in the Ordovician (Lefebvre et al., 2022 and references therein). The presence of *P. mobilis* in the Hope Shale is more unexpected because, in the Middle Ordovician, Shropshire was part of Avalonia, which was then an independent micro-continent separated from Gondwana by the opening of the Rheic Ocean. However, several other examples of echinoderm taxa with Gondwanan affinities have been reported in the Middle Ordovician of Avalonia (see, e.g., Jefferies, 1987; Fone, 2003; Lefebvre et al., 2012; Botting et al., 2013; Lefebvre et al., 2022). These shared taxa suggest that they originated from the same pool of organisms before Avalonia rifted away from Gondwana and/or that exchanges were still possible on both sides of the Rheic Ocean in the Middle Ordovician.

Conclusions

The systematic description of solutans from the Fezouata Shale reveals an unexpectedly diverse assemblage comprising a *Castericystis*-like syringocrinid and at least two minervaecystids (*N. agterbosi* and *P. mobilis*) in the Lower Ordovician of the Anti-Atlas (Morocco). The *Castericystis*-like solutan represents the first evidence of exceptionally preserved soft tissues (part of the digestive system) in this class. The description of *Nimchacystis* fills the morphological gap between *Minervaecystis* and *Plasiacystis*, thus supporting their placement within the same family (Minervaecystidae), along with *Pahvanticystis*. The abundant and well-preserved material of *P. mobilis* makes it possible to describe several previously unknown or poorly documented morphological features of this taxon. The new Moroccan material also provides new insights into the palaeobiogeographic dispersion of minervaecystids from Laurentia to high-latitude Gondwana and, subsequently, to Avalonia, as well as their presumed mode of life as active *detritus feeder*s crawling backwards on soft substrates.

Data availability statement

The original contributions presented in the study are included in the article/supplementary material. Further inquiries can be directed to the corresponding authors.

Ethics statement

The manuscript presents research on animals that do not require ethical approval for their study.

Author contributions

CD: Data curation, Methodology, Software, Visualization, Writing – original draft, Writing – review & editing. BL: Conceptualization, Data curation, Investigation, Methodology, Supervision, Visualization, Writing – original draft, Writing – review & editing. CM: Writing – review & editing. RM: Writing – review & editing. MN: Methodology, Supervision, Writing – review & editing. RR: Data curation, Methodology, Writing – review & editing. FS: Writing – review & editing, Funding acquisition. SZ: Writing – review & editing.

Funding

The author(s) declare financial support was received for the research, authorship, and/or publication of this article. This study was supported by Faculty of Geoscience and Environment of the University of Lausanne and the SNF Ambizione grant number PZ00P2_209102.

Acknowledgments

This paper is a contribution to IGCP 735 "Rocks and the Rise of Ordovician Life" (Rocks n'ROL) and to the ANR project "Evolution of the Cambrian-Ordovician Biodiversification Onset Over Space and Time" (ECO-BOOST). FS thanks funding from the Faculty of Geoscience and Environment of the University of Lausanne and the SNF Ambizione grant number PZ00P2_209102. MN was supported by an internal grant from the Czech Geological Survey no. 311410, which is a contribution to the Strategic Research Plan of the Czech Geological Survey (DKRVO/CGS 2023-2027). RM was supported through NSF grant 2036298. SZ was supported by the Spanish Ministry of Science and Innovation (PID2021-125585NB-100), co-financed by the European Regional Development Fund, project "Aragosaurus: Recursos Geológicos y Paleoambientales" (E18_17R) funded by the Government of Aragón. The authors are especially grateful to Marine Fau and Loïc Villier for their comments on an early draft of this paper, as well as to the two reviewers for their careful and insightful reviews. Ton Agterbos, Thierry Castel, Patrick Catto, Vaáclav Micka, Myriam Prost, Roland and Véronique Reboul, Daniel Vizcaïno, Andries Weug, and Ondřej Zicha are warmly thanked for having collected, provided access to, and/or photographed important specimens of solutans from the Lower Ordovician of Morocco. The authors would also like to thank Didier Berthet (Musée des Confluences, Lyon), Denis Demarque, and Serge Régnault (Natural History Museum, Nantes), Khadija El Hariri (Cadi Ayyad University, Marrakech), Tim Ewin (Natural History Museum, London), Yves Laurent, and Pierre Dalous

(Natural History Museum, Toulouse), Stéphane Jouve, Anne Médard, and Vincent Poncet (Natural History Museum, Marseille), Rudy Lerosey-Aubril (Senckenberg Museum, Frankfurt), Abel Prieur and Emmanuel Robert (Lyon 1 University, Villeurbanne), and Jessica Utrup (Yale Peabody Museum, New Haven) for access to specimens housed in the public collections over which they have oversight. Vincent Perrier provided invaluable help with photographs.

Conflict of interest

The authors declare that the research was conducted in the absence of any commercial or financial relationships that could be construed as a potential conflict of interest.

The authors BL and FS declared that they were editorial board members of Frontiers, at the time of submission. This had no impact on the peer review process and the final decision.

Publisher's note

All claims expressed in this article are solely those of the authors and do not necessarily represent those of their affiliated organizations, or those of the publisher, the editors and the reviewers. Any product that may be evaluated in this article, or claim that may be made by its manufacturer, is not guaranteed or endorsed by the publisher.

References

Ausich, W. I. (2001). "Echinoderm taphonomy," in *Echinoderm Studies*. Eds. M. Jangoux and J. M. Lawrence (Rotterdam: Balkema), 171–227.

Bather, F. A. (1913). Caradocian cystidea from Girvan. *Trans. R. Soc. Edinburgh* 49, 359–529. doi: 10.1017/S0080456800003999

Botting, J. P. (2016). Diversity and ecology of sponges in the Early Ordovician Fezouata Biota, Morocco. *Palaeogeography Palaeoclimatology Palaeoecol.* 460, 75–86. doi: 10.1016/j.palaeo.2016.05.018

Botting, J. P., Muir, L. A., and Lefebvre, B. (2013). Echinoderm diversity and environmental distribution in the Ordovician of the Builth Inlier, Wales. *Palaios* 28, 293–304. doi: 10.2110/palo.2012.p12-118r

Brett, C. E., Moffat, H. A., and Taylor, W. (1997). Echinoderm taphonomy, taphofacies, and Lagerstätten. *In* Waters, J. A., and Maples, C. G. (eds), *Geobiology of Echinoderms. Paleontological Soc. Papers* 3, 147–190. doi: 10.1017/S1089332600000243

Caster, K. E. (1968). "Homoiostelea," in *Treatise on Invertebrate Paleontology, part S, Echinodermata*, vol. 1 . Ed. R. C. Moore (Boulder: Colorado for Goelogical Society of America Lawrence, Kansas for the University of Kansas Press), S581–S627.

Daley, P. E. J. (1995). Anatomy, locomotion and ontogeny of the solute *Castericystis vali* from the Middle Cambrian of Utah. *Geobios* 28, 585–615. doi: 10.1016/S0016-6995(95)80214-2

Daley, P. E. J. (1996). The first solute which is attached as an adult: a Mid-Cambrian fossil from Utah with echinoderm and chordate affinities. *Zoological J. Linn. Soc.* 117, 405–440. doi: 10.1111/j.1096-3642.1996.tb01659.x

David, B., Lefebvre, B., Mooi, R., and Parsley, R. (2000). Are homalozoans echinoderms? An answer from the extraxial-axial theory. *Paleobiology* 26, 529–555. doi: 10.1666/0094-8373(2000)026<0529:AHEAAF>2.0.CO;2

Dehm, R. (1934). Untersuchungen an Cystoideen des rheinischen Unterdevons. *Sitzungsberichte Bayerischen Akademie der Wissenschaften Mathematisch-naturwissenschaftliche Abteilung* 1934, 19–43.

Destombes, J. (2006). Carte géologique au 1/200 000 de l'Anti-Atlas marocain. Notice explicative. Paléozoïque inférieur : Cambrien moyen et supérieur – Ordovicien – Base du Silurien. Feuille Tafilalt – Taouz. Chapitre E. *Notes Mémoires du Service géologique du Maroc* 244bis, 1–69.

Destombes, J., Hollard, H., and Willefert, S. (1985). "Lower Palaeozoic rocks of Morocco," in *Lower Palaeozoic Rocks of the World. 4. Lower Palaeozoic of North Western - Central Africa*. Ed. C. H. Holland (New York: Wiley), 91–336.

Donovan, S. K. (1991). "The taphonomy of echinoderms: calcareous multi-element skeletons in the marine environment," in *The processes of fossilization*. Ed. S. K. Donovan (London: Belhaven Press), 241–269.

Dupichaud, C., and Lefebvre, B. (2022). "Solutan echinoderms from the Fezouata Shale Lagerstätte (Lower Ordovician, Morocco): diversity, exceptional preservation and palaeobiogeographic implications," in *Abstract book, Second Annual Meeting of IGCP 735*, Cadi Ayyad University, Marrakesh, October 19-20 2022. 23–28.

Dupichaud, C., Lefebvre, B., and Nohejlová, M. (2023). Solutan echinoderms from the Lower Ordovician of the Montagne Noire (France): new data and palaeobiogeographic implications. *Estonian J. Earth Sci.* 72, 26–29. doi: 10.3176/earth.2023.80

Ebbestad, J. O. R. (2016). Tergomya and Paragastropoda (Mollusca) from the Lower Ordovician Fezouata Formation. *Palaeogeography Palaeoclimatology Palaeoecol.* 460, 87–96. doi: 10.1016/j.palaeo.2016.01.003

Fone, W. (2003). "The first occurence of the mitrate *Promitrocystites barrandei* (Jaekel 1918) in Great Britain and some questions it raises," in *Programme and abstracts, The Palaeontological Association, 47th Annual Meeting*, Leicester, 14th-17th December. 59–60.

Gorzelak, P., and Salamon, M. A. (2013). Experimental tumbling of echinoderms—taphonomic patterns and implications. *Palaeogeography Palaeoclimatology Palaeoecol.* 386, 569–574. doi: 10.1016/j.palaeo.2013.06.023

Gorzelak, P., and Zamora, S. (2016). Understanding form and function of the stem in early flattened echinoderms (pleurocystitids) using a microstructural approach. *PeerJ* 4 (e1820), 1–10. doi: 10.7717/peerj.1820

Havlíček, V. (1971). Brachiopodes de l'Ordovicien du Maroc. *Notes Mémoires du Service Géologique du Maroc* 230, 1–135.

Hunter, A. W., Lefebvre, B., Nardin, E., Régnault, S., Van Roy, P., and Zamora, S. (2010). "Preliminary report on echinoderm Lagerstätten from the Upper Ordovician of the eastern Anti-Atlas, Morocco," in *Echinoderms: Durham*. Eds. L. G. Harris, S. A. Böttger, C. W. Walker and M. P. Lesser (Rotterdam: Balkema), 23–30.

Jaekel, O. (1901). Ueber Carpoideen; eine neue Classe von Pelmatozoen. *Z. der Deutschen Geologischen Gesellschaft* 52, 661–677.

Jaekel, O. (1918). Phylogenie und System der Pelmatozoen. *Paläontologische Z.* 3, 1–124. doi: 10.1007/BF03190413

Jefferies, R. P. S. (1987). "The chordates - a preliminary note," in *Bulletin of the British Museum (Natural History) Geology* 41, 285–290.

Kerr, T. J. V., and Twitchett, R. J. (2004). "Experimental decay and disarticulation of *Ophiura texturata*: implications for the fossil record of ophiuroids," in *Echinoderms: München*. Eds. T. Heinzeller and J. H. Nebelsick (Rotterdam: Balkema), 439–446.

Kidwell, S. M., and Baumiller, T. (1990). Experimental disintegration of regular echinoids: roles of temperature, oxygen, and decay thresholds. *Paleobiology* 16, 247–271. doi: 10.1017/S0094837300009982

Klein, J. T. (1778). *Naturalis Dispositio Echinodermatum. Accessit Lucubratiuncula de Aculeis Echinorum Marinorum et Specilegium de Belemnitis. Edita et Descriptionibus Novisque Inventis et Synonymis Auctorum Auca a Nathanaele Godofredo Leske* (Leipzig: Officina Gleditdchiana), 278. pp.

Kouraïss, K., El Hariri, K., El Albani, A., Azizi, A., Mazurier, A., and Lefebvre, B. (2019). Digitization of fossils from the Fezouata Biota (Lower Ordovician, Morocco): evaluating computed tomography and photogrammetry in collections enhancement. *Geoheritage* 11, 1889–1901. doi: 10.1007/s12371-019-00403-z

Kröger, B., and Lefebvre, B. (2012). Palaeogeography and palaeoecology of early Floian (Lower Ordovician) cephalopods from the Upper Fezouata Formation, Anti-Atlas, Morocco. *Fossil Rec.* 15, 61–75. doi: 10.1002/mmng.201200004

Lefebvre, B. (2007). Early Palaeozoic palaeobiogeography and palaeoecology of stylophoran echinoderms. *Palaeogeography Palaeoclimatology Palaeoecol.* 245, 156–199. doi: 10.1016/j.palaeo.2006.02.021

Lefebvre, B., Allaire, N., Guensburg, T. E., Hunter, A. W., Kouraïss, K., Martin, E. L. O., et al. (2016). Palaeoecological aspects of the diversification of echinoderms in the Lower Ordovician of central Anti-Atlas, Morocco. *Palaeogeography Palaeoclimatology Palaeoecol.* 460, 97–121. doi: 10.1016/j.palaeo.2016.02.039

Lefebvre, B., Derstler, K., and Sumrall, C. D. (2012). A reinterpretation of the solutan *Plasiacystis mobilis* (Echinodermata) from the Middle Ordovician of Bohemia. *Zoosymposia* 7, 287–306. doi: 10.11646/zoosymposia.7.1.27

Lefebvre, B., and Fatka, O. (2003). Palaeogeographical and palaeoecological aspects of the Cambro-Ordovician radiation of echinoderms in Gondwanan Africa and peri-Gondwanan Europe. *Palaeogeography Palaeoclimatology Palaeoecol.* 195, 73–97. doi: 10.1016/S0031-0182(03)00303-1

Lefebvre, B., Guensburg, T. E., Martin, E. L. O., Mooi, R., Nardin, E., Nohejlová, M., et al. (2019). Exceptionally preserved soft parts in fossils from the Lower Ordovician of Morocco clarify stylophoran affinities within basal deuterostomes. *Geobios* 52, 27–36. doi: 10.1016/j.geobios.2018.11.001

Lefebvre, B., Gutiérrez-Marco, J. C., Lehnert, O., Martin, E. L. O., Nowak, H., Akodad, M., et al. (2018). Age calibration of the Lower Ordovician Fezouata Lagerstätte, Morocco. *Lethaia* 51, 296–311. doi: 10.1111/let.12240

Lefebvre, B., and Lerosey-Aubril, R. (2018). Laurentian origin of solutan echinoderms: new evidence from the Guzhangian (Cambrian Series 3) Weeks Formation of Utah, USA. *Geological Magazine* 155, 1190–1204. doi: 10.1017/S0016756817000152

Lefebvre, B., Nohejlová, M., Martin, E. L. O., Kašička, L., Zicha, O., and Gutiérrez-Marco, J. C. (2022). "New Middle and Late Ordovician cornute stylophorans (Echinodermata) from Morocco and other peri-Gondwanan areas," in *The Great Ordovician Biodiversification Event: Insights from the Tafilalt Biota, Morocco*, vol. 485 . Eds. A. W. Hunter, J. J. Álvaro, B. Lefebvre, P. Van Roy and S. Zamora (London: The Geological Society, London, Special Publications), 345–522.

Lefebvre, B., Sumrall, C. D., Shroat-Lewis, R. A., Reich, M., Webster, G. D., Hunter, A. W., et al. (2013). "Palaeobiogeography of Ordovician echinoderms," in *Early Palaeozoic Biogeography and Palaeogeography*, vol. 38 . Eds. D. A. T. Harper and T. Servais (London, Memoirs: Geological Society), 173–198.

Loi, A., and Dabard, M. P. (1999). Stratigraphic significance of siliceous-argilaceous nodules in Ordovician formations of the Armorican massif (France) and Sardinia (Italy). *Acta Universitatis Carolinae Geologica* 43, 89–92.

Loi, A., and Dabard, M. P. (2002). Controls of sea-level fluctuations on the formation of Ordovician siliceous nodules in terrigeneous offshore environments. *Sedimentary Geology* 153, 65–84. doi: 10.1016/S0037-0738(02)00102-1

Marek, L. (1983). The Ordovician hyoliths of anti-atlas (Morocco). *Sborník Národního Musea v Praze* 39, 1–36.

Martin, E. L. O., Vidal, M., Vizcaïno, D., Vaucher, R., Sansjofre, P., Lefebvre, B., et al. (2016). Biostratigraphic and palaeoenvironmental controls on the trilobite associations from the Lower Ordovician Fezouata Shale of the central Anti-Atlas, Morocco. *Palaeogeography Palaeoclimatology Palaeoecol.* 460, 142–154. doi: 10.1016/j.palaeo.2016.06.003

Meyer, D. L. (1971). Post-mortem disintegration of Recent crinoids and ophiuroids under natural conditions. *Geological Soc. America Abstracts Programs* 3, 645–646.

Muir, L. A., and Gutiérrez-Marco, J. C. (2023). A new species of the problematic organism *Webbyites* from the Early Ordovician Fezouata Biota of Morocco. *Estonian J. Earth Sci.* 72, 74–77. doi: 10.3176/earth.2023.24

Nebelsick, J. H. (1995). "Actuopalaeontological investigations on echinoids: the potential for taphonomic interpretation," in *Echinoderm Research 1995*. Eds. R. H. Emson, A. B. Smith and A. C. Campbell (Rotterdam: Balkema), 209–214.

Noailles, F., Lefebvre, B., and Kašička, L. (2014). A probable case of heterochrony in the solutan *Dendrocystites* Barrande 1887 (Echinodermata: Blastozoa) from the Upper Ordovician of the Prague Basin (Czech Republic) and a revision of the family Dendrocystitidae Bassler 1938. *Bull. Geosciences* 89, 451–476. doi: 10.3140/bull.geosci.1475

Nohejlová, M., and Fatka, O. (2016). Ontogeny and morphology of Cambrian eocrinoid *Akadocrinus* (Barrandian area, Czech Republic). *Bull. Geosciences* 91, 141–153. doi: 10.3140/bull.geosci.1583

Nohejlová, M., and Lefebvre, B. (2022). "Late Ordovician solutan echinoderms from the western Tafilalt, Morocco," in *The Great Ordovician Biodiversification Event: Insights from the Tafilalt Biota, Morocco*, vol. 485 . Eds. A. W. Hunter, J. J. Álvaro, B. Lefebvre, P. Van Roy and S. Zamora (London: The Geological Society, London, Special Publications), 523–539.

Nohejlová, M., Lefebvre, B., Nardin, E., Fatka, O., and Budil, P. (2019). "New echinoderm Lagerstätte from the Letná Formation (Sandbian, Upper Ordovician) of Bohemia," in *Abstracts, 10th European Conference on Echinoderms*, Moscow, September 16-19, 2019, Vol. 69.

Parsley, R. L. (2012). Ontogeny, functional morphology, and comparative morphology of lower (Stage 4) and basal middle (Stage 5) Cambrian gogiids, Guizhou Province, China. *J. Paleontology* 86, 569–583. doi: 10.1666/10-153R2.1

Polechová, M. (2016). The bivalve fauna from the Fezouata Formation (Lower Ordovician) of Morocco and its significance for palaeobiogeography, palaeoecology and early diversification of bivalves. *Palaeogeography Palaeoclimatology Palaeoecol.* 460, 155–169. doi: 10.1016/j.palaeo.2015.12.016

Prokop, R. V., and Petr, V. (2003). *Plasiacystis mobilis*, gen. et sp. n., a strange "carpoid" (Echinodermata, ?Homoiostelea: Soluta) in the Bohemian Ordovician (Czech Republic). *Sborník Národního muzea (B: Přírodní vědy) [= Acta Musei Nationalis Pragae (B: Natural History)]* 59, 151–162.

Rahman, I. A., and Lintz, H. (2012). *Dehmicystis globulus*, an enigmatic solute (Echinodermata) from the Lower Devonian Hunsrück Slate, Germany. *Paläontologische Z.* 86, 59–70. doi: 10.1007/s12542-011-0116-y

Rozhnov, S. V. (2022). Solutans (Echinoderms): Evolution frozen between torsion and pentaradiality. *Paleontological J.* 56, 1306–1321. doi: 10.1134/S0031030122110144

Saleh, F., Guenser, P., Gibert, C., Balseiro, D., Serra, F., Waisfeld, B. G., et al. (2022b). Contrasting Early Ordovician assembly patterns highlight the complex initial stages of the Ordovician Radiation. *Sci. Rep.* 12 (3852), 1–8.

Saleh, F., Pittet, B., Perrillat, J. P., and Lefebvre, B. (2019). Orbital control on exceptional fossil preservation. *Geology* 47 (2), 103–106. doi: 10.1130/G45598.1

Saleh, F., Pittet, B., Sansjofre, P., Guériau, P., Lalonde, S., Perrillat, J. P., et al. (2020). Taphonomic pathway of exceptionally preserved fossils in the Lower Ordovician of Morocco. *Geobios* 60, 99–115. doi: 10.1016/j.geobios.2020.04.001

Saleh, F., Vaucher, R., Antcliffe, J. B., Daley, A. C., El Hariri, K., Kouraïss, K., et al. (2021). Insights into soft-part preservation from the Early Ordovician Fezouata Biota. *Earth Sci. Rev.* 213 (103464), 1–12. doi: 10.1016/j.earscirev.2020.103464

Saleh, F., Vaucher, R., Vidal, M., El Hariri, K., Laibl, L., Daley, A. C., et al. (2022a). New fossil assemblages from the Early Ordovician Fezouata Biota. *Sci. Rep.* 12 (20773), 1–10. doi: 10.1038/s41598-022-25000-z

Smith, A. B. (1988). Patterns of diversification and extinction in Early Palaeozoic echinoderms. *Palaeontology* 31, 799–828.

Smith, A. B. (2005). The pre-radial history of echinoderms. *Geological J.* 40, 255–280. doi: 10.1002/gj.1018

Sprinkle, J., and Guensburg, T. E. (1993). "Echinoderm biostratigraphy," in *Paleozoic Biochronology of the Great Basin, Western United States. Open-File Report*, vol. 598 . Ed. M. E. Taylor (New York, Oklahoma City: US Geological Survey Open-File Report), 61–63.

Sprinkle, J., and Guensburg, T. E. (1997). "Early radiation of echinoderms," in *Geobiology of Echinoderms* The Paleontological Society Papers, vol. 3 . Eds. J. A. Waters and C. G. Maples, 205–224.

Sprinkle, J., and Guensburg, T. E. (2004). "Crinozoan, blastozoan, echinozoan, asterozoan, and homalozoan echinoderms," in *The Great Ordovician Biodiversification Event*. Eds. B. D. Webby, F. Paris, M. L. Droser and I. G. Percival (Columbia University Press), 266–280.

Sumrall, C. D., Sprinkle, J., and Guensburg, T. E. (1997). Systematics and paleoecology of Late Cambrian echinoderms from the western United States. *J. Paleontology* 71, 1091–1109. doi: 10.1017/S0022336000036052

Thoral, M. (1935). *Contribution à l'étude Paléontologique de l'Ordovicien inférieur de la Montagne Noire et Révision Sommaire de la Faune Cambrienne de la Montagne Noire* (Montpellier: Imprimerie de la Charité), 362. p.

Ubaghs, G. (1963). *Cothurnocystis* Bather, *Phyllocystis* Thoral and an undetermined member of the order Soluta (Echinodermata, Carpoidea) in the uppermost Cambrian of Nevada. *J. Paleontology* 37, 1133–1142.

Ubaghs, G. (1970). *Les Echinodermes «Carpoïdes» de l'Ordovicien inférieur de la Montagne Noire (France)* (Paris: Editions du CNRS, Cahiers de Paléontologie), 110. p.

Ubaghs, G., and Robison, R. A. (1985). A new homoiostelean and a new eocrinoid from the Middle Cambrian of Utah. *Univ. Kansas Paleontological Contributions* 115, 1–24.

Ubaghs, G., and Robison, R. A. (1988). Homalozoan echinoderms of the Wheeler Formation (Middle Cambrian) of western Utah. *Univ. Kansas Paleontological Contributions* 120, 1–17.

Vaucher, R., Pittet, B., Martin, E. L. O., Lefebvre, B., and Hormière, H. (2017). A wave-dominated tide-modulated model for the Lower Ordovician of the Anti-Atlas. *Sedimentology* 64, 777–807. doi: 10.1111/sed.12327

Zamora, S., Deline, B., Álvaro, J. J., and Rahman, I. A. (2017). The Cambrian Substrate Revolution and the early evolution of attachment in suspension-feeding echinoderms. *Earth-Science Rev.* 171, 478–491. doi: 10.1016/j.earscirev.2017.06.018

Zamora, S., and Gutiérrez-Marco, J. C. (2023). Filling the Silurian gap of solutan echinoderms with the description of new species of *Dehmicystis* from Spain. *Acta Palaeontologica Polonica* 68, 185–192. doi: 10.4202/app.01054.2023

Zamora, S., Lefebvre, B., Álvaro, J. J., Clausen, S., Elicki, O., Fatka, O., et al. (2013). "Cambrian echinoderm diversity and palaeobiogeography," in *Early Palaeozoic Biogeography and Palaeogeography*, vol. 38. (London: Geological Society, London, Memoirs), 157–171.

Zamora, S., and Rahman, I. A. (2014). Deciphering the early evolution of echinoderms with Cambrian fossils. *Palaeontology* 57, 1105–1119. doi: 10.1111/pala.12138

Frontiers in
Ecology and Evolution

Ecological and evolutionary research into our natural and anthropogenic world

This multidisciplinary journal covers the spectrum of ecological and evolutionary inquiry. It provides insights into our natural and anthropogenic world, and how it can best be managed.

Discover the latest Research Topics

See more →

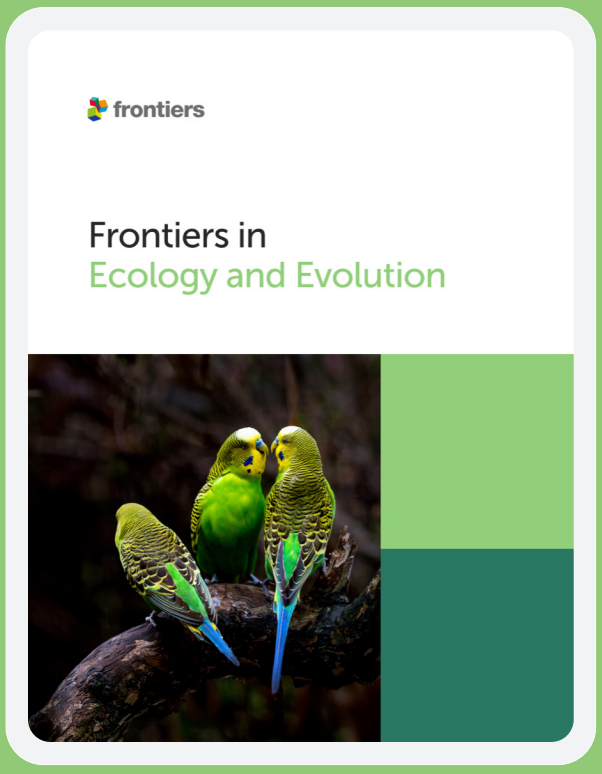

Frontiers

Avenue du Tribunal-Fédéral 34
1005 Lausanne, Switzerland
frontiersin.org

Contact us

+41 (0)21 510 17 00
frontiersin.org/about/contact